Hypericin-mediated photodynamic therapy in two- and three-dimensional models of colorectal cancer: optimisation using a novel microfluidic device

Mohammed Ibrahim Husenmiya Khot

200978790

Submitted in accordance with the requirements for the degree of Doctor of Philosophy

School of Medicine

Faculty of Medicine and Health

University of Leeds

April 2019

The candidate confirms that the work submitted is his own, except where work which has formed part of jointly authored publications has been included. The contribution of the candidate and the other authors to this work has been explicitly indicated below. The candidate confirms that appropriate credit has been given within the thesis where reference has been made to the work of others.

The work in **Chapter 1** of this thesis has appeared in publication as follows:

Khot, M.I., Andrew, H., Svavarsdottir, H.S., Armstrong, G., Quyn, A.J. and Jayne, D.G., 2019. A review on the scope of Photothermal Therapy-based nanomedicines in pre-clinical models of colorectal cancer. *Clinical Colorectal Cancer*, 18(2), e200-e209. https://doi.org/10.1016/j.clcc.2019.02.001

I was responsible for conducting the literature search, reviewing the articles and drafting and editing the manuscript.

The work in **Chapters 1, 5** and **7** of this thesis has appeared in publication as follows:

Khot, M.I., Downey, C.L., Armstrong, G., Svavarsdottir, H.S., Jarral, F., Andrew, H. and Jayne, D.G., 2019. The role of ABCG2 in modulating responses to anti-cancer photodynamic therapy. *Photodiagnosis and Photodynamic Therapy*. https://doi.org/10.1016/j.pdpdt.2019.10.014

I was responsible for conducting the literature search, reviewing the articles and drafting and editing the manuscript.

The work in **Chapters 1, 6** and **7** of this thesis has appeared in publication as follows:

Khot, M.I., Levenstein, M.A., Kapur, N. and Jayne, D.G., 2019. A review on the recent advancement in 'Tumour spheroids-on-a-chip'. *Journal of Cancer Research and Practice*, 6, 55-63.

I was responsible for conducting the literature search, reviewing the articles and drafting and editing the manuscript.

The work in **Chapters 5** and **7** of this thesis has appeared in publication as follows:

Khot, M.I., Perry, S.L., Maisey, T., Armstrong, G., Andrew, H., Hughes, T.A., Kapur, N. and Jayne, D.G., 2018. Inhibiting ABCG2 could potentially enhance the efficacy of hypericin-mediated photodynamic therapy in spheroidal cell models of colorectal cancer. *Photodiagnosis and Photodynamic Therapy*, 23, pp.221-229. https://doi.org/10.1016/j.pdpdt.2018.06.027

I was responsible for the conception of the research plan, developing methodology, planning and executing experiments, analysing data and drafting and editing the manuscript.

ACKNOWLEDGEMENTS

Firstly, I would like to express my eternal gratitude to my supervisor and mentor, Professor David G. Jayne, for giving me the opportunity to study and conduct research under his tutelage and also for being a constant source of guidance, motivation, inspiration and encouragement. I would also like to acknowledge and thank, Professor Nikil Kapur, for overseeing and supervising the entire engineering aspect of my research.

I would like to thank the following people for their invaluable support:-

School of Medicine: *Sarah Perry, Gemma Armstrong, Helen Andrew, Annabelle Williams, Candice Downey, Hafdis Svavarsdottir, Yazan Khaled, Thomas Maisey, Ailsa Rose, Sonny Gunadi, Amanda Smith, Thomas Hughes and David Jayne*

School of Mechanical Engineering: *Nicholas Fry, Mark Levenstein and Nikil Kapur*

School of Physics and Astronomy: *Matthew Bourn and Sally Peyman*

A special thank you to my amazing and lovely surgical ladies: Gemma Armstrong, Helen Andrew, Hafdis Svavarsdottir and Candice Downey for keeping me socially engaged during my PhD.

I am grateful to my parents for their continued support and for encouraging me to seek knowledge and continually make progress. Additionally, a big thank you to my sister, Shaheen and my brother, Sannaan.

Finally, I would like to thank my dear and very close friends; Amirul, Zohaib, Bakhtyar, Akik, Khurram, Inzamam and Amir. Their support was a driving force, in getting me through my PhD. *'Thank you guys, for putting up with me and being there, when I needed all of you'.*

رَّبِّ زِدْنِى عِلْمًا

"O Lord! Increase me in my knowledge"

For Mum and Dad

ABSTRACT

Introduction

Surgery, chemotherapy and radiation therapy are the main treatment options in colorectal cancer (CRC), which is a major cause of global mortality. Photodynamic therapy (PDT) is an emerging field in oncological research, involving light mediated activation of a photosensitiser and subsequent cytotoxicity. Hypericin is a promising photosensitiser, however its potential in clinical oncology is under review. Three-dimensional (3D) multicellular spheroids are recognised as better representations of cancer as compared to two-dimensional (2D) cell cultures. Conventional 3D cell culturing methods are complex procedures. Integrating 3D cell culturing into microfluidics, can scale down traditional protocols and allow precise high throughput experiments to be conducted on a microfluidic platform.

Methods

HT29, HCT116, Caco2 colorectal cancer and HFFF2 human foetal foreskin fibroblast cell lines were used in this project. Non-cell adherent coating, ultra-low attachment plates, hanging drop and spinner flask techniques were used to generate 3D spheroids. For PDT, cell cultures were treated with Hypericin, then subjected to $1J/cm^2$ of light. Western blot and immunofluorescence was conducted to detect ABCG2 protein. Designs of microfluidic devices were drawn in SolidWorks and produced using 3D printing and laser cutting. Fluid flow was driven using a syringe pump. HT29 spheroids were cultured and treated with 5-Fluorouracil (5-FU) in the microfluidic device. Trypan blue, fluorescent dyes and the Lactate Dehydrogenase assay were used to analyse cytotoxicity.

Results

The agarose-coated plate and spinner flasks methods were found to be successful methods for culturing 3D spheroids. Light and Hypericin-dose dependant reduction in cell viability was observed in all cell lines ($p < 0.0001$). Spheroids were more resistant than 2D cultures to Hypericin-PDT (HT29: $p = 0.003$, HCT116: $p = 0.006$) and also had a greater expression of ABCG2 protein. Inhibition of ABCG2 protein in spheroids with Ko143 resulted in an enhanced Hypericin-PDT effect compared to Hypericin-PDT alone (HT29: $p = 0.04$, HCT116: $p = 0.01$). HT29 spheroids were successfully cultured in the 'version 3' microfluidic device. 5-FU treatment and cytotoxic analysis was achievable 'on-chip' through flow.

Conclusions

Hypericin-PDT is an effective method for treating CRC, with potential clinical application. 3D spheroids are better representations of *in vivo* cancers and could improve pre-clinical to clinical translation of Hypericin-PDT in CRC. Microfluidic platforms provide a convenient route for streamlining and downsizing traditional laboratory-based experiments and techniques. Combining complex 3D cell culturing methods and microfluidics can enhance the routine incorporation of spheroids in pre-clinical investigations.

TABLE OF CONTENTS

LIST OF TABLES

LIST OF FIGURES

LIST OF VIDEOS

Video 1 - Fluid flow through Version 1 microfluidic device

Video 2 - Fluid flow through Version 2 microfluidic device

Video 3 - Fluid flow through Version 3 microfluidic device

LIST OF ABBREVIATIONS

2D	Two-dimensional
3D	Three-dimensional
3Rs	'Reduction', 'Refinement' and 'Replacement'
5-ALA	5-aminolevulinic acid
5-FU	5-Fluorouracil
ABC	ATP-binding cassette
ABCG2	ATP-binding cassette superfamily G member 2
ABS	Acrylonitrile Butadiene Styrene
AlPcS2a	Aluminium Phthalocyanine Chloride Disulfonic acid
AlPcS4	Aluminum Phthalocyanine Tetrasulfonic acid
AMG	Advanced Microscopy Group
ANOVA	Analysis of Variance
APC	Adenomatous polyposis coli
AuNP	Gold-based nanoparticles
Bax	Bcl-2-associated X protein
Bcl-2	B-cell lymphoma 2
BCRP	Breast Cancer Resistance Protein
CAFs	Cancer-associated fibroblasts
CEA	Carcinoembryonic antigen
CRC	Colorectal Cancer
CRS	Cytoreductive Surgery
CRYSTAL	Cetuximab combined with iRinotecan in first-line therapY for metaSTatic colorectAL cancer
CTGF	Connective Tissue Growth Factor

DAPI	4′,6-diamidino-2-phenylindole
DMEM	Dulbecco's Modified Eagle Medium
DNA	Deoxyribonucleic acid
DPBS	Dulbecco's Phosphate-Buffered Saline
DPX	Depex Mounting Medium
ECM	Extracellular Matrix
EDTA	Ethylenediaminetetraacetic acid
EGFR	Epithelial Growth Factor Receptor
Em:	Emission
EMT	Epithelial-Mesenchymal Transition
Ex:	Excitation
FBS	Fetal Bovine Serum
FC	Ferrochelatase
FGS	Fluorescence-guided surgery
FOLFIRI	Leucovorin, 5-FU and Irinotecan
FOLFOX	Leucovorin, 5-FU and Oxaliplatin
FOLFOXIRI	Leucovorin, 5-FU, Oxaliplatin and Irinotecan
Gy	Gray
H&E	Haematoxylin and Eosin staining
HIF1α	Hypoxia Inducible factor 1α
HIPEC	Hyperthermic Intraperitoneal Chemotherapy
HpD	Hematoporphyrin Derivative
HSP60	Heat Shock Protein 60
HYP	Hypericin
ICG	Indocyanine Green

IFN-γ	Interferon gamma
IL-6	Interleukin 6
J/cm²	Joule per centimetre squared
KRAS	Kirsten RAt Sarcoma
LDH	Lactate Dehydrogenase
LDL	Low-density lipoproteins
LDS	Lithium Dodecyl Sulfate
LED	light-emitting diode
MCTS	Multicellular Tumour Spheroids
Methyl ALA	Methylaminolevulinic acid
MIF	Macrophage Migration Inhibitory Factor
MMR	DNA Mismatch Repair
MPM	Malignant Pleural Mesothelioma
mTHPC	meta(tetrahydroxyphenyl)chlorin
NFκB	Nuclear Factor-κB
NICE	National Institute for Health and Care Excellence
NIR	Near-infrared
nm	nanometres
NP	Nanoparticles
NPe6	mono-L-aspartyl chlorin e6
PARP	Poly (ADP-ribose) polymerase
PBGD	Porphobilinogen Deaminase
PBS	Phosphate-Buffered Saline
PCI	Photochemical internalisation
PDMS	Polydimethylsiloxane

PDT	Photodynamic Therapy
PI	Propidium Iodide
PMMA	Poly(methyl methacrylate)
PolyHEMA	Poly(2-hydroxyethyl methacrylate)
PpIX	Protoporphyrin IX
PPME	Pyropheophorbide-a Methyl Ester
PRIME	Panitumumab Randomized Trial In Combination with Chemotherapy for MEtastatic Colorectal Cancer to Determine Efficacy
PS	Photosensitiser
PTT	Photothermal Therapy
PVDF	Polyvinylidene Difluoride
RH	Relative Humidity
RIPA	Radioimmunoprecipitation assay
ROS	Reactive Oxygen Species
RPMI	Roswell Park Memorial Institute
SCC	Squamous Cell Carcinoma
SEM	Scanning Electron Microscopy
TBS-T	Tris-buffered saline with Tween 20
TNFα	Tumour Necrosis Factor α
TPCS2a	Disulfonated Tetraphenyl chlorin
UK	United Kingdom
ULA	Ultra-Low Attachment
USA	United States of America
UV	Ultraviolet

v/v   Volume/Volume

w/v   Weight/Volume

Chapter One

INTRODUCTION

1 INTRODUCTION

1.1 COLORECTAL CANCER

1.1.1 Incidence and survival

In the UK alone, colorectal cancer (CRC) is the fourth most common form of cancer, accounting for 12% of all newly diagnosed cancer cases (Cancer Research UK, 2015). Furthermore, CRC is the second most common cause of cancer related deaths, accounting for 10% of all cancer related mortalities. Since the early 1990's, the incidence rate of CRC has increased by 4%, and between 2013 and 2015, there were over 40,000 new CRC cases each year. The incidence of CRC strongly correlates with age, with elderly people being more susceptible to developing the disease (75 years and older). Around 76%, 59% and 57% of individuals diagnosed with CRC will survive their disease for one, five and ten years respectively (Cancer Research UK, 2016).

1.1.2 Current methods of treatment for colorectal cancers

1.1.2.1 Surgery

Surgery has remained central to managing and treating CRC. This includes complete surgical excision of the primary tumour, along with the draining lymphatics. Around 80% of newly diagnosed CRC cases, present with localised diseased that can be treated with surgical resection (Gustavsson et al., 2015). The remaining patients present with advanced disease, and only a small proportion of patients with advanced and metastatic disease are suitable for aggressive surgery to resect multi-site disease. For the remainder, surgery is palliative (Edwards et al., 2012). Even for patients who undergo initial surgery with curative intent, there is a risk of disease recurrence. This may be within the

surgical field, termed locoregional recurrence or to distant organs (Riihimäki et al., 2016; Liska et al., 2017). To highlight this, Pugh *et al.* (2016) investigated the post-operative recurrence of disease in patients staged with Dukes' A-C CRC (Pugh et al., 2016). The study found 17% (189/1132) of patients had experienced recurrence after a median of 4 years after surgery. Pulmonary recurrence was most frequently associated with rectal cancers, whereas multi-site and non-colonic recurrences were more frequently seen in right-sided colonic tumours. Disease recurrence also correlated with the initial tumour staging, and recurrence from lower-stage tumours were more likely to be treatable. Lymph node metastasis at the time of initial surgery is highly predictive of locoregional and distant disease recurrence, highlighting the importance of radical lymphadenectomy to increase the chances of cure (McDonald et al., 2012; Andrew et al., 2016).

With regards to the type of surgery performed, laparoscopic surgery for colorectal cancer, has been shown to achieve similar outcomes to conventional open surgery, but with short-term advantages in terms of more rapid recovery, shorter hospital stays, fewer complications and overall better quality of life (Milsom et al., 1998; Braga et al., 2002; Green et al., 2013). Furthermore, laparoscopic hepatectomy is also as safe as open surgery for liver resection in selected patients with CRC liver metastases (Xie et al., 2017).

1.1.2.2 Chemotherapy and Radiation Therapy

Chemotherapy is often used as an adjunct to surgery, to reduce the chance of metastatic disease. 5-fluorouracil (5-FU) is genotoxic and is the foundation chemotherapeutic agent used in CRC treatment. 5-FU is frequently

administered in combination with folinic acid (leucovorin) and it can be effective, as a stand-alone treatment in advanced CRC (Poon et al., 1989; Thirion et al., 2004), achieving a survival benefit in patients with stage II and III CRC, as compared to those who are treated with surgery alone (Wilkinson et al., 2010).

The topoisomerase I inhibitor, Irinotecan, and the platinum DNA alkylating agent, Oxaliplatin, have also been incorporated into treatment regimens for metastatic CRC. In the 1990's and 2000's, many clinical trials were conducted to identify the optimal doses and combinations of these chemotherapeutic compounds to treat advanced and metastatic CRC. This lead to the development of the FOLFOX (Leucovorin, 5-FU and Oxaliplatin) and FOLFIRI (Leucovorin, 5-FU and Irinotecan) treatment regimens. In comparison to 5-FU and Leucovorin alone, the addition of oxaliplatin or irinotecan, demonstrated greater efficacy in previously untreated patients with advanced CRC. In comparison to each other, the FOLFOX and FOLFIRI regimens were found to achieve similar treatment responses, progression-free and overall survival rates. However, differences were observed in the toxicity profiles (Goldberg et al., 2004; Tournigand et al., 2004; Colucci et al., 2005). Recently, the combination of both oxaliplatin and irinotecan along with 5-FU and leucovorin (FOLFOXIRI), was developed as a more aggressive approach to treat metastatic CRC. Studies found FOLFOXIRI to be greatly beneficial in terms of overall survival, progression-free survival and overall response rates, as compared to the standard FOLFIRI regimen, but with greater toxicity in FOLFOXIRI treated patients (Leal et al., 2017).

In an attempt to reduce the toxicity of systemic chemotherapy regimens, targeted therapies have been introduced. Many clinical studies have attempted to find an effective targeting monoclonal antibody that could be used as a second-line of treatment in combination with FOLFOX and FOLFIRI. The advantages of targeted therapies using monoclonal antibodies and small molecule inhibitors, are their ability to antagonise overexpressed growth factor receptors, supressing the growth of the tumour and the potential to overcome chemotherapy resistance. Targeted therapies can be used to deliver a wide range of cytotoxic agents to cancer cells bearing the target antigen and with potentially less systemic side effects (J. Li et al., 2012). Examples of studies using targeted therapies, include the Eastern Cooperative Oncology Group 3200 study, which investigated the combination of the pro-angiogenic vascular endothelial growth factor inhibitor, Bevacizumab, and FOLFOX. The study showed an improvement in survival in patients with previously treated metastatic CRC, when they received Bevacizumab and FOLFOX as compared to FOLFOX alone (Giantonio et al., 2007). Many colorectal cancers possess inactivating mutations, in the tumour suppressor gene, APC, resulting in the increased expression of the epithelial growth factor receptor (EGFR) with subsequent uncontrolled cell division and tumour growth (van Houdt et al., 2010). The CRYSTAL study investigated the combination of the EGFR inhibitor, Cetuximab, and FOLFIRI as first-line treatment in metastatic CRC patients. The results demonstrated an improved progression-free and overall survival in patients with wild-type KRAS as compared to those who received FOLFIRI alone (van Cutsem et al., 2009; van Cutsem et al., 2011). Furthermore, the PRIME study evaluated the combination of the EGFR inhibitor, Panitumumab, and FOLFOX, and found a significant improvement in progression-free survival

in metastatic CRC patients with wild-type KRAS as compared to those who received FOLFOX alone (Douillard et al., 2010). From the above, it can be seen that the key milestones in chemotherapy for CRC, includes the discovery of 5-FU, the identification of leucovorin as a potentiator of 5-FU cytotoxicity, the incorporation of irinotecan/oxaliplatin to treatment regimens and more recently the use of targeting biological agents (Gustavsson et al., 2015). Within the UK, the NICE guidelines support these treatments as standard of care, in patients with advanced metastatic CRC (National Institute for Health and Care Excellence, 2011).

Radiotherapy is commonly used in combination with surgery and chemotherapy for rectal cancers to improve local disease control and long-term survival (Kye and Cho, 2014). Radiotherapy may be used alone, usually as a short course of 5 x 5Gy, to "sterilise" the surgical field prior to operation and reduce the risk of local recurrence. Alternatively it can be given in combination with chemotherapy when it is commonly given over a 6 week period followed by a "recovery period" of 6 weeks prior to surgical resection (Petrelli et al., 2016). This latter regimen is used when tumour down-staging is required to facilitate surgical resection with a clear circumferential resection margin (Du et al., 2018).

1.1.2.3 Cytoreductive surgery and hyperthermic intraperitoneal chemotherapy

Cytoreductive surgery and hyperthermic intraperitoneal chemotherapy (CRS & HIPEC) is an aggressive approach in treating patients with advanced stage IV disease. CRS & HIPEC is reserved for those with hepatic and peritoneal metastases and otherwise very poor prognosis. This treatment initially involves

the surgical removal of tumour deposits within the abdomen along with any involved organs as necessary, followed by the delivery of a heated and concentrated form of a chemotherapeutic solution to the abdominal region. CRS & HIPEC offers a chance for long-term survival in patients, with peritoneal metastasis (Halkia et al., 2015; Simkens et al., 2017). Morbidity and mortality associated with CRS & HIPEC varies according to patient factors, chemotherapeutic drug used, spread of disease, tumour histology and also the experience of the operating surgeon and treatment centre (Newton et al., 2016).

1.2 PHOTODYNAMIC THERAPY

1.2.1 The use of photosensitisers

Oscar Raab, a German medical student whose name is synonymous with Photodynamic Therapy (PDT), is credited as being the first scientist to discover the cytotoxic properties of light absorbing chemicals at the start of the 20th century (Mohanty et al., 2013). During the next few decades, the biological effects of photosensitive chemicals and compounds in various organisms were considered to be 'oddities'. It wasn't until around the 1960's and 1970's, when it was identified that injections of crude preparations of haematoporphyrin led to fluorescence in cancerous lesions, that could be visualised during surgery (Sibata et al., 2000). Additionally, the serendipitous addition of a porphyrin derivative into a culture of cells that were left next to a window in a laboratory resulting in cytotoxicity, led to the use of photosensitive chemicals for therapeutic purposes and the inception of modern day PDT (Allison et al., 2004). Since then, the medicinal application of photosensitisers has been explored in age-related macular degeneration, anti-cancer PDT, anti-microbial PDT and fluorescent imaging and diagnosis (Verteporfin In Photodynamic

Therapy Study Group, 2001; Dolmans et al., 2003; Motoori et al., 2015; Carrera et al., 2016).

1.2.2 Anti-cancer applications of photosensitisers

1.2.2.1 Phototoxic and Photodynamic treatment of cancers

PDT involves the administration of a photosensitiser, which is selectively taken up and retained by tumours. Photoexcitation of the photosensitiser using light of a specific wavelength within the visible light region of the electromagnetic spectrum, results in the production of reactive oxygen species (ROS), followed by oxidative stress and anti-cancer effects resulting in cell death (Figure 1.1). In addition to inducing cell death by necrosis and apoptosis, an immunogenic response is elicited at the site of tumour growth combined with the collapse and shutdown of the tumour microvasculature (Castano et al., 2006; Robertson et al., 2009; Hatakeyama et al., 2013). The attractiveness of PDT is that it is a site-specific method of treatment by virtue of the fact that the activating light can be directed to a specific target lesion (Z. Huang et al., 2008; Mathews et al., 2009). PDT also addresses some of the limitations with conventional chemotherapy treatments, such as systemic toxicity, resistance to treatment and tumour selectivity (Robertson et al., 2009; Maduray and Davids, 2011; Kawczyk-Krupka et al., 2016).
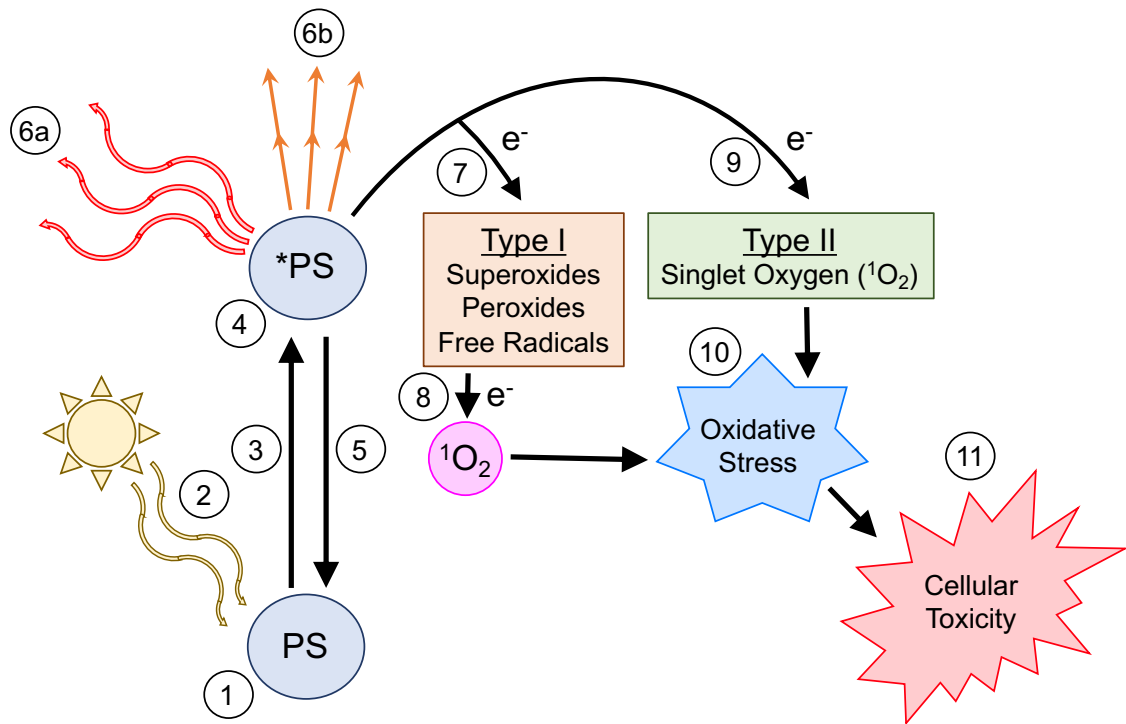
Figure 1.1 – The molecular mechanism of action in PDT

1) Ground state of energy photosensitiser (PS) absorbs photon energy from *2)* irradiating light of a specific wavelength. *3)* The excited photosensitiser (*PS) then achieves a higher state of energy. *4)* At high energy states, *PS is unstable and will *5)* lose energy returning to ground state. Energy is lost through *6a)* fluorescence, *6b)* kinetic energy or by transferring energy to *7)* intracellular oxidising agents to generate radical ions which then *8)* transfer energy to molecules of oxygen to form highly reactive singlet oxygen ($^1O_2$) (Type I reaction) or *9)* directly to oxygen to form $^1O_2$ (Type II reaction). *10)* Oxidative stress is experienced by the cell due to increased production and accumulation of $^1O_2$, resulting in *11)* cellular toxicity and cell death.

Following the identification of Hematoporphyrin derivative (HpD) as a potent mediator of PDT, Dougherty *et al.* (1978) reported the first large clinical study evaluating PDT. As this was the first study of its kind, many tumours were reported to be treated, including skin (basal cell carcinoma and malignant melanoma), chondrosarcoma, colon adenocarcinoma, prostate cancer, endometrial carcinoma, breast carcinoma and angiosarcoma. In this study, they reported a complete response in 88% (98/113) of lesions treated with HpD and

exposed to red light (Dougherty et al., 1978). The importance of this study is that it was the first to establish the efficacy of clinical PDT, and also demonstrate the ability of PDT to treat tumours, that have previously failed to respond to traditional treatment. Since then, years of research has gone into understanding and evaluating the influencing variables of PDT i.e. type and concentration of photosensitiser, total light dose and drug-light interval to improve the therapeutic index of PDT (Cengel et al., 2016). The success of early clinical trials led to the first clinical approval of PDT in 1993 using the HpD, porfimer sodium (Photofrin), in bladder cancer (Dolmans et al., 2003; Ormond and Freeman, 2013).

The success of Photofrin quickly propelled this photosensitiser into being approved for many other malignancies (Table 1.1). However, it was identified quite early on that there were some limitations in Photofrin-mediated PDT. At Photofrin's wavelength of maximum light absorption (~630nm), the molar absorption of photons is low, therefore a higher concentration of light and photosensitiser was required. The wavelength of maximum activation was also found to be short for effective tissue penetration. Additionally, compared to the newer generation of photosensitisers, the rate of tumour-to-normal tissue accumulation was low and Photofrin had a longer half-life meaning that patients were more likely to experience adverse effects such as cutaneous photosensitivity which can last for six to ten weeks (Dolmans et al., 2003; Ormond and Freeman, 2013; Zhang et al., 2017). HpD and Photofrin are first generation photosensitisers and are considered to be impure and generally composed of a crude mixture of hematoporphyrins and porphyrinic compounds. To address the unfavourable events associated with Photofrin-PDT; a lot of

emphasis has been put into the production of newer and more refined second-generation photosensitisers. This includes the modification of existing porphyrin structures and also the creation of several new non-porphyrin based photosensitisers that have better tumour retention, activation at longer wavelengths of light (up to 800nm) and reduced skin phototoxicity (Gomer, 1991; Ormond and Freeman, 2013; Zhang et al., 2017).

Table 1.1 – Current clinically approved photosensitisers for PDT

Photosensitiser	Trade Name	Application
Porfimer sodium	Photofrin	Bladder cancer
		Oesophageal cancer
		Lung cancer
		Barrett's oesophagus
		Cervical cancer
		Endobronchial cancer
5-ALA (PpIX)	Levulan	Actinic Keratosis
Methyl ALA (PpIX)	Metvix	Actinic Keratosis
		Basal cell carcinoma
		Bowen's disease
Verteporfin	Visudyne	Age-related macular degeneration
mTHPC	Foscan	Head and neck cancer
NPe6	Laserphyrin	Lung cancer
AlPcS4	Photosens	Head and Neck cancer
		Skin cancer
		Stomach cancer
		Breast cancer

Of the many second-generation photosensitisers that have been developed, one successful example is Protoporphyrin IX (PpIX) and its precursor 5-

aminolevulinic acid (5-ALA). Exogenously administered 5-ALA is taken up by metabolically active cells, such as cancer cells, where it is utilised in the heme biosynthesis pathway in the mitochondria to produce PpIX and subsequently the haemoglobin co-factor, heme. A negative feedback mechanism prevents an excess production of endogenous 5-ALA, which can result in phototoxicity. However, this can be overridden by the administration of exogenous 5-ALA (Rick et al., 1997). Several 5-ALA/PpIX derived clinical compounds such as Levulan®, Alacare® and Metvix®, are currently being used, to successfully treat a large variety of superficial dermatological lesions including basal cell carcinoma, actinic keratosis on the face and scalp and also squamous cell carcinoma (SCC) *in situ* (Bowen's disease) (Ibbotson, 2011; Wan and Lin, 2014; M. Kim et al., 2015) (Table 1.1). 5-ALA/PpIX has now superseded Photofrin to become one of the most popular and commercially available photosensitisers for PDT. Many current approved clinical PDT protocols focus on dermatological lesions, which is vastly more popular than the use of PDT to ablate solid tumours (Z. Huang et al., 2008).

Dermatological PDT protocols typically involve the topical application of the photosensitiser, followed by light treatment using a simple "lamp like" device. This is clearly easier to administer as compared to treatment of solid tumours involving internal organs, where the photosensitiser has to be administered systemically, and the light delivered by endoscopic means. However, there have been some significant advances in the more complex applications of PDT, especially in treating thoracic malignancies. Kato *et al.* (2003) conducted a clinical study, where PDT was evaluated in patients with early stage SCC of the lung. The second-generation photosensitiser, mono-L-aspartyl chlorin e6

(NPe6), was administered intravenously, followed by light treatment using a fibre optic diode laser. A complete response rate was observed in 83% (29/35) of patients and 85% (33/39) of lesions treated with NPe6-PDT. No serious adverse effects and low skin photosensitivity was observed (Kato et al., 2003). Minnich *et al.* (2010) evaluated Photofrin-PDT in patients with endobronchial lesions obstructing the airway and found that 74% (94/127) of patients achieved significant improvement in dyspnoea (Minnich et al., 2010). Other studies have confirmed the efficacy and safety of PDT in treating lung cancers (Furukawa et al., 1999; Moghissi et al., 1999).

The above studies are examples of where PDT has been used as an alternative to surgery and usually in the palliative setting. However, when PDT was investigated as an adjunct to surgery in tracheobronchial malignancies, it was found to be safe and effective, even in surgically high-risk patients (Jheon et al., 2011). In treating malignant pleural mesothelioma (MPM), surgery has been recommended as part of an overall treatment regime. Combined intraoperative PDT and surgery appears promising in improving local control and potentially prolonging survival in selective MPM patients (Simone and Cengel, 2014). Intraoperative PDT has also been investigated in brain malignancies, with many clinical studies having looked at its efficacy and compared it to the current standard of care. Although the results in brain cancers are promising, the evidence from randomised clinical trials is not convincing and there is still a long way to go before PDT is accepted as routine treatment for brain cancer (Eljamel, 2010; Quirk et al., 2015). PDT is ideally suited for treating lesions ranging from mild dysplasia to superficial SCC in head and neck cancers, which can be easily accessed. Similar to dermatological lesions, PDT in head and

neck cancers is relatively easy to perform and attractive for its ability to preserve normal anatomy and function. PDT can also be repeated and with the development of new photosensitisers, the risk of photosensitivity reactions can be reduced (Mimikos et al., 2016).

PDT works independently to conventional chemotherapy, radiation and surgery, which means it can have an additive effect in combination therapies. However, in comparison to dermatological and endoscopic PDT applications, intraoperative PDT to treat solid intra-abdominal malignancies has attracted less attention and is not widely used. A review by Moghissi *et al.* (2015), evaluated the current position of PDT in surgery. The authors described PDT as an effective tool for surgeons, by virtue of it being i) safe and efficient treatment, ii) administered through routine endoscopic applications, iii) used alone on precancerous lesions with long-term clearance if surgery is prohibitively risky, iv) used neoadjuvantly to reduce tumour volume and v) does not affect post-surgical adjuvant therapy (Moghissi et al., 2015).

After decades of research into anti-cancer PDT, criteria have been established for the ideal photosensitiser, which includes: i) availability of the compound in a chemically pure form, ii) strong phototoxicity, iii) negligible dark toxicity, iv) long light wavelengths (>600nm) for photoactivation, v) rapid clearance from the body, vi) longer and stable triple excited energy state to yield a high production of ROS and vii) multiple routes for administration (Z. Huang et al., 2008; I. Yoon et al., 2013).

Outside of dermatology, the use of PDT is not supported by a strong evidence-base for the treatment in cancer. A major limitation that is hindering the progression of PDT into mainstream medicine, is the lack of high-quality, multicentred and internationally collaborative randomised clinical trials that evaluate meaningful outcomes, such as safety and efficacy, functional outcomes, quality of life, survival rates and cost effectiveness (Bown, 2012). The situation is made more complex by the wide number of variables involved in delivering PDT, including the doses of photosensitiser and light treatment used.

1.2.2.2 Fluorescence guided surgery

Historically, surgeons have relied on their surgical training and experience to distinguish tumours from surrounding normal tissue and therefore guide the extent of surgical resection. Reliance on vision and touch to distinguish tumour and healthy tissue can be inaccurate, leading to either incomplete tumour removal with early tumour recurrence, or unnecessary resection of healthy tissue that compromises postoperative function. Pre- and perioperative imaging are now heavily relied on, to assist surgeons to improve outcomes of cancer surgery. Photosensitisers are increasingly being used as visualising agents, for real-time intraoperative fluorescent imaging, to aid surgeons in identifying surgical margins and identifying metastatic disease (Mondal et al., 2014; Mochida et al., 2017).

PDT involves the administration of a total dose of light (usually measured in J/cm^2), which is required to allow photons to maximally transfer energy to ground energy state photosensitisers and allowing them to achieve a higher

excited state of energy. When the photosensitisers return to ground state, the energy is transferred to oxygen and superoxides to form ROS. For fluorescence guided surgery a dose of light is required that is sufficient to excite the photosensitisers to a higher state of energy, which is then quickly emitted as fluorescent light. (Figure 1.1) (Loschenov et al., 2000).

The earliest example of using a fluorophore in humans was recorded in 1957 and involved the use of indocyanine green (ICG) (Koonce and Newman, 2017). Then in 1960, it was found that injection of crude preparations of HpD into neoplastic lesions allowed them to be fluorescently visualised during surgery (Dougherty et al., 1998; Sibata et al., 2000). Since then, ICG has become one of the most frequently used fluorescent probes because it is readily available, binds rapidly to serum lipoproteins, absorbs and emits light in the near-infrared (NIR) spectrum, possesses low toxicity and clears from tumours at a slower rate than normal tissues (Ogawa et al., 2009; Mochida et al., 2017; Armstrong et al., 2017).

In Europe, 5-ALA/PpIX has been extensively investigated since the start of the 21st century for its role in fluorescence-guided surgery (FGS). Stummer *et al.* (2000) published the first European clinical study in 5-ALA/PpIX mediated FGS in glioblastoma, and found it to be a safe method that aided the completeness of tumour removal (Stummer et al., 2000). The authors then undertook a large multicentre randomised phase III trial and found that tumour resection was complete in 65% (90/139) of patients who were given 5-ALA as compared to 36% (47/131) of patients who received conventional white light imaging. Furthermore, patients who received 5-ALA/PpIX mediated FGS were found to

have a higher 6-month progression free survival in comparison to those who received white light (41% vs 21% respectively) (Stummer et al., 2006). 5-ALA mediated FGS has subsequently been adopted for intraoperative fluorescence visualisation of several types of cancers, but most notably in brain cancer (Vansevičiūtė et al., 2014; Inoue et al., 2015; Namikawa et al., 2015).

Recent attempts to improve FGS and fluorescence diagnosis have concentrated on the development of fluorescent molecular probes and photosensitisers with improved specificity and efficacy i.e. using targeting antibodies and nanoparticles (Landau et al., 2016). This includes the development of dual-function photosensitisers, for simultaneous FGS and intraoperative PDT (Patel et al., 2016). These developments are still in their early stage and for the most part, require further preclinical testing prior to translation into clinical practice.

1.2.2.3 Photothermal Therapy

Similar to PDT and fluorescence utilised for guiding surgery, Photothermal Therapy (PTT) is another non-invasive anti-cancer technique, which utilises photosensitising agents (Norouzi et al., 2018). Following the administration of the photosensitiser to cancer cells, NIR light radiation is emitted which is absorbed by the photosensitiser and converted into kinetic energy (Figure 1.1). The released kinetic energy can overheat the intracellular environment, inducing hyperthermia, which results in cell death (Huang et al., 2008; Huang and El-Sayed, 2011). Intracellular temperatures between 40°C to 47°C cause irreversible damage to cellular proteins and impair DNA function, often resulting in apoptotic cell death. In PTT, it is common for the intracellular temperature of

cancer cells to reach 50°C, resulting in necrosis and rapid cell death as indicated by the instant denature of proteins and cells disintegrate as the lipid bilayer is compromised (Cherukuri et al., 2010; Mouratidis et al., 2015; Spyratou et al., 2017).

Many different photosensitising materials have been evaluated for mediating PTT, including graphene oxide, carbon nanotubes and various hydrophobic NIR light-absorbing dyes. However, the most popular photosensitising material in PTT related studies is gold (Huang and El-Sayed, 2010). Gold-based nanoparticles (AuNP) are efficient in converting light energy into heat, can be structurally tuned to absorb maximum light in the NIR range and are biocompatible (Riley and Day, 2017). Furthermore, AuNP can also be used for optical imaging, due to their capacity to absorb and scatter light in the visible and NIR regions (Tong et al., 2009).

Examples of studies which have evaluated PTT in CRC models includes studies conducted by O'Neal *et al.* (2004) and Goodrich *et al.* (2010), that observed substantial tumour growth regression *in vivo* in murine CT26 CRC tumour xenografts, following treatment with AuNP and NIR light radiation. No adverse toxicity was found in the vital organs (O'Neal et al., 2004; Goodrich et al., 2010). Due to the nano-scale sized of PTT mediating photosensitising materials, multimodal nanomedicines have been developed and evaluated, incorporating PTT agents with chemotherapeutics, cancer-imaging agents and cancer-targeting moieties. These multimodal nanomedicines have demonstrated improved uptake into cancer cells, improved imaging of cancers and synergistic anti-cancer effects with combined chemotherapy and PTT (Kirui et al., 2013;

Azhdarzadeh et al., 2016; Hosseinzadeh et al., 2017; Tsai et al., 2017; Chen et al., 2017; Yang et al., 2017; Lu et al., 2018; Einafshar et al., 2018; Lin and Shieh, 2018).

Both PTT and PDT utilise photosensitive agents, which absorb light energy to elicit anti-cancer effects (Chitgupi et al., 2017). Whereas light energy is converted into heat energy in PTT (Jaque et al., 2014), with PDT the light energy is transferred to oxygen to produce reactive oxygen species, which is mediated by the photosensitive agent (Dolmans et al., 2003). Hypoxia is known to drive the progression of cancers and resistance to treatment (Muz et al., 2015; Petrova et al., 2018). Unlike PDT, PTT does not require oxygen to induce cytotoxicity and is better suited to treat solid cancers with predominant hypoxic and anoxic regions.

1.2.2.4 Photochemical internalisation

Photochemical internalisation (PCI) utilises the concept of PDT, to augment the intracellular delivery of macromolecules, including chemotherapeutic agents (Adigbli and MacRobert, 2012). In PCI, lysosomal or endosomal vesicles containing therapeutic agents are combined with a photosensitiser which binds to the membrane of the vesicle. The photosensitiser-vesicle complex is administered and is taken up by target cells through endocytosis. The chemical polarity of the photosensitiser keeps it in close proximity to the membrane of the vesicle and upon light irradiation, the photo-activated photosensitiser generates local ROS that disrupt the vesicular membrane with resultant release of the therapeutics (Selbo et al., 2010). The idea behind PCI is to improve the delivery of drugs, providing an efficient and targeted delivery system. Tumour selectivity

and destruction is substantially improved because i) toxic compounds are packaged into delivery vesicles with targeting moieties i.e. tumour specific antibodies or peptide-conjugates, ii) the photosensitiser can also exert PDT effect and iii) localised site-directed light radiation improves the specificity of treatment (Weyergang et al., 2006).

To highlight the advantages of PCI, Weyergang *et al.* (2006) observed a highly synergistic toxic effect in EGFR-positive NuTu-19 rat epithelial ovarian cancer cell line, subjected to the PCI of the EGFR-targeting toxin, Saporin (Weyergang et al., 2006). Norum *et al.* (2017) used the photosensitiser Aluminium Phthalocyanine Chloride Disulfonic acid (AlPcS2a), to conduct *in vivo* PDT and PCI with bleomycin in CT26 murine colon carcinomas (Norum et al., 2017). Recently, Olsen *et al.* (2017) demonstrated the use of PCI to eliminate MA11 human breast cancer cells that were resistant to PDT (Olsen et al., 2017). The potential advantages of PCI in pre-clinical investigations, has had some success in clinical studies. A recent phase I trial evaluated the safety of Disulfonated Tetraphenyl chlorin (TPCS2a) mediated PCI with bleomycin in patients with advanced and recurrent solid malignancies. The study found TPCS2a-PCI with bleomycin to be effective in eliminating tumour tissue whilst preserving adjacent, non-malignant healthy tissue. Adverse effects such as skin photosensitivity to TPCS2a and other mild and tolerable events were observed. However, TPCS2a-PCI was overall deemed to be safe and tolerable (Sultan et al., 2016).

In comparison to PDT, PCI can substantially enhance cell killing because the intravesicular therapeutic can continue to cause cell death, after the

phototoxicity of the photosensitiser has ceased. Additionally, the high tumour to normal tissue specificity of targeted vesicles means low doses of light and drugs can be used, thereby improving the therapeutic index (Selbo et al., 2010). PCI offers potential as an alternative therapy for solid cancers, but much work needs to be done to optimise the photosensitisers and therapeutic agents used.

1.2.2.5 Current clinical state of PDT in colorectal cancers

PDT is a safe method of treatment and is successfully being applied to treat many types of cancers. In colorectal cancers (CRC), the first reported study evaluating PDT as a treatment modality was published in 1986. In this pilot study, a group of 14 patients with post-surgical residual, unresectable or recurrent CRC were treated with HpD and Photofrin and an argon-pumped dye laser. Half of the patients (50%, 3/6) with unresectable tumour recurrences, and 40% (2/5) with incomplete resection experienced a significant relief in pain following PDT. In one patient, histological analysis confirmed the complete elimination of disease following several sessions of PDT. In another two patients, PDT was used adjuvantly after surgical resection and was found to be safe and tolerable (Herrera-Ornelas et al., 1986). This study was the first to show PDT as an effective anti-cancer technique, that can be used repeatedly and be applied to prevent and manage unresectable and recurrent CRC. Following the study in 1986, additional pilot and phase I/II studies were conducted to evaluate HpD and Photofrin mediated PDT in colonic, rectal and gastrointestinal cancers. PDT was evaluated as an adjuvant intraoperative procedure and also as an alternative to surgery in inoperable cases (Krasner, 1989; Patrice et al., 1990; Barr et al., 1990; Kashtan et al., 1991; Allardice et al., 1994; Harlow et al., 1995). These studies also found PDT to be an effective

method in eradicating small tumours and treating minimal residual disease. However, the early use of PDT in colorectal cancer was limited by the use of Photofrin as the photosensitiser, with many patients experiencing prolonged mild to severe skin photosensitivity. The low tumour-to-normal tissue uptake and retention of the photosensitiser also meant that its therapeutic index in CRC was narrow (Hahn et al., 2006). New photosensitisers are therefore needed for application in CRC (Kawczyk-Krupka, Bugaj, Latos, Zaremba, et al., 2015).

5-ALA/PpIX has been investigated in multiple clinical studies of PDT in CRC. Collectively, the findings show that 5-ALA/PpIX mediated PDT is a simple and relatively non-invasive method of treatment, with no serious side effects. Moreover, PDT could be repeated multiple times to treat advanced disease (Fromm et al., 1996; Hamdan et al., 2003; Kawczyk-Krupka, Bugaj, Latos, Zaremba, et al., 2015). Mlkvy *et al.* (1995) reported a study in which patients with inoperable duodenal or colonic polyps were subjected to either 5-ALA/PpIX or Photofrin mediated PDT. All patients healed safely with no major complications. It was founded that Photofrin tended to have a better effect, inducing deep penetrative tissue necrosis as compared to the superficial necrosis observed with 5-ALA/PpIX. However, patients treated with Photofrin experienced cutaneous photosensitivity for up to 3 months post-treatment, whereas 5-ALA/PpIX had cleared by 2 days (Mlkvy et al., 1995). Mlkvy and colleagues then evaluated Photofrin, 5-ALA/PpIX and a chlorin-based photosensitier Foscan (mTHPC, Temoporfin) in patients with gastrointestinal cancers as an alternative to surgery. Similar to the previous study, Photofrin was found to be the most effective in causing necrosis and superficial necrosis was observed with 5-ALA/PpIX. Foscan treated tumours showed a 60-80%

reduction in size depending on the drug-light interval. Although Photofrin and Foscan were found to be most effective, cutaneous photosensitivity lasted on average 12 weeks and 5 weeks respectively (MÍkvy et al., 1998).

Recently, additional clinical studies have evaluated PDT using second generation photosensitisers in CRC. Lustig *et al.* (2003) evaluated intratumoural light administration in patients treated with the chlorin-based photosensitiser, Talaporfin sodium. The light source used was a safe, non-laser based device. No cutaneous photosensitivity was observed and the overall tumour response rate was found to be 33% (Lustig et al., 2003). Van Duijnhoven *et al.* (2005) evaluated interstitial PDT in patients with non-resectable liver metastases of CRC origin using the bacteriochlorin photosensitiser, mTHPBC. No serious complications were observed and patients only experienced mild skin photosensitivity after an excessive amount of light exposure. Tumour necrosis was observed at 1 month after PDT in all treated lesions (van Duijnhoven et al., 2005).

To date, the many pilot and phase I/II clinical studies that have evaluated PDT as a method of treatment in CRC, have identified it to be a safe and precise technique, due to the selective accumulation and targeted activation of photosensitisers. Adverse phototoxicity is manageable with the newer generation photosensitisers. In comparison to chemotherapy, PDT is well tolerated and can be repeated without a risk of complications or adverse events. The versatility of PDT means that it can potentially be used as an alternative to other methods to treat CRC, or in combination as a multi-modality regimen. With respect to the application of PDT in CRC, much of the clinical evidence as

described above is proof of principle, conducted in small scale pilot studies. Additional phase I/II studies are needed to establish the optimal doses of the ideal photosensitiser and light. This can eventually lead on to a decisive large scale, multicentered, controlled study that will inform the wider clinical community on thoroughly developed and specific uses of PDT protocols in CRC (Kawczyk-Krupka, Bugaj, Latos, Zaremba, et al., 2015).

1.2.2.6 Current pre-clinical state of PDT in colorectal cancers

1.2.2.6.1 *In vitro* cell based studies

Before going into human clinical trials, novel anti-cancer techniques are evaluated pre-clinically in simple models of cancer. A key component in evaluating PDT in a certain type of cancer is the comparison of the different types of photosensitisers and the diverse intracellular events that occur with each photosensitiser (Kawczyk-Krupka et al., 2016). With the rising popularity of Photofrin and porphyrin derivatives in the mid to late 20th century, there were many studies which investigated Photofrin mediated PDT in CRC cell lines. The advantage of simple cell models is that they allow investigations to focus on the molecular interactions between different intracellular components and how they respond to photodynamic effects. Hanlon *et al.* (2001) investigated the effects of Photofrin mediated PDT on the molecular chaperone Heat shock protein 60 (Hsp60) in the CRC cell line, HT29. Hsp60 has been implicated in regulating apoptosis (Ghosh et al., 2008) and oxidative stress associated with PDT. An increase in Hsp60 expression was observed in cells treated with Photofrin and irradiated with light, indicating a potential protective role played by Hsp60 against PDT (Hanlon et al., 2001). In another study, Fisher *et al.* (1998) looked at the role of the tumour suppressor p53 in PDT in CRC cells. p53 plays a

crucial role in responding to cellular stress by promoting intracellular signalling to induce cell cycle arrest, senescence and apoptosis (Bieging et al., 2014). Cancers with wild-type p53 are generally more sensitive to anti-cancer treatment than cancers with mutated or deleted p53, and in this study, wild-type p53 CRC cells were found to be more sensitive to Photofrin-mediated PDT than mutant p53 cells, despite the amount of photosensitiser being taken up by the two different types of cells being equivalent (Fisher et al., 1998). Zawacka-Pankau *et al.* (2007) found that PpIX is able to bind to p53 and disrupt the interaction between p53 and its negative regulator, HDM2, in the wild-type p53 HCT116 CRC cell line, leading to the upregulation of p53 targeted pro-apoptotic genes. However, PpIX mediated PDT in p53-null HCT116 cells also resulted in growth suppression, albeit p53-positive cells were more sensitive to PDT (Zawacka-Pankau et al., 2007). Interestingly, another study found that PpIX mediated photodynamic therapy induced apoptosis in p53-null HCT116 cells through binding of PpIX to another member of the p53 family, p73, in a similar fashion (Sznarkowska et al., 2011).

Newer and improved porphyrin-based photosensitisers were investigated in HCT116 cells and were found to be more effective than Photofrin (Banfi et al., 2004). A follow-up study found that similar porphyrin derivatives were also more effective than the chlorin photosensitiser, Foscan in HCT116 cells (Gariboldi et al., 2009).

Similar to Photofrin, the cellular localisation of 5-ALA converted PpIX initially occurs at the plasma membrane, followed by redistribution to the nuclear membrane, endoplasmic reticulum and the mitochondria, as well as other

organelles (Wilson et al., 1997). To highlight the importance of intracellular localisation of porphyrin photosensitisers, Gederaas *et al.* (1999) observed substantial damage to mitochondrial function in WiDr CRC cells subjected to 5-ALA/PpIX mediated PDT, leading to irreversible cell death (Gederaas et al., 1999). As mentioned previously, the conversion of exogenously administered 5-ALA to PpIX occurs in metabolically active cells via the heme biosynthesis pathway. This means that the success of 5-ALA/PpIX mediated PDT is dependent on the production of intracellular PpIX. Krieg *et al.* (2002) investigated the uptake and kinetics of 5-ALA metabolism in HT29, Caco2 and SW480 CRC cell lines. Porphobilinogen deaminase (PBGD) and ferrochelatase (FC) are enzymes, which are involved in the heme biosynthesis pathway and mediate the production of PpIX and conversion of PpIX into heme respectively (Franken et al., 2011). The study found differential enzymatic expression and activity between the different cell lines, resulting in varied levels of PpIX production. This suggests that analysis of PBGD and FC levels in CRC may be of use in determining response to 5-ALA/PpIX mediated PDT (Krieg et al., 2002).

An explanation for the prolonged photosensitivity seen with Photofrin, as compared to 5-ALA/PpIX, is due to the clearance rate of the different photosensitisers. FC converts intracellular PpIX into heme and iron is a co-factor used by FC in the process. Juzeniene *et al.* (2009) found that along with the concentration and incubation times of 5-ALA administered to WiDr cells, temperature and pH (factors which affect FC enzymatic activity) and the intracellular content of iron also influenced the rate at which PpIX is converted into non-photosensitive heme (Juzeniene et al., 2009). As described in *1.3.2.4,*

the phototoxic effects of 5-ALA/PpIX appear to be limited to superficial necrosis with poor penetration of the deeper tissues. Brunner *et al.* (2001) investigated the pharmacokinetics of 5-ALA. Due to the low lipophilicity of 5-ALA, it has poor binding affinity to lipoproteins and poor penetration across cell membranes. The study looked at the uptake and PpIX production levels of 5-ALA and 5-ALA esters (modified 5-ALA) in HT29, Caco2 and SW480 cell lines. The results showed that the uptake of 5-ALA esters into cells was markedly improved as compared to 5-ALA, achieving significantly higher levels of PpIX in CRC cells. Equivalent amounts of PpIX was observed in cells treated with lower doses of 5-ALA esters, as compared to the higher dosed 5-ALA (Brunner et al., 2001). Kawczyk-Krupka et al. (2015b) studied the effects of 5-ALA/PpIX mediated PDT on the secretion of cytokines, including the Macrophage Migration Inhibitory Factor (MIF). Hypoxia Inducible factor 1α (HIF1α) is stabilised under low oxygen and hypoxic conditions and promotes the upregulation of MIF, which has been shown to promote cell proliferation, migration and angiogenesis (Winner et al., 2007). The study found that MIF increased in both SW480 and SW620 cell lines following 5-ALA/PpIX mediated PDT, potentially indicating a protective role played by MIF in promoting cell survival in low oxygen conditions typically found following PDT (Kawczyk-Krupka, Bugaj, Latos, Wawrzyniec, et al., 2015).

The European approved chlorin photosensitiser, Foscan, was evaluated in Colo 201 CRC cells. Foscan mediated PDT was found to be effective in exhibiting drug- and light-dependent apoptosis. Unlike the porphyrin based photosensitisers, Foscan was found to localise in lysosomes rather than the mitochondria in Colo 201 cells. This demonstrates that, in addition to cell-type specific mechanisms, the type of photosensitiser used also influences the action

of PDT mediated cell death (Leung et al., 2002). Mitochondrial localising photosensitisers, such as the porphyrins, can cause rapid damage to the mitochondrial membrane, resulting in the release of cytochrome c and subsequent apoptosis (Cai et al., 1998). However, chlorin photosensitisers that localise to lysosomes, can induce apoptosis through photodamage to lysosomes with release of lysosomal proteases and cathepsins and subsequent mitochondrial destabilisation, release of cytochrome c and activation of pro-apoptotic factors and caspases (Stoka et al., 2006). This was also highlighted by Mitsunaga *et al.* (2007), who identified an apoptotic cell death induced in HCT116 cells subjected to PDT using the chlorin photosensitiser, ATX-S10Na (II) (Mitsunaga et al., 2007).

DNA mismatch repair mechanisms (MMR) are responsible for eliminating and amending DNA base pair mismatches and genetic mutations which may occur during DNA synthesis. Loss of MMR function can lead to genetic instability, potentially resulting in the unregulated growth of cells and tissue. Furthermore, cancers that are deficient in MMR mechanism are known to be resistant to anti-cancer treatments (Peltomäki, 2001). Schwarz *et al.* (2002) found Foscan mediated PDT to be effective in both MMR proficient and deficient HCT116 cells, suggesting PDT as a strategy for bypassing resistance in MMR deficient cancers (Schwarz et al., 2002).

Sharma *et al.* (2005) investigated the effect of extracellular pH on PDT in Colo 205 CRC cells. Cells were treated with the chlorin photosensitiser, chlorin p6, and subjected to light irradiation. The study found that an extracellular pH of 7.4 resulted in apoptotic cell death as suggested by the condensation of chromatin,

partial reduction in mitochondrial membrane potential and an increase in activity of the pro-apoptotic enzyme, caspase-3. In contrast, a slightly acidic extracellular pH of 6.5 resulted in a necrotic mode of death, as suggested by the total loss of mitochondrial membrane potential and increased damage to the plasma membrane. The fine balance in the homeostatic regulation of H^+ ions is an important factor in regulating cell survival and also plays a role in the progression of cancers and may determine the mode of cell death during PDT (Sharma et al., 2005; Swietach et al., 2014).

Similar to the chlorin photosensitisers, bacteriochlorin photosensitisers such as pheophorbide-a have also shown been shown to be effective PDT agents when assessed *in vitro* in HT29 cells (Xu et al., 2010). Matroule *et al.* (1999) highlighted that inducing PDT using a methyl ester derivative of Pyropheophorbide-a (PPME) in HCT116 cells resulted in the activation of the transcription factor Nuclear Factor-κB (NFκB). The importance of NFκB in PDT is that this redox-activated transcription factor is involved in the regulation of genes which produce vital cytokines, such as interleukins-1,2,6 and Tumour Necrosis Factor α (TNFα). The resulting effect of the transcriptional activities of NFκB is to regulate apoptosis in cells, depending on the type of cell and the stress insults inducing its activation (Matroule, Bonizzi, et al., 1999; Barkett and Gilmore, 1999). The authors used another pheophorbide-a derived photosensitiser and found this compound to localise predominantly in the lysosomes, and not the mitochondria, and also induced apoptosis in HCT116 cells through an NFκB pathway (Matroule, Hellin, et al., 1999).

Similar to porphyrins and chlorins, the silicon (IV) phthalocyanines are another class of second-generation photosensitsers that have recently gained attention as effective mediators of PDT, specifically in CRC cell lines (Lo et al., 2007). The silicon phthalocyanine photosensitiser, Pc4, is well-known in eliciting an intrinsic apoptotic response in cells treated with PDT (Miller et al., 2007). To evaluate the role of the apoptosis modulating factor, Bax, Chiu *et al.* (2005) subjected Bax proficient and knockout HCT116 cells to Pc4 mediated PDT. As expected, in Bax proficient cells, PDT induced the activation of Bax and release of cytochrome c from the mitochondria leading to an intrinsic apoptotic response. However, in Bax deficient cells, a slower apoptotic response was observed, characterised by the activation of caspases and DNA and chromatin degradation. Although the release of cytochrome c was not observed in Bax deficient cells, both cell types underwent apoptosis showing a Bax independent role in Pc4 mediated apoptosis (Chiu et al., 2005). Other studies have investigated the intracellular localisation and its effect on cell death using phthalocyanine photosensitisers in DLD1 and Caco2 CRC cells. These studies found the photosensitisers to localise to lysosomes and the mitochondria, in a similar fashion to porphyrin and chlorin photosensitisers. Activation of the photosensitiser resulted in the release of cathepsins from lysosomes and cytochrome c from the mitochondria, leading to apoptosis (Manoto et al., 2012; Sekhejane et al., 2014).

As described in *1.2.2.2*, ICG has been used for intraoperative fluorescence visualisation of cancers. However, ICG also possess phototoxic properties and was investigated by Bäumler *et al.* (1999) in HT29 cells. ICG mediated PDT was exhibited in HT29 cells and showed promise as an effective mediator of

PDT (Bäumler et al., 1999). However, it appears that ICG was superseded by Photofrin as the preferred photosensitiser in the early 1990's and so its efficacy as a PDT agent in clinical trials has never been tested.

1.2.2.6.2 *In vitro* Targeted PDT in CRC cells

The lipophilic and hydrophobic nature of photosensitisers means that they are naturally selective for cancer cells, where they can localise to organelles and are intracellularly retained (Allison et al., 1994). However, photosensitisers can also accumulate in healthy tissues, resulting in adverse phototoxicity. To address this, targeted therapy techniques have been developed to improve the delivery of photosensitisers to cancers, whilst simultaneously increasing the specificity of PDT (Kawczyk-Krupka et al., 2016). These targeted photosensitisers are termed "third generation" photosensitisers. Second generation photosensitisers were developed to address the issues of first generation photosensitisers such as Photofrin i.e. phototoxicity and delayed clearance. Third generation targeted photosensitisers attempt to improve the specificity in delivering existing photosensitisers to cancers (Z. Huang et al., 2008; I. Yoon et al., 2013).

Nanoparticles (NPs) are increasingly being investigated as drug delivery vehicles to improve the delivery of chemotherapeutics to tumours without affecting normal tissue. NPs are designed to release drugs at the tumour site, by exploiting the physical interaction between the NP and cancer cells. NPs are an ideal delivery system because they are biodegradable, non-immunogenic, easy to manufacture and can deliver large payloads to targeted sites (Yu et al., 2016). To this effect, Hu *et al.* (2009) showed significant uptake of NP

encapsulated porphyrins via clathrin-mediated endocytosis in SW480 cells, as compared to free porphyrins. Due to the rapid and improved uptake of NP encapsulated porphyrins, a higher phototoxic effect was observed in treated cells (Hu et al., 2009). Similarly, Simon *et al.* 2010 showed that silica NP encapsulated PpIX had increased accumulation in HCT116 cells as compared to free PpIX. They also found a stronger generation of ROS in NP treated cells, suggesting an improved photodynamic effect (Simon et al., 2010).

Liposomes are another form of drug delivery system that have been used to improve the delivery of anti-cancer drugs. Liposomes consist of a phospholipid bilayer membrane, meaning they can easily fuse with the plasma membrane of cells to deliver their payload (Slingerland et al., 2012). Fospeg, a liposomal formulation of the chlorin photosensitiser Foscan, has been investigated in HT29 cells. The study found Fospeg mediated PDT to trigger apoptotic cell death in a drug and light dose-dependent manner (Wu et al., 2015). However, a direct comparison in cellular uptake and cell viability post-PDT between Fospeg and Foscan was not conducted. Another study looked at the use of oligonucleotide aptamers to improve the delivery of NPe6 to HT29 cells. The aptamers used were designed to target short glycan-peptide molecules on the surfaces of cancer cells, which are not present on normal epithelial cells. The study found a >500-fold increase in toxicity in cells treated with the aptamer-conjugated NPe6 compared to free NPe6 and subjected to light irradiation (Ferreira et al., 2009). The direct conjugation of a photosensitiser to targeting antibody fragments has also been shown to be better than free photosensitisers, allowing a lower dosage of the PS agent to be used (Bhatti et al., 2008).

1.2.2.6.3 *In vivo* animal studies

Animal studies are essential in bridging the translational gap between *in vitro* studies and clinical application (Denayer et al., 2014). With respect to PDT, animal- studies have been used to evaluate the *in vivo* mechanism, efficacy and safety of PDT in complex organisms (Kawczyk-Krupka et al., 2016).

Similar to *in vitro* cell based studies, the earliest pre-clinical *in vivo* studies that evaluated PDT in animal models of CRC utilised Photofrin as the photosensitiser (Lantz et al., 1992). As expected, Porphyrin derived photosensitisers were effective in mediating PDT producing extensive tumour necrosis (Bugaj et al., 2007). The effect of adjuvant intraoperative PDT was also evaluated very early in animal models. Abulafi *et al.* (1997) found that the local recurrence rate of colonic tumours in Balb/c mice subjected to combined surgery and Photofrin or Foscan mediated intraoperative PDT was substantially lower (~70%) as compared to control groups, signifying the added benefit of intraoperative PDT (Abulafi et al., 1997).

As described earlier, 5-ALA/PpIX is an attractive photosensitiser mainly due to its rapid clearance from the body, resulting in a shorter period of adverse phototoxicity. However, in comparison to Photofrin or Foscan, 5-ALA/PpIX is not as effective in inducing deeply penetrative necrosis. To explore this further, Messmann *et al.* (1995) found that 5-ALA/PpIX mediated PDT-induced necrosis did not improve by increasing the dose of 5-ALA or light above a certain threshold. However, they did identify an increase in the area of necrosis when animals were subjected to fractionated light treatment during laparotomy as

compared to a single continuous dose of light (Messmann et al., 1995). On the other hand, Webber *et al.* (2005) found that fractionated administration of the photosensitiser, NPe6, was more effective at promoting photodamage to subcutaneously implanted CRC cells, as compared to a single dose of NPe6. This was attributed to the rapid clearance of NPe6 *in vivo*. Unlike Photofrin and 5-ALA, the rapid clearance rate of NPe6 is beneficial to reduce periods of adverse photosensitivity, but it results in a narrower time-frame for optimal accumulation of the photosensitiser in cancers (Webber et al., 2005). Other studies have evaluated novel chlorin based photosensitisers in mice with CRC and gastric cancer cell line xenografts, and found them to be effective mediators of PDT *in vivo* as illustrated by significant suppression in xenograft growth (Lim et al., 2009; Tanaka et al., 2011).

As part of the transition from first to second generation photosensitisers, many studies evaluated the *in vivo* efficacy of Photofrin in comparison to newer photosensitisers in CRC xenografts. Vonarx-Coinsmann *et al.* (1994) compared Photofrin and Foscan mediated PDT in HT29 xenografts in mice. Foscan treated mice were irradiated with 650nm light and Photofrin treated mice with 630nm light. Foscan was found to be more effective than Photofrin due, in part, to the better light penetration at 650nm and also the ability of Foscan to produce a higher quantum yield (Vonarx-Coinsmann et al., 1994). Orenstein *et al.* (1996) compared NPe6, 5-ALA/PpIX and Photofrin mediated PDT in mice bearing colon carcinomas and observed differences in distribution and tissue damage between the different agents, indicating that the selection of a specific photosensitiser is vital for a desired anti-cancer effect (Orenstein et al., 1996). Hajri *et al.* (2002) found that Photofrin was preferentially taken up and retained

by tumours cells as compared to the bacteriochlorin pheophorbide-a, which cleared out rapidly from HT29 tumour-bearing mice. This is in contrary to their *in vitro* results, which showed a higher uptake of pheophorbide-a in HT29 cells, and highlights the difference in uptake and retention of photosensitisers depending on the type of tumour model being used (Hajri et al., 2002).

Studies have also evaluated the phthalocyanine photosensitisers, Pc4 and AlSPc, in animal models of CRC and found them to be effective in inducing changes to tumour vasculature and tumour regression through apoptosis and necrosis. The photosensitisers were retained in tumours for longer than normal tissue, limiting the phototoxic damage to healthy tissue (Tralau et al., 1987; Barr et al., 1987; Whitacre et al., 2000).

Many patients with CRC will develop either synchronous or metachronous liver metastases (Misiakos et al., 2011). Rovers *et al.* (1999) implanted colon carcinomas into the livers of mice and found Foscan mediated PDT to be effective in inducing complete tumour remission, with mild and transient damage to normal tissue. Tissue kinetics showed a rapid clearance of Foscan from hepatic tissue, with prolonged retention in tumours (Rovers et al., 1999).

In concordance with *in vitro* investigations, drug-delivery targeted photosensitiser mediated PDT was found to be more effective than free photosensitisers, with improved tumour uptake, retention and PDT mediated tumour regression *in vivo*. This includes NP encapsulated porphyrins in SW480 xenografts (Hu et al., 2009), silica NP encapsulated PpIX in HCT116 xenografts (Simon et al., 2010) and anti-carcinoembryonic antigen (CEA) antibody

conjugated AlPcS$_4$ in human colonic carcinoma xenografts (Carcenac et al., 1999).

Pre-clinical investigation of the different classes of photosensitisers has sought to improve our understanding of their effects and the intracellular changes induced upon light irradiation. Many *in vitro* investigations focus on simple experimental endpoints i.e. cell viability, intracellular pharmacokinetics and the effects of PDT on protein/gene expression. Animal models are then used to investigate PDT in complex organisms, taking into consideration the effects of tumour vascularisation, tissue oxygenation and other physiological factors that influence PDT efficacy. However, a prevailing disadvantage of pre-clinical investigations is the risk of over extrapolating results and making clinical predictions based on the results from animal studies that cannot always be replicated in a clinical setting (Kawczyk-Krupka et al., 2016). Accepting this, the various photosensitisers and PDT protocols used in CRC have collectively shown PDT to be an effective and beneficial method of treatment. The identification of the optimal photosensitiser for PDT in CRC is still ongoing, but will probably involve a "third generation" photosensitiser that offers targeted delivery with improved specificity and enhanced efficacy.

1.2.3 Intracellular mechanisms of PDT

The type of cell death observed in PDT is dependent on the concentration of photosensitiser, dose of light administered, type of tumour and intracellular localisation of photosensitiser (Kubin et al., 2005). It was previously thought that necrosis was the primary mode of cell death in PDT. However, studies have shown that the activation of a photosensitiser and production of ROS are

usually the first step in a cascade of events resulting in cell death (Castano et al., 2006; Karioti and Bilia, 2010). The production of ROS will generally promote changes in the mitochondria and subsequent release of cytochrome c, which in turn, induces the activation of downstream caspases and apoptosis (Panzarini et al., 2009). The initiation of apoptosis can be both caspase-dependant and -independent and is influenced by the intracellular environment and interplay between pro- and anti-apoptotic factors (Panzarini et al., 2011). The induction of autophagy following PDT has also been reported, as a mechanism to remove oxidatively damaged organelles and aggregated proteins produced by photochemical reactions. However, the role of autophagy remains unclear in whether it protects cells from further destruction or terminally commits them to cell death (Panzarini et al., 2011; Dewaele et al., 2011).

1.2.4 The role of ABCG2 in PDT

The ATP-binding cassette (ABC) superfamily G member 2 (ABCG2) transporter, also known as the breast cancer resistance protein (BCRP), is predominantly located in the cell membrane. The primary role of ABCG2 is to actively pump out endogenous metabolites, xenobiotics and toxins from cells or into intracellular compartments such as the endoplasmic reticulum for elimination (Mo and Zhang, 2012; Westover and Li, 2015). In cancer research, ABCG2 has long been identified as one of the major contributors to multidrug resistance and treatment failure. Chemotherapeutic compounds such as doxorubicin, methotrexate, mitoxantrone and topotecan have been identified as substrates of ABCG2 activity (Stacy et al., 2013). Clinically, high ABCG2 expression correlates with poor prognosis in acute myeloid leukaemia patients, as indicated by poor complete response, disease-free survival and overall

survival (Benderra et al., 2005). Additionally, key genetic alterations such as the R482G 'gain-of-function' mutation have been identified in increasing drug efflux activity (Honjo et al., 2001; Morisaki et al., 2005; Clark et al., 2006; Westover and Li, 2015; Khunweeraphong et al., 2017).

The role of ABCG2 in conferring chemoresistance has been well-documented and also extends to PDT. ABCG2 has been shown to influence the intracellular uptake and retention of photosensitisers and affect photosensitiser-mediated fluorescence and PDT in cells. (Jonker et al., 2002; Palasuberniam et al., 2015; J.H. Kim et al., 2015; Abdel Gaber et al., 2018; Baglo et al., 2019; Kurokawa et al., 2019). Blocking ABCG2 through the use of small molecule inhibitors such as Ko143 and Fumitremorgin C, has shown to improve the retention of photosensitisers and enhance PDT. Many studies have been conducted to investigate the interplay between ABCG2, the pharmacokinetics of various photosensitisers and the effect they have on the efficiency of PDT. Compared to other well-documented multidrug resistant proteins such as P-glycoprotein and Multidrug resistance-associated protein 1, ABCG2 has been found to have the largest impact on influencing the accumulation of photosensitisers and impeding PDT (Robey et al., 2005).

In addition to the elimination of photosensitisers from cells, ABCG2 has also been shown to play an anti-oxidative role by interfering with the generation of ROS and decreasing the expression of inflammatory factors associated with oxidative stress. In PDT, the production of ROS is crucial to effectively induce cytotoxicity (Figure 1.1), and blocking ABCG2 activity has been reported to

increase the production of singlet oxygen and superoxides (Shen et al., 2010; Poleshko and Volotovski, 2016).

1.3 HYPERICIN

1.3.1 Background to Hypericin

St. John's wort *(Hypericum perforatum)* is a herbaceous plant, which is best known for possessing sedative properties. Extracts of St. John's wort has classically been used to treat various illnesses and disorders, and is still being used in modern times to treat mild-to-moderate depression, anxiety and seasonal affective disorder (Wheatley, 1999; Barnes et al., 2001). St. John's wort is made up of various chemical constituents, with the predominant compound being the anthraquinone derivative, Hypericin (Figure 1.2) (Barnes et al., 2001). Hypericin and its other proto-forms are found as dark-coloured granules in the glands, stem, leaves, petals and stamens of the plant (Agostinis et al., 2002; Crockett and Robson, 2011). Hypericin has received interest for its uses in anti-depressive, anti-microbial, anti-viral, anti-tumoural and photodynamic activities.
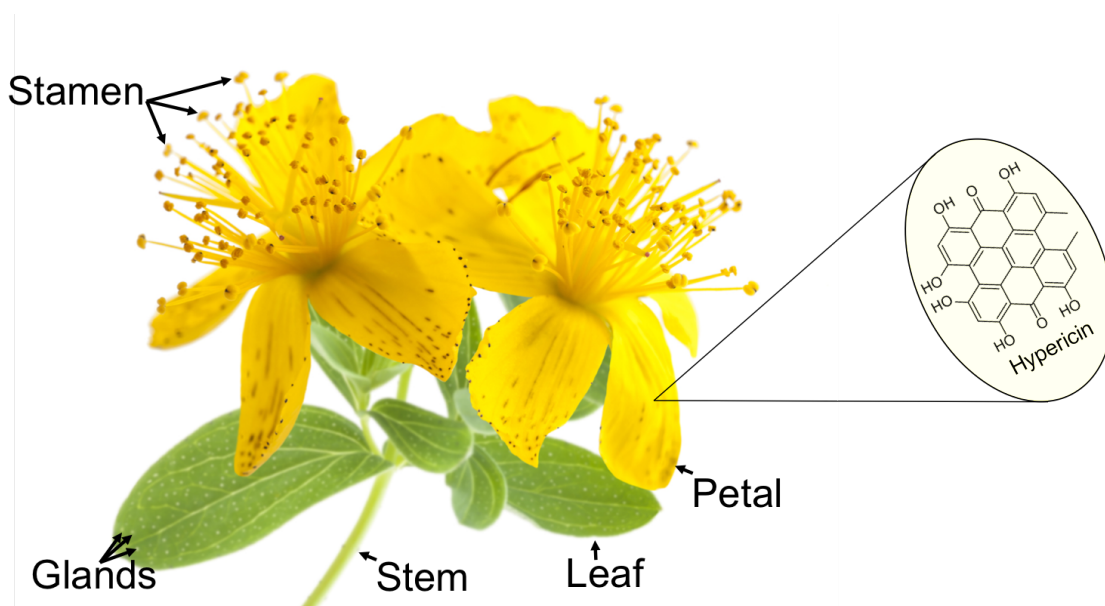
Figure 1.2 - St. John's Wort (Hypericum Perforatum)

Hypericin is a naturally occurring photosensitiser and is the main chemical constituent of the *Hypericum* genus.

1.3.2 Hypericin and PDT

Unlike the other well-established classes of photosensitisers (porphyrins and chlorins), which have been extensively studied over the past few decades, Hypericin is a naturally occurring photoactive compound (Nakajima and Kawashima, 2012). It exhibits light dependant toxicity, produces a substantial quantum yield, intense light absorption and excitation in the visible light region, low photo-bleaching, resulting in potent photosensitising properties and bright fluorescence (Kubin et al., 2005; Maduray and Davids, 2011; Ritz et al., 2012; Xu et al., 2015; Zheng et al., 2016). Similar to other photosensitisers, Hypericin is a potent lipophilic compound, which is advantageous for its uptake and retention in cancer cells. Due to the high demand for cholesterol in cancer cells, they have an increased expression of lipoprotein receptors as compared to normal cells (Damiano et al., 2013). The increased endocytic activity results in the preferential uptake of photosensitisers into tumour cells. Hypericin has a

high affinity (30:1 molar ratio) for cholesterol-delivering low-density lipoproteins (LDL). The aggregation of Hypericin into LDL does not impair its ability to be recognised and taken up by LDL receptors, and once internalised into cells, lysosomal degradation of LDL results in the intracellular release of Hypericin (Polo et al., 2002; Haylett and Moore, 2002). Interestingly, Siboni *et al.* (2002) investigated the mechanisms by which LDL-bound and unbound Hypericin was taken up into cells, and found unbound Hypericin to be taken up more rapidly than LDL-bound Hypericin. This may be due to differences in hydrophilicity, allowing free Hypericin to passively diffuse into cells a lot quicker than the slower LDL-receptor mediated route (Siboni et al., 2002).

Once internalised into cells, Hypericin localises predominantly in the perinuclear region, as well as other membranous organelles, such as the endoplasmic reticulum, golgi apparatus and lysosomes (Uzdensky et al., 2001; Siboni et al., 2002). Upon light activation, cellular necrosis, apoptosis and autophagy are observed, which is dependent on the dose of Hypericin and light administered (Karioti and Bilia, 2010; Jendželovská et al., 2016).

With specific regard to Hypericin mediated PDT in CRC cell lines, a small number of studies have identified Hypericin as an effective photosensitiser. A study by Mikes *et al.* (2011) found that despite HT29 cells having a lower accumulation of Hypericin and production of ROS, as compared to normal human foetal colon epithelial cells, the normal colonic cells were more resistant to Hypericin mediated PDT. This suggests that the cell's ability to manage ROS and respond to oxidative stress, as well as the subcellular distribution of Hypericin, can affect the efficacy of PDT (Mikeš et al., 2011). The same group

also investigated the role of p53 in apoptosis in HCT116 cells treated with Hypericin mediated PDT (Mikes et al., 2009). The results showed that the lack of p53 did not significantly impact overall cell death, however a delayed activation of caspase-3 was observed in p53-null cells. They also showed that in HT29 cells with mutated p53 protein, Hypericin mediated PDT resulted in necrosis as the principal mode of death (Mikes et al., 2007). This suggests that p53 as a mechanism for inducing apoptotic killing in Hypericin mediated PDT is redundant in colon cancer cells. In the absence of the tumour suppressor p53, Hypericin mediated PDT is still an effective inducer of cell death, but by a necrosis-mediated pathway.

Sackova *et al.* (2005) evaluated the differences in response to Hypericin treatment in HT29 cells followed by a single or unequally fractionated dose of light. Cells treated with an unequally fractionated dose of light *(1J/cm^2 followed by 6 hours in dark followed by 11J/cm^2)* were more resistant to treatment as compared to those given a single continuous dose of light *(12J/cm^2)*. The rationale behind this study was to highlight the importance of dark intervals between light treatments in fractionated light delivery. Other studies have found fractionated light delivery to be more effective as it allows the re-oxygenation of tissue between periods of light treatment (Xiao et al., 2007; De Bruijn et al., 2016). However, an extended dark interval, as used in the above study, could downplay the effect of PDT and instead allow the cells to acquire resistance to PDT during another round of light treatment (Sacková et al., 2005). A follow-up study found that HT29 cells subjected to fractionated light with Hypericin mediated PDT, had suppressed plasma membrane externalisation of the apoptotic signaling factor phosphatidylserine, decreased levels of intracellular

ROS and Hypericin and differential expression profile of various cytokines. This resulted in an overall better cell survival (Fadok et al., 1998; Kuliková et al., 2010).

With respect to Hypericin related *in vivo* studies, Blank *et al.* (2002) investigated the toxicity of Hypericin mediated PDT in murine colon carcinoma models. Hypericin mediated PDT induced tumour necrosis and caused extensive damage to the tumour vasculature. Compared to other photosensitisers, the wavelength of maximum light absorption with Hypericin is shorter (590nm), however this does not hinder its ability to be used as an effective mediator of PDT (Blank et al., 2002).

One of the primary objectives of the research described in this thesis, is to evaluate Hypericin as a potential photosensitiser for PDT in CRC. Unlike other well established photosensitisers, such as the second-generation porphyrin and chlorin based photosensitisers, Hypericin has not been intensively investigated and its role in photodiagnosis and PDT still remains unclear. The above studies which have thus far attempted to elucidate this, have shown promising results. This research aims to build upon these findings, and add to the evidence base to support the potential clinical application of Hypericin mediated PDT in treating CRC.

1.3.3 Hypericin-PDT and ABCG2

As described in *1.2.4*, ABCG2 plays an important role in influencing cellular responses to PDT. Investigating the interaction between Hypericin and ABCG2, Jendzelovsky *et al.* (2009) found Hypericin to be a preferential substrate of

ABCG2, and blocking ABCG2 activity resulted in an increased intracellular accumulation and retention of Hypericin. The authors also identified an increase in the protein expression of ABCG2 in Hypericin-treated HT29 cells, indicating a possible defence mechanism employed by cells against foreign xenobiotics (Jendzelovsky et al., 2009; Šemeláková et al., 2016). Compared to more prominent photosensitisers i.e. Photofrin, 5-ALA and Foscan. Studies investigating the relationship between Hypericin and ABCG2 have been very limited. More specifically, studies have not been reported which decisively show the synergistic effects of inhibiting ABCG2 and administering Hypericin-PDT. Therefore, a main focus of this research project, is to highlight the impact of ABCG2 in influencing Hypericin-PDT cytotoxicity.

1.4 PRE-CLINICAL MODELS OF CANCER

1.4.1 Monolayered two-dimensional cell cultures

Although the number of potential anti-cancer agents being put through clinical trials has increased over the past decade, the proportion of newly developed products that progress successfully through clinical development is very low (Breslin and O'Driscoll, 2013). Since the clinical evaluation of drugs is based upon their efficacy in pre-clinical models, it is essential that these models are reliable and as representative of the clinical scenario as possible (Stock et al., 2016). *In vitro* models of cancers are valuable tools that serve as cost effective and efficient platforms for screening anti-cancer treatments (Katt et al., 2016). Immortalised mammalian cells have become important laboratory models for the *in vitro* testing of drug activity, metabolism and toxicity (Antoni et al., 2015). Monolayered, two-dimensional (2D) cell cultures have traditionally been used for pre-clinical evaluation. 2D cell cultures offer an easy, robust and convenient

method of analyses. But, 2D cell cultures are dissimilar to *in vivo* cancers in terms of their lack of tissue-specific architecture, gene and protein expression, cellular heterogeneity and response to treatment (Fang and Eglen, 2017). Monolayer cultures are grown by allowing cells to adhere to an artificial substrate, where they are in contact with adjacent cells in a two-dimensional plane. Due to the lack of oxygen, nutrient and waste gradients, the environment in a 2D cell culture is not physiologically similar to the *in vivo* situation (Antoni et al., 2015). This disparity makes the extrapolation of laboratory results to the clinic challenging. The failure of many anti-cancer clinical trials, which have relied on positive pre-clinical results, questions the reliability of conventional cell cultures for evaluating novel treatments.

1.4.2 Animal models

Animal models provide a more complete pre-clinical *in vivo* system for translational research. The additional physiological and anatomical elements, such as the structure of organs and tumours, stromal vasculature and immune system, make them ideal models for understanding human diseases and evaluating treatment. Animal models are used to establish proof of concept for evaluating the efficacy and toxicology of novel therapeutics before transitioning into clinical trials in humans (Cekanova and Rathore, 2014; Salahudeen and Kuo, 2015). However, a major drawback in using animal models is the extensive resource consumption in both time and financial costs (Mak et al., 2014). Furthermore, animal studies are expensive and require stringent ethical considerations. The 3R's ('Reduction', 'Refinement' and 'Replacement') initiative aims to address the limitations associated with using animals in research. 'Replacement' describes the identification and use of alternatives to

animal models, such as sophisticated *in vitro* and computational models. The ultimate aim is to maintain or improve the quality of research, whilst progressively reducing the reliance on animal-based experiments (Balls, 2002; Doke and Dhawale, 2015). However, in the UK alone, the total number of animal-based experimental procedures increased by 23% between 2007 and 2016 (Home Office, 2018). This indicates the use of animal models as compensation for the poor and inadequate state of pre-clinical *in vitro* models, especially in cancer research. There is a need for improved pre-clinical models that build upon simple monolayered cell cultures and provide a better representation to the *in vivo* situation.

1.4.3 Three-dimensional multicellular tumour spheroidal cell models

Cellular aggregations resulting in three-dimensional (3D) multicellular tumour spheroids (MCTS) are emerging as more effective tools for biomedical research as they more closely simulate *in vivo* cancers (Figure 1.3) (Chen et al., 2015). Unlike 2D cell cultures, MCTS are better able to replicate the tissue architecture, cell to cell and cell to extracellular matrix (ECM) interactions of *in vivo* cancers (Breslin and O'Driscoll, 2013). Furthermore, the spatial arrangement of cells within a 3D structure means that concentration gradients of nutrients, oxygen, waste products, deposition of extracellular matrix and intra-spheroidal distribution of anti-cancer compounds are generated. Overall, the significance of intracellular interactions within MCTS, coupled with their ability to mimic the natural physiological environment of solid tumours, allows MCTS to utilise alternative intracellular mechanisms to promote growth, survival and resistance to treatment (Pickl and Ries, 2009).

2D Monolayer
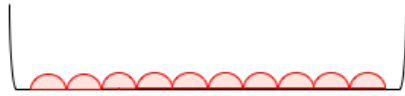
1. Cells mostly in contact with plastic

2. Minimal contact between cells

3. Uniform cell proliferation rate

4. Uniform access to O_2, nutrients and drug treatment

5. Differential gene and protein expression compared to *in vivo* cancers

6. Cells are generally sensitive to anti-cancer drugs

3D Spheroid
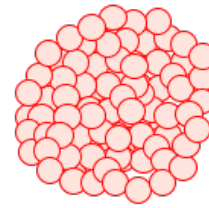
1. Cell to cell contact is dominant

2. Differential cell proliferation rates throughout spheroids

3. Gradients of access O_2/nutrients/drug penetration are created

4. Gene and protein expression is similar to *in vivo* cancers

5. Cells are generally resistant to anti-cancer drugs and often good predictors of *in vivo* responses.

Figure 1.3 – 2D Monolayer and 3D Spheroid cell models of cancer

2D monolayer and 3D spheroidal *in vitro* cell models of cancer are generated using the same cancer cell lines. However, the differences in the spatial arrangement of cells within the cultures results in the generation of two distinct cell cultures (Edmondson et al., 2014).

Compared to 2D models, cells in a 3D arrangement provide a much more effective platform for studying basic biological mechanisms. An example includes the ability to monitor the migration and invasion of cells from a tumour spheroid through the network of extracellular matrices. In pharmacological studies, 2D models are used to identify suitable anti-proliferative agents through simple drug-screening and cytotoxicity assays with the end-results providing limited information. In comparison, MCTS can be used to study the penetration and diffusion of drugs that replicates the situation *in vivo*. Spheroids can also be used to study the effect of drugs on cancer stem cells or similar tumour-initiating cells, which can be difficult to model in simple cell cultures (Mehta et al., 2012).

Additionally, MCTS can be cultured for longer periods (up to a few weeks), whereas many 2D cancer cell lines have to be passaged at least once a week. This allows the long-term analysis of cell growth and pharmacokinetic effects of anti-cancer compounds to be studied. Finally, gene expression analysis, metabolomics, proliferation and drug sensitivity assays have shown MCTS to be substantially more relevant to *in vivo* tumours as compared to their 2D monolayered counterparts (Hirschhaeuser et al., 2010; Edmondson et al., 2014; Antoni et al., 2015).

Many techniques have been established and are currently being applied for producing 3D spheroidal *in vitro* cell models of cancers. These include the culture of 3D cell cultures on non-cell adherent biomaterials, in hanging drops, in constant agitation and encapsulation into collagen gels and scaffolds. The application of the different techniques depends on the type of assay and experimental procedure being conducted. Each technique carries its own of advantages and limitations (Table 1.2) and requires optimisation for different cell lines and experience to carry out the different protocols (Ravi et al., 2015). For this research project, the different 3D cell culturing techniques will be evaluated and subsequently chosen for further experiments.

Table 1.2 – Advantages and limitations of the different 3D cell culturing techniques (Breslin and O'Driscoll, 2013; Edmondson et al., 2014; Katt et al., 2016)

3D cell culturing Method	Spheroid formation	Advantages	Limitations
Non-adherent Coating	Cells are cultured on non-cell adherent surfaces promoting cell-cell contact and formation of spheroids	Simple Inexpensive Spheroids form with minimum effort Suitable for high throughput experiments	Expensive if using specialised plates Variability in spheroid size can occur if volumes per well are not the same Coating wells is labour intensive and can often result in uneven coating
Hanging Drop	Cells are suspended in inverted droplets and spheroids form through gravity initiating cell aggregation	Inexpensive Homogenous spheroids Spheroids are easily accessible	Expensive if using specialised plates Labour intensive when manually pipetting droplets Spheroids can easily break if droplets are slightly disturbed
Agitation-based techniques	Cells in suspension, are added to a spinner or rotating vessel and kept in constant agitation, forming spheroids	Easy to culture spheroids Large scale production of spheroids is achievable Spheroids are easily accessible Constant motion of medium assists in transporting nutrients	Requires specialised equipment Quite expensive to operate Variable sizes of spheroids
Matrices and Scaffolds	Cells are embedded into matrix and in between scaffold fibers and cultured to form spheroids.	3D structures are externally supported	Difficult to access spheroids in matrix irregular spheroid sizes No control over the spatial distribution of spheroids

1.4.3.1 3D cell culturing techniques

1.4.3.1.1 Non-adherent method

The non-cell adherent method also known as the liquid overlay method is one of the common and frequently applied techniques for producing multicellular spheroids. Non-cell adherence is achieved by coating cell culturing plates, with a substrate that prevents cells from adhering to the plastic cell culturing surface, resulting in more prominent cell-cell interactions. The advantage of this method is that it can be used to consistently produce uniform shaped and sized spheroids in conventional 96-well plates, which is optimal for high-throughput applications, such as the screening of anti-cancer compounds (Costa et al., 2014; Costa et al., 2018). Aside from preparing tissue-culturing plates 'in house' with non-cell adherent surfaces, commercially prepared plates are available from manufacturers e.g. Corning® Costar® Ultra-Low Attachment Multiple Well Plates, that eliminate the need for preparing plates 'in house'.

1.4.3.1.2 Hanging Drop method

The hanging drop method is another well-established technique, for generating 3D spheroids. In comparison to the other 3D cell culturing techniques, the hanging drop method does not require specialist equipment, specific 3D cell culturing matrigels and synthetic material or preparation of cell culturing plates before the introduction of cells (Kelm et al., 2003; Foty, 2011). Simply, cells in suspension are deposited in droplets onto the surface of a cell culturing plate or dish. The plate/dish is then inverted and cells aggregate at the liquid-air interface, at the base of the droplet. Aside from gravity, no other forces are required in the formation of 3D spheroids. Similar to the non-cell adherent

method, the sizes of spheroids can be controlled by adjusting cell seeding densities and the volume of droplets.

1.4.3.1.3 Agitation-based techniques

The idea behind agitation-based techniques, is that cells in suspension are kept in constant motion in a culturing flask. The agitation-based techniques for producing 3D spheroids, can be divided into two different methods (Breslin and O'Driscoll, 2013). The first of the two agitation-based techniques is the spinner flask method. Cells in suspension are gently stirred continuously in a flask, preventing them from settling down, adhering to the sides and instead forming cell-cell interactions leading to cell aggregates and subsequent 3D spheroids. The advantage of using spinner flasks over the other methods for producing 3D spheroids, is that large numbers of spheroids can be produced in a single flask with relative ease. Spheroid cultures can be cultured for long periods of time, providing they are kept in constant agitation and cell media is replenished regularly. The constant movement of fluid can aid in the transport of nutrients and waste products to and away from spheroids respectively (Kim, 2005). This is unlike the non-cell adherent method, whereby spheroids are cultured individually (one spheroid per well in a 96-well plate), in a static environment and are best suited for high-throughput screening applications (Ho et al., 2012). Spheroids in spinner flasks are cultured collectively, and are extracted from flasks as required and re-plated to perform experiments. The ability to culture spheroids in spinner flasks for weeks at a time means that you can easily achieve the desired sizes of spheroids for experiments.

The second agitation-based technique is the rotating flask method. Unlike the spinner flask method, whereby cells in suspension are kept in motion through stirring rods in the flask. Cells in suspension in this method, are kept in constant motion by keeping the culturing flask itself in constant gyratory rotation on a horizontal axis (Kim, 2005).

1.4.3.1.4 Matrices and scaffolds

Another method for producing 3D spheroidal cell structures, is through the use of extracellular matrices and supporting scaffolds. Cell matrices and matrigels are gelatinous mixtures of proteins, comprised of laminin, collagen, fibronectin and enactin and considered to be reconstituted variants of tissue ECM and basement membrane (Hughes et al., 2010). Matrix and matrigel embedded spheroids is an effective *in vitro* tool as it simulates the tumour (spheroid) and its microenvironment (matrix and matrigel), allowing cell-ECM interactions to be observed. Furthermore, the matrix used for embedding and culturing spheroids also facilitates in the delivery of nutrients and growth factors as well as providing vital structural support to the 3D spheroid cultures (Härmä et al., 2010). Spheroids can be embedded into the matrigel or on top of a layer of matrigel, resembling the basement membrane. Many variants of the standard matrigel is prepared, and are made with specific growth factors and nutrients depending on the type of specimen being cultured (Kleinman and Martin, 2005). Unlike the other 3D cell culturing techniques, where a 'one size fits all' approach is used to culture spheroids, the molecular composition of Matrigel can be tailored for specific requirement, however this can be costly for the large-scale production of spheroids and high-throughput applications. Another advantage of Matrigel embedded cells and spheroids, is that it can also be used for assays to

model angiogenesis (endothelial cells forming capillary structures) and the migration of cells through the matrigel network (Kleinman and Martin, 2005).

Similar to matrix and matrigel embedded spheroids, scaffold structures are also used to produce 3D spheroid cell models. Alginate, collagen and laminin are used for building biodegradable scaffolds, whereas polyethylene glycol, polyvinyl alcohol, polylactide-co-glycolide, and polycaprolactone are commonly used as materials for constructing biofriendly synthetic scaffolds (Breslin and O'Driscoll, 2013; Edmondson et al., 2014). Cells can attach themselves to the scaffold fibres and migrate along these as they divide, forming 3D spheroidal structures within the interstitial spaces (Kim, 2005). Additional benefits of scaffold-based 3D cell culturing include the incorporation of nutrients, soluble growth factors and ECM molecules into scaffold structures to sustain spheroid growth. The type of scaffold and presence of ECM proteins can affect growth and morphology of the spheroids. In addition, the sizes of the pores within the scaffold structure can be controlled by modifying the cross-linking density building materials thus facilitating the exchange of gases, delivery of nutrients and drugs and also the removal of waste products (Schmidt et al., 2008; Breslin and O'Driscoll, 2013).

There is growing evidence that MCTS and 3D models are superior to 2D models. However, there are limitations in the routine incorporation of MCTS based investigations into drug discovery programs. These include cost, manual labour and time to setup 3D models, plus the ability to perform high throughput screening and analysis is limited and can be difficult to perform. Furthermore, a major hurdle in the widespread acceptance of MCTS is the lack of studies which

directly compare MCTS and 2D models (Stock et al., 2016). However, the potential advantages of incorporating MCTS into mainstream anti-cancer research is still being recognised (Hirschhaeuser et al., 2010).

For this research project, 3D spheroidal models will be used for investigating Hypericin-PDT and compared to responses observed in 2D models. Similar to the very limited number of studies investigating the relationship between Hypericin and ABCG2, there is a lack of reported studies which directly compare PDT, between 2D monolayer and 3D spheroidal cell models. This is crucial as 3D spheroids are better representations of clinical cancers that 2D cultures do not recapitulate, and a direct comparison between the two distinct cell models will offer more clinically translatable results.

1.4.4 Advanced 3D co-culture *in vitro* models of cancer

3D *in vitro* models provide an alternative platform to whole *in vivo* organisms and 2D cell cultures. Although MCTS offer many advantages over 2D monolayered cell cultures, they still do not fully replicate the natural microenvironment of tumour *in vivo* (Nyga et al., 2011). In comparison to *in vivo* models, MCTS are still too simplistic and fail to consider the different stromal cell types and extracellular components that make up the tumour microenvironment (Nyga et al., 2011). Components of the tumoural microenvironment play a vital role in tumour initiation, progression, invasion, metastasis and resistance to treatment. Solid tumours are surrounded by the extracellular matrix (ECM) and various stromal cells, such as fibroblasts, adipocytes, vascular endothelial cells and inflammatory cells (Figure 1.4) (Wang et al., 2017). Heterocellular interactions within the tumour microenvironment can

re-shape the metabolic environment to support tumour growth. Cancer cells have the ability to effectively 'hijack' and rewire many normal cellular signalling mechanisms within the different stromal cells to promote growth and survival (Lyssiotis and Kimmelman, 2017). Recent focus has been on the development of composite *in vitro* models, to study the role of different cell types and the tumour microenvironment within complex 3D models.
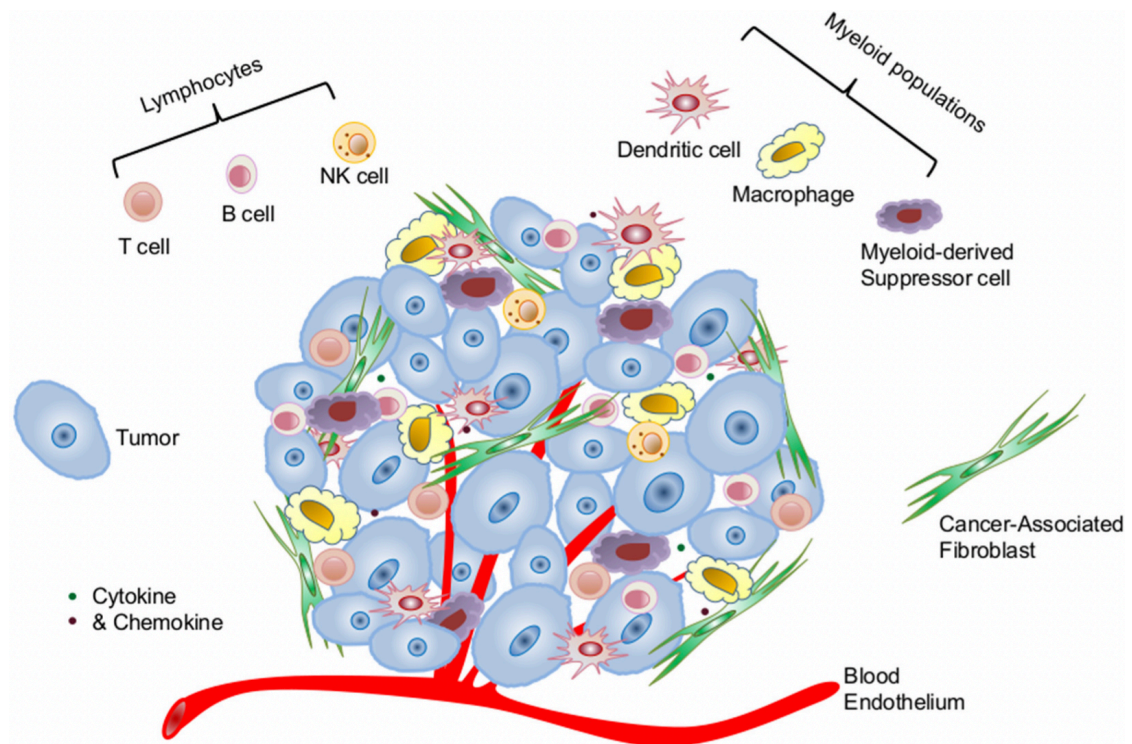
Figure 1.4 – Advanced co-cultured in vitro 3D models

Co-cultured *in vitro* models represent the dynamic tumour and microenvironment. The various constituents of the stroma can support the growth and survival of tumours and can also modulate response to treatment (Cui and Guo, 2016).

Cancer-associated fibroblasts (CAFs) have gained a lot of attention for their role in promoting tumour progression. CAFs can secrete growth factors, cytokines and chemokines to promote angiogenesis and tumour growth, secrete proteases to degrade the ECM and promote invasion and metastasis and also

modulate sensitivity to anti-cancer treatment (Shiga et al., 2015). To highlight the role played by CAFs, Jeong *et al.* co-cultured CAFs in a 3D cancer model with HT29 CRC spheroids. The authors found HT29 spheroids co-cultured with CAFs to be significantly more resistant to anti-cancer treatment, as compared to mono-cultured spheroids. Additionally, co-cultured spheroids were on average larger in size and also morphologically different compared to monocultures. Migration of fibroblasts towards the HT29 spheroids was also observed (Jeong et al., 2016). Eder *et al.* investigated the influence of co-culturing CAFs with 3D models of LAPC4 and LNCaP prostate cancer cell lines and found that CAFs were able to decrease the sensitivity of prostate cancer cell lines to anti-androgenic treatment (Eder et al., 2016). Furthermore, Kim *et al.* studied the induction of epithelial-mesenchymal transition (EMT), which is a typical characteristic of malignant tumours, in HT29 spheroids co-cultured with CAFs during the early stages of invasion and metastasis. The authors found that co-cultured models were able to replicate EMT at the invasive tumour margin. HT29 cells migrated away from the spheroid when co-cultured with CAFs and exhibited an increased expression of EGFR and CTGF with downregulation of membranous E-cadherin; events which are typically observed in metastasising cells (S.A. Kim et al., 2015).

Conventional MCTS models are simple cell aggregates that have been cultured for several days resulting in compact spheroidal structures. These structures are effective for replicating micro-metastases, avascular tumour nodules and poorly vascularised tumours (Katt et al., 2016). Angiogenesis and the tumour vasculature plays an essential role in facilitating the growth and survival of solid tumours. Due to its importance, angiogenesis has been identified as one of the

defining hallmarks of cancer (Hanahan and Weinberg, 2000). In order to receive sufficient oxygen and nutrients to grow and proliferate, tumour cells need to have a blood vessel within close proximity. For this reason, many advanced tumours promote angiogenesis and recruit endothelial cells from existing blood vessels to fabricate their own vasculature and sustain growth. Additionally, the tumour vasculature also provides an escape route for metastasising tumour cells to enter the systemic circulation and disseminate to other parts of the body (Bielenberg and Zetter, 2015; Forster et al., 2017). Thus, anti-angiogenic and anti-vascular therapies are a huge focus in anti-cancer research (Eichhorn et al., 2004; Niu and Chen, 2010). Drug discovery studies also focus on the tumour vasculature, but as a route to deliver anti-cancer agents (Narang and Varia, 2011).

To study the role of tumour vasculature in promoting growth and survival, Amann *et al.* described a complex co-culture model composed of non-small cell lung cancer cell lines, fibroblasts and endothelial cells. The authors were able to illustrate angiogenesis *in vitro* through the migration of endothelial cells towards tumour cells and also show the effect of anti-angiogenic drugs in an *in vivo*-like 3D cell culture model (Amann et al., 2017). Furthermore, Upreti *et al.* (2011) investigated the differences between tumour-endothelial cell 3D co-culture and 3D tumour cell monoculture models. The authors found that co-cultured models were more sensitive to the chemotherapeutic, paclitaxel, compared to monoculture models, suggesting that crosstalk between the different cell types is important in determining response to treatment (Upreti et al., 2011).

Other researchers have produced advanced co-culture *in vitro* models of cancer including: the creation of a lung carcinoma, fibroblast and pro-inflammatory monocyte co-culture model (Yamazoe et al., 2016); breast cancer and mesenchymal stem cells (Karnoub et al., 2007); and other examples of co-culturing cancer cell lines with stromal cells (Moriyama et al., 2010; Fang et al., 2013). These studies highlight the differences between simple and more complex models of cancer in terms of their phenotype, growth, survival, response to treatment and more importantly show how a more *in vivo*-like model of cancer is better for understanding disease processes.

1.5 3D CELL CULTURING AND MICROFLUIDICS

Microfluidics is the precise manipulation of volumes of fluid (in micro- and nanoscales) through micro-fabricated devices, typically where there is a length scale of less than 1mm within the device (Gale et al., 2018). Microfluidics offers many advantages over traditional laboratory-based assays for evaluating cell biology. Most notably is the ability to streamline assays by allowing complex experiments to be performed on a single all-encompassing platform. Furthermore, the miniaturised systems reduce the amount and volumes of samples and reagents consumed as compared to traditional protocols, thereby reducing costs, preserving precious samples and reducing experimental times (Sackmann et al., 2014). Microfluidics can also be used to produce perfused cultures and represent the dynamic *in vivo* state of vascularised tumours (Hirschhaeuser et al., 2010). Microfluidic platforms are custom designed and manufactured and allow tailored experiments to be conducted to a great degree of control. Coupled with an automated setup, microfluidics offers spatial and temporal control of the chemical and physical environment of the sample and

provides insights into real-time dynamic cellular processes (Figure 1.5) (Duncombe et al., 2015).

As described in *1.4.3*, 3D spheroids are better *in vitro* models of cancers as compared to traditional 2D cell cultures. In recent years, combined 3D cell culturing and microfluidics has become an increasingly evolving area. Substantial advancements have been made in the quality of microfluidic platforms for culturing, treating and evaluating 3D spheroids (Patra et al., 2013; Shin et al., 2013; Frey et al., 2014; Ayuso et al., 2015; Aijian and Garrell, 2015; Patra et al., 2016; McMillan et al., 2016; Sabhachandani et al., 2016). Existing 3D cell culturing techniques have allowed microfluidic devices to be designed around these techniques, as well as incorporating different methods of analyses. The use of microfluidics for culturing and analysing 3D spheroids is still in the early stages. However, the combination of 3D spheroids and microfluidic systems, offers a potentially powerful tool to aid cancer research.
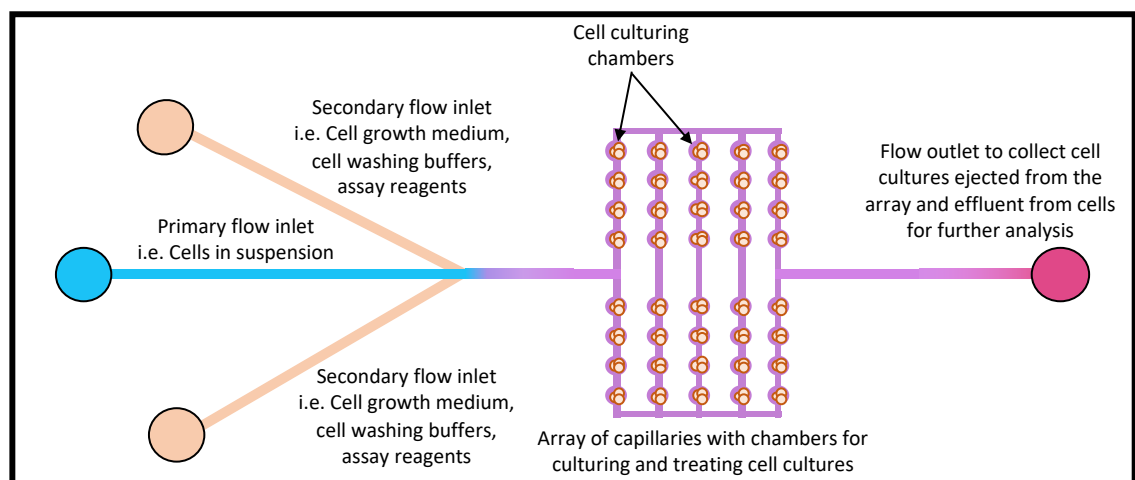
Figure 1.5 – Microfluidic chip for culturing cells in vitro

Schematic diagram of a microfluidic chip highlighting the ports on the chip for introducing and extracting fluids, capillaries through which the fluid flows and cell culturing chambers.

1.6 SUMMARY

CRC is one of the most commonly diagnosed cancers and a leading cause of death. Current treatment regimens have improved disease-free and overall survival rates. However, these improvements are at best modest and current treatment has not changed significantly in recent years. PDT is an effective anti-cancer treatment, applicable to many types of cancer. Rapid advances in our understanding of the mechanisms of PDT, combined with the development of novel photosensitisers, has allowed PDT to be considered as an alternative or adjunct to surgery and chemotherapy in some solid cancers. In CRC, many pre-clinical studies and a limited number of small clinical trials have evaluated PDT and shown it to be effective as a stand-alone treatment or in conjunction with other modalities. However, the optimal photosensitisers and conditions for PDT in CRC are yet to be established.

3D spheroid cell cultures have been shown to be better models of tumour *in vitro* in comparison to 2D cultures. Spheroid cultures mimic the cell-to-cell and cell-to-ECM interactions, physiological gradients and response to treatment of *in vivo* cancers. They bridge the gap between basic cell-based experiments and complex, resource-intensive animal models. The combination of microfluidics applied to 3D cell culturing offers a powerful new tool for advancing our understanding of anti-cancer treatments in a more efficient way.

Chapter Two

HYPOTHESIS AND AIMS

2 HYPOTHESIS AND AIMS

The hypotheses for my research is that Hypericin-mediated PDT is an effective method for treating CRC. Furthermore, 3D spheroidal cell models of CRC will better replicate the *in vivo* response to Hypericin-mediated PDT as compared to conventional 2D cell cultures. Finally, a microfluidic flow platform for culturing 3D spheroids will enable streamline 3D cell culturing and analysis.

The aims of my research are to:

1. Optimise cell culturing techniques to reliably produce 3D CRC spheroids.

2. Investigate the differences in responses to Hypericin-mediated Photodynamic Therapy in 2D CRC monolayers and 3D CRC spheroids.

3. Conceptualise, develop and optimise a microfluidic flow system that can accommodate the production, culture, treatment and evaluation of 3D spheroids.

Chapter Three

MATERIALS AND METHODS

3 MATERIALS AND METHODS

3.1 Cell lines and culturing conditions

Human colon cancer (HT29, HCT116, Caco2) and human foetal foreskin fibroblast (HFFF2) cell lines were obtained from the European Collection of Authenticated Cell Cultures (Salisbury, UK). HT29, HCT116, Caco2 were cultured in Roswell Park Memorial Institute (RPMI) 1640 Medium + GlutaMAX™ (Gibco® by Life Technologies™, Paisley, UK) supplemented with 10% (v/v) Fetal Bovine Serum (FBS) (Sigma Aldrich, Gillingham, UK). HFFF2 was cultured in Dulbecco's Modified Eagle Medium (DMEM) + GlutaMAX™ supplemented with 10% (v/v) FBS. Cell cultures were maintained at 37°C, under 5% CO_2 air enriched environment and relative humidity (RH) of 95%. Upon reaching 80-90% confluency, cell cultures were washed with Dulbecco's Phosphate-Buffered Saline (DPBS, Gibco® by Life Technologies™) and incubated for 5 minutes with 0.05% (v/v) trypsin and 0.5% (v/v) ethylenediaminetetraacetic acid (EDTA, Gibco® by Life Technologies™) in DPBS. Cell culture medium containing 10% (v/v) FBS was added to trypsinised cells, and the cell suspensions were centrifuged at 400g for 5 minutes. The supernatant was discarded and the pelleted cells were resuspended in fresh medium, seeded into 75cm^2 tissue culture flasks (Corning Inc., New York, USA) and grown to 80-90% confluence for the experiments.

3.2 3D cell culturing techniques

3.2.1 PolyHEMA coated plates

5mg/ml Poly(2-hydroxyethyl methacrylate) (PolyHEMA) solution was created by completely dissolving 250mg Poly(2-hydroxyethyl methacrylate) (PolyHEMA) (Sigma Aldrich) into 50mL of 95% (v/v) ethanol. 60μL of the 5mg/ml PolyHEMA solution was pipetted into each well of a round-bottomed 96-well plate. The plates were kept at 37°C for 2 days with the lids on to allow the ethanol to evaporate. Dry plates were wrapped in parafilm and stored at 4°C. Before use the plates were sterilised with UV light for 30 minutes at room temperature with the lids off. Confluent cells were washed with DPBS, trypsinised, centrifuged at 400g for 5 minutes and resuspended in fresh medium. 200μL of a 1x10^4 cells/mL cell suspension was added to each well, the plate was centrifuged at 500g for 10 minutes and incubated at 37°C/5% CO_2/95% RH. On Day 7, images of spheroids were taken using the Advanced Microscopy Group (AMG) EVOS® FL digital inverted microscope (Life Technologies, Loughborough, UK).

3.2.2 Hanging Drop

Cells were washed with DPBS, trypsinised, centrifuged at 400g for 5 minutes and resuspended in fresh medium. 20μL droplets of a 1x10^6 cells/mL cell suspension solution was deposited, on to the inside surface of the lid of a Corning® 100mm Tissue Culture Dish. The lid was then placed back on top of the bottom dish, which was filled with DPBS and incubated at 37°C/5% CO_2/95% RH. On Day 4, images were taken as described in *3.2.1*.

3.2.3 Agarose-coated plates

1% (w/v) agarose solution was made by dissolving 1g of agarose powder (Sigma) into 100mL deionised water. 50µL of the 1% (w/v) agarose solution was added into each well of a round-bottomed 96-well plate and left to gel at room temperature for 20 minutes. 100µL of varying concentrations of cells in suspension was added to each well and the plate was centrifuged at 360g for 10 minutes and incubated at 37°C/5% CO_2/95% RH. Images were taken as described in *3.2.1*.

3.2.4 Commercial Ultra-Low Attachment (ULA) plates

100µL of varying concentrations of cells in suspension was seeded into Corning® Costar® Ultra-Low Attachment 96-well plates (Corning Inc., New York, USA) and incubated at 37°C/5% CO_2/95% RH. Images were taken as described in *3.2.1*.

3.2.5 Spinner Flasks

3.2.5.1 Generating and culturing spheroids in spinner flasks

Cells were grown to 90% confluency in a 75cm^2 tissue-culturing flask. Cells were trypsinised, centrifuged and resuspended in 10mL of cell media. 140mL of cell media was added to a CELLSPIN 250 spinner flask (INTEGRA Biosciences Ltd, Egham, UK) followed by the 10mL cell suspension solution. The flask was placed onto a stirring platform (INTEGRA Biosciences) that was connected to a module control unit (INTEGRA Biosciences). Spinner flasks were kept at 37°C/5% CO_2/95% RH. Cells were kept in suspension by continuous rotational agitation at 75rpm. Spheroids were cultured for up to 25 days. Every 3 days,

90% of cell media was aspirated from the flasks and replaced with fresh cell media.

3.2.5.2 Embedding, sectioning and staining spheroids

Spheroids were generated in spinner flasks. Spheroids were aspirated from the spinner flasks and embedded into Cryo-M-bed (Bright Instruments, Luton, UK). Sections (5µm) were cut from the block of embedded spheroids onto glass slides using a Leica CM3050 S Research Cryostat (Leica Microsystems (UK) Ltd, Milton Keynes, UK). Slides were stained in Mayer's Haematoxylin Solution for 3 minutes, followed by washing in Scott's tap water for 1 minute and counterstained with Eosin for 1 minute. Slides were then dehydrated in ethanol, rehydrated in xylene and mounted on to coverslips using DPX. Slides were then imaged on the Nikon Eclipse E1000 (Nikon UK Ltd, Kingston upon Thames, UK).

3.3 *In vitro* Photodynamic Therapy

3.3.1 Preparation and storage of Hypericin

Hypericin was purchased from Molecular Probes® by Life Technologies™ (Eugene, Oregon, USA) in a powdered form. 100µM Hypericin stock solution was prepared in 100% ethanol and was stored as 1mL aliquots at -20°C in the dark. Working solutions of Hypericin were prepared for each experiment in cell media.

3.3.2 Mapping the light absorption spectrum of Hypericin

The light absorption spectrum of Hypericin was measured using a Nanodrop 1000 Spectrophotometer (Thermo Fisher Scientific Inc., Wilmington, Delaware, USA). The Nanodrop was initially calibrated with deionised water and the absorption spectrum of 100% ethanol was measured as a blank control to normalise the Hypericin absorption spectrum. Absorption was measured between 220nm and 750nm.

3.3.3 Light source for Photodynamic Therapy

The light-radiating device comprised of a series of LED's (one hundred and ninety-two HLMP-EL3B-WXKDD Amber LEDs (Avago Technologies, California, USA)) with maximum peak emission wavelength at 594nm. The light emission spectrum was mapped out using an Ocean Optics USB4000 spectrometer (Ocean Optics Inc., Oxford, UK). A light diffuser was built directly above the surface of light emission, with an internal fan to prevent overheating. The irradiation fluency at the surface of emission was $230\mu W/cm^2$, as measured with a Newport 843-R Laser Power Meter and a Newport 918D-SL-OD3R Photodiode Sensor (Newport Corporation, California, USA). Light treatment lasted for 72 minutes and 28 seconds, which equates to a total light dose of $1J/cm^2$ (see Appendix for calculation of light dose). The light-radiating device was custom built by the Electronics Services Department, School of Mechanical Engineering, University of Leeds, Leeds, UK.

3.3.4 Monitoring light fluency readings and operating temperature of light radiating device over a prolonged period

The light radiating device described in *3.3.3* was switched on and left to run for 4 hours. Light fluency readings were taken every 30 minutes using a Newport 843-R Laser Power Meter and a Newport 918D-SL-OD3R Photodiode Sensor. Temperature readings were taken every 30 minutes using a Tekpower DT8380 Non-contact Infrared Thermometer (Tekpower, California, USA).

3.3.5 Treating cells with Hypericin-PDT

For 2D cultures, cells were seeded at 6×10^5 and 5×10^4 cells per well into 6- and 96-well tissue culture plates respectively and incubated at 37°C/5% CO_2/95% RH for 24 hours. For 3D spheroid cultures, 500 cells per well were seeded into agarose-coated plates as described in *3.2.3* and incubated at 37°C/5% CO_2/95% RH for 48 hours. Cell cultures were treated with varying concentrations (0-200nM) of Hypericin in the dark for 16 hours. Cultures were then washed with DPBS and phenol red-free cell media supplemented with 10% (v/v) FBS was added to cultures. Depending on experimental conditions, cultures were either irradiated with light or kept in the dark at room temperature. The light treated cultures were placed on top of the diffuser surface of the light-radiating device described in *3.3.3* and treated with a light dose of 1J/cm^2.

3.3.6 Co-treating cell cultures with Ko143 and Hypericin-PDT

Cell cultures were incubated with 10µM Ko143 for 90 minutes, followed by varying concentrations (0-200nM) of Hypericin in the dark for an additional 16 hours. Cultures were then washed and treated with light as described above.

3.3.7 Assessing cytotoxicity in cell cultures

3.3.7.1 Quantifying cytotoxicity in 2D and 3D cultures

Twenty-four hours after light irradiation, cell viability was assessed in 2D cultures by initially aspirating and collecting the floating cells in culture. Adherent cells were washed with DPBS and briefly incubated with trypsin for 5 minutes at 37°C. Cell culture medium supplemented with 10% (v/v) FBS was added to trypsinised cells, and the cells were gently lifted using a cell scraper (Greiner Bio-One Ltd., Stonehouse, UK). Cells in suspension were collected and centrifuged at 400g for 5 minutes. 90% of the supernatant was discarded and cells were resuspended in the remaining supernatant. 10µL of resuspended cells were mixed in a 1:1 ratio with 0.4% Trypan Blue solution and loaded into the Countess® Cell Counting Chamber Slides (Fisher Scientific UK Ltd, Loughborough, UK; Cat). Cell Viability was measured using a Countess® II Automated Cell Counter (Thermo Fisher, Paisley, UK). Alternatively, 2D and 3D cultures were treated with 1.3µg/mL propidium iodide (Biotium Inc., California, USA) for 15 minutes. Cell cultures were then washed twice with DPBS and fresh cell culture medium added. Fluorescence was measured on a Mithras LB 940 Microplate Reader (Ex: 540nm, Em: 620nm) (Berthold Technologies Ltd., Harpenden, UK).

3.3.7.2 Visualising cytotoxicity in 3D cultures

Twenty-four hours following irradiation, 3D spheroids cultures were incubated with 1.3µg/mL propidium iodide and 5µg/mL Hoechst 33342 (Thermo Fisher) for 15 and 60 minutes respectively. Spheroids were then washed and fluorescence visualised using the EVOS™ FL Imaging System (Thermo Fisher).

3.3.8 Evaluating the penetration of Hypericin through 3D spheroids

Spheroids generated in spinner flasks were aspirated from the flasks, seeded into 6-well plates and treated with 200nM Hypericin for 16 hours in the dark. Spheroids were then embedded into Cryo-M-bed (Bright Instruments, Luton, UK) and sections (5µm) were cut onto glass slides using a Leica CM3050 S Research Cryostat (Leica Microsystems (UK) Ltd, Milton Keynes, UK). Glass coverslips were mounted onto glass slides using ProLong™ Gold Antifade Mountant with DAPI (Thermo Fisher) and cured overnight. Slides were then sealed and imaged on the Nikon A1R Confocal Microscope (Nikon UK Ltd, Kingston upon Thames, UK).

3.3.9 Evaluating the long-term changes in spheroid volume following Ko143 treatment and Hypericin-PDT

Spheroids were grown in 1% agarose-coated plates and subjected to Ko143 treatment and Hypericin-PDT as described in *3.3.5* and *3.3.6.* Images of spheroids were taken using the EVOS™ FL Imaging System (Thermo Fisher). Images of spheroids were analysed using ImageJ (National Institutes of Health, Maryland, USA) and the equation to calculate the volume of a sphere ($V = \frac{4}{3}\pi r^3$) was used to calculate the volume of spheroids (see Appendix for step-by-step calculation of spheroid volumes). On Day 10, spheroid cultures were incubated with propidium iodide and Hoechst 33342 and imaged as described in *3.3.7.2*.

3.4 Characterising ABCG2 protein

3.4.1 Quantifying ABCG2 protein in 2D and 3D cell models (Western Blot)

3.4.1.1 Preparation and quantifying protein lysates

Spinner flask spheroids were washed with ice-cold DPBS and sonicated in radioimmunoprecipitation assay (RIPA) buffer with protease inhibitor for 15 minutes at 4°C. 2D cell cultures were grown to 90% confluency, washed with ice-cold DPBS and lysed by incubating with RIPA buffer with protease inhibitor for 15 minutes at 4°C. Lysed cells were collected and centrifuged at 14,000rpm (13,200g) for 10 minutes. Supernatants containing protein extracts were aliquoted at 100µL and stored at -80°C. Concentration of protein in lysates were determined using the DC™ Protein Assay kit (Bio-Rad, Watford, UK) according to the manufacturer's instructions. A linear standard curve ($R^2 \geq 0.98$) was generated using varying concentrations of bovine serum albumin and the concentration of protein in lysates was then determined.

3.4.1.2 Gel electrophoresis and protein transfer

Protein lysates were prepared by mixing protein lysates with NuPAGE® lithium dodecyl sulfate (LDS) Sample Buffer (Thermo Fisher) and deionised water. Samples were loaded into and resolved on LDS-PAGE 12% gel (NuPAGE Novex 12% Bis-Tris Gel 1.0mm, 10 well) (Thermo Fisher) in NuPAGE® MOPS SDS running buffer (Thermo Fisher). Pre-stained SeeBlue™ Plus2 (Thermo Fisher) and MagicMark™ XP Western Protein Standard (Thermo Fisher) were prepared in 50% (v/v) and used as molecular markers. Gels were run for 90 minutes at 180 volts. Resolved proteins were transferred onto methanol activated polyvinylidene difluoride (PVDF) membrane in NuPAGE® transfer buffer for 90 minutes at 30 volts.

3.4.1.3 Immunoblotting and imaging

Following protein transfer, membranes were blocked in 5% skimmed milk in TBS-T for 30 minutes, followed by blocking in 1% skimmed milk in TBS-T for 30 minutes. Membranes were incubated with mouse anti-BCRP (BXP-21) monoclonal primary antibody (1:200 in 1% skimmed milk in TBS-T, Millipore, Watford, UK) overnight at 4°C. Membranes were then washed with TBS-T and incubated with horseradish peroxidase-conjugated Rabbit anti-mouse polyclonal secondary antibody (1:2000 in 1% skimmed milk in TBS-T, Thermo Fisher) for 1 hour at room temperature. Protein bands were developed using the SuperSignal™ West Femto Maximum Sensitivity Substrate (Thermo Fisher) and imaged on the ChemiDoc™ XRS+ System (Bio-Rad). β-actin served as the protein loading control.

3.4.2 Immunofluorescence for detecting ABCG2

Fifteen-days old spinner flask spheroids were embedded into Cryo-M-bed (Bright Instruments, Luton, UK) and sections (5µm) were cut onto glass slides using the Leica CM3050 S Research Cryostat (Leica Microsystems (UK) Ltd, Milton Keynes, UK). Monolayered cell cultures were grown to confluency on glass coverslips. Spheroid sections and monolayered cells on glass slides and coverslips respectively were fixed with 4% paraformaldehyde for 15 minutes. Slide and coverslips were then washed with phosphate buffered saline (PBS), blocked with 0.5% skimmed milk in PBS and incubated with anti-BCRP primary antibody (same antibody described in *3.4.1.3*, 1:20 in 0.5% skimmed milk in PBS) for 1 hour at room temperature. Slides and coverslips were then washed with PBS and incubated with Alexa Fluor 488-conjugated goat anti-mouse

secondary antibody (1:300 in 0.5% skimmed milk in PBS, Thermo Fisher) for 30 minutes at room temperature. Slides and coverslips were washed and mounted using ProLong™ Gold Antifade Mountant with DAPI (Thermo Fisher) overnight at room temperature. Slides were imaged using the Zeiss Axio Imager Z1 (Carl Zeiss Ltd, Cambridge, UK).

3.5 Microfluidic flow systems

3.5.1 Version 1

3.5.1.1 Designing and creating fluid flow device

The schematic designs for the flow device were drawn in SolidWorks (Dassault Systèmes, Vélizy-Villacoublay, France). The designs were printed onto photocurable acrylonitrile butadiene styrene thermoplastic polymer (ABS) resin using an EnvisionTEC 3D printer (EnvisionTEC GmbH, Gladbeck, Germany).

3.5.1.2 Forming droplets in wells

Rubber tubings were connected to the device and used to flow fluids through the device. The Aladdin Single-Syringe Pump (AL-2000) (World Precision Instruments, Florida, USA) was used to drive the flow of fluid at 100µL/min.

3.5.2 Version 2

3.5.2.1 Designing, creating and assembling the flow device

The schematic designs were drawn in SolidWorks. The different layers of the microfluidic device were cut using a Universal Laser Systems PLS6.150D laser cutter (Universal Laser Systems GmbH, Vienna, Austria). The top and bottom layers of the device were made from Poly(methyl methacrylate) (PMMA). The

inner top and inner bottom layers were made from silicone rubber and the central layer with the cell culturing wells was made from the polyimide film, Kapton. The device was fashioned together using screws on each corner of the microfluidic device.

3.5.2.2 Seeding cells through fluid flow

Confluent HT29 cells were washed with DPBS, trypsinised, centrifuged at 400g for 5 minutes and resuspended in fresh cell medium. 1x10^6 cells/mL cell suspension solution was loaded into a 10mL syringe and cells were seeded at 5µL/min into the device, using an Aladdin Single-Syringe Pump (AL-2000). The device was then incubated at 37°C/5% CO_2/95% RH and images were taken using the EVOS® FL digital inverted microscope.

3.5.3 Version 3

3.5.3.1 Designing, creating and assembling the flow device

Schematic designs were drawn in SolidWorks. To create the central cell culturing fluid flow chip, a master mould was initially created by printing the designs onto ABS using an EnvisionTEC 3D printer (EnvisionTEC GmbH, Gladbeck, Germany). Flow chips were then cast from the master mould using Polydimethylsiloxane (PDMS) as the casting material. The top and bottom layers of the device were fabricated from PMMA using the laser cutter system as described in *3.5.2.1*. The device was fashioned together using bolts on each corner of the microfluidic device.

3.5.3.2 Seeding cells and culturing spheroids on PDMS flow chip

Confluent HT29 cells were washed with DPBS, trypsinised, centrifuged at 400g for 5 minutes and resuspended in fresh medium. 20µL of a 2x10^7 cells/mL cell suspension was deposited on top of the spheroid culturing wells on the PDMS flow chip, and incubated at 37°C/5% CO_2/95% RH. Cell media was exchanged every 24 hours. Images were taken using the EVOS® FL digital inverted microscope.

3.5.3.3 Preparing and imaging spheroids via scanning electron microscopy

HT29 spheroids were prepared as described in *3.5.3.2*. Spheroids were briefly washed with pre-warmed DPBS and fixed in 2.5% (v/v) glutaraldehyde for 20 minutes. Spheroids were then subjected to dehydration in increasing gradients of ethanol (25%, 40%, 60%, 80%, 90% and 100%). For imaging, the PDMS chip containing the spheroids was coated with 4nm of iridium and imaged using a Nova NanoSEM450 scanning electron microscope (Thermo Fisher).

3.5.4 Recording fluid flow

Methylene Blue hydrate (Sigma Aldrich) was dissolved into deionised water, and flowed through the microfluidic devices at 50µL/min. A OnePlus 3T (A3010) smartphone (Android version 8.0.0) (OnePlus, China) was used to record the video footage. The video was edited using iMovie version 10.1.2 (Apple Inc., California, USA).

3.6 Combining microfluidics and fluid flow

3.6.1 Culturing spheroids in microfluidic flow chip

HT29 cells were washed with DPBS, trypsinised, centrifuged at 400g for 5 minutes and resuspended in fresh cell medium to create a 2×10^7 cells/mL cell suspension solution. 20µL of cell suspension was deposited onto the spheroid culturing wells through the central port on the top PMMA layer. Fresh cell medium was then flowed through the microfluidic device at 10µL/min, using a syringe pump and a 10mL syringe loaded with cell medium, to flush out excess cells that had not settled into the wells. The microfluidic device was then incubated at 37°C/5% CO_2/95% RH. After 24 hours, fresh cell medium was flowed through the device at 20µL/min using a syringe pump and a 10mL syringe loaded with cell medium. Following complete cell media exchange in the microfluidic device, the device was placed back into incubation. The Aladdin Single-Syringe Pump (AL-2000) was used to drive the flow of fluid.

3.6.2 Treating spheroids with 5-Fluorouracil through fluid flow

5-Fluorouracil (5-FU) was purchased in powdered form from Sigma-Aldrich. A stock solution of 5-FU (20mM) was prepared in deionised water. Further dilutions were prepared from the stock solution in cell culturing media. Forty-eight hours after seeding the cells into the microfluidic device, 500µM 5-FU was prepared and flowed through the device at 20µL/min as described in *3.6.1*. The microfluidic device was then incubated for another 24 hours.

3.6.3 Analysing cell viability in spheroids

3.6.3.1 Lactate dehydrogenase (LDH) assay

Following 5-FU treatment, the supernatant was collected from the microfluidic device, by flowing DPBS into the device at 20µL/min as described in *3.6.1*. The supernatant was used to conduct the LDH cytotoxicity assay using the Pierce™ LDH Cytotoxicity Assay Kit (Thermo Fisher) and carried out as per the manufacturer's instructions and guidelines.

3.6.3.2 Visualising cytotoxicity in 3D spheroids

A solution containing 1.3µg/mL propidium iodide and 5µg/mL Hoechst 33342 was prepared in cell culture media and flowed through the device at 20µL/min as described in *3.6.1*. Spheroids were incubated with the dyes for 30 minutes, washed with DPBS through flow (as described in *3.6.3.1*) and fluorescently imaged using the EVOS™ FL Imaging System.

3.7 Statistical Analysis

Two-way ANOVA, one-way ANOVA and Student's *t*-test were used to perform statistical analysis using GraphPad Prism 7 (GraphPad Software, Inc., California, USA). $p<0.05$ was considered to be statistically significant. Data are presented as the mean ± standard deviation.

3.8 Recipes for solutions

RIPA Buffer supplemented with protease inhibitor

50mM Tris-HCl, pH 7.4

150mM NaCl

1% NP-40

1x cOmplete™ Protease Inhibitor Cocktail (Sigma Aldrich)

Buffer solution was prepared in deionised water

TBS-T

20mM Tris-HCl, pH 7.4

150mM NaCl

0.1% Tween-20

Buffer solution was prepared in deionised water

Chapter Four

RESULTS (1) – Techniques for culturing 3D *in vitro* multicellular tumour spheroids

4 RESULTS (1) - TECHNIQUES FOR CULTURING 3D *IN VITRO* MULTICELLULAR TUMOUR SPHEROIDS

4.1 Introduction

2D monolayer cell cultures have conventionally been used, to understand the function and mechanism of disease such as cancer. However, it has been recognised that 2D models do not fully represent disease *in vivo*, and this limitation hinders the successful translation and progression of novel anti-cancer techniques from being evaluated in simple *in vitro* cell models to complex organisms such as animal models and human clinical trials. Cells in 2D models are presented by being adhered to the plastic surfaces of tissue culturing flasks and plates in a static environment. This is unlike *in vivo* cancers where cells are in contact with each other and the ECM, resulting in a more dynamic environment that influences the behaviour of cell growth (Achilli et al., 2012). To address the gap in translating the efficacy of treatment techniques, 3D multicellular tumour spheroidal models have been recognised as better representative models of cancers. Spheroids (also referred to as 3D microtissues) mimic the architectural and functional characteristics of the native tissue (Achilli et al., 2012). Various techniques have been designed and developed to generate 3D multicellular tumour spheroidal models of carcinoma cell lines. The application of these different methods, depends on the type of spheroidal model required for the experimental question that is being

addressed. In my research, I investigate the different techniques for producing spheroids, which would then inform me on the techniques that I could use for subsequent spheroid related experiments.

4.2 Methods

The PolyHEMA coating, hanging drop, agarose coating, commercial ultra-low attachment and spinner flask methods were used for generating 3D spheroids of HT29 and HCT116 cell lines. Details of each 3D cell culturing method are described in *3.2*. Spinner flask spheroids were embedded, sectioned and subjected to haematoxylin and eosin staining, as described in *3.2.5.2*.

4.3 Results

4.3.1 Evaluating different 3D cell culturing techniques

Different 3D cell culturing techniques (PolyHEMA non-adherent coating, agarose non-adherent coating, hanging drop and spinner flask) were evaluated to identify the techniques which would best be suited for producing 3D spheroids for further experiments in this research project (Figure 4.1).
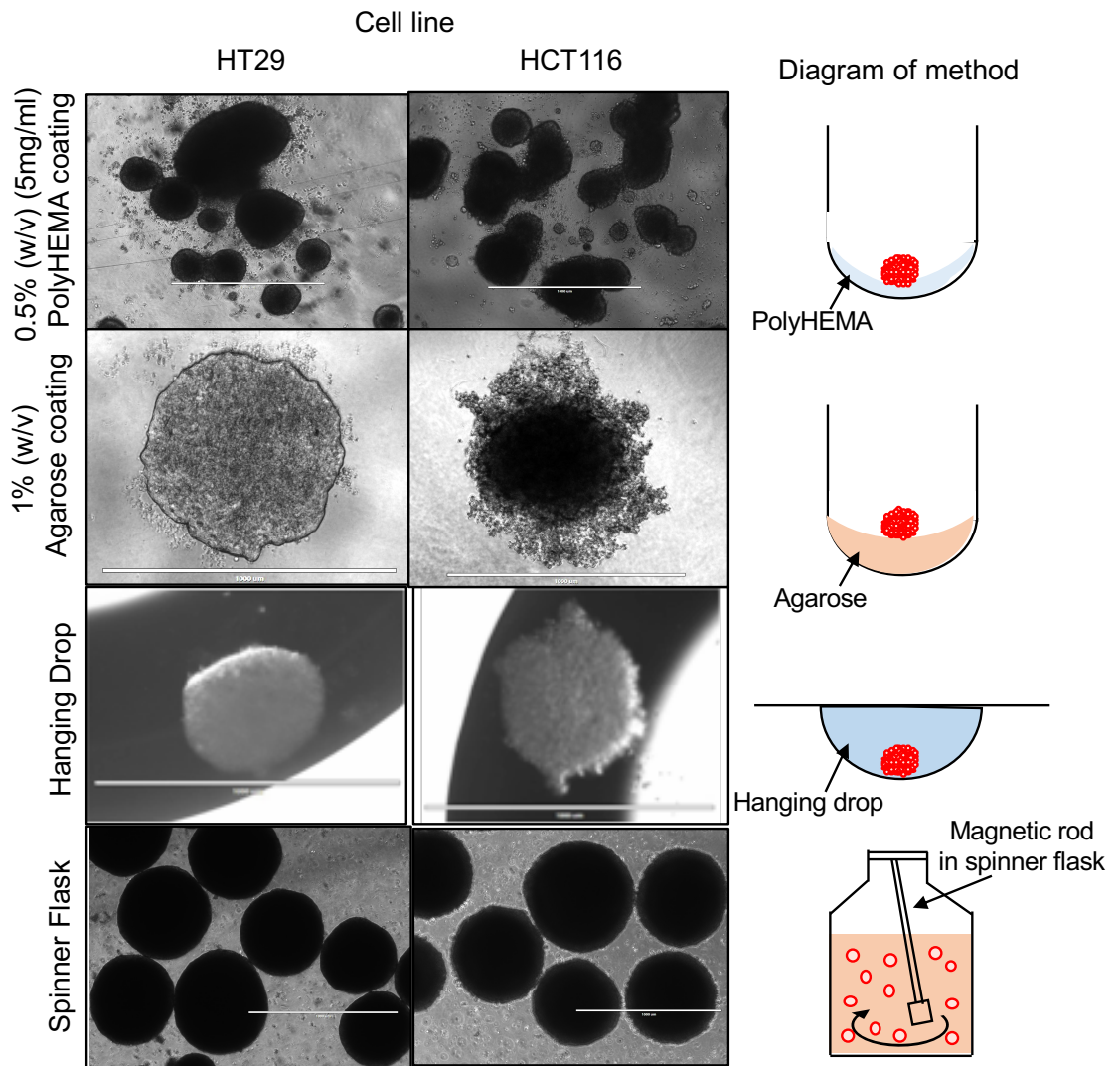
Figure 4.1 - Overview of the techniques used for generating 3D spheroids

Different 3D cell culturing techniques were evaluated to produce 3D spheroid models of HT29 and HCT116 cell line. 96-well plates were coated with PolyHEMA or agarose and cells in suspension was added to the wells. For hanging drop spheroids, droplets of cells in suspension were deposited on to the inner surface of a petri dish and inverted to form a hanging drop. For spinner flask spheroids, cells in suspension were added into a spinner flask containing cell media and kept in constant agitation. Scalebar = 1000µm. Images in this figure are representative of at least 3 independent experiments. See *3.2.1, 3.2.2, 3.2.3* and *3.2.5* of Material and Methods for the detailed protocol.

4.3.2 PolyHEMA coating

HT29 and HCT116 cells seeded into 0.5% (w/v) (5mg/ml) PolyHEMA coated 96-well plates were unable to form uniform spheroidal structures. Instead, cells were found to form multiple irregular globular structures in the wells (Figure 4.2). Due to the ineffectiveness of this technique and inconsistencies in producing 3D spheroids, this technique was not further utilised for producing 3D spheroid cell cultures.

4.3.3 Agarose coating

HT29 and HCT116 cells were seeded into 96-well plates coated with 1% (w/v) agarose. Cells were found to form aggregates and subsequently produce uniform spheroidal structures (Figure 4.3). This technique was found to be easy in application, effective and consistent in producing 3D spheroids. The agarose coating method was chosen for further experiments.

4.3.4 Hanging Drop

Similar to the agarose coated method, the hanging drop method was also found to produce 3D spheroid structures (Figure 4.4). However, this technique is more difficult to perform in comparison to the agarose method and the lack of a physical supporting component results in fragile 3D spheroidal structures in the droplets. The hanging drop method is a simple technique for producing 3D spheroids. However, the difficulties in manually handling cultures and complications in maintaining the spheroid structures were reasons for not using this technique for further experiments.

Figure 4.2 - Generating 3D spheroids using PolyHEMA coating

HT29 and HCT116 cells were seeded into 0.5% (w/v) PolyHEMA coated 96-wells plates at 1250, 5000 and 10000 cells per well. Images taken after 2 days of culturing. Scalebar = 1000µm. Images in this figure are representative of at least 3 independent experiments. See *3.2.1* of Material and Methods for the detailed protocol.

1% (w/v)
Agarose coating

Number of
cells seeded
per well

Cell line

HT29

HCT116
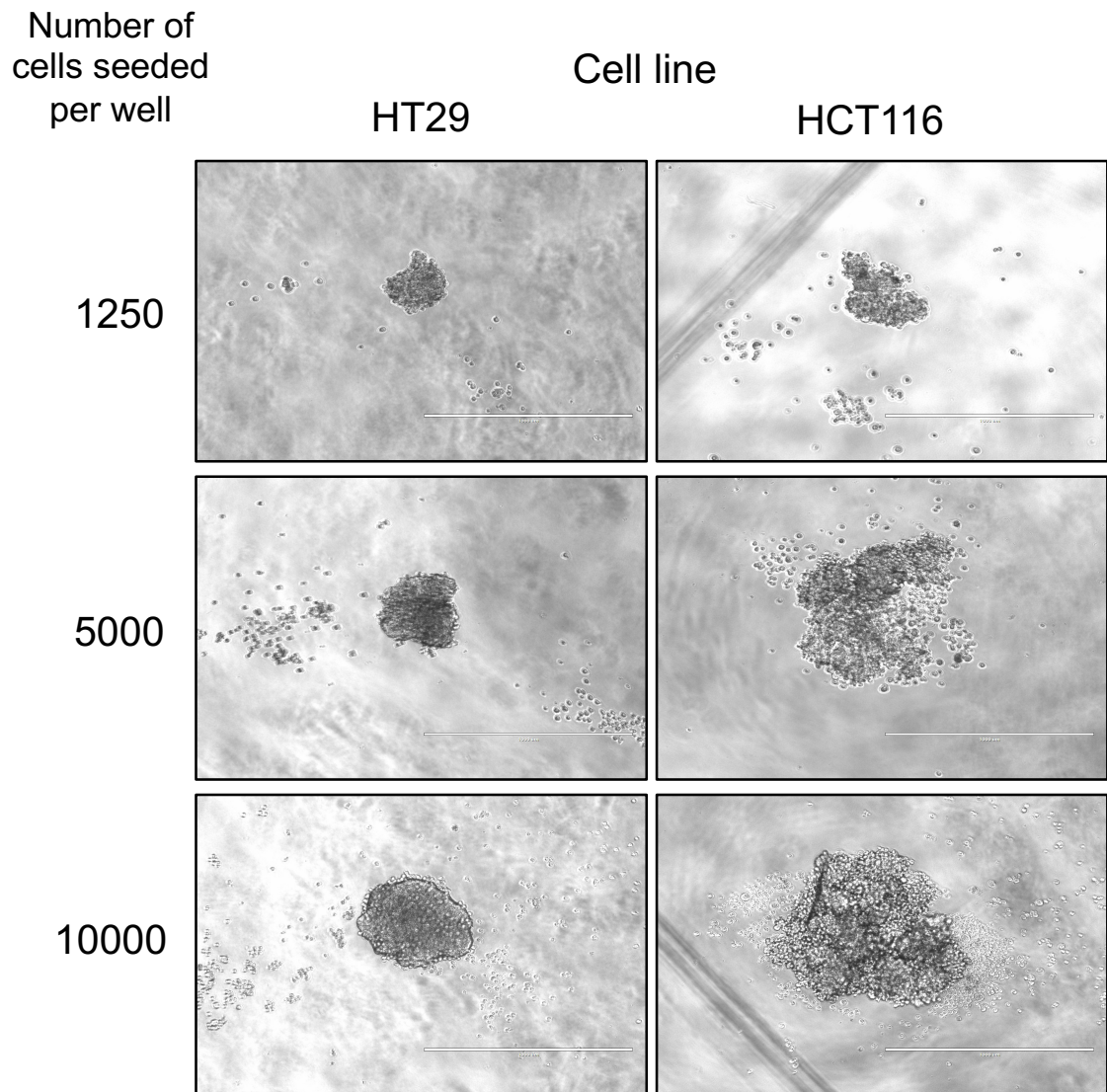
1250

5000

10000

Figure 4.3 - Generating 3D spheroids using agarose coating

HT29 and HCT116 cells were seeded into 1% (w/v) agarose coated 96-wells plates at 1250, 5000 and 10000 cells per well. Images taken after 2 days of culturing. Scalebar = 1000μm. Images in this figure are representative of at least 3 independent experiments. See *3.2.3* of Material and Methods for the detailed protocol.

Hanging Drop

Number of
cells seeded
per droplet

Cell line

HT29   HCT116
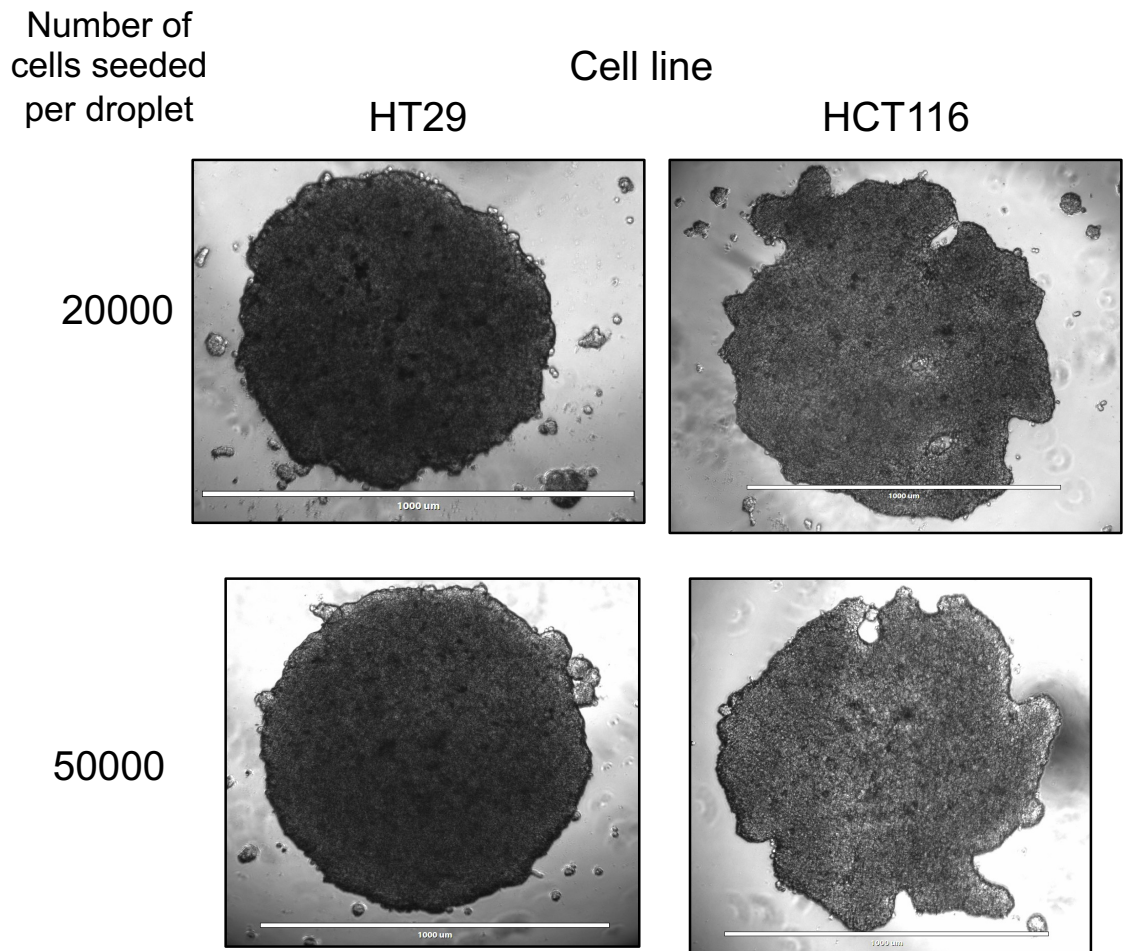
20000

50000

Figure 4.4 - Generating 3D spheroids using hanging drops

HT29 and HCT116 cells were seeded in 20µL hanging droplets at 20000 and 50000 cells per droplet. Images taken after 2 days of culturing. Scalebar = 1000µm. Images in this figure are representative of at least 3 independent experiments. See *3.2.2* of Material and Methods for the detailed protocol.

4.3.5 Spinner Flask

In the spinner flasks, HT29 and HCT116 cells were kept in constant agitation, allowing mature 3D spheroids to form over 20 days (Figure 4.5). This technique is useful for generating a large number of spheroids and serves as a reserve for when 3D spheroids are required for experiments. The spinner flask method was also chosen for further experiments.

Spinner Flask
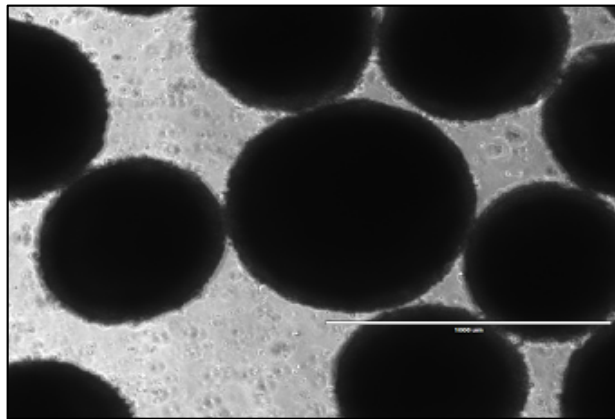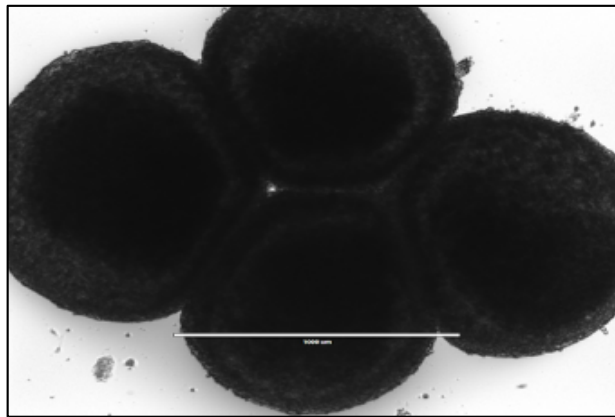
Figure 4.5 - Generating 3D spheroids using spinner flasks

HT29 and HCT116 cells were seeded into and cultured in spinner flasks. Images taken at Day 20. Scalebar = 1000µm. Images in this figure are representative of at least 3 independent experiments. See *3.2.5* of Material and Methods for the detailed protocol.

4.3.6 Selecting techniques for producing 3D spheroids

Following the evaluation of the different 3D cell culturing techniques. The agarose-coated plate and spinner flask techniques were chosen for producing spheroids, for experiments described in Chapter 5. The agarose-coated plate method is a simple and effective technique, which can be used to consistently produce uniform-sized spheroids. Spheroids are generated in 96-well plates, permitting high throughput screening experiments and standard assays to be performed on the plate without manually handling spheroids. For the PDT experiments in Chapter 5, generating spheroids and performing PDT could be done conveniently in 96-well plates. The spinner flask method was also chosen for its versatility as the flasks serve as a bank of spheroids, specifically for experiments to be conducted in Chapter 5. Spheroids in spinner flasks are constantly in suspension, making it easy and convenient to extract spheroids from flasks that can be used for many different experimental techniques. This includes lysing spheroids to generate protein lysates, embedding and sectioning spheroids for immunohistochemistry and seeding spheroids into plates for any desired experiment.

The agarose-coated plate technique was chosen as a method for producing 3D spheroids for subsequent experiments. Different cell seeding densities were evaluated, and showed that HT29 and HCT116 spheroids were able to form spheroids within two days after initial cellular aggregation (Figure 4.2). In comparison, HT29 and HCT116 cells were seeded into similar commercially available pre-coated Ultra-Low Attachment (ULA) plate (Figure 4.3). Cell aggregates were formed within one day of seeding cells and compact spheroids

had formed by the second day. For both 'non-adherent' techniques, the original

cell seeding densities dictated the sizes of resulting spheroids.
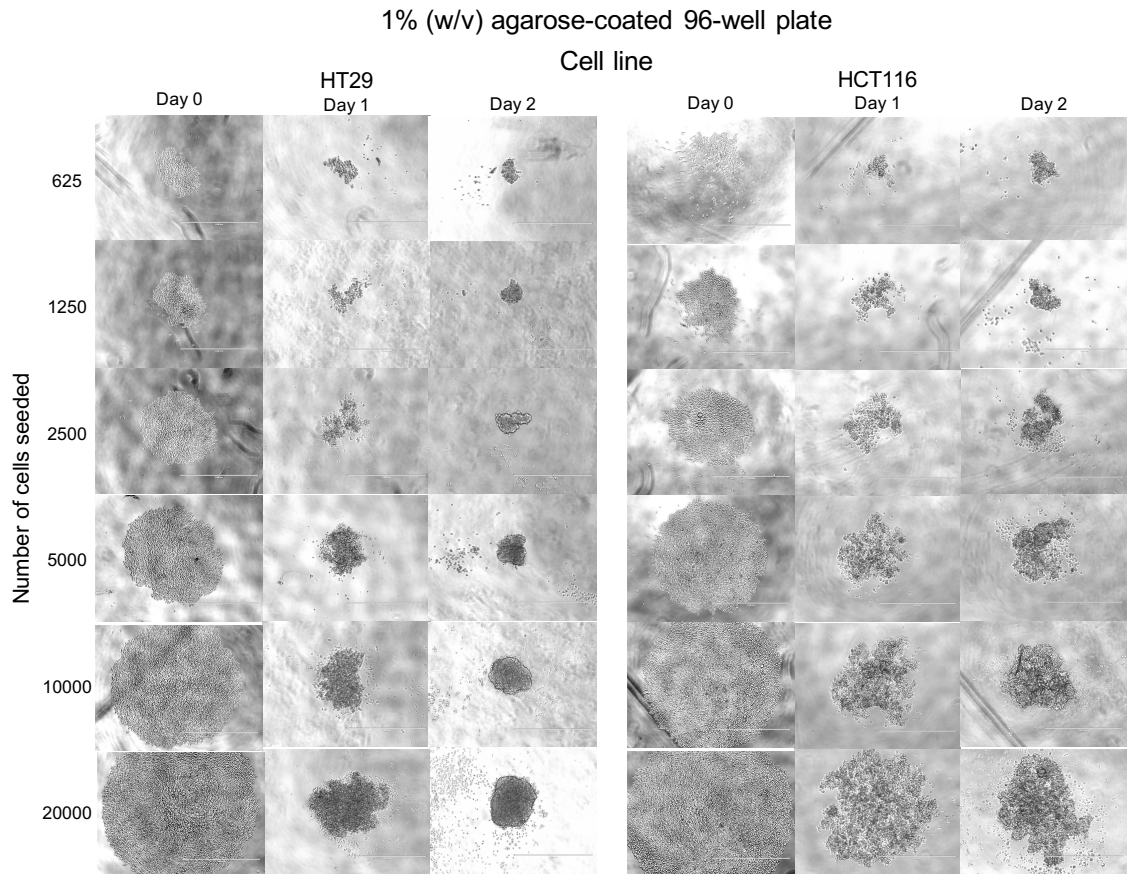
Figure 4.6 – 3D spheroids cultured in 1% (w/v) agarose-coated 96-well plates

Varying concentrations of HT29 and HCT116 cells in suspension were prepared
and seeded into 96-well plates pre-coated with 1% (w/v) agarose and centrifuged
to form cell aggregates. Cell aggregates/spheroids were cultured for 2 days.
Scalebar = 1000μm. Images in this figure are representative of at least 3
independent experiments. See *3.2.3* of Material and Methods for the detailed
protocol.

Commercial Ultra-Low Attachment 96-well plate

Cell line
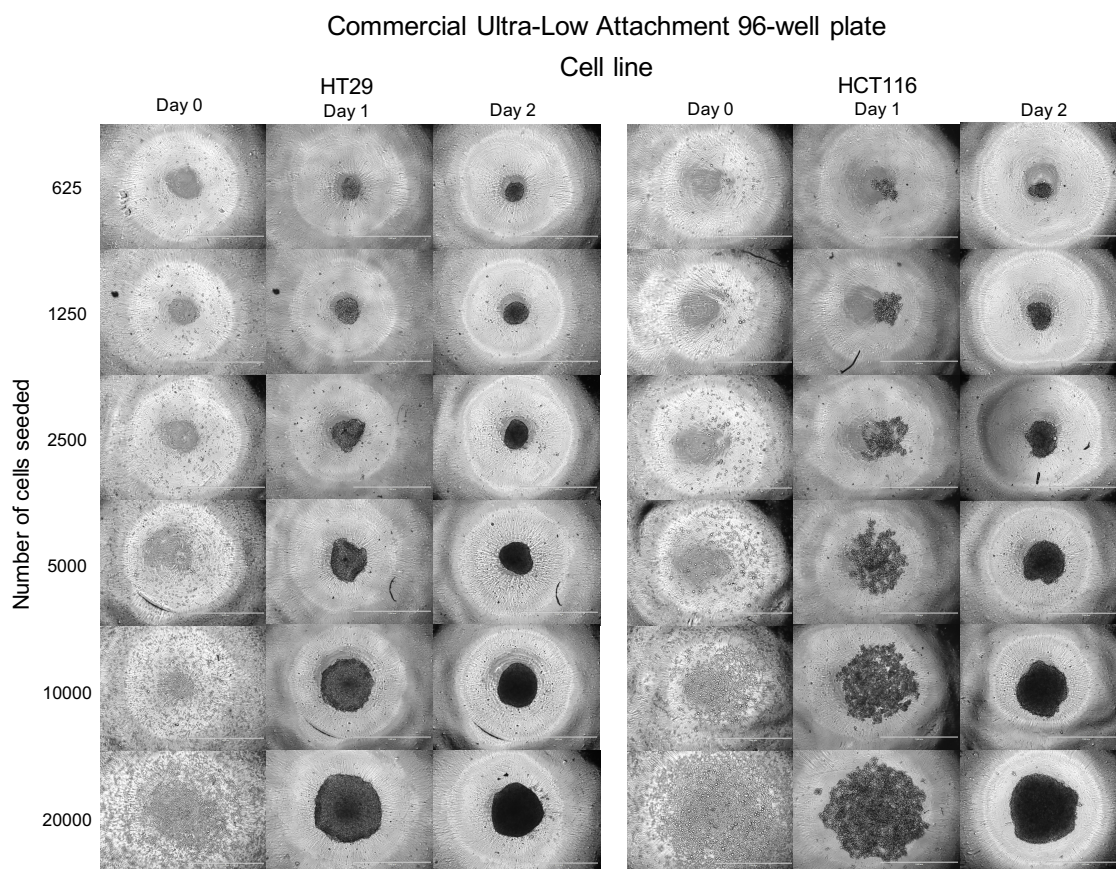
Figure 4.7 – 3D spheroids cultured in commercial ULA 96-well plates

Varying concentrations of HT29 and HCT116 cells in suspension were prepared and seeded into commercially available ULA 96-well plates. Cell aggregates/spheroids were cultured for 2 days. Scalebar = 1000µm. Images in this figure are representative of at least 3 independent experiments. See *3.2.4* of Material and Methods for the detailed protocol.

The spinner flask technique for producing spheroids was also chosen for further experiments. Spheroids were able to be cultured for long periods of time, which allowed them to grow in size and mature into solid 3D spheroidal structures (Figures 4.4A, 4.4B and 4.4C). Following an initial rapid growth phase, the rate of spheroid growth slowed down after day 20 (Figure 4.4B). Furthermore, spheroids cultured for extended periods of time, were also noted to have necrotic central cores as illustrated by the loss of cell-cell connections and loose cellular debris (Figure 4.4D).

A) Growth of spinner flask spheroids over 25 days (1)
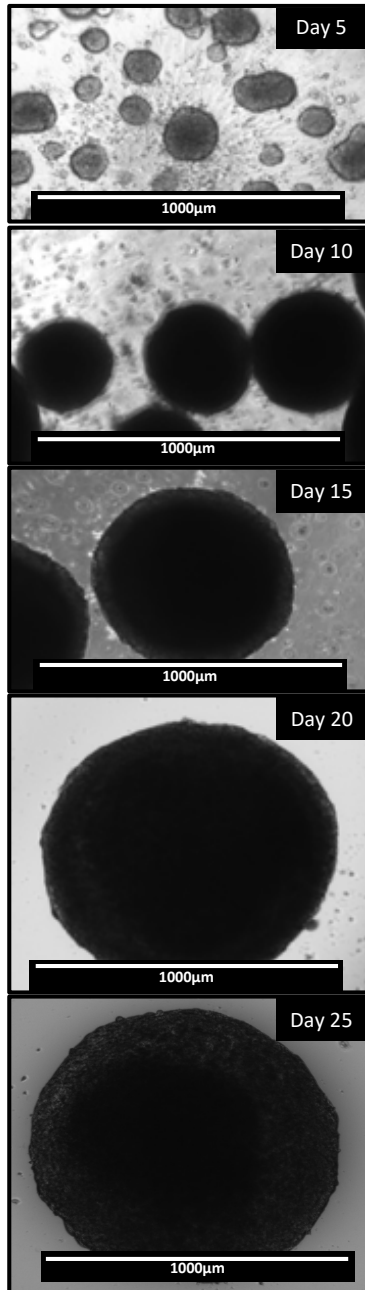
B) Growth of spinner flask spheroids over 25 days (2)
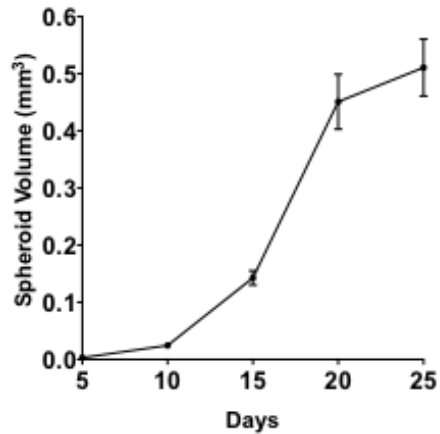
C) Hoechst 33342 fluorescent staining (Day 20)
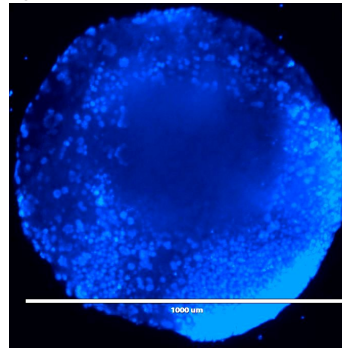
D) Section and H&E staining (Day 20)
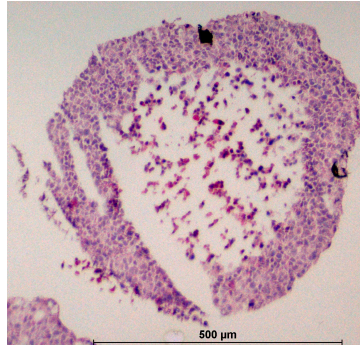
Figure 4.8 – 3D HCT116 spheroid cultured in a spinner flask

HCT116 cells were cultured for 25 days in a spinner flask. **A)** Trans illumination images and **B)** Volumes of spheroids taken at Days 5, 10, 15, 20 and 25. Scalebar = 1000μm. Data represents means with standard deviation of 3 independent experiments. Experiments were performed in triplicate. **C)** Hoechst 33342 fluorescent Images were taken to confirm the generation of the 3D spheroidal structures at Day 20. Scalebar = 1000μm. **D)** Spheroids were cryoembedded, sectioned and stained with Haematoxylin and Eosin (H&E) dyes. Scalebar = 500μm. Images in this figure are representative of at least 3 independent experiments. See *3.2.5* of Material and Methods for the detailed protocol.

Chapter Five

RESULTS (2) - Photodynamic properties of Hypericin

5 RESULTS (2) - PHOTODYNAMIC PROPERTIES OF HYPERICIN

5.1 Introduction

Photodynamic therapy (PDT) is a cytotoxic treatment that involves the administration of a tumour-retaining photosensitiser followed by light irradiation. As described in detail in Chapter 1, PDT is an effective method for treating cancers, including lung, bladder, head and neck, and skin. Furthermore, PDT can be used in conjunction with other treatments, without interfering with their mechanism of action. In regards to the use of PDT in colorectal cancers (CRC), many clinical and pre-clinical studies over the past few decades have shown PDT to be effective in inhibiting tumour growth and therefore making cancers more manageable. Many different classes of photosensitisers i.e. porphyrins, chlorins and phthalocyanines, have been investigated and generally show promising results for clinical application (Dolmans et al., 2003; Dos Santos et al., 2019).

Hypericin is the photosensitising agent that will primarily be investigated in this research project. Aside from its wide traditional medicinal applications, especially as an anti-depressant, hypericin has become widely recognised as a potent natural photosensitiser in anti-cancer PDT and photodiagnosis (Jendželovská et al., 2016). Unlike other well-known and established photosensitisers, hypericin does not belong to one of the traditional classes of photosensitisers. As highlighted in Chapter 1, pre-clinical studies have been

conducted, which investigated the phototoxicity of hypericin in *in vitro* models of CRC. However, many of these investigations relied on simple 2D monolayered cancer models. As described in Chapters 1, and explored in Chapter 4, 3D spheroidal models are increasingly being recognised as better representations of *in vivo* tumours, as compared to traditional monolayer cell cultures. This chapter aims to build upon previous findings and investigate the differences between 2D and 3D models in response to hypericin-PDT. This chapter will also look at the role played by the multidrug resistance protein, ABCG2, in influencing the responses in 2D and 3D models of CRC to hypericin-PDT.

5.2 Methods

2D monolayer and 3D spheroidal models of HT29 and HCT116 were treated with hypericin for 16h, followed by a light treatment of $1J/cm^2$ at 590nm. Hypericin mediated PDT cytotoxicity was evaluated, using the trypan blue assay, fluorescent imaging and through quantifying propidium iodide fluorescence. 3D spheroids were treated with hypericin for 16h, embedded, sectioned and fluorescently imaged to visualise the penetration of the photosensitiser through spheroids. ABCG2 protein was detected and semi-quantified using western blotting and immunofluorescence assays. Details of methods are described in *3.3* and *3.4*.

5.3 Results

5.3.1 PDT lightbox and light mediated activation of Hypericin

A custom lightbox (described in *3.3.3*) was manufactured for *in vitro* PDT experiments, with an average light fluency rate of $230\mu W/cm^2$ at 590nm

(Figures 5.1). The peak wavelength of light absorption for hypericin was found to be 590nm, which coincides with the peak wavelength of light emission from the lightbox (Figure 5.1C).

A) A custom lightbox was manufactured for conducting the *in vitro* hypericin-PDT experiments. Cells are seeded into culturing plates, treated with hypericin for 16 hours and placed on top of the lightbox. **B)** The output of light at 590nm from the lightbox was measured, and used to calculate the light dose. **C)** The peak wavelengths of light emission and absorption were mapped out for the lightbox and hypericin respectively. **D)** Calculations for determining the duration of light treatment using the lightbox. See *3.3.2* and *3.3.3* of Material and Methods for the detailed protocol.

Figure 5.1 – Source of light for Hypericin-PDT

D)
1) $J/cm^2 = W/cm^2 \times seconds$

2) $1J/cm^2 = 0.00023W/cm^2 \times seconds$

3) $Seconds = \dfrac{1J/cm^2}{0.00023W/cm^2} = 4348$ **(72mins & 28 secs)**

5.3.2 Continuous operation of the lightbox to evaluate reliability

The lightbox was further characterised, specifically for its feasibility and reliability to radiate light consistently for prolonged periods of time. As shown in Figure 5.2, the lightbox was ran continuously for 4 hours and the operating temperature at the light diffuser surface remained stable between 20-23°C (ambient room temperature) for the entire duration of its operation (Figure 5.2A). During this period, light fluency rates also remained stable between 230-233µW/cm^2 at the light diffuser surface (Figure 5.2B).
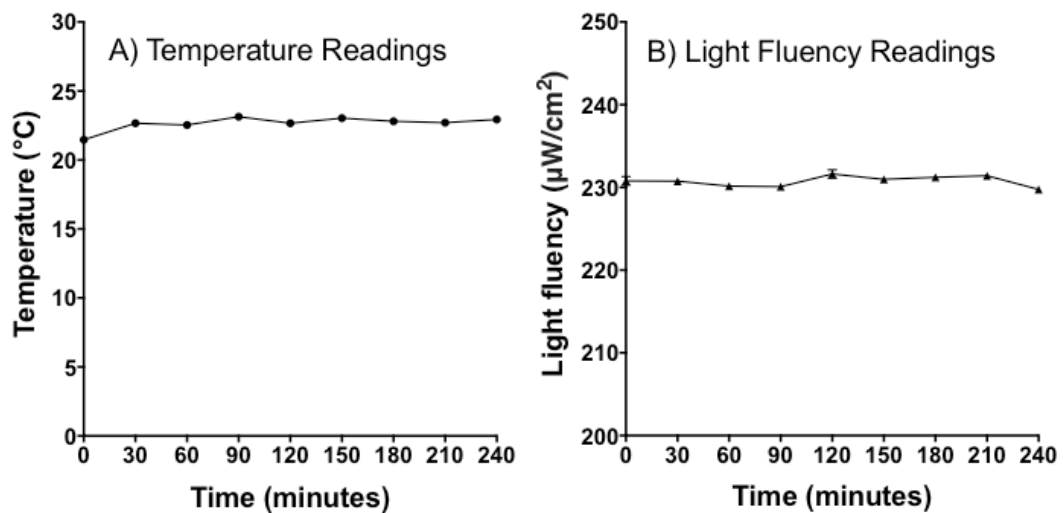
Figure 5.2 - Assessing the reliability of the lightbox

The light radiating device/lightbox was switched on and left to run continuously at ambient room temperature for 240 minutes (4 hours). A) The operating temperature on the light diffuser surface and B) light fluency rate was monitored and recorded at 30-minute intervals. Data represents means with standard deviation of 3 independent experiments. Experiments were performed in triplicate. See *3.3.3* and *3.3.4* of Material and Methods for the detailed protocol.

5.3.3 Light dependant cytotoxicity of Hypericin

To highlight the light dependant cytotoxicity of hypericin, HT29, HCT116, Caco2 and HFFF2 cell lines were treated with varying concentrations of hypericin and then treated with light or kept in the dark (Figure 5.3). 1J/cm^2 of light and

hypericin dose dependant cytotoxicity was observed in all cell lines. Cell viability decreased with increasing concentrations of hypericin and 1J/cm^2 of light as compared to light only treated controls (200nM hypericin: HT29 77% reduction in cell viability, p=0.0002, HCT116 91% reduction in cell viability, p<0.0001, Caco2 73% reduction in cell viability, p=0.0006, HFFF2 86% reduction in cell viability, p=0.0002). However, cell cultures treated with hypericin and subsequently kept in the dark, did not respond to treatment as indicated by negligible reduction in cell viability with increasing concentrations of hypericin as compared to untreated controls (200nM hypericin: HT29 1.6% reduction in cell viability, p=0.75, HCT116 1.9% reduction in cell viability, p=0.73, Caco2 3% reduction in cell viability, p=0.36, HFFF2 4.5% reduction in cell viability, p=0.68). The HT29, HCT116 and Caco2 cell lines were selected as they represent three different grades and stages of colorectal carcinomas (Figures 5.3A, 5.3B and 5.3C). PDT does not specifically target cancer cells and does not discriminate between different cell types. To highlight this, the normal fibroblast cell line, HFFF2, was also treated with hypericin-PDT and was found to respond to treatment by exhibiting significant cell death (Figures 5.3D).

Similarly, HT29 and HCT116 spheroids treated with hypericin and then kept in the dark were viable at 200nM hypericin, as indicated by the lack of uptake of propidium iodide. Spheroids treated with hypericin and then irradiated with light, responded to treatment as indicated by the increasing uptake of propidium iodide (Figure 5.4). HT29 and HCT116 cell lines were chosen to generate 3D spheroids, as both cell lines are able to successfully produce spheroids with a high rate of success (see Chapter 4). Caco2 cells have previously been

described to be difficult to use when preparing spheroids and fail to produce compact 3D structures (Hoffmann et al., 2015).

For the hypericin-PDT experiments conducted in this research project, the concentrations of hypericin I used ranged from 0 – 200nM. As shown in Figure 5.3, a dose-dependent response is observed in all four cell lines and the IC_{50} values (a crucial indicator of the efficacy of treatment) can be determined. IC_{50} values: HT29 = 88nM, HCT116 = 30nM, Caco2 = 165nM, HFFF2 = 45nM. Cell viability of all four cell lines decreased with increasing concentrations of Hypericin. At 200nM Hypericin, cell viability is around 20% in all cell lines (Figure 5.3). A previous study by Mikes *et al.* (2007) evaluated hypericin-PDT in HT29 cells under variable light doses and concentrations of hypericin (Mikes et al., 2007). Similar to the results shown in Figure 5.3, this study found a hypericin dose-dependent reduction in cell viability between 0 – 200nM hypericin. The authors additionally show that increasing the concentration of hypericin to 300nM and 400nM did not result in increased cytotoxicity. Cell viability was found to plateau at 20% between 200nM – 400nM hypericin. This study shows 0 – 200nM hypericin to be the most effective therapeutic range for PDT. Subsequent studies investigating hypericin-PDT have also described using 0 – 200nM hypericin for their experiments (Mikes et al., 2009; Jendzelovsky et al., 2009; Mikeš et al., 2011; Šemeláková et al., 2012; Jendželovská et al., 2014; Kuchárová et al., 2015; Šemeláková et al., 2016; Jendželovský et al., 2019).
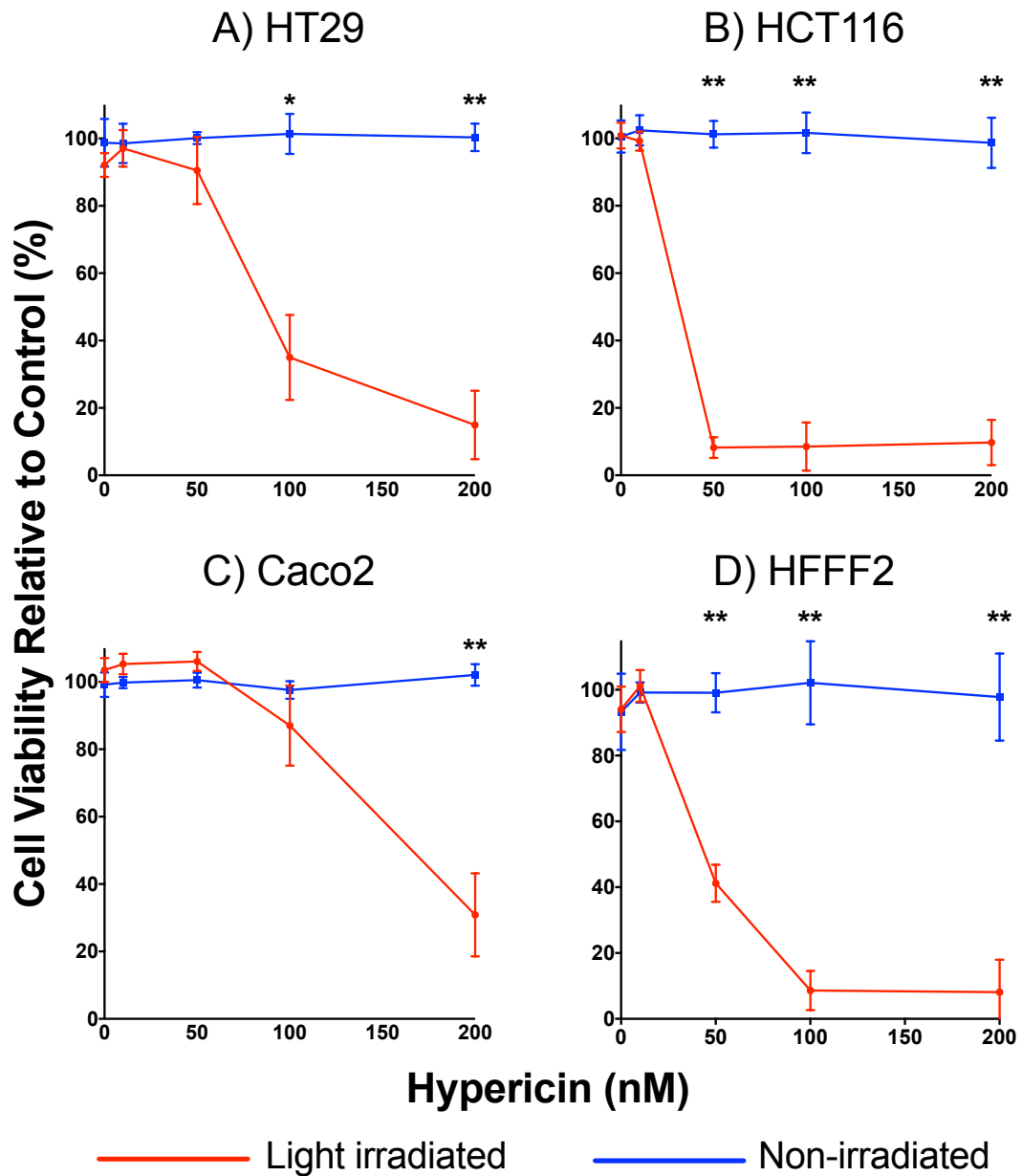
Figure 5.3 – Light-dependent cytotoxicity of Hypericin in 2D cultures

A) HT29 **B)** HCT116 **C)** Caco2 and **D)** HFFF2 cell cultures were treated with hypericin and treated with light (1J/cm^2) or kept in the dark. After 24 hours, cell viability was assessed using the Trypan blue dye exclusion assay. Data are shown relative to control treated cultures and represent means with standard deviation of 3 independent experiments. Experiments were performed in triplicate. *$p<0.005$, **$p<0.001$. See *3.3.5* and *3.3.7* of Material and Methods for the detailed protocol.
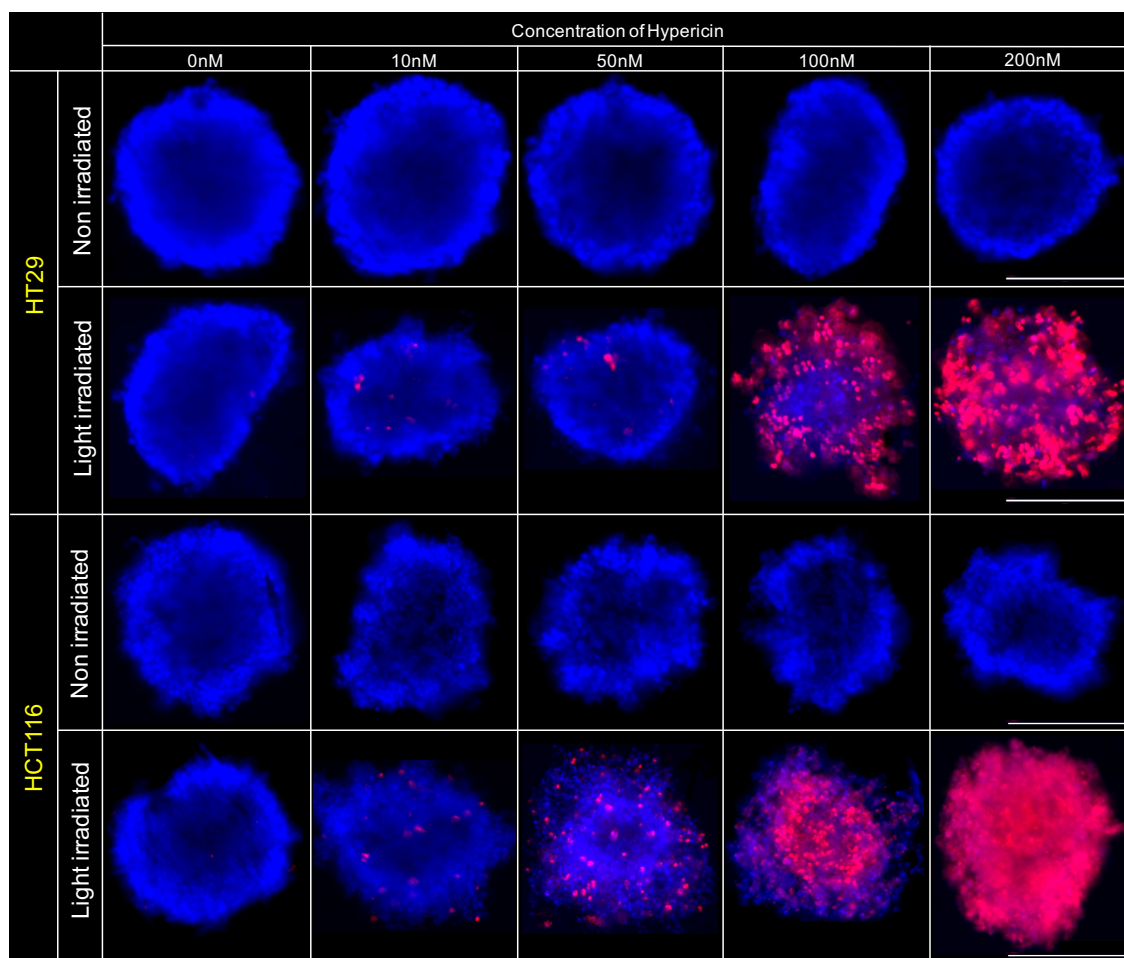
Figure 5.4 – Light-dependent cytotoxicity of Hypericin in 3D spheroids

HT29 and HCT116 cell line spheroids were cultured on 1% agarose-coated plates for 48 hours. Spheroids were then subjected to hypericin-PDT. After 24 hours, spheroids were stained with Hoechst 33342 (Blue) and propidium iodide (Red) and fluorescently imaged. Scalebar = 400µm. Images in this figure are representative of at least 3 independent experiments. See *3.3.5* and *3.3.7* of Material and Methods for the detailed protocol.

5.3.4 Hypericin-PDT in 2D and 3D models

The response to hypericin-PDT between 2D monolayer and 3D spheroid models of HT29 and HCT116 cell lines was evaluated. As highlighted in Figure 5.5, HT29 and HCT116 3D spheroids were significantly more resistant to hypericin as compared to their 2D monolayer counterparts (100nM hypericin: HT29 spheroids 35% more viable, $p<0.0001$ and HCT116 spheroids are 32% more viable, $p=0.01$).
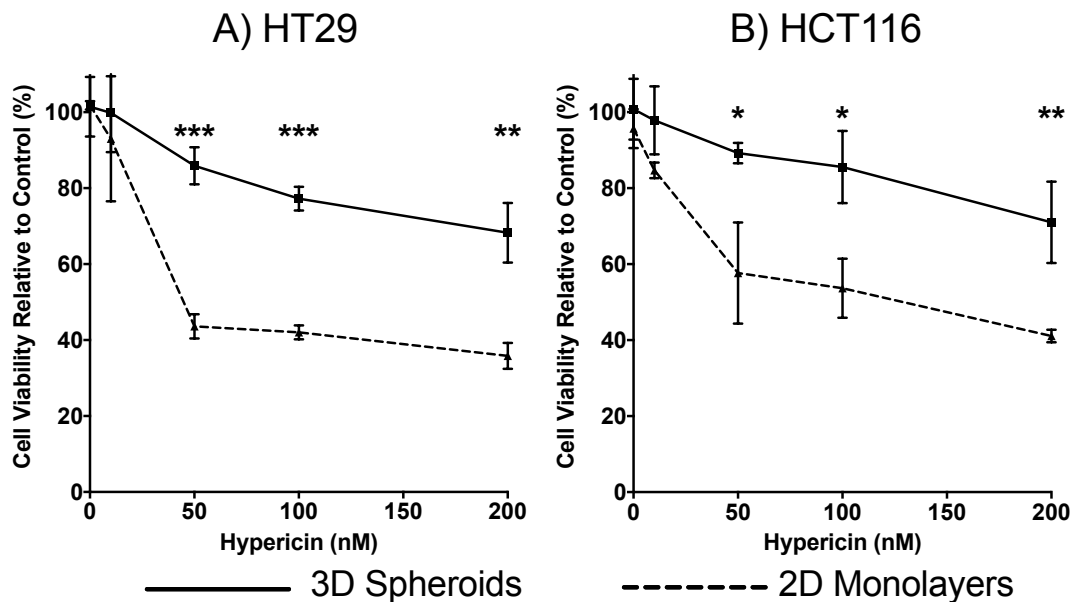
Figure 5.5 – Differences in response to Hypericin-PDT between 3D and 2D models

A) HT29 and **B)** HCT116 3D spheroids and 2D monolayers were subjected to hypericin-PDT. After 24 hours, cultures were treated with propidium iodide and fluorescence was quantified, correlating to cell viability. Data are shown relative to control treated cultures and represent means with standard deviation of 3 independent experiments. Experiments were performed in triplicate. *$p<0.05$, **$p<0.01$, ***$p<0.001$. See *3.3.5* and *3.3.7* of Material and Methods for the detailed protocol.

A limitation of the experiments comparing responses to hypericin-PDT between 2D and 3D models in this research project, was not utilising the trypan blue assay to validate the findings shown in Figure 5.5. Propidium iodide fluorescence was quantified to determine cell viability for 2D and 3D models (Figure 5.5) and the trypan blue assay was used for results shown in Figure 5.3. The trypan blue assay involves the uptake of the trypan blue dye, into cells with damaged plasma membranes i.e. dead cells. The dye would then irreversibly stain intracellular organelles. Staining 2D cell cultures is straightforward, whereas staining 3D spheroids would first involve disrupting and breaking up the 3D structure, prior to the addition of the dye (Piccinini et al., 2017).

5.3.5 The expression of ABCG2 in 2D and 3D models of CRC

The expression of the ATP-binding cassette (ABC) transporter, ABCG2, was evaluated in 2D monolayer and 3D spheroid models of HT29 and HCT116 cell lines. The expression and cellular location of the ABCG2 protein was predominantly found at the cellular membrane (Figure 5.6A and 5.6B). In the 3D spheroids, ABCG2 was found to be differentially expressed throughout the spheroidal structure. The outer layers of cells in the spheroids were found to be highly expressing ABCG2 as compared to the inner central mass of cells (Figure 5.6C and 5.6D).

Western blot analysis was conducted to semi-quantify the expression of the ABCG2 protein in 2D and 3D models of HT29 and HCT116. As shown in Figure 5.7, a reduction in expression of the ABCG2 protein was observed in 2D monolayer cultures as compared to the 3D spheroidal cultures for both HT29 and HCT116.
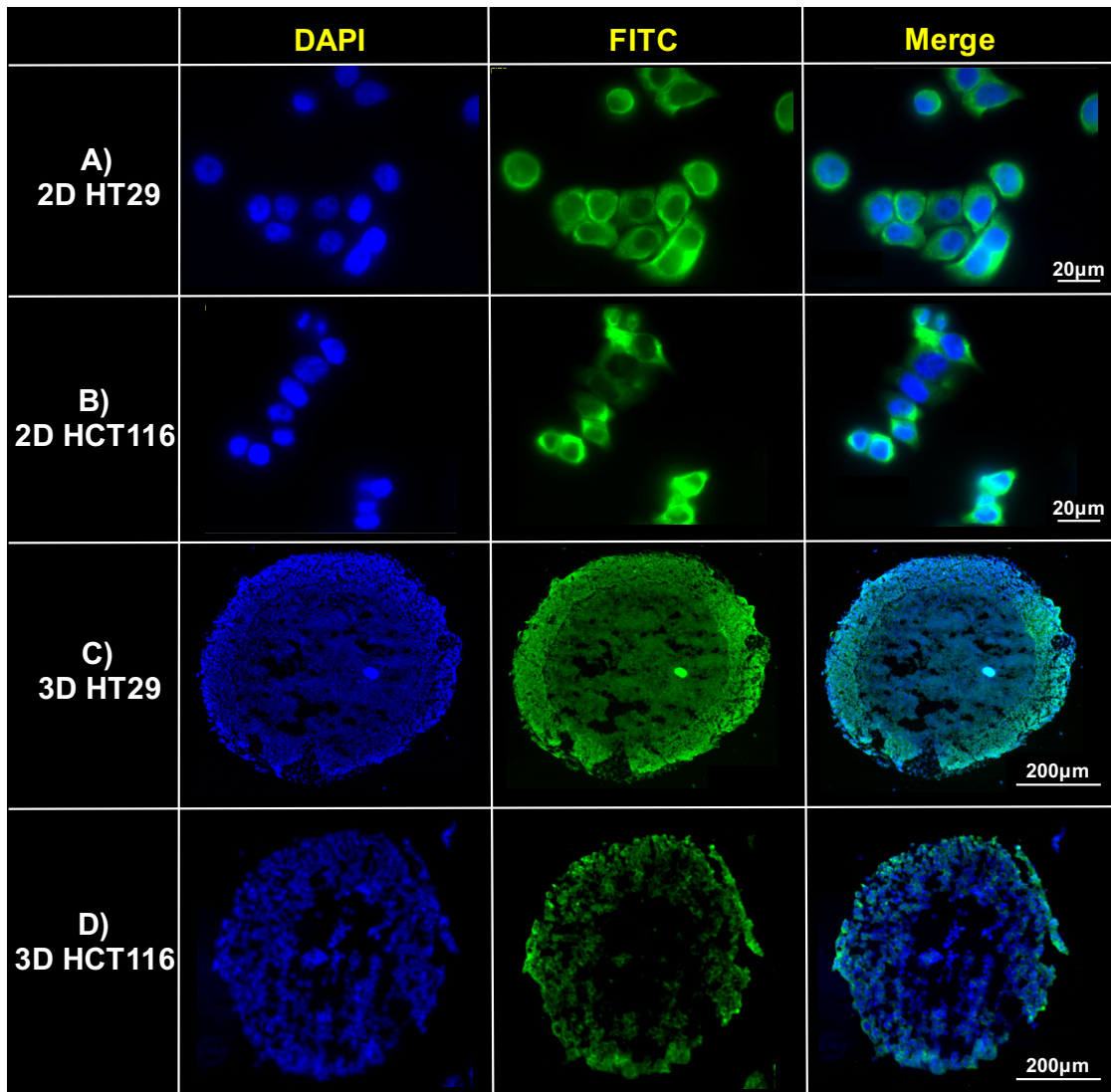
Figure 5.6 – ABCG2 protein expression in 3D and 2D models (1)

A) 2D HT29 **B)** 2D HCT116 **C)** 3D HT29 spinner flask spheroids and **D)** 3D HCT116 spinner flask spheroids were sectioned, fixed in 4% paraformaldehyde, blocked with 0.5% skimmed milk and incubated with a primary anti-BCRP (ABCG2) monoclonal antibody (1:200) at room temperature for 1 hour. Slides were then incubated with secondary Alexa Fluor 488 antibody (Green) (1:300) for 30 minutes at room temperature and mounted with DAPI (Blue). Slides were imaged using fluorescent microscopy. Images in this figure are representative of at least 3 independent experiments. See *3.4.2* of Material and Methods for the detailed protocol.
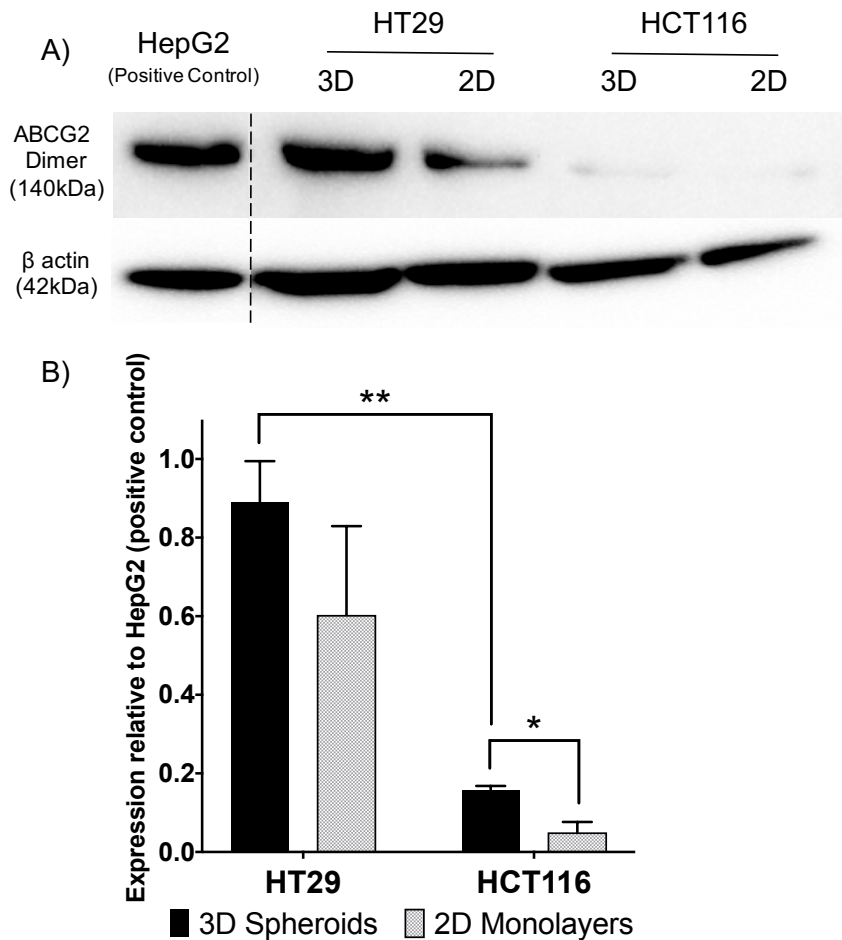
Figure 5.7 – ABCG2 protein expression in 3D and 2D models (2)

A) Western blot analysis and **B)** Semi-quantification of ABCG2 in protein extracts from 3D spheroid and 2D models of HT29 and HCT116 (HepG2 cell lysates served as positive control). 10μg of protein lysates per sample was loaded into and resolved on 12% Bis-Tris gel in SDS running buffer for 90 minutes at 180 volts. Resolved proteins were transferred onto methanol activated PVDF membrane in transfer buffer for 90 minutes at 30 volts. Membranes were blocked using 5% and then 1% skimmed milk for 30 minutes each. Membranes were incubated with anti-BCRP (ABCG2) monoclonal primary antibody (1:200) overnight at 4°C and then incubated with horseradish peroxidase-conjugated polyclonal secondary antibody (1:2000) for 1 hour at room temperature. Protein bands were developed using chemiluminescent substrates and imaged. β-actin served as the protein loading control. Data are shown relative to the protein expression of ABCG2 in HepG2 lysates and represent means with SD of 3 independent experiments. Experiments were performed in triplicate. *$p<0.005$, **$p<0.0005$. Western blot image in this figure is representative of at least 3 independent experiments. See *3.4.1* of Material and Methods for the detailed protocol.

5.3.6 The effect of ABCG2 inhibition on Hypericin-PDT

Monolayer and spheroidal models of HT29 and HCT116 cell lines were co-treated with 10µM Ko143 (ABCG2 inhibitor) and then subjected to hypericin-PDT. In 2D monolayer cell cultures, Ko143 and hypericin-PDT co-treated HT29 cultures were found to be significantly more sensitive to treatment, as compared to hypericin-PDT alone treated HT29 cell cultures (10nM hypericin: 38% decrease in cell viability, p=0.02). Additionally, with increasing concentrations of hypericin, co-treated 2D HT29 cells showed a dose dependant reduction in cell viability. However, at higher concentrations of hypericin, the differences in cell viability between co-treated and hypericin-PDT alone treated cultures had diminished (Figure 5.8A). No significant difference was observed between co-treated and hypericin-PDT alone treated 2D HCT116 cell cultures (p=0.94) (Figure 5.8B). In 3D spheroid cell cultures, a significant difference in sensitivity to treatment between co-treated and hypericin-PDT alone treated cultures was observed in both HT29 and HCT116 spheroidal cultures (100nM hypericin: co-treated HT29 spheroids 11% less viable, p=0.01 and co-treated HCT116 spheroids 9% less viable, p=0.02) (Figure 5.8C and 5.8D). Unlike 2D cultures, the effect of Ko143 on both HT29 and HCT116 spheroid viability was still apparent at higher doses of hypericin-PDT.
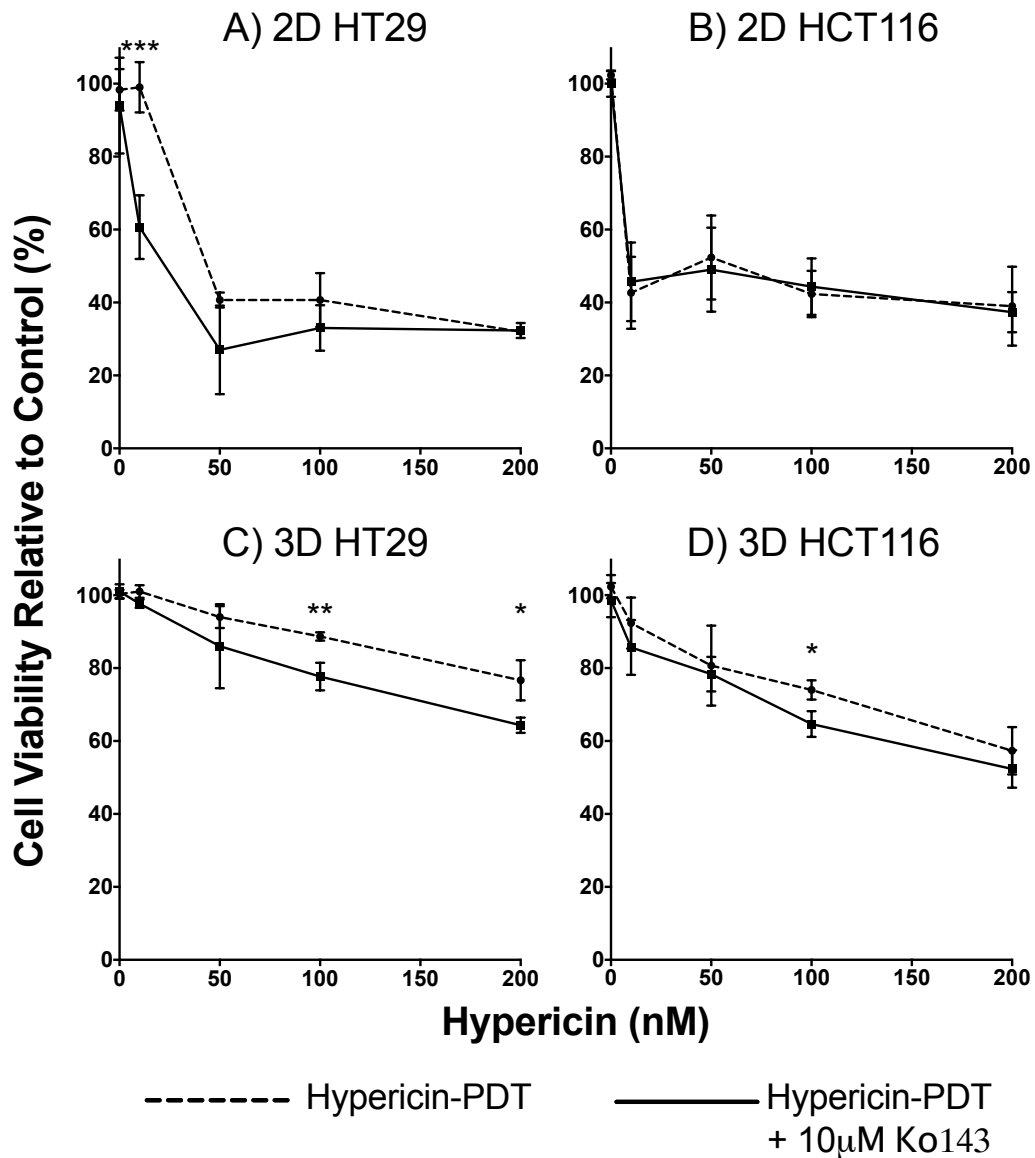
Figure 5.8 – The effect of Ko143 on Hypericin-PDT in 3D and 2D models

A) 2D HT29 and **B)** 2D HCT116 cell cultures were generated by seeding cells into 96-well plates at 5×10^3 cells per well and cultured for 2 days. **C)** HT29 spheroid and **D)** HCT116 spheroid cultures were generated by seeding cells into 1% agarose-coated 96-well plates at 5×10^2 cells per well and cultured for 2 days. Cell cultures were treated with 10µM Ko143 for 90 minutes and then co-treated with varying concentrations (0-200nM) of Hypericin or treated with Hypericin alone in the dark for an additional 16 hours. Cultures were then irradiated with light at 1J/cm². After 24 hours, cultures were stained with propidium Iodide for 15 minutes and fluorescence was quantified using a microplate reader (Ex: 540nm, Em: 620nm). Data are shown relative to control treated cultures and represent means with SD of 3 independent experiments. Experiments were performed in triplicate. *$p<0.05$, **$p<0.01$, ***$p<0.005$. See *3.3.5*, *3.3.6* and *3.3.7* of Material and Methods for the detailed protocol.

Different studies have evaluated the effect of Ko143 on ABCG2 activity and the intracellular retention of photosensitisers. Jonker *et al.* (2002) was the first to show that 10µM Ko143 significantly antagonised, the efflux pump activity of ABCG2 in eliminating different photosensitisers from cells (Jonker et al., 2002). Since then other studies have reported the use of Ko143, with concentrations around 10µM. Due to this, 10µM Ko143 was chosen for PDT experiments with the inhibition of ABCG2 activity (Šemeláková et al., 2016; Abdel Gaber et al., 2018). As shown in Figure 5.8, 10µM Ko143 was found to improve hypericin-PDT, specifically in 3D and 2D HT29 cell cultures, where the protein expression of levels of ABCG2 were found to be high (Figure 5.7).

5.3.7 Distribution of Hypericin in 3D spheroids

HT29 and HCT116 3D spheroids were treated with 200nM hypericin and the diffusion of hypericin was found to extend through to the core of both HT29 and HCT116 spheroids (Figure 5.9). HT29 spheroids exhibited a higher expression of the ABCG2 protein as compared to HCT116 spheroids. This is highlighted by the expression of ABCG2 in the thicker outer layers of cells in HT29 spheroids (Figure 5.6C and 5.6D) and also overall ABCG2 protein levels (Figure 5.9). This corresponds with the cell uptake and distribution of hypericin through spheroids, as hypericin was more prominently observed in the outer layers of HCT116 spheroids as compared to HT29 spheroids (Figure 5.9).
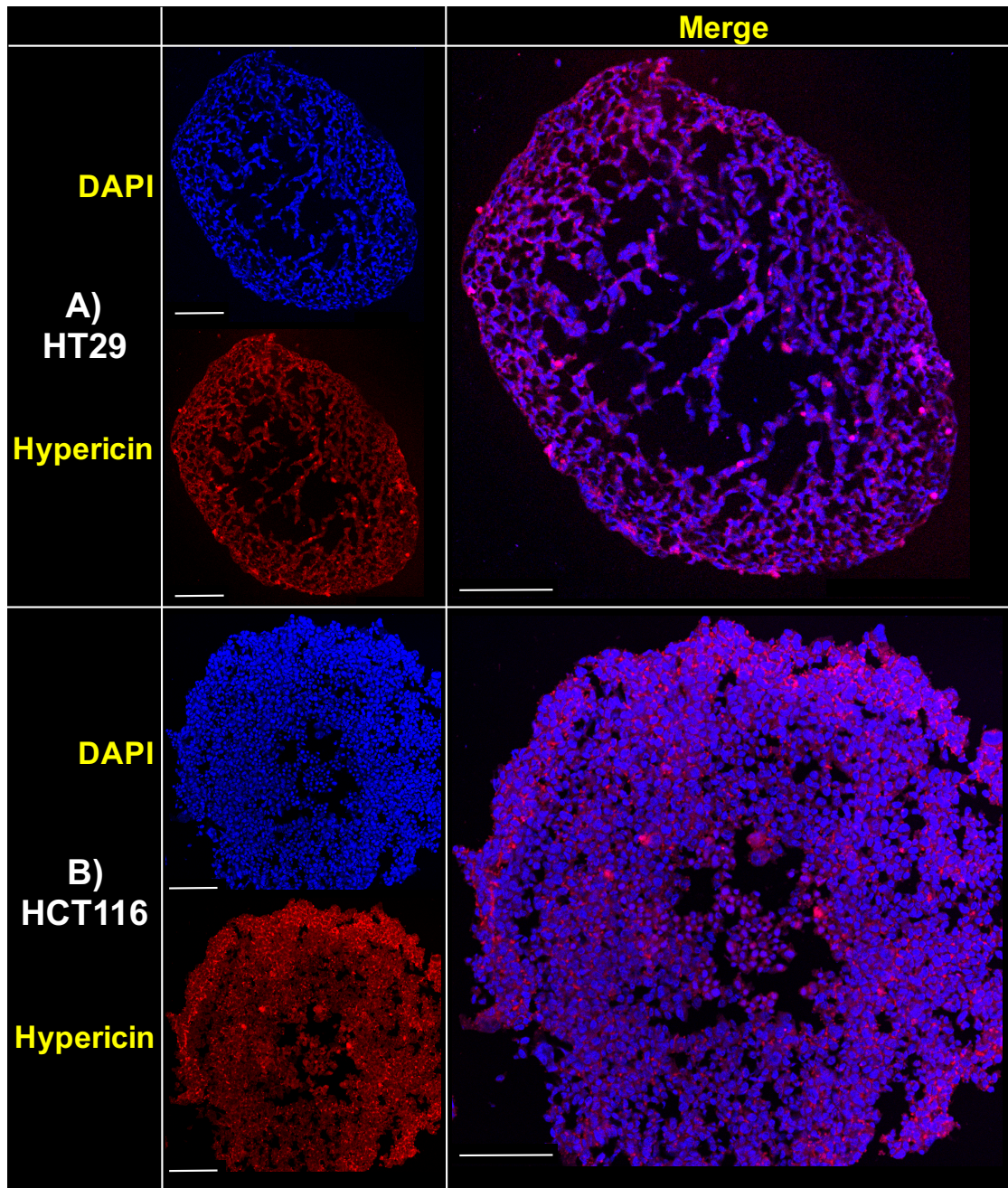
Figure 5.9 – Penetration of Hypericin through multicellular spheroids

A) HT29 and **B)** HCT116 spinner flask spheroids were incubated with 200nM Hypericin (Red) for 16 hours in the dark. Spheroids were then fixed in OCT, sectioned, mounted with DAPI (Blue) and fluorescently imaged. Scalebar = 100µm. Images in this figure are representative of at least 3 independent experiments. See *3.3.8* of Material and Methods for the detailed protocol.

5.3.8 Prolonged culture of spheroids following ABCG2 inhibition and Hypericin-PDT

Spheroids were subjected to ABCG2 inhibition and hypericin-PDT and then cultured for an additional 10 days. As shown in Figure 5.10, both HT29 and HCT116 spheroids started to regrow by Day 4 and continued to increase in volume. By day 10, Ko143 and 200nM hypericin co-treated spheroids were significantly larger as compared to the sizes of spheroids on day 0 (HT29 spheroids: $0.22mm^3$ increased volume, $p<0.005$ and HCT116 spheroids: $0.44mm^3$ increased volume, $p<0.02$). One day after PDT, cytotoxicity was observed in spheroids as indicated by the loose cellular debris and loss of compact spheroidal structure in HT29 and HCT116 spheroids co-treated with $10\mu M$ Ko143 and 200nM hypericin. By day 4, spheroids had re-formed their compact structure and continued to increase in volume (Figure 5.11A). Fluorescent imaging confirmed the presence of no dead cells in the spheroids as indicated by the lack of propidium iodide fluorescence (Figure 5.11B).

Following the initial growth phase, the rate at which 3D spheroids grow would eventually slow down. At this stage, the spheroid is postulated to be fully mature and will stop growing in size. Mature 3D spheroids comprise of three distinct layers of cells. The outer layers of cells consist of actively proliferating cells, with secondary layers of metabolically inactive quiescent cells and necrotic cells in the central core. Following hypericin-PDT, cell death would primarily be localised to the outer layers of proliferating cells, that would shed off as cellular debris (Figure 5.11A). This would allow oxygen and nutrients in the cell media to diffuse through to the quiescent cells and stimulate these cells to re-enter cell

growth by switching to an active state of metabolic activity and subsequently regrow and reform the structure of the 3D spheroid (Wallace and Guo, 2013).
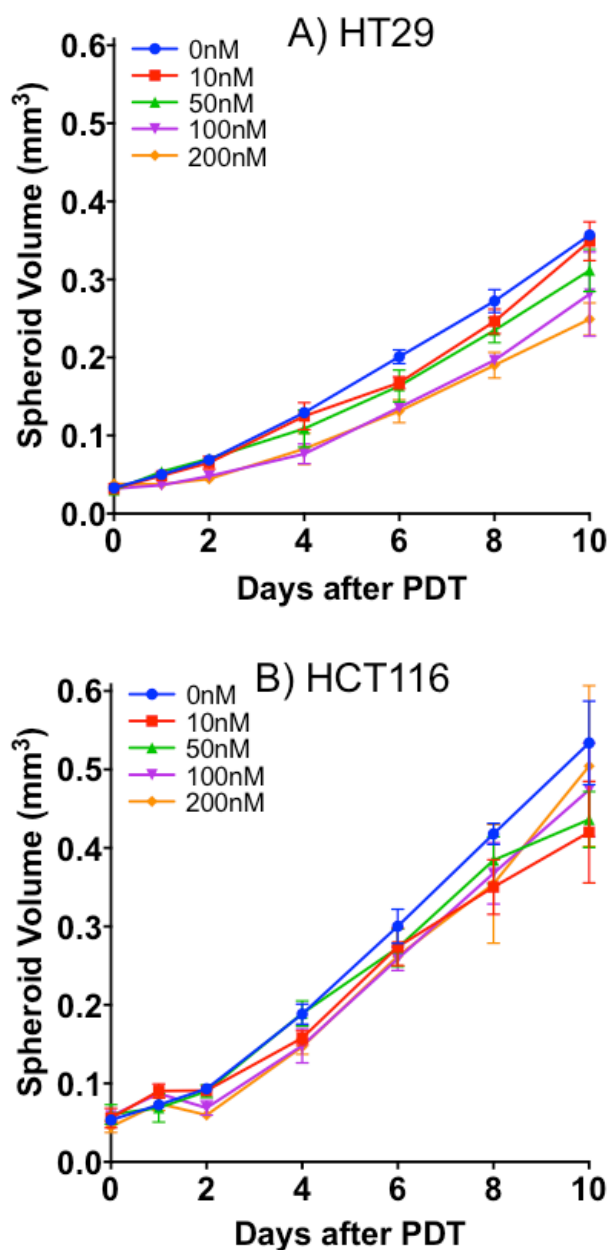
Figure 5.10 – Prolonged culture of 3D spheroids following Ko143 and Hypericin-PDT co-treatment (1)

A) HT29 and **B)** HCT116 3D spheroids were co-incubated with 10µM Ko143 and varying concentrations of hypericin and irradiated with light. Measurements of spheroid volume were taken over 10 days after PDT. Data are shown relative to control treated cultures and represent means with SD of 3 independent experiments. Experiments were performed in triplicate. See *3.3.9* of Material and Methods for the detailed protocol.
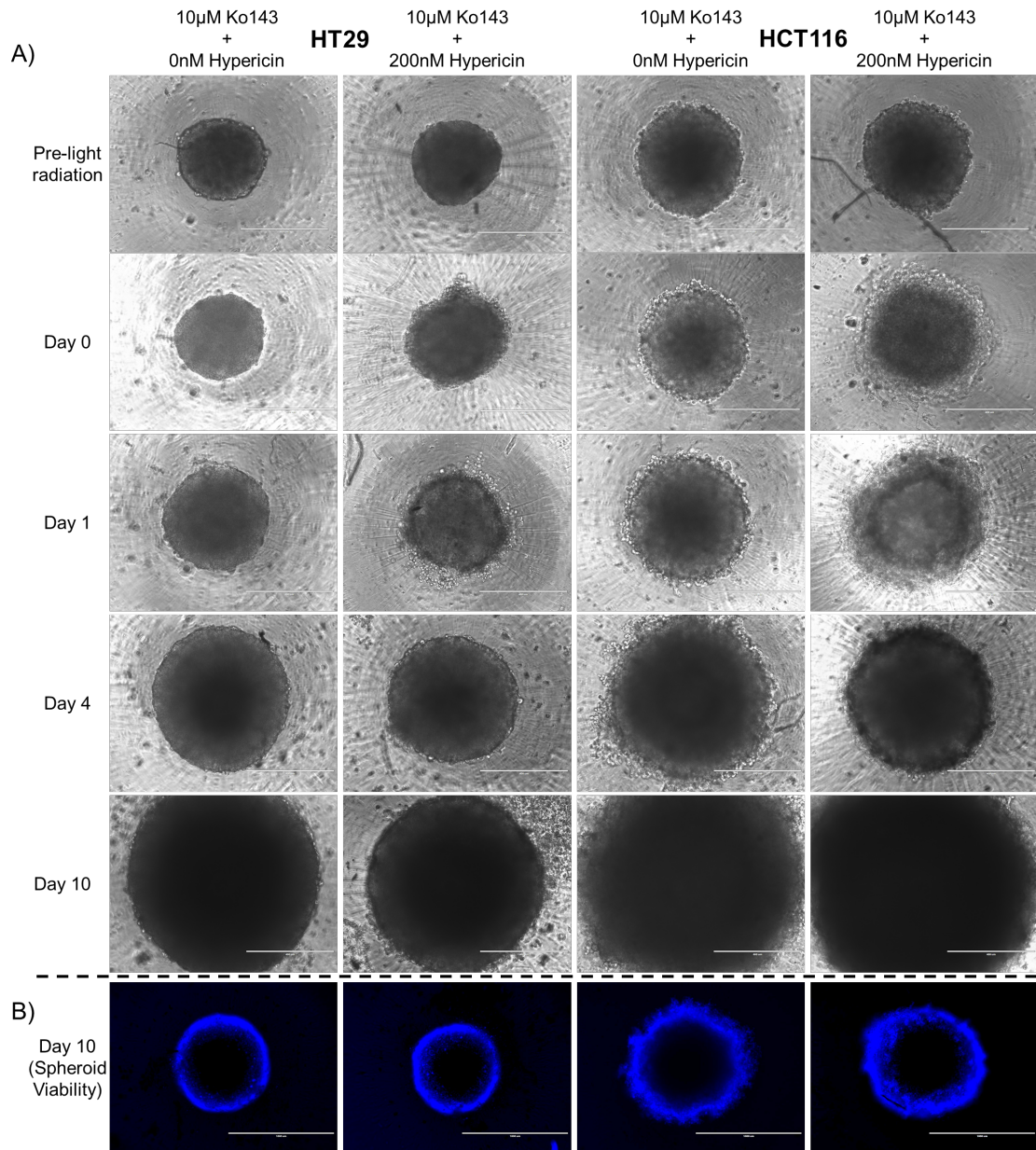
Figure 5.11 – Prolonged culture of 3D spheroids following Ko143 and Hypericin-PDT co-treatment (2)

A) HT29 and HCT116 3D spheroids were co-incubated with 10µM Ko143 and hypericin (0nM and 200nM) and irradiated with light. Transillumination images of spheroids were taken pre-light radiation and also at days 0, 1, 4 and 10. Scalebar = 400µm. **B)** On Day 10, HT29 and HCT116 3D spheroids were stained with Hoechst 33342 (Blue) and propidium iodide (Red) and fluorescently imaged. Scalebar = 1000µm. Images in this figure are representative of at least 3 independent experiments. See *3.3.9* of Material and Methods for the detailed protocol.

Chapter Six

RESULTS (3) – The Development of a Microfluidic Device for 3D Cell Culture

6 RESULTS (3) - THE DEVELOPMENT OF A MICROFLUIDIC DEVICE FOR 3D CELL CULTURE

6.1 Introduction

The need for newer and better i*n vitro* models of cancer is essential in order to advance our understanding of basic cancer biology and to reduce the reliance on *in vivo* animal models. As described in Chapters 1 and 4, and demonstrated in Chapter 5, 3D spheroidal *in vitro* cell models are recognised as better models than 2D cell cultures for the pre-clinical evaluation of anti-cancer treatments (Breslin and O'Driscoll, 2013; Ishiguro et al., 2017). Similar to *in vivo* cancers, 3D spheroids possess a layered spatial arrangement of cells with differing rates of cell proliferation, unsynchronised cell cycles and physiologically relevant gradients of oxygen, nutrients and waste products (Ludwig et al., 2013; Edmondson et al., 2014). Spheroids also offer a more clinically accurate response to treatment, as compared to the unnatural responses observed in traditional 2D monolayer cell cultures.

In Chapter 4, various 3D cell culturing techniques were evaluated in order to identify the best method for evaluating anti-cancer therapies. All the 3D spheroid culturing techniques share similar limitations, namely the cost and manual labour involved, with experiments requiring a few days to setup up the culture 3D spheroids prior to investigation. On the other hand, commercial

spheroid culturing plates are readily available, however, they can be expensive, particularly when large numbers of experiments are performed. Manually preparing spheroids using conventional cell culturing equipment, can be time-consuming and can often be difficult to carry out without experience (Costa et al., 2018).

Microfluidics is the concept whereby conventional macroscale laboratory experiments are scaled down and conducted on custom manufactured platforms. This is achieved by accurately directing the flow of fluid on a micro- and nanoscale through the microfluidic device in order to complete a desired effect e.g. treating cells with a drug. In the past decade, there has been growing interest in combining conventional 3D cell culturing and microfluidics in an effort to address the limitations associated with 3D spheroid culturing techniques (Young and Beebe, 2010; Sackmann et al., 2014). This chapter looks at the development of a microfluidic device, which can be used to culture, treat and evaluate 3D spheroids.

6.2 Methods

Schematic designs for the microfluidic devices were drawn in Solidworks and manufactured using various materials. Manufacturing details are described in *3.5*. HT29 cells were used to generate 3D spheroids in the 'version 3' microfluidic device (see *3.5.3.2* and *3.5.3.3*). HT29 spheroids were generated on chip, treated with 5-FU and cytotoxicity was evaluated using fluorescent imaging and the LDH assay. A single-syringe pump was used to drive fluid flow through the microfluidic device. Details of the microfluidic experiments are described in *3.6*.

6.3 Results

6.3.1 Version 1

Microfluidic platforms for culturing and analysing 3D spheroids have evolved from existing 3D cell culturing methods by incorporating a fluid flow element. As depicted in Chapter 4, the hanging drop technique is one the simplest and most convenient methods for generating spheroids. Therefore, this technique was chosen as the basis for designing the 'version 1' microfluidic device (Figure 6.1). The design incorporated 5 interconnected wells with two ports on either side of the interconnected wells to allow fluids to flow through the wells. Cells in suspension would be flowed through and droplets form in the wells, forming cell aggregates and eventually spheroids (Figure 6.2). As seen in Video 1 and highlighted in Figure 6.3, the introduction of fluid through the 'Flow IN' port in 'version 1' resulted in the fluid accumulating in the first well and unable to flow through the interconnecting channel to the rest of wells.

Due to the difficulties and failure in generating seamless fluid flow and hanging drops through the 'version 1' microfluidic device, further work on the 'version 1' microfluidic device was discontinued.
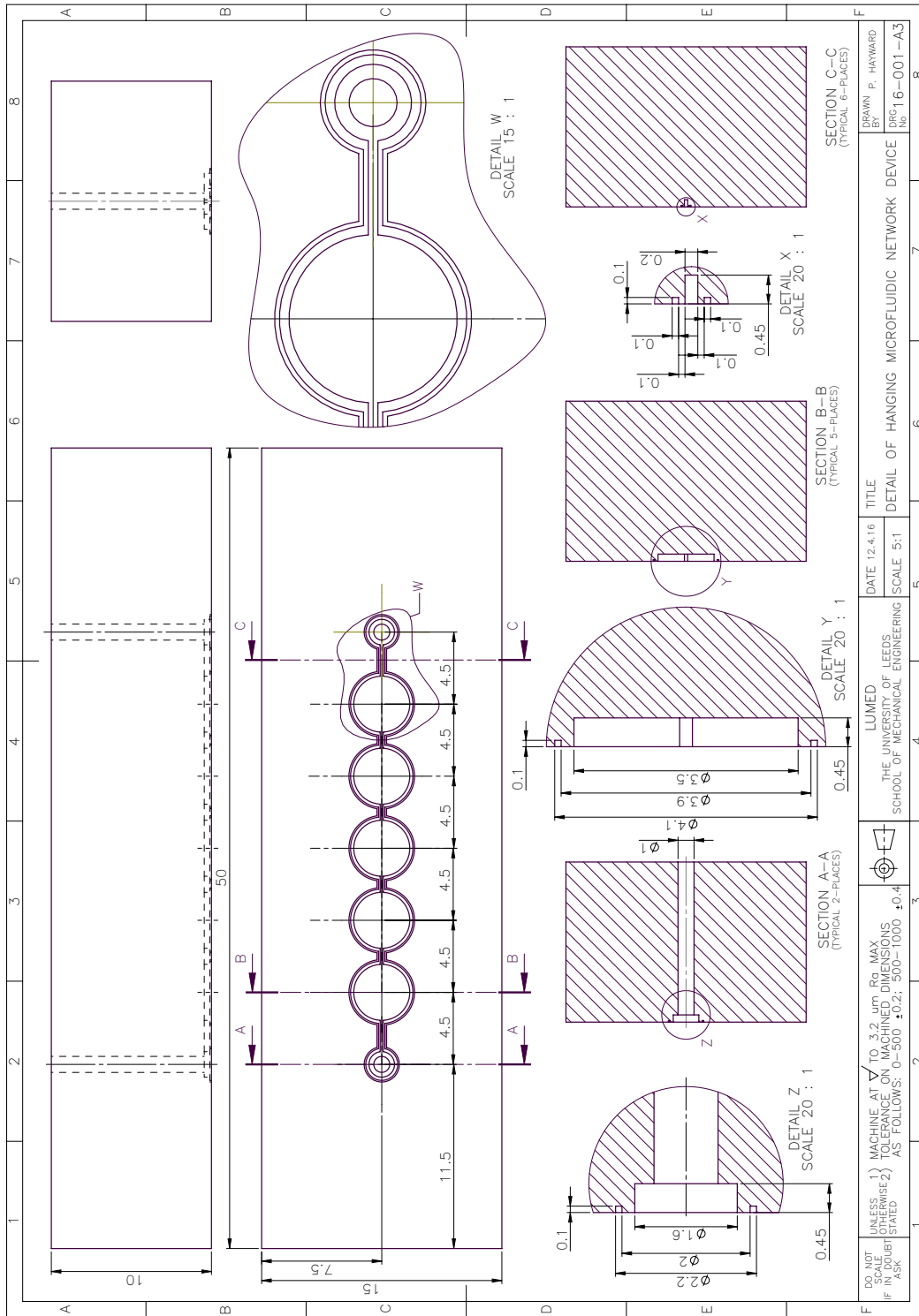
Figure 6.1 – Designing the Hanging drop Version 1 microfluidic device

Schematic diagram of the Hanging drop Version 1 microfluidic model. Dimensions are in mm.
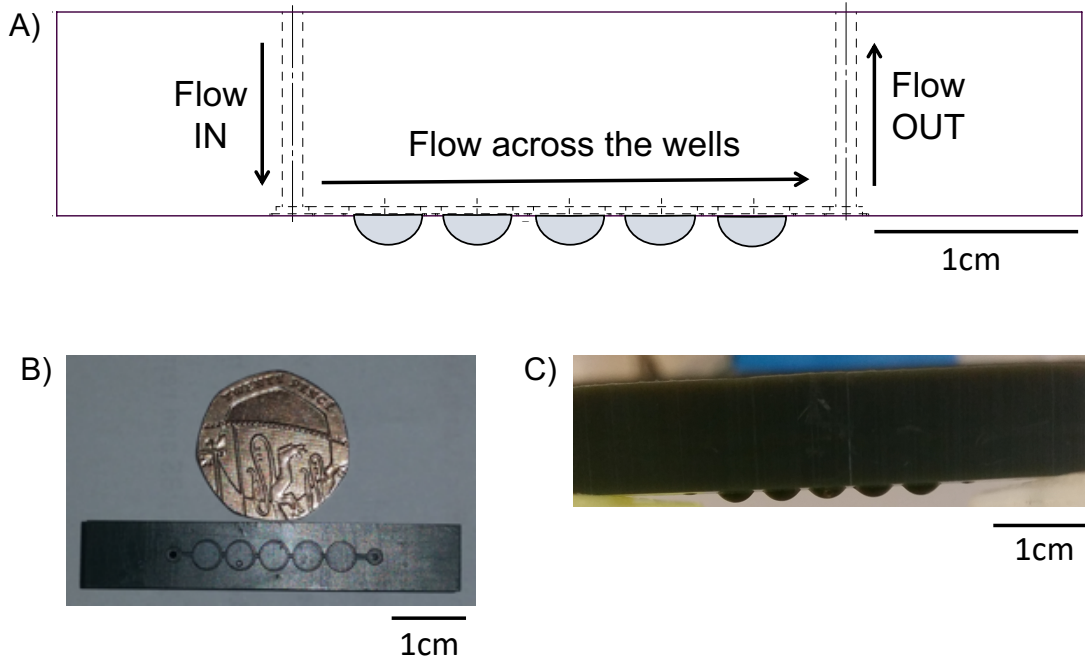
Figure 6.2 – Version 1 microfluidic device

A) The concept behind the Version 1 microfluidic device was to form hanging drops in the wells as fluid passed over the wells. **B)** and **C)** are photographic images of the Version 1 microfluidic device.
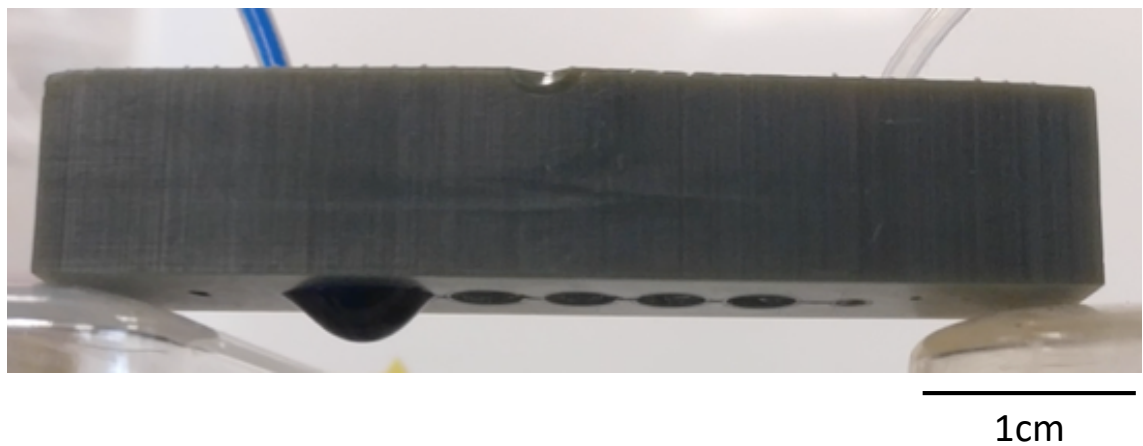
Figure 6.3 - Failure of hanging drops forming in the Version 1 microfluidic device

Fluid was flowed through the inlet port of the 'version 1'microfluidic device. A large droplet was formed at the inlet port opening and fluid accumulated in this droplet and failed to flow through the capillary and interconnected wells to form hanging drops. See *3.5.1.2 o*f Material and Methods for the detailed protocol.

6.3.2 Version 2

In Chapter 4, it was illustrated that the forced-floating method carries many advantages for 3D cell culturing, and was selected as one of the techniques for spheroid-based experiments in this research project. The forced-floating method involves the seeding of cells onto a non-cell adherent substrate. The 'version 2' microfluidic device was designed using the forced-floating method for culturing 3D spheroids and comprised of different layers of material to build a 3D spheroid culturing microfluidic flow platform (Figure 6.4). Sandwiched between the Poly(methyl methacrylate) (PMMA) layers, are two layers of silicone. Silicone was used as it is an established non-cell adherent material (Hauser et al., 2009). The polyimide film, Kapton, was chosen as the central layer in between the upper and lower layers of silicone, due to the ease of cutting with a short wavelength laser and contained the wells for the spheroids (Koren, 1984).

As shown in Video 2, flow of fluid through the inlet port resulted in fluid flowing over the wells and exiting through the outlet port (Figure 6.4B). Flow of HT29 cells in suspension into the device resulted in cells being seeded into the micro-wells cut into the Kapton, on top of the non-cell adherent silicone (Figure 6.5). However, upon seeding, cells settled down into the wells and continued to grow from the position in which they settled (Figure 6.5). By Day 2, the cells had failed to grow in a 3D spheroidal structure and instead the growth resembled a 2D monolayered cell culture. The issue regarding the flow of fluid through the 'version 1' microfluidic device, was resolved in the 'version 2 microfluidic device (Video 2). However, 3D spheroids were unable to be formed and cultured on the 'version 2' microfluidic device.
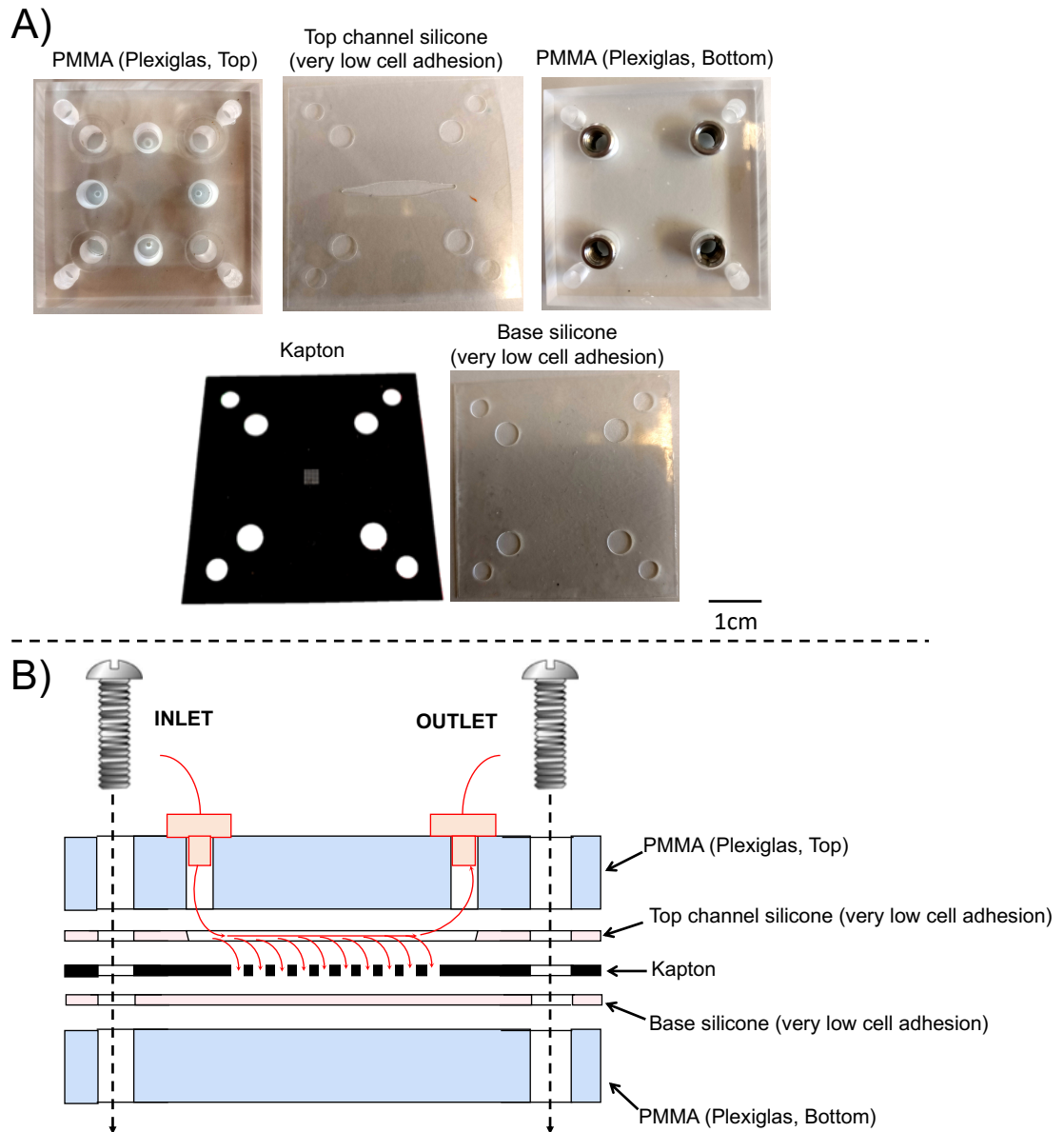
Figure 6.4 – Design and fabrication of the Version 2 microfluidic device

A) The Version 2 microfluidic device was created using different materials. **B)** The different materials were assembled to make the flow device and fluid flow through the device was designed to allow cells to be deposited into the wells printed in the middle Kapton layer.
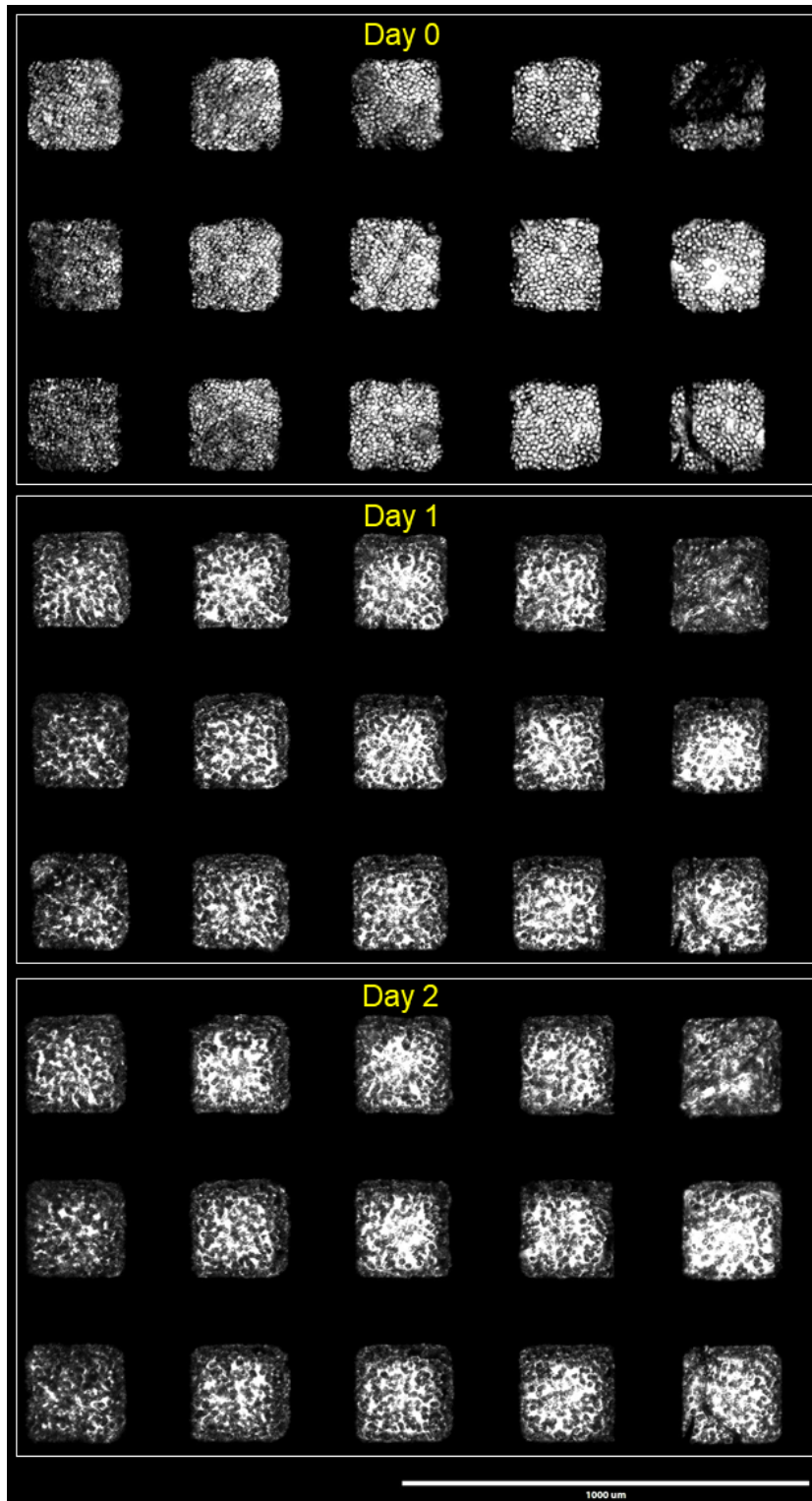
Figure 6.5 – Culturing cells in the Version 2 microfluidic device

HT29 cells in suspension were seeded through flow into the microwells (printed in Kapton layer) of the microfluidic device. Images were taken on days 0, 1 and 2. Cell growth at day 2 resembled that of 2D cell monolayers. Scalebar = 1000µm. Images in this figure are representative of at least 3 independent experiments. See *3.5.2 of* Material and Methods for the detailed protocol.

6.3.3 Version 3

6.3.3.1 Designing the 3D spheroidal culturing microfluidic chip

Following the failure of the 'version 2' microfluidic device, specifically the inability to generate 3D spheroids, a 'version 3' of the 3D cell culturing microfluidic flow device was designed and fabricated (Figure 6.6). Similar to 'version 2', the 'version 3' was based upon the generation of 3D spheroids on a non-cell adherent substrate. Instead of constructing the design with upper and lower layers of a non-cell adherent substrate and a middle layer with the microwells, the 'version 3' combined all three components into one single central 3D spheroid-culturing unit (Figure 6.6B).

A mould was created from the schematic designs in Figure 6.5 (Figure 6.6A) and a Polydimethylsiloxane (PDMS) flow chip was cast from the mould (Figure 6.6B). The flow channel contains an array of concave shaped wells in the centre for culturing 3D spheroids through fluid flow (Figure 6.6C and 6.6D). In comparison to the polygonal 'square' shaped wells of the 'version 2' microfluidic device, the concave shaped wells in 'version 3' would aid in the cell seeding process, by assisting cells in forming initial cell aggregates (Figure 6.7). Upon seeding of HT29 cells into the concave shaped wells, cell aggregates formed immediately (Day 0). By Day 2, 3D spheroids had started to form and continued to grow in cell density and size (Figure 6.8). Scanning electron microscopy confirmed the presence of the 3D spheroidal cell cultures in the wells of the PDMS flow chip (Figure 6.9). Once it was established that the geometry of the wells in the PDMS flow chip were able to successfully generate 3D spheroids, the next step in developing and optimising 'version 3' microfluidic device was to incorporate a fluid flow element.
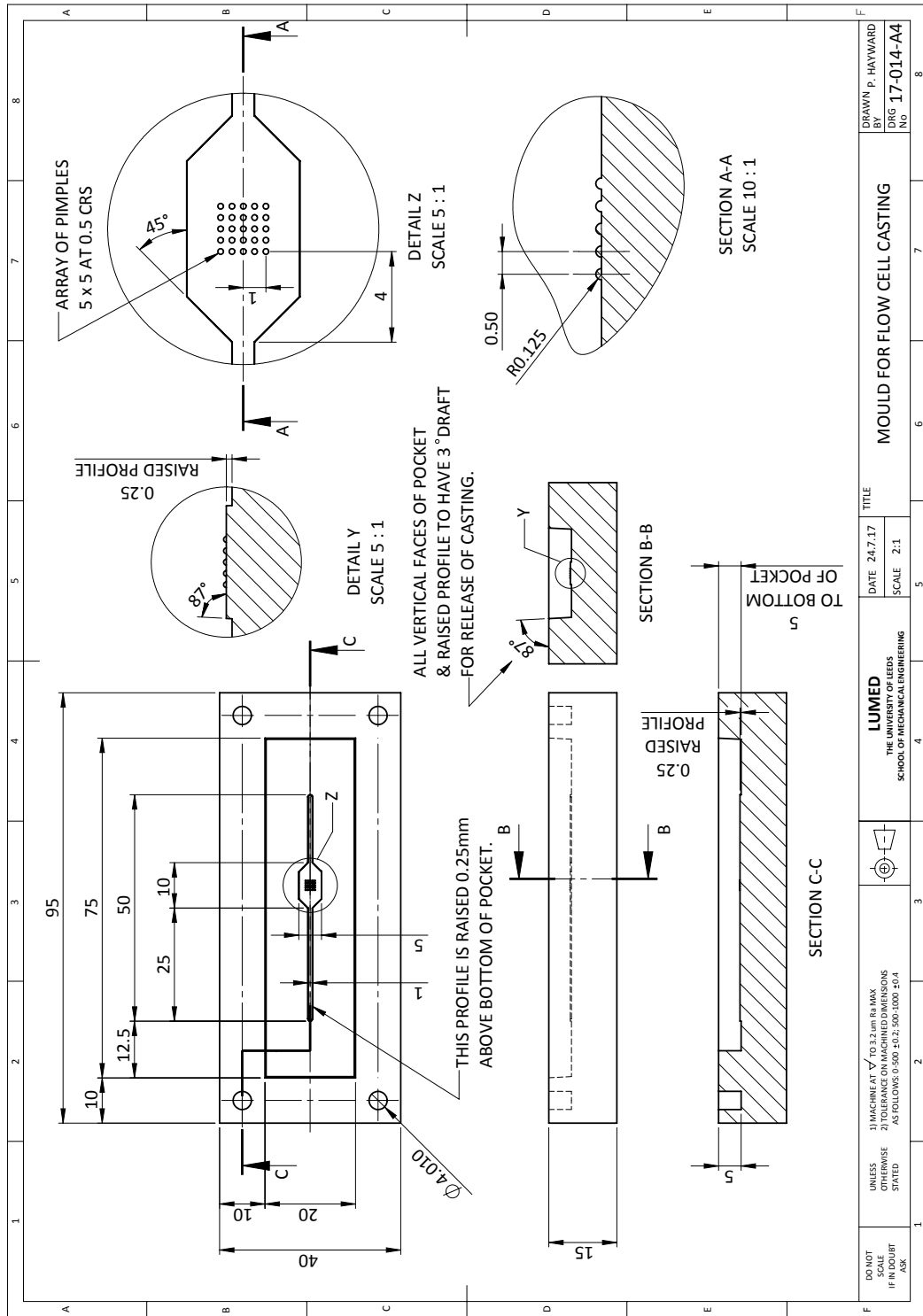
Figure 6.6 – Designing the mould for the low cell attachment Version 3 microfluidic chip

Schematic diagram of the mould for casting the low cell attachment Version 3 microfluidic flow chip. Dimensions are in mm.
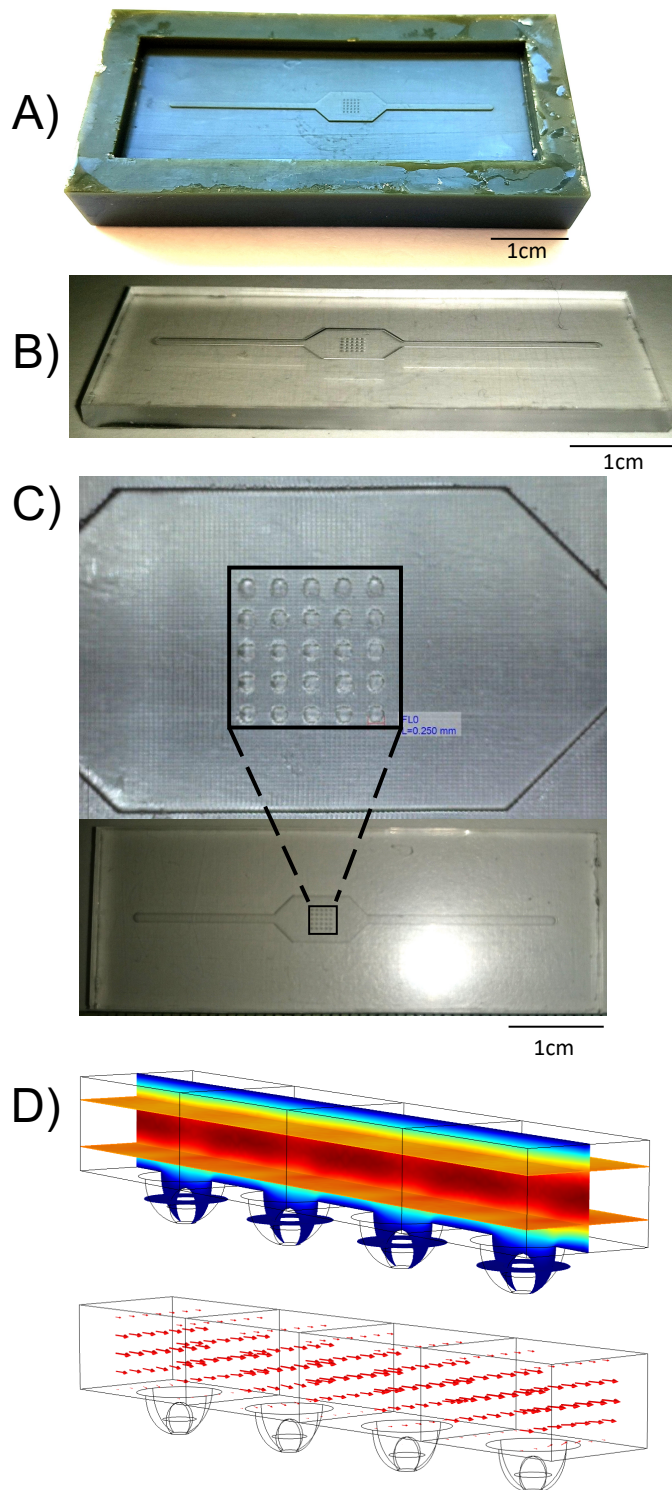
Figure 6.7 – PDMS flow chip of the Version 3 microfluidic device

A) The mould used to cast the low cell attachment version 3 microfluidic flow chip. **B)** PDMS flow chips were casted from the mould. **C)** The PDMS flow chip contains a 5x5 array of wells, that was specifically designed for culturing spheroids. **D)** Computational fluid dynamics showing the flow of fluid over the wells containing spheroids. Red = 20µL/min, orange = 15µL/min, yellow = 10µL/min, teal = 7µL/min, blue = 5µL/min.

A) Version 2

Layer of Kapton with wells

Layer of silicone

B) Version 3

Concave shaped wells

PDMS flow chip
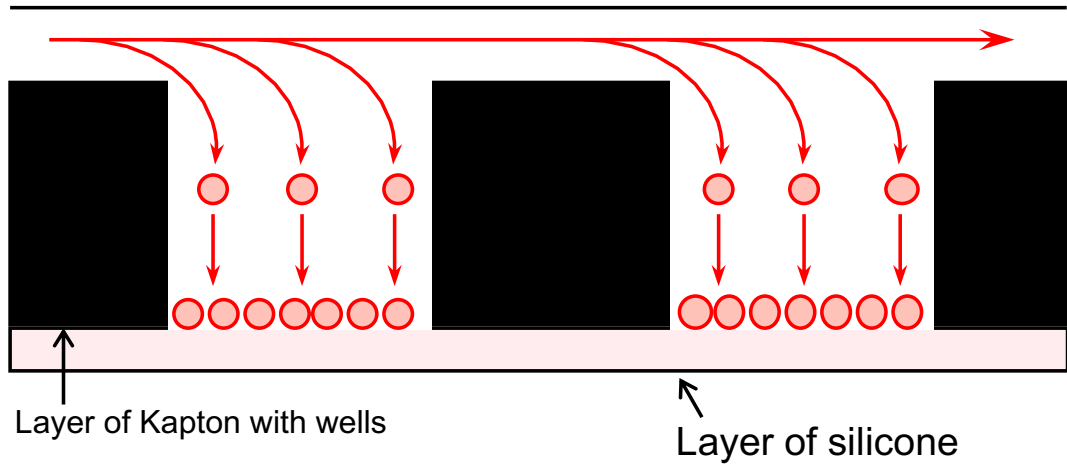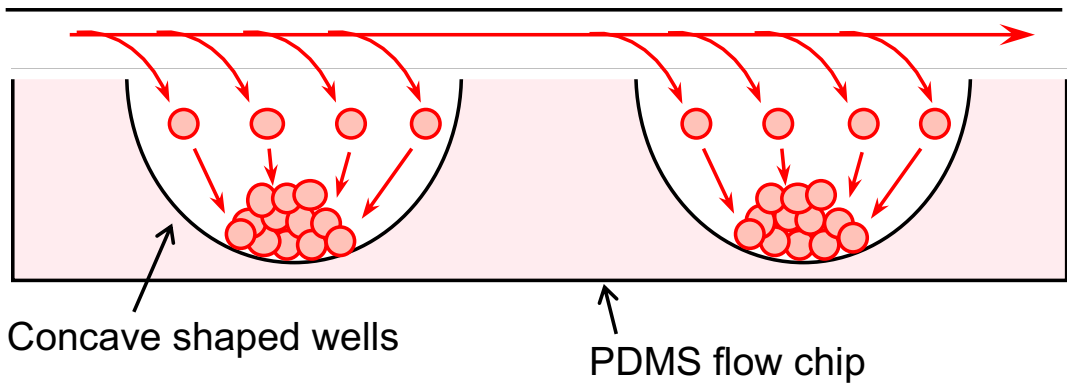
Figure 6.8 – Differences in the geometrical shapes of the cell culturing wells between Version 2 and Version 3 microfluidic devices

A) Version 2 was designed in layers with flat a layer of Kapton sandwiched between two flat layers of silicone, resulting in 'square' shaped wells. **B)** Version 3 was designed by casting PDMS flow chips from a 3D printed mould. The resulting wells have a concave shape.
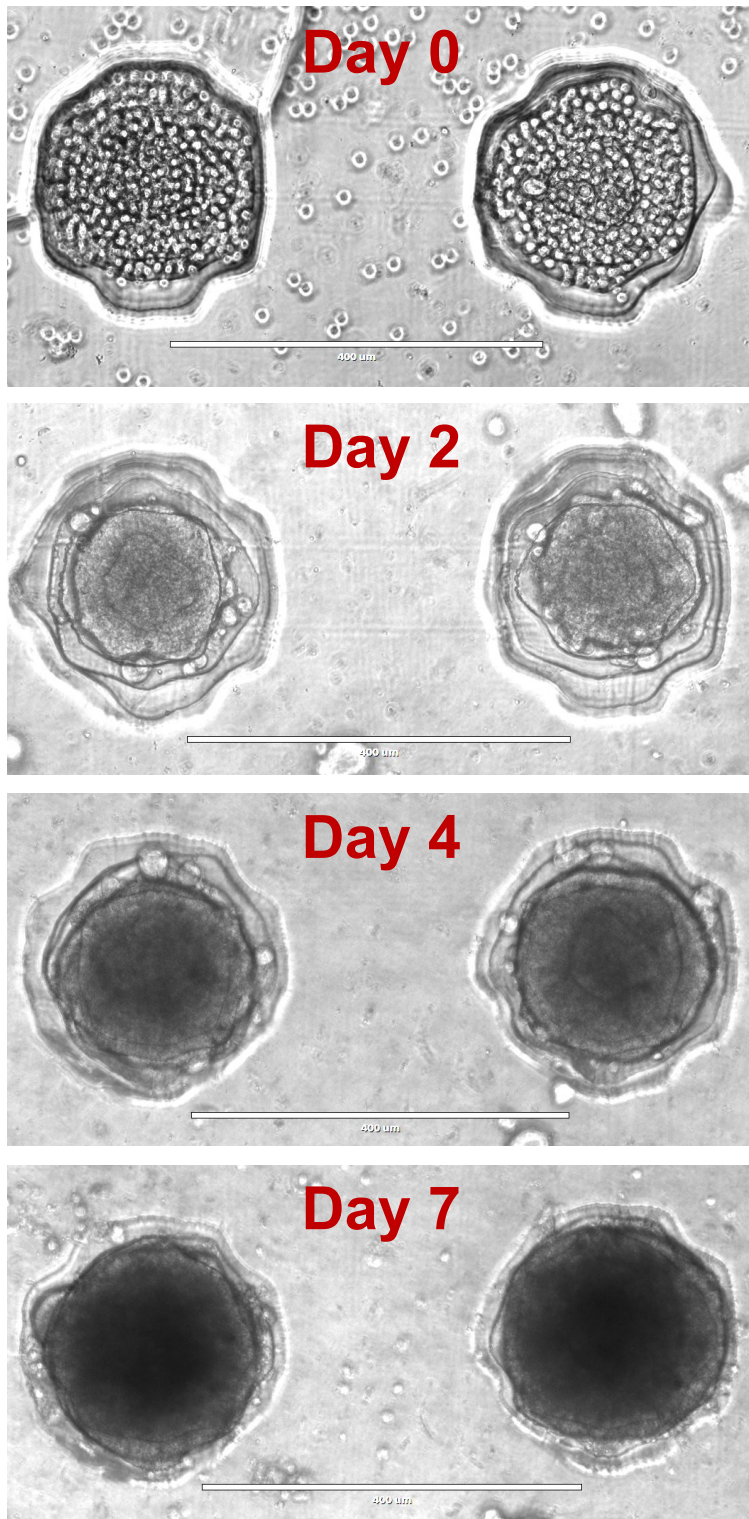
Figure 6.9 – Culturing 3D spheroids in the Version 3 PDMS microfluidic chip

HT29 cells were seeded into the wells of the microfluidic flow chip and cultured for several days. Transillumination images of cell aggregates and spheroids were taken on days 0, 2, 4 and 7. Scalebar = 400µm. Images in this figure are representative of at least 3 independent experiments. See *3.5.3 o*f Material and Methods for the detailed protocol.
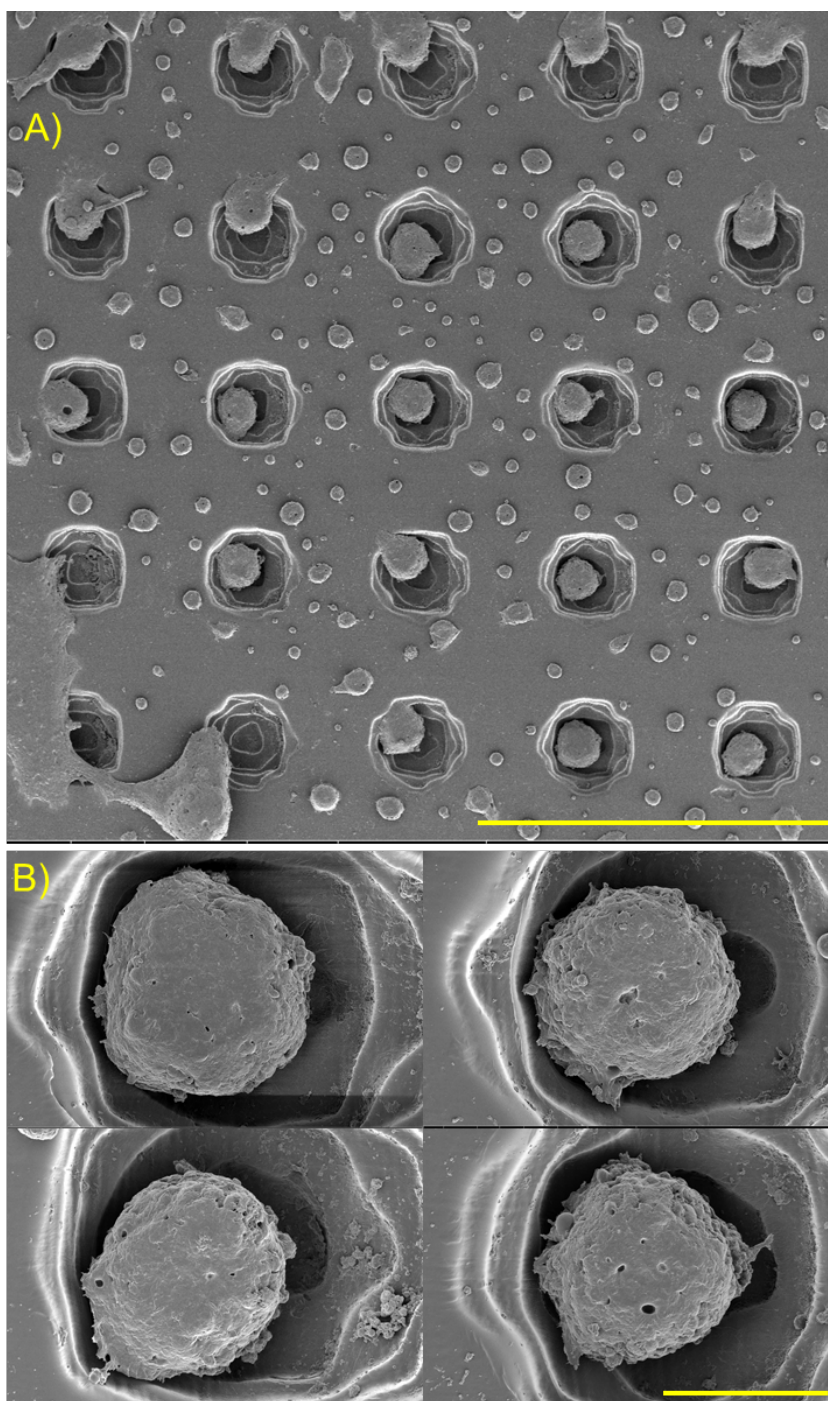
Figure 6.10 – Scanning electron microscopy (SEM) images of 3D spheroids cultured in the Version 3 PDMS microfluidic chip

HT29 3D spheroids were cultured in the microfluidic flow chip for 10 days. Spheroids were fixed with 2.5% glutaraldehyde and subjected to ethanol gradient dehydration. The microfluidic chip was coated with iridium before imaging. **A)** 35x magnification of the array of wells containing spheroids. Scalebar = 1000µm. **B)** 500x magnification of individual spheroids. Scalebar = 100µm. Images in this figure are representative of at least 3 independent experiments. See *3.5.3 of* Material and Methods for the detailed protocol.

6.3.3.2 Optimising and further refining the 'version 3' microfluidic device

Through the development of the 'version 2' microfluidic device, it was identified that the use of the two layers of PMMA to create fluid flow should be combined with the PDMS microfluidic flow chip to create the 'version 3' microfluidic device (Figure 6.11).
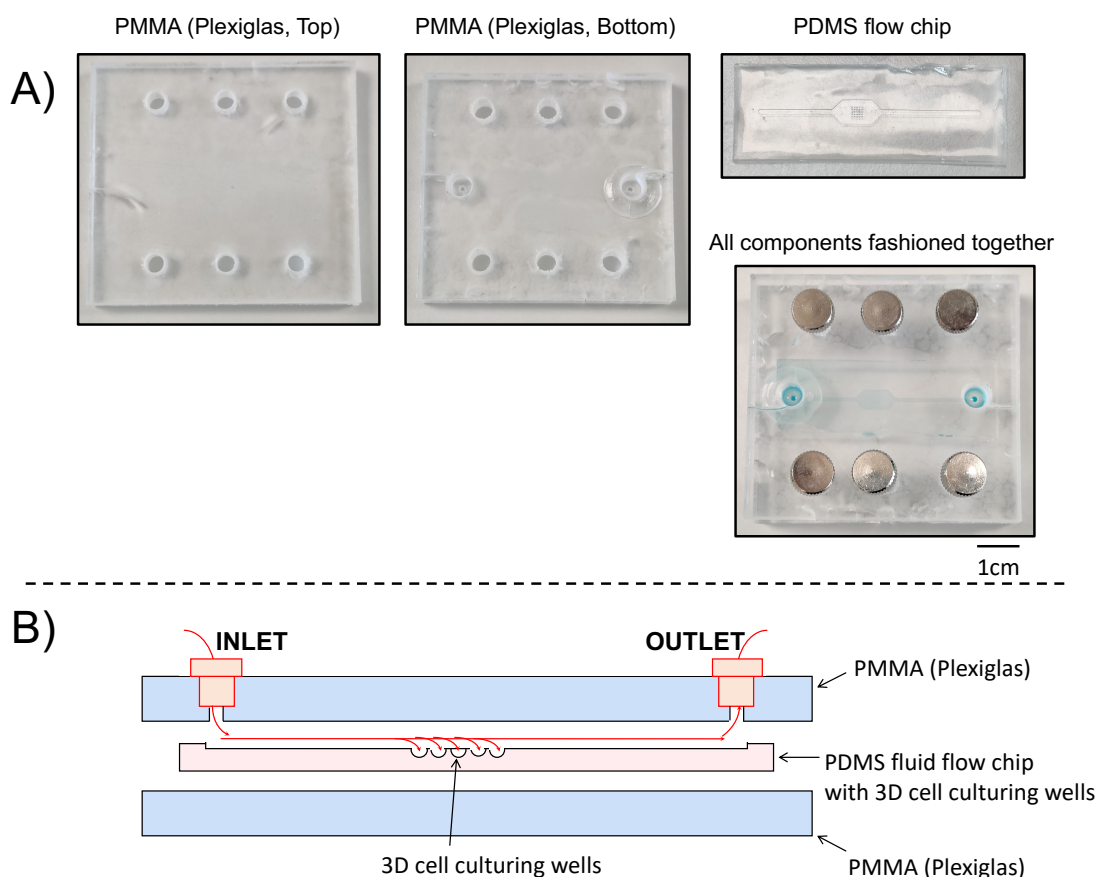
Figure 6.11 - Design and fabrication of the Version 3 microfluidic device

A) Photographic Images and **B)** Schematic diagram of the Version 3 microfluidic device. The device was created using two layers of PMMA and a PDMS fluid flow chip in the middle.

HT29 cells in suspension were perfused into the 'version 3' microfluidic device and cultured 2 days. As shown in Figure 6.12, upon the introduction of fluid through the device, pockets of air had formed in the wells of the PDMS microfluidic chip. Roughly half the number of wells had cells seeded into them, whilst the rest had air bubbles occupying the wells (Figure 6.12A). After 2 days of culturing, only a few wells had formed 3D spheroids and the rest of the wells had no spheroids in the wells (Figure 6.12B).

The presence of air bubbles in the wells of the PDMS flow chip, was restricting the successful seeding of cells and generation of 3D spheroids in the 'version 3' microfluidic device. To address this issue, a cell seeding port was designed into a modified version of the top layer of PMMA, which allowed cells to be seeded into the microfluidic device and directly into the wells without fluid flow (Figures 6.13A and 6.13B). Following the seeding of HT29 cells through the cell seeding port in the 'version 3'microfluidic device, 3D spheroids had successfully formed in all the wells of the PDMS chip after 2 days of culturing (Figure 6.13C). the implementation of the cell seeding port into the 'version 3' microfluidic device, eliminated the generation of air bubbles in the wells, that were present during cell seeding through fluid flow. This pragmatic modification improved the culturing of 3D spheroids in the 'version 3' microfluidic device.
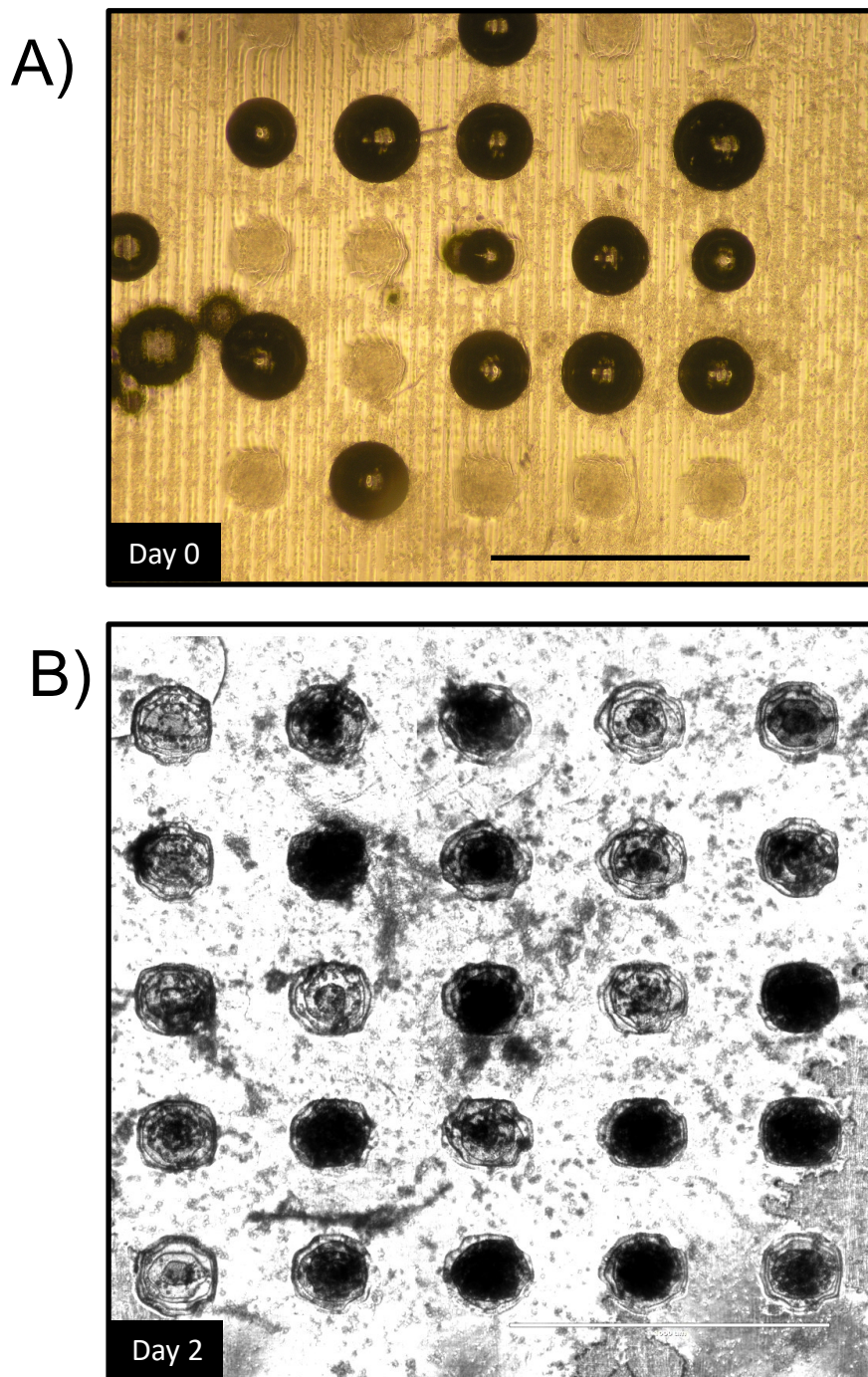
Figure 6.12 - Seeding HT29 cells in suspension through fluid flow in the Version 3 microfluidic device

A) HT29 cells in suspension were seeded through fluid flow into the 'version 3' microfluidic device. **B)** After 2 days, images were taken of cells and spheroids in the microfluidic device. Scalebars = 1000μm. Images in this figure are representative of at least 3 independent experiments. See *3.5.2.2 o*f Material and Methods for the detailed protocol.
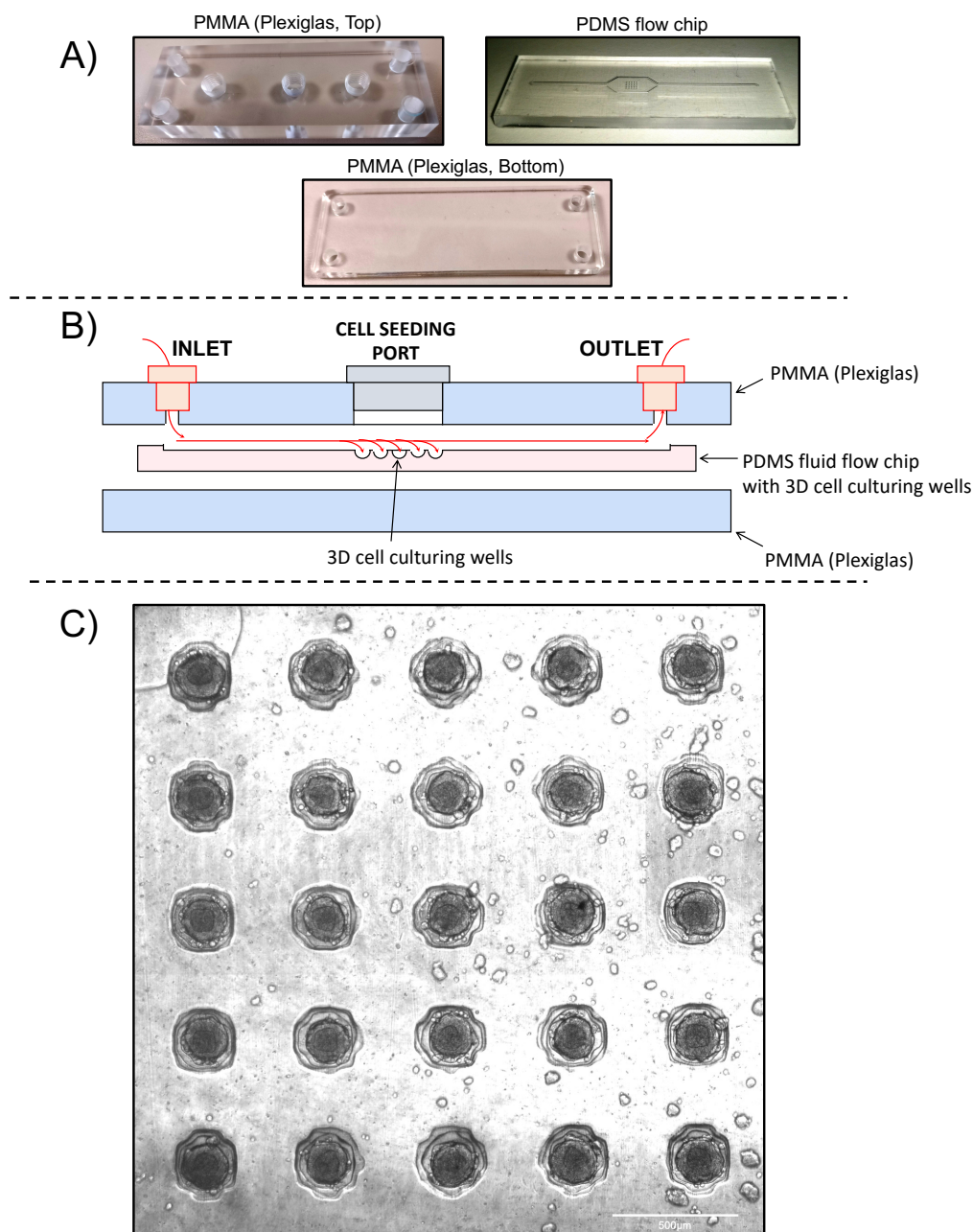
Figure 6.13 - Further refining and optimising the Version 3 microfluidic device

A) The optimised Version 3 microfluidic device was created using two layers of PMMA and a PDMS fluid flow chip. The top layer of PMMA has a cell seeding port in the middle to deposit cells directly into the 3D cell culturing wells in the PDMS flow chip. **B)** The different pieces are assembled to make the flow device and fluid flow through the device was designed to allow cells to be deposited into the wells in the PDMS chip. **C)** HT29 cells were seeded through the cell seeding port in the 'version 3' microfluidic device, cultured for 2 days and then imaged. Scalebars = 500µm. Images in this figure are representative of at least 3 independent experiments. See *3.5.3 o*f Material and Methods for the detailed protocol.

The three versions of the 3D cell culturing microfluidic devices that were developed in this research project, were designed and optimised in order to streamline 3D cell culturing experiments. Table 6.1 provides an overview of the three microfluidic devices. In this research project, we identified and aimed to investigate the three microfluidic concepts. From the three devices, the 'version 3' microfluidic device proved to be the most promising for further development. The 'version 3' microfluidic device was designed with a port for convenient cell seeding and loading, standard low pressure high-performance liquid chromatography fittings, simple in culturing 3D spheroids and easy to use in a tissue culturing laboratory.

Table 6.1 – An overview of the three versions of 3D cell culturing microfluidic devices

		Microfluidic Device		
		Version 1	**Version 2**	**Version 3**
3D cell culturing	Image			
	3D spheroid culturing method	Hanging drop	Non-cell adherent surface	Non-cell adherent surface
	Previous track record of a similar microfluidic concept	(Frey et al., 2014)	(Okuyama et al., 2010; Ziółkowska et al., 2013; Patra et al., 2016)	(Lee et al., 2013; Sun et al., 2014; Kwapiszewska et al., 2014; Chen et al., 2015)
	Ability to culture 3D spheroid	Spheroids were unable to be cultured	The geometry of the well prevented the formation of spheroids	Spheroids were formed upon the seeding of cells into wells
User friendliness	Ability to flow fluid	Fluid did not flow through device	Fluid flowed through successfully	Fluid flowed through successfully
	Setting up and Handling the device	Simple to setup by screwing fluid flow connector to either side	Can be difficult to assemble and align the different layers	Simple to assemble
	Ability to image spheroids	Lateral microscopy would be required to image droplets	Imaging could be performed on a conventional inverted microscope	Imaging could be performed on a conventional inverted microscope

6.3.4 Culturing, treating and evaluating 3D spheroids through fluid flow

The optimised and refined 'version 3' microfluidic device could successfully culture 3D spheroids, together with seamless flow of fluid through the microfluidic device (Figure 6.14). As illustrated in Video 3, upon introduction of fluid flow, the fluid was able to move through the capillary and pass over the spheroid culturing wells as it flowed out of the microfluidic device.
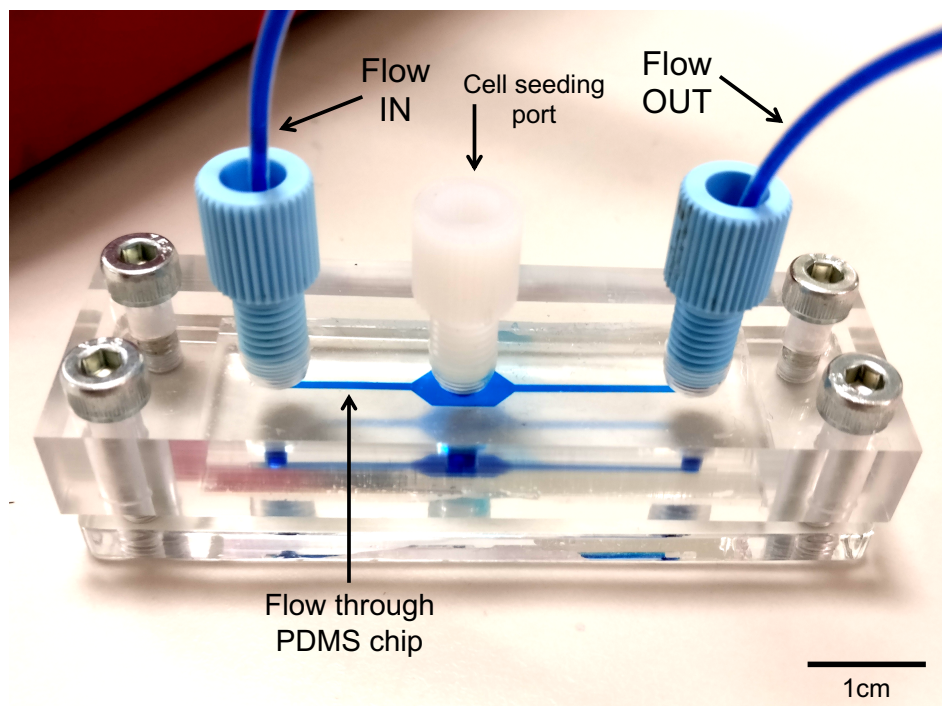
Figure 6.14 – Fluid flow through the optimised Version 3 microfluidic device

Version 3 microfluidic device combined the fluid flow element of Version 2 microfluidic device together with the non-cell adherent based technique for culturing 3D spheroids.

3D HT29 spheroids were cultured in the microfluidic device and then treated with 500µM 5-Fluorouracil (5-FU) through fluid flow. After 24 hours, cell viability analysis was performed on the spheroids by 1) collecting the supernatant through flow and performing the Lactate Dehydrogenase (LDH) assay and 2) treating spheroids with Hoechst 33342 and propidium iodide through fluid flow and fluorescently visualising cell death. Untreated spheroids were found to be significantly more viable as compared to 5-FU treated spheroids (74% difference in spheroid cell viability, p=0.0001) (Figures 6.15A and 6.15B). This is confirmed by the uptake of propidium iodide dye in 5-FU treated spheroids and lack of dye uptake in untreated spheroids (Figure 6.15C).

The 3D spheroids produced in the 'version 3' microfluidic device grew to 200µm (Figure 6.15C). This was due to the geometrical sizes of the concave shaped wells in the PDMS flow chip, which were designed with diameters of 250µm (Figure 6.6). Although there are smaller in size when compared to the spheroids generated in Chapter 4 *(4.3.2)* in 1% agarose-coated 96-well plates, they are still large enough to develop clinically relevant physiological gradients i.e. oxygen, catabolites and nutrients with hypoxic cores. Chemosensitivity results obtained using the 'version 3' microfluidic device spheroids still have potential clinical translation. Langan *et al.* (2016) evaluate the correlation between the sizes of spheroids and the development of hypoxic/necrotic cores. This study found that spheroids larger than 150µm in diameter begin to develop clinical physiological gradients and hypoxic cores (Langan et al., 2016). In the 'version 3' microfluidic device, the 200µm diameter sized spheroids would therefore be large enough to adequately represent clinical tumours, yet small

enough to fit in the microfluidic devices without outgrowing the microwells and obstructing the path of fluid flow.

A) Bar graph showing Cell Viability Relative to Control (%) for Untreated (~100%) and 5-FU Treated (~30%), $p=0.0001$.

B) Raw LDH assay absorbance values

Treatment conditions	Experiment 1			Experiment 2			Experiment 3			Average values of all experiments	% Cell Viability
	1	2	3	1	2	3	1	2	3		
Untreated	0.769	0.765	0.755	0.752	0.734	0.712	0.695	0.669	0.734	0.732	100
5-FU Treated	0.197	0.196	0.193	0.186	0.198	0.19	0.202	0.193	0.186	0.193	26

C) Fluorescent images of Untreated and 5-FU Treated spheroids.

Figure 6.15 – Culturing, treating and evaluating anti-cancer activity in spheroids through microfluidic flow

HT29 3D spheroids were cultured in the microfluidic flow chip for 2 days. Spheroids were then treated with 5-Fluorouracil (5-FU, 500µM) through fluid flow and incubated for 24 hours. **A)** The supernatant was then collected through fluid flow and the Lactate dehydrogenase (LDH) assay was performed. Data are shown relative to control treated cultures and represent means with standard deviation of 3 independent experiments. Experiments were performed in triplicate. **B)** Raw absorbance values from the experiments performed for the LDH assay. **C)** Spheroids were also stained with Hoechst 33342 (Blue) and propidium iodide (Red) and fluorescently imaged. Scalebar = 400µm. Images in this figure are representative of at least 3 independent experiments. See *3.6* of Material and Methods for the detailed protocol.
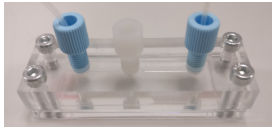
Chapter Seven

DISCUSSION

7 DISCUSSION

7.1 Techniques for culturing 3D *in vitro* multicellular tumour spheroids

7.1.1 Non-adherent method

For my research, I looked at two commonly used substrates, agarose and PolyHEMA. Agarose-coated plates for producing spheroids is a low-cost and facile method, as it simply requires preparing powdered agarose in water or cell culture medium, which is then sterilised. Liquid agarose is added to the wells of the plate, which gels at room temperature. Cells in suspension are then added on top of the gelled agarose, and cell aggregates are formed. PolyHEMA is another biomaterial which has been investigated for its use as a non-adherent substrate. PolyHEMA is usually prepared in ethanol and added to the wells of cell culturing plates. Ethanol is left to evaporate at room temperature, leaving the PolyHEMA polymer coating on the surface.

As shown in Figures 4.1 and 4.2, in my experiments, PolyHEMA coated plates were unable to form uniformly shaped and sized spherical cell structures. Furthermore, at room temperature, agarose is able to gel within a few minutes, in comparison to ethanol which takes substantially longer to evaporate. Regardless of the type of polymer used, preparation of cell culturing plates is a prerequisite to adding cells, which is a time-consuming process. Alternatively, commercially available pre-coated ULA plates can eliminate the need to prepare cell culturing plates with a non-adherent surface. Figures 4.6 and 4.7 highlight the shape, structure and the quality of spheroids being produced between 'in-house' prepared agarose-coated and commercial ULA 96-well

plates. For both techniques, loose cell aggregates and spheroids were formed by days one and two respectively. However, it was noted that the structures of spheroids produced in the commercial ULA plates were more refined than spheroids cultured in agarose-coated plates (specifically comparing HT29 Day 1 and HCT116 Day 2 for both techniques). This observation may be due to the differences in the accuracy, quality and standards in preparing plates, between the two methods. On one hand, the commercial ULA plates are prepared on a large industrial scale with automated machinery carrying out the manufacturing process. Whereas the agarose-coated plates are prepared manually, resulting in discrepancies from well-to-well with respect to the layer and thickness of agarose, in addition to the rate at which the agarose gels. However, the superior quality of commercial ULA plates also translates into increased costs per plate, which may not be feasible for carrying out experiments where large numbers of spheroid culturing plates are required (See Appendix for a detailed breakdown of the costs) (Breslin and O'Driscoll, 2013).

Another advantage of applying this spheroid-generating technique in standard tissue culturing plates, is that the desired size of spheroids can be achieved by adjusting the cell seeding densities and total spheroid culturing time. As described earlier, the non-cell adherent technique simply requires preparing standard cell culturing plates, with a non-adherent polymer coating on the surface. This allows for functional and cytotoxicity assays to be performed with ease. Furthermore, ordinary laboratory equipment such as microscopes, multichannel pipettes and microplate readers, that were designed to be compatible with standard cell culturing plates could be utilised to monitor spheroid formation and growth in real time and evaluate responses to treatment

(Vinci et al., 2012). The simplicity in application, low cost-effectiveness, consistent production of uniform spheroids, precise control of the sizes of spheroids, compatibility for high-throughput screening and the ability to culture 2D and 3D models on the same plate was the reason for using this technique for to produce 3D spheroids used in experiments described in Chapter 5.

7.1.2 Hanging Drop method

The hanging drop method is an attractive, simple and ideal approach to producing effectual 3D spheroids (Figure 4.1), however, this technique is technically challenging and requires practice to produce 3D spheroids consistently. The limitations of the hanging drop have also been described by others, who have used this technique (Shri et al., 2017). A major disadvantage of this technique is the delicateness and fragility of the spheroidal structures in the droplets. Replenishment of cell media at regular intervals is vital for continued growth and spheroids will very often disintegrate if the droplets are disturbed during the exchange of cell media. This can be overcome by the use of commercially available hanging drop plates, instead of petri dishes used in this investigation. However, similar to commercial ULA plates, specialised plates can be expensive to purchase and may not be a viable option for performing large numbers of experiments.

Another cause of 3D spheroids fragmenting is the lack of extracellular matrices to structurally support the growth of spheroids. Spheroids in suspension, like the hanging drop, solely rely on intercellular interactions to uphold the structure. This is unlike other 3D cell culturing techniques, where external structural support is provided. Another disadvantage of the hanging drop method, is the

very limited volumes of the droplets to accommodate the aggregation of cells. Droplets are usually restricted to 50μL or less to maintain the hanging drops on an inverted surface by surface tension (Kurosawa, 2007). Taken together, the fragile nature of spheroids in hanging drops, the inability to easily exchange cell media, and the limited volume of cell media means that spheroids cannot be cultured for extended periods of time. Petri dishes and standard cell culturing 12-, 24- and 48-welled plates have conventionally been used to produce spheroids in hanging drops. To preserve the structures of spheroids for experimental application, it is vital to keep them suspended in the droplets which is not possible in inverted dishes and welled plates. For this reason, purpose-built commercial hanging drop plates are an option but as highlighted above, may not be an effective route. Recently, advancements to the conventional hanging drop protocol have been reported, that improve the application of this technique. Kuo *et al.* (2017) describe a custom fabricated hanging drop platform to generate spheroids, and highlight the addition of collagen fibrils to the cell culture media droplet, in an effort to improve spheroid durability and structural rigidity (Kuo et al., 2017). Similarly, Bender *et al.* (2016) describe an automated hanging drop platform for producing spheroids. The authors highlight the substantial improvement to the conventional hanging drop by improving structural rigidity through the addition of collagen to the droplet (Bender et al., 2016). In principle, the hanging drop method is effective for generating spheroids. However, in comparison to the more popular non-cell adherent method, the hanging drop technique is less favoured due to the user-friendliness, effective spheroid production and high-throughput applications of the former method.

7.1.3 Agitation-based techniques

The first of the two agitation-based techniques is the spinner flask method and a technique, that I evaluated and chose for generating 3D spheroids for experiments described in Chapter 5. As shown in Figures 4.5 and 4.8, 3D spheroids can grow up to 1mm in size, which is far larger than the sizes of 3D spheroids grown using the other 3D cell culturing methods. A downside to culturing spheroids in spinner flasks, is the shear stress exerted upon spheroids through fluid motion which may influence spheroid physiology (Lin and Chang, 2008). In comparison to culturing spheroids in 96-well plates and hanging drops which require microliter volumes of cell media, spinner flasks require around 200mL of cell media to be replenished multiple times a week to sustain spheroid growth which may be cost ineffective (Rodday et al., 2011). Also, spinner flasks require specialised equipment and setups in the laboratory to operate continuously, which can be quite expensive to maintain. Furthermore, spheroids produced in spinner flasks can vary in sizes, however this can be addressed by seeding a controlled number of cells into spinner flasks or by initially producing spheroids through other techniques (non-cell adherent or hanging drop) which are then transferred to spinner flasks for long-term culturing (Smith et al., 2005).

The ability to culture large numbers of spheroids easily for prolong periods of times and utilise them as required for experiments, was the reason the spinner flask method was chosen for further experiments. During experimentation for this research project, the need for large volumes of cell culturing media was taken into consideration and financial resources had to be considered when running spinner flask cultures. Another criticism for using this technique as

experienced through this research project, is that the entire spinner flasks and platform setup have to be placed into cell culturing incubators, to maintain optimal culturing conditions. Unlike hanging drop and non-cell adherent plates, spinner flask setups require large amounts of space in the incubator, often resulting in the incubator solely being used to accommodate the spinner flask setup.

I was unable to evaluate the rotating flask method in this research project. As opposed to the spinner flask method, spheroids in the rotating flask method experience a lower shear stress due to the entire flask rotating (Goodwin et al., 1993). Aside from that, the advantages and limitations of the rotating flask are similar to the spinner flask method, such as large numbers of spheroids, long-term culture, costs and varying sizes of spheroids (Breslin and O'Driscoll, 2013).

7.1.4 Matrices and scaffolds

For this research project, I was unable to evaluate the use of matrices and scaffolds for generating 3D spheroids. A major advantage of using this method in comparison to those mentioned above is the structural support provided and by the matrices/scaffolds and availability of nutrients and growth factors in the constructs that can influence the growth of 3D spheroids (Langhans, 2018). The techniques I have evaluated in this research project, utilised cell media only to facilitate growth in cells in 3D spheroids. Investigating the use of matrices/scaffolds for my research project would have improved my assessments and comparison of the different techniques.

A limitation of matrices/scaffolds is the inherent inability to rapidly screen drugs in embedded spheroids. Other limitations of these techniques are that spheroids grow at different rates in the matrix/scaffold, resulting in unequal sized and shaped structures. Upon the seeding of cells, their distribution within the matrigel and along the scaffold is random, and thus the resulting location of spheroid in the culturing vessel cannot be controlled. Finally, it is often quite technically challenging to extract spheroids from the matrices/scaffolds for invasive analysis, without compromising the structures of the spheroids (Sodunke et al., 2007; Justice et al., 2009; Breslin and O'Driscoll, 2013).

For my research, I investigated two colorectal cancer cell lines, HT29 and HCT116. These cell lines have been identified to be molecularly heterogeneous and originate from differing clinically relevant subtypes of colorectal cancer (Berg et al., 2017). Interestingly, both cell lines showed to form morphologically and structurally distinct spheroid structures (Figures 4.1, 4.2 and 4.3). Depending on the cell type, culturing time and techniques, spheroids can form tight compact spheroids or looser cell aggregates (Ivascu and Kubbies, 2006).

The 'non-adherent' and 'spinner flask' techniques were the chosen methods for producing 3D spheroids for further experiments in this research project. In keeping with the theme of transitioning from basic 2D cell models to more clinical-like 3D spheroidal cell models, specifically for drug development and screening purposes, this research project utilised 3D spheroidal cell models of HT29 and HCT116 colorectal cancer cell lines to evaluate PDT. The routine incorporation of spheroid-based experiments into *in vitro* drug efficacy investigations, will very likely produce more clinically accurate results as

compared to monolayer cultures, due to their more accurate recapitulation of solid tumour architecture, biology and physiology (Sant and Johnston, 2017). Additionally, spheroids can serve to bridge the gap between cell-based *in vitro* and animal-based *in vivo* studies.

Regardless of the technique used for generating 3D spheroidal cell models, the application of 3D spheroids has primarily been used as a representation of a better and more relevant model of clinical cancers (Breslin and O'Driscoll, 2013). As mentioned previously, 3D spheroids recapitulate the physiological gradients, tissue architecture and heterogeneity in cell growth and proliferation of *in vivo* cancers. These qualities are usually never observed in simple 2D monolayered cell cultures. Although 3D spheroids are advantageous for pre-clinical studies, they still do not fully bridge the gap between *in vitro* models and *in vivo* cancers (Costa et al., 2018). 3D spheroids lack the complexity of the tumour microenvironment (tumour vasculature, ECM, immune response) and heterogenous cellular composition (fibroblasts, endothelial cells, immune cells, mesenchymal cells) (Katt et al., 2016). These factors play a vital role in tumour progression. Tumour cells can recruit stromal cells in the microenvironment, which in turn, provide tumour cell growth signals and an environment for tumour progression as well as metastasis. The reciprocal communication between cancer cells and stromal cells in the tumour microenvironment is not captured in 3D spheroids (Yuan et al., 2016). Simple 3D spheroidal cell models also fail to recapitulate the physiology of the tumour microenvironment, specifically mimicking the enhanced permeability and retention effect and interstitial fluid pressures; factors which are well-known to influence the delivery of anti-cancer drugs to the tumour (Liu et al., 2016; Nakamura et al., 2016).

My research project used simple 3D spheroid models, comprised of one type of cell line. For future experiments, it would be beneficial to incorporate tumour microenvironment-like co-culture models, incorporating stromal cells into 3D spheroids, as platforms for evaluating PDT. The useful of such models would provide more clinically translatable results.

7.2 Photodynamic properties of Hypericin

7.2.1 Hypericin as a PDT mediating photosensitiser

One of the main objectives of my research was to evaluate the natural anthraquinone based compound, hypericin, as a photosensitising agent to mediate PDT. As described in Chapter 1, many pre-clinical and small scale clinical studies have evaluated PDT to treat CRC. However, a defined clinical protocol for PDT (including the choice of photosensitiser) is yet to be established. The use of hypericin in PDT attempts to expand the current scope of second generation photosensitisers. As shown in Figures 5.3 and 5.4, hypericin possess minimal dark toxicity, yet exhibits potent phototoxicity. Furthermore, hypericin preserves its chemical structure as it is not subjected to xenobiotic metabolism in the body by drug metabolising enzymes, such as cytochrome P450s (Kubin et al., 2005; Maduray and Davids, 2011).

Following the administration of hypericin-PDT, an apoptotic cell death is usually observed *in vitro* using sub-lethal doses (<100nM) of hypericin. Post-PDT events such as DNA fragmentation, blebbing of the cell membrane, loss of mitochondrial function, up- and down-regulation of Bax and Bcl-2 respectively, PARP cleavage and activation of caspase-9 have been reported (Zhang et al.,

2015). In addition to an intrinsic apoptotic response, the activation of an inflammatory response, mediated by the secretion of TNF-α, IL-6 and IFN-γ pro-inflammatory factors to further supress cell growth has also been reported (Zhang et al., 2015).

A major limitation of the experiments described in Chapter 5, is that although this research project primarily focussed on Hypericin, another photosensitiser was not included in experiments. As summarised in Chapter 1, Hypericin is relatively unknown when compared to more prominent and clinically approved photosensitisers e.g. Photofrin, Foscan or 5-ALA/PpIX. This research project would have benefitted from the inclusion of the these photosensitisers, as it would have demonstrated the efficacy of the up and coming Hypericin in comparison to PDT mediated by clinically available and well characterised photosensitisers.

7.2.2 Resistance in 3D *in vitro* models to PDT

Another objective of my research was to compare the responses between 2D monolayer and 3D spheroidal cell cultures of CRC to hypericin-PDT. The results presented in Chapter 5, show that 3D spheroidal cultures of HT29 and HCT116 are significantly more resistant to hypericin-PDT as compared to their monolayer counterparts (Figure 5.5). As described in Chapters 1 and 4, 3D spheroids provide a better representation of *in vivo* cancer, in comparison to conventional 2D monolayers cell cultures. This is achieved by the architectural and physiological elements of 3D spheroids, mimicking the *in vivo* environment. Other studies have also identified 3D spheroid cancer models to be more resistant to PDT as compared to 2D monolayers. Examples include treating

A549 and MRC-5 lung cancer and MCF7 breast cancer spheroids and monolayers with 5-ALA-PDT (Yang et al., 2015; Zuchowska et al., 2016), glycosylated porphyrin-PDT in HCT116, MCF7 and HeLa spheroids (Pereira et al., 2017) and also the differential expression of apoptotic related genes in phthalocyanine-PDT treated 2D and 3D models of the A549 cell line (Manoto et al., 2017).

As previously stated, spheroids are better models of *in vivo* cancers as compared to conventional 2D cell cultures. Physiological gradients of oxygen, catabolites and drug diffusion through the spheroidal model as well as the spheroid architecture, allows for more clinically relevant *in vitro* data to be generated. Spheroids used to assess hypericin-PDT in this research project were grown to 400-500µm, and it has previously been identified that spheroids of this size have prominent hypoxic cores (Langan et al., 2016). Although hypericin was observed to be able to diffuse through to the core of spheroids, resistance in spheroids to PDT was quite apparent. Overall, the findings from this research corroborates with those of other researchers, highlighting the importance of evaluating PDT in 3D cell models. The findings from this research project in addition to the findings of others, strongly suggests the use of 3D spheroids for evaluating PDT for clinical translation.

7.2.3 ABCG2 and 3D spheroids

Many previous studies that have examined the role of ABCG2 in PDT, have for the most part been conducted in 2D monolayer cell cultures. This research project investigated ABCG2 and PDT in both 2D and 3D *in vitro* cell models. Cells in 2D monolayer cell cultures are uniformly exposed to growth factors and

oxygen and their cell cycles are also synchronised. This is unlike cells in 3D spheroids, that are exposed to varying gradients of growth factors and oxygen and also have differential rates of cell proliferation (Breslin and O'Driscoll, 2013). In this study, it was observed that 3D CRC spheroids had upregulated ABCG2 protein expression as compared to their respective 2D monolayer counterparts (Figure 5.7). Furthermore, unlike the uniform expression of ABCG2 protein in 2D monolayer cells, this study found an increased expression in the outer layers of cells in spheroids, as compared to the inner central mass of cells.

Unlike the current scope of publications and reported studies, this research project is the first to report on the comparison in the expression of ABCG2 protein between 2D and 3D models of the same cell line. The use of 3D spheroids in this research project to characterise the ABCG2, could potentially improve clinical translation. The clinical significance of ABCG2 has previously been identified as a useful predictive biomarker of resistance to chemotherapy in advanced and metastatic colorectal cancers, as indicated by the elevated ABCG2 expression levels, in comparison to normal colonic tissue (H.G. Liu et al., 2010; Tuy et al., 2016). Exploiting the overexpression of ABCG2 in colorectal cancers through the inhibition of this transmembrane protein, could substantially improve clinical PDT applications.

7.2.4 Improving responses to PDT in 3D *in vitro* models

Oxygen is a crucial element in the production of ROS and the lack of oxygen in the hypoxic core of spheroids, can limit the production of ROS and reduce overall cytotoxicity (Kareliotis et al., 2018). Resistance to PDT is not easily

observed in 2D models, but is readily observed in spheroids with prolonged culture, when they were able to re-form their original compact spheroidal shape and continued to grow in volume. An improved understanding of the mechanism of PDT resistance, derived through 3D spheroid models, could help to develop more effective clinical PDT protocols. One such example might be the application of prolonged low dose fractionated PDT. Conventional PDT involves the administration of a single dose of photosensitiser, prior to light treatment. Whereas in fractionated PDT, a lower dose of a photosensitiser is given multiple times (*i.e. 2x dose of 1mg/ml instead of 1x dose of 2mg/ml*) in combination with a lower light fluency rate but equal amount of total light dose *(i.e. 2x light treatment at 0.25mW/cm^2 for 2x 2000 seconds = 1J/cm^2 instead of 0.5mW/cm^2 for 2000 seconds = 1J/cm^2).* An example of low dose fractionated PDT, is the study conducted by Mathews *et al.* (2009). The authors found that administering light at low fluency rates for longer periods (3J/cm^2 over 24h) resulted in significantly greater inhibition of growth of glioma cell line spheroids as compared to high fluence light treatment for a short period (3J/cm^2 over 1h). Additionally, splitting the doses of 5-ALA into two (2x 100µg/mL) and administering the second dose at the midpoint of light treatment had a more profound effect in reducing spheroid growth as compared to a single dose (200µg/mL) given pre-light treatment. Histological analysis of spheroids revealed superficial necrosis of spheroids, in the outer layers of cells treated with 3J/cm^2 of light over 1h, as compared to the deeper necrosis observed in spheroids treated with 3J/cm^2 of light over 24h (Mathews et al., 2009). An *in vivo* study by Xiao *et al.* (2007) found fractionated light delivery to prostate tumour xenografts in rats to be significantly more effective in complete tumour cure rates as compared to rats that received continuous light treatment (Xiao et

al., 2007). Clinical studies by Star *et al.* (2006) and De Vijlder *et al.* (2012) also found that patients who received fractionated 5-ALA-PDT in superficial basal cell carcinoma had better long-term complete remission and complete response rates as compared to those who received 5-ALA-PDT with single light treatment (Star et al., 2006; de Vijlder et al., 2012). With oxygen being a crucial factor in PDT, the rate of oxygen consumption in high light dose PDT is believed to be very fast. Therefore, lower light fluency rates slows down the rate at which oxygen is consumed and prolongs the generation of ROS. In addition, the 'dark' intervals between light treatment in fractionated treatment permits the reoxygenation of cells and tissues with extended phototoxicity (Xiao et al., 2007).

In this research project, Hypericin was evaluated and found to be a potent photosensitiser to mediate PDT in CRC *in vitro* models. Hypericin showed strong photo-cytotoxicity with negligible toxicity in the dark. HT29 and HCT116 spheroids were found to be more resistant to hypericin-PDT, as compared to their monolayered counterparts. The resistance in spheroids may be due in part to the effect of the multidrug resistance protein, ABCG2. Inhibiting ABCG2 activity improved sensitivity in 3D spheroids to hypericin-PDT. However, after hypericin-PDT, the re-growth of both HT29 and HCT116 3D spheroids was observed. This finding may suggest a transient and/or partial cytotoxic effect of hypericin-PDT in the spheroidal cell models, enabling cells to recover and spheroids to re-grow. Recently, Weijer *et al.* (2015) conducted a study, investigating the activation of survival pathways in SK-ChA-1 cells, subjected to PDT. The study found cells to induce cell survival signalling pathways via the upregulation of HIF1α and NFκB, following PDT treatment. The activation of

these key cell survival signalling mechanisms, is vital for cells to persist and survive through treatment (Weijer et al., 2015).

A limitation of this research project is that the PDT-influencing and expression of ABCG2, was the only intracellular mechanism that was investigated. As suggested above, PDT induces a myriad of intracellular changes on a molecular level. These include signalling pathways involved in regulating apoptosis, response to oxidative stress, autophagy, cell survival, hypoxia and inflammation (Castano et al., 2005). For future experiments, it would be beneficial to characterise the different signalling pathways affected by PDT, specifically when comparing responses to treatment between 2D monolayer and 3D spheroidal cell models.

With the current scope of literature, evaluating Hypericin-PDT, predominantly being carried out in 2D cell models (Jendželovská et al., 2016). This research project is the first to use 3D spheroids and highlights the importance of using 3D spheroids as a means of evaluating PDT, and the implications of resistance to PDT for future clinical applications.

7.3 The development of a microfluidic device for 3D cell culture

There has been growing interest in the integration of 3D cell culturing into microfluidic platforms. Microfluidics has allowed conventional 3D cell culturing techniques, such as those described in Chapter 4, and also the experimental treatment and analysis of 3D spheroids to be performed in a convenient, streamlined fashion on an integrated platform (X.J. Li et al., 2012). A main

objective of this research project, was to develop a 3D cell culturing microfluidic device that could accommodate the culture, treatment and evaluation of anti-cancer activity in 3D spheroids through fluid flow.

7.3.1 Version 1

The Hanging drop 'version 1' microfluidic device was designed in a way similar to that described by Frey *et al.* (2014). In the study, the authors were able to generate HCT116 spheroids by loading cells in suspension on to the device through a pipette. The cell suspension solution would fill all channels and wells and cells would settle at the bottom of the hanging drops, initiating the formation of a spheroid (Frey et al., 2014). The idea behind the 'version 1' microfluidic device was to flow cells in suspension through the microfluidic device via the inlet/outlet ports and hanging drop wells. However, as depicted in Video 1, upon the introduction of fluid flow into the device, fluid failed to flow across the wells. In the aforementioned study, Frey *et al.* (2014) describe the use of oxygen plasma treatment to increase the wettability of PDMS prior to cell seeding and the strategic positioning of a thin layer of PDMS, to locally modify the surface of the microfluidic device. The resulting surface modification created a hydrophobic barrier around the wells and interconnecting channels, which prevented the overflow of liquid out of the wells and channels (Frey et al., 2014). Acrylonitrile butadiene styrene (ABS) was chosen as the material to create the 'version 1' device as it had previously been shown to possess good durability and resilience, high impact strength, simple processing properties, lightweight, chemical resistance and relatively low consumer costs (Kamelian et al., 2018; Martinez et al., 2018). The failure of fluid flowing through the channels and wells in the 'version 1' device is potentially due to the

hydrophobicity, low surface energy and poor adhesive properties of ABS (Wang et al., 2014; Martinez et al., 2018). Techniques such as chemical surface treatment, oxygen plasma treatment and atmospheric plasma torch treatment have been shown to 'activate the surface' and increase the wettability of ABS (Abenojar et al., 2009; Shu and Wang, 2012). These techniques could potentially be applied to improve the flow of fluid in future iterations of the 'version 1' microfluidic device.

Aside from the limitations of the surface properties of untreated ABS, other limitations of the 'version 1' microfluidic device include the limitations associated with hanging drops. As described in Chapter 4, the fragility of droplets and the spheroids contained within droplets is a major obstacle, making it difficult to maintain spheroid structures. The hanging drop system is therefore technically and logistically challenging to perform.

7.3.2 Version 2

The 'version 2' 3D cell culturing microfluidic device was designed around the forced-floating method, also known as the non-cell adherent method. As highlighted in Chapters 4 and 5, this technique is simple in application and carries many advantages. The non-cell adherent substrate prevents cells from adhering to the culturing surface, forcing them to aggregate and grow as 3D spheroidal structures (Costa et al., 2018).

The 'version 2' microfluidic device was constructed using three different materials: 1) Silicone, 2) Kapton and 3) PMMA (Figure 6.3). Silicone was used to create the fluid flow channel and the base of the wells, above and below the

cell culturing wells respectively. Silicone is frequently used for bioengineering applications and is commonly used in medical devices. This is due to its physiological inertness, biocompatibility and the surface properties of silicone prevent protein and cell adhesion (Hauser et al., 2009; Shin et al., 2018). Therefore, it was chosen as a practical candidate for designing the non-cell adherent surface in the 'version 2' microfluidic device. Next, sandwiched between the two layers of silicone, is a layer of the polyimide film, Kapton. This central layer of the 'version 2' microfluidic device is crucial, as it contains the wells in which the cells would be seeded into. The dimensions, geometry and sizes of cell culturing wells, for culturing 3D spheroids is important, as it can often influence the size and shape of the resulting spheroidal structure (Ratnayaka et al., 2013). Polyimide films, such as Kapton, are routinely used to create microscale electrical components. High-energy laser cutting has been shown to be effective in cutting polyimide films, as it can achieve micromachining with the highest degree of precision, whilst negating the effect of heat and surface damage to the film (Ganin et al., 2018). Therefore, the Kapton films used to construct the 'version 2' microfluidic device were cut using a laser to precisely control the shape and size of cell culturing wells. In addition to its advantageous engineering properties, which includes excellent mechanical strength, flexibility and chemical and radiation resistance, Kapton has also previously shown to be biocompatible and non-cytotoxic (Sun et al., 2009; Hadler et al., 2017). The third material, PMMA, was used to create the top and bottom layers i.e. the encasing of the microfluidic device. Similar to silicone, PMMA has been used extensively for biomedical applications due to its biocompatibility, low manufacturing costs and easy processability. The main advantage of PMMA for fabricating microfluidic devices is its inherent optical

clarity and refractive index (Ali et al., 2015). The clear optical transparency of PMMA allows light to pass through with ease, making it an ideal material for microscopic imaging. Therefore, imaging cells in the 'version 2' microfluidic device was achievable.

In practise, upon seeding of cells into the 'version 2' microfluidic device, cells settled into the wells and formed 2D monolayered cell cultures, instead of 3D spheroidal cultures (Figures 6.4 and 6.7). This may have been due to the polygonal quadrilateral shape of the wells, as formed by the layer of Kapton sandwiched between parallel layers of silicone. The geometry of cell culturing wells for generating 3D spheroidal cell structures is important in initiating cell aggregation and spheroid formation. Many studies culturing 3D spheroids have been described using concave shaped (also known as 'U-shaped' or 'round-bottomed') 96-well or 384-well cell culturing plates (Friedrich et al., 2009; Phung et al., 2011; Sirenko et al., 2015; Gaskell et al., 2016). Non-cell adherent concave shaped plates are commercially available, or can be prepared in-house using agarose (Costa et al., 2014). This has been described in Chapter 4 and used to generate 3D spheroids for experiments described in Chapter 5. The inability to form cell aggregates in the 'version 2' microfluidic device, suggested that it was not possible to use this design to generate and culture 3D spheroids.

7.3.3 Version 3

The 'version 3' microfluidic device was also based upon the forced-floating method for generating 3D spheroids. However, unlike the layered approach used for creating the cell culturing wells and the top flow channel in the 'version

2' microfluidic device, the 'version 3' microfluidic device combined these elements into one single central piece fabricated from PDMS. PDMS is a commonly used material for manufacturing 3D cell culturing microfluidic devices (Okuyama et al., 2010; Yu et al., 2010; T. Liu et al., 2010; Jin et al., 2011; Patra et al., 2013; Lee et al., 2013; Ziółkowska et al., 2013; Toley et al., 2013; Shin et al., 2013; S. Yoon et al., 2013; Chan et al., 2013; Albanese et al., 2013; Ruppen et al., 2014; Wang and Wang, 2014; Frey et al., 2014; Sun et al., 2014; Kwapiszewska et al., 2014; Yu et al., 2015; Prabhakarpandian et al., 2015; Chen et al., 2015; J.-Y.J.-Y. Kim et al., 2015; Aijian and Garrell, 2015; Sabhachandani et al., 2016; Patra et al., 2016; Jeong et al., 2016; McMillan et al., 2016). PDMS is biocompatible, permits gas exchange, is inexpensive, easy to mould and manipulate and is optically transparent (Li et al., 2013). The PDMS flow chips created for the 'version 3' microfluidic device were designed with concave shaped wells (Figure 6.5), allowing cells to aggregate at the bottom tip of the well and successfully generate 3D spheroids (Figures 6.7, 6.8 and 6.9).

During the creation of the 'version 2' microfluidic device it was recognised that PMMA was a suitable material for creating the top and bottom enclosing layers. This is due to its effectiveness in allowing fluid flow ports to be fashioned into the material, and also the ability to image through optically transparent PMMA. Therefore, PMMA was chosen for creating the top and bottom enclosing layers, of the 'version 3' microfluidic device. Another material which could have potentially been used is polycarbonate, which is durable, biocompatible, possess suitable optical properties for imaging and can be sterilised through autoclaving (Khan et al., 2005).

The concept of microfluidic devices is to streamline and improve traditional laboratory-based experiments and protocols. Following the optimisation of the 'version 3' microfluidic device, the ability to successfully generate 3D spheroids on the PDMS flow chip was demonstrated and a proof-of-concept experiment was conducted to illustrate its potential application. The evaluation of chemotherapeutics in 3D spheroids is a popular field in anti-cancer research. However, this can be challenging when undertaken using conventional 3D cell culturing methods. As highlighted in Chapter 1, 5-FU is the most commonly used chemotherapeutic for treating CRC (Poon et al., 1989; Thirion et al., 2004). Therefore, 5-FU was selected as the chemotherapeutic agent to treat the 3D HT29 CRC spheroids cultured in the 'version 3' microfluidic device. Cell culturing, 5-FU treatment and cytotoxic analysis of HT29 spheroids were all performed 'on-chip' and excluding the initial cell seeding, every step was conducted through fluid flow. Using the 'version 3' microfluidic device, both quantitative (LDH Assay) and qualitative (fluorescent imaging) data were obtained on the cytotoxic effects of 5-FU on HT29 spheroids (Figure 6.12).

Through evaluating and improving upon 'version 1' and 'version 2' of the microfluidic devices described in this project, the 'version 3' microfluidic device was found to culture, treat and evaluate treatment in 3D spheroids on-chip. This project validates the work on 3D spheroidal cell culturing microfluidic models developed by other researchers (Okuyama et al., 2010; Sun et al., 2014; Chen et al., 2015; Patra et al., 2016). These microfluidic platforms are designed to conveniently screen anti-cancer drugs in a streamlined, high-throughput fashion

on complex 3D cell models. The 'version 3' microfluidic device is another platform, that potentially offers this option for convenience.

There is still the need for further refinement and improvement of the 'version 3' microfluidic device to take it to the next level as a potential product that can be used commercially for clinical application. Like many 3D cell culturing microfluidic devices that have been described in the literature, PDMS is the most commonly used material used for fabrication. However, there are limitations to using PDMS, including the ability to easily absorb organic solvents and small molecules, such as proteins, which can hinder biological experiments and affect their outcomes. In addition, the logistics of preparing and treating PDMS-based devices can be technically challenging for non-specialist users (Mukhopadhyay, 2007; Levenstein et al., 2016). For the purposes of designing and demonstrating "one-off" prototype microfluidic models, PDMS has thus far proven to be effective. However, alternative materials will need to be investigated to transition PDMS-based devices from prototypes into industry standard commercial products.

Next, cell seeding in the 'version 3' microfluidic device was done using a pipette and through the central cell loading/seeding port. The implementation of this port assisted in introducing cells into the device and help improve the workflow. Cell medium exchange, 5-FU treatment, collection of supernatant for the LDH assay and fluorescent dye staining were performed through fluid flow. Patra and co-authors describe a 3D cell culturing microfluidic device, similar to our 'version 3' microfluidic device. The authors used mathematical simulation to calculate fluid flow rates, based upon the geometrical shape of the chambers,

in order to seed cells inside the cell culturing chambers (Patra et al., 2013; Patra et al., 2016). Therefore, for future experiments, cell seeding through fluid flow would be an ideal step to implement and establish the microfluidic device as a full fluid flow system.

Another factor which may need to be considered when improving the 'version 3' microfluidic device, is the continuous perfusion of cell media and fluids. Currently, the fluidic environment in the 'version 3' microfluidic device is both static and dynamic. The environment is dynamic when fluid is flowing through the device and static when in incubation. A fully dynamic and continuous fluid flow environment would mimic systemic circulation and create a more clinically relevant microfluidic model (van Duinen et al., 2015). The LDH assay and fluorescent imaging techniques were used in this study for evaluation. Although these methods are adequate for quickly analysing cytotoxicity in spheroids, it would be ideal to perform further invasive and in-depth histological analyses, which would require the physical extraction of 3D spheroids from the microfluidic device (Patra et al., 2013; Clayton et al., 2018). Finally, the microfluidic setup described in this study relied on an external single syringe pump setup to drive fluid flow. Although the path of fluid flow through the device is pre-set to reduce manual labour, setting up the syringe pump and loading independent syringes still requires manual input and would benefit from an automated delivery system with multiple preloaded fluid reservoirs following a pre-programmed sequence, flow rate and timing schedule (Safavieh and Juncker, 2013; Korir and Prakash, 2015).

In summary, three versions of a 3D cell culturing microfluidic device were created in this research project. It was found that the 'version 3' microfluidic device was the most effective as a streamlined 3D cell culturing platform. This included the culture, treatment and evaluation of cytotoxicity in 3D HT29 CRC spheroids through fluid flow on a single microfluidic device.

7.4 Research summary, conclusions and future work

The aims of this research project were to 1) evaluate different 3D cell culturing methods for generating 3D spheroidal cell models of CRC, 2) evaluate Hypericin mediated PDT as a potential treatment technique for CRC, and 3) develop a novel 3D cell culturing microfluidic device.

First, as shown in Chapter 4, different 3D cell culturing methods were evaluated to illustrate their inherent advantages and limitations. As described in Chapter 1, 3D spheroidal cell models are better representations of cancers as compared to conventional and traditional 2D monolayered cell cultures. Recently, there has been emerging research in further complex *in vitro* models of cancers. These include advanced 3D co-culture models, as described in Chapter 1, which aim to incorporate stromal, mesenchymal and endothelial cell lines into 3D carcinoma cell models and organoids. Colorectal organoids, produced from patient tumour tissue specimens and driven by the self-renewing capabilities of the colonic epithelium, have recently been investigated as enhanced *in vitro* models of CRC (Sato et al., 2011). In comparison to 3D spheroidal cell models, generated from commercially available immortalised cell lines, patient-specific organoids are derived from primary patient tumour tissue and reflect similar genetic expression, tissue architecture and treatment response to anti-cancer

therapies as the primary tumour (van De Wetering et al., 2015). Organoids can therefore potentially be used for designing personalised medicines, in addition to serving as useful tools for anti-cancer research.

In this research project, Hypericin mediated PDT was evaluated in 2D and 3D cell models of CRC and was found to be an effective method of killing both cancer cell models. Therefore, there is potential for Hypericin mediated PDT to be clinically applied in treating and managing CRC. However, as identified in this research project, 3D spheroidal models of HT29 and HCT116 CRC cell lines were more resistant to PDT as compared to their 2D monolayered counterparts. For future experiments, identifying and addressing the contributors of resistance to Hypericin mediated PDT, such as ABCG2, could potentially improve cell response. Re-designing the PDT experimental protocol, to include periods of reoxygenation and delivering light over a prolonged period of time through low light fluency, could further enhance PDT cell killing in 3D spheroidal cell models and other complex *in vitro* cell cultures. Following *in vitro* investigations, further pre-clinical evaluation in small animal models, will be required to be undertaken to confirm the findings from this research project.

The final part of this research project was the development of a 3D cell culturing microfluidic device. Three different versions of the microfluidic device were designed and tested, and the 'version 3' microfluidic device was found to be an effective platform for culturing, treating and evaluating cell death in 3D spheroids. The wider implication of 3D cell culturing microfluidic devices is that they can potentially address many needs in contemporary research. These microfluidic platforms can replace conventional 3D cell culturing methods by

accommodating the culture, treatment and evaluation of 3D spheroids "on-chip". As described above, organoids can potentially replace 3D spheroidal cell cultures and the combination of organoids and microfluidics could provide a platform that can 1) be used by clinicians to design and rapidly evaluate personalised medicines, and 2) provide an alternative to the use of animals in research. Taken into consideration the scope of potential applications, the 'version 3' microfluidic device is exciting and will benefit from further development to take it to a level where routine usage in the laboratory is possible.

REFERENCES

8 REFERENCES

Abdel Gaber, S.A., Müller, P., Zimmermann, W., Hüttenberger, D., Wittig, R., Abdel Kader, M.H. and Stepp, H. 2018. ABCG2-mediated suppression of chlorin e6 accumulation and photodynamic therapy efficiency in glioblastoma cell lines can be reversed by KO143. *Journal of Photochemistry and Photobiology B: Biology*. **178**(July), pp.182–191.

Abenojar, J., Torregrosa-Coque, R., Martínez, M.A. and Martín-Martínez, J.M. 2009. Surface modifications of polycarbonate (PC) and acrylonitrile butadiene styrene (ABS) copolymer by treatment with atmospheric plasma. *Surface and Coatings Technology*. **203**(16), pp.2173–2180.

Abulafi, A.M., DeJode, M.L., Allardice, J.T., Ansell, J.K. and Williams, N.S. 1997. Adjuvant intraoperative photodynamic therapy in experimental colorectal cancer using a new photosensitizer. *British Journal of Surgery*. **84**(3), pp.368–71.

Achilli, T., Meyer, J. and Morgan, J.R. 2012. Advances in the formation, use and understanding of multi- cellular spheroids. *Expert Opin Biol Ther*. **12**(10), pp.1347–1360.

Adigbli, D.K. and MacRobert, A.J. 2012. Photochemical internalisation: the journey from basic scientific concept to the threshold of clinical application. *Current Opinion in Pharmacology*. **12**(4), pp.434–8.

Agostinis, P., Vantieghem, A., Merlevede, W. and De Witte, P.A.M. 2002. Hypericin in cancer treatment: More light on the way. *The International Journal of Biochemistry and Cell Biology*. **34**(3), pp.221–241.

Aijian, A.P. and Garrell, R.L. 2015. Digital Microfluidics for Automated Hanging Drop Cell Spheroid Culture. *Journal of Laboratory Automation*. **20**(3), pp.283–295.

Albanese, A., Lam, A.K., Sykes, E.A., Rocheleau, J. V. and Chan, W.C.W. 2013. Tumour-on-a-chip provides an optical window into nanoparticle tissue transport. *Nature Communications*. **4**(1), p.2718.

Ali, U., Karim, K.J.B.A. and Buang, N.A. 2015. A Review of the Properties and Applications of Poly (Methyl Methacrylate) (PMMA). *Polymer Reviews*. **55**(4), pp.678–705.

Allardice, J.T., Abulafi, A.M., Grahn, M.F. and Williams, N.S. 1994. Adjuvant intraoperative photodynamic therapy for colorectal carcinoma: a clinical study. *Surgical Oncology*. **3**(1), pp.1–10.

Allison, B.A., Pritchard, P.H. and Levy, J.G. 1994. Evidence for low-density lipoprotein receptor-mediated uptake of benzoporphyrin derivative. *British Journal of Cancer*. **69**(5), pp.833–839.

Allison, R.R., Downie, G.H., Cuenca, R., Hu, X.H., Childs, C.J.H. and Sibata, C.H. 2004. Photosensitizers in clinical PDT. *Photodiagnosis and Photodynamic Therapy*. **1**(1), pp.27–42.

Amann, A., Zwierzina, M., Koeck, S., Gamerith, G., Pechriggl, E., Huber, J.M., Lorenz, E., Kelm, J.M., Hilbe, W., Zwierzina, H. and Kern, J. 2017. Development of a 3D angiogenesis model to study tumour - endothelial cell interactions and the effects of anti-angiogenic drugs. *Scientific Reports*. **7**(1), pp.1–13.

Andrew, H., Gossedge, G., Croft, J., Corrigan, N., Brown, J.M., West, N., Quirke, P., Tolan, D., Cahill, R. and Jayne, D.G. 2016. Next Generation intraoperative Lymph node staging for Stratified colon cancer surgery (GLiSten): a multicentre, multinational feasibility study of fluorescence in predicting lymph node-positive disease. *Efficacy and Mechanism Evaluation*. **3**(6), pp.1–122.

Antoni, D., Burckel, H., Josset, E. and Noel, G. 2015. Three-dimensional cell culture: a breakthrough in vivo. *International Journal of Molecular Sciences*. **16**(3), pp.5517–5527.

Armstrong, G., Smith, A. and Toogood, G. 2017. An Overview of Near Infrared Fluorescent Cholangiography with Indocyanine Green during Cholecystectomy. *J Surg Transplant Sci*. **5**(2), p.e1051.

Ayuso, J.M., Basheer, H.A., Monge, R., Sánchez-Álvarez, P., Doblaré, M., Shnyder, S.D., Vinader, V., Afarinkia, K., Fernández, L.J. and Ochoa, I. 2015. Study of the chemotactic response of multicellular spheroids in a microfluidic device. *PLoS ONE*. **10**(10), pp.1–16.

Azhdarzadeh, M., Atyabi, F., Saei, A.A., Varnamkhasti, B.S., Omidi, Y., Fateh, M., Ghavami, M., Shanehsazzadeh, S. and Dinarvand, R. 2016. Theranostic MUC-1 aptamer targeted gold coated superparamagnetic iron oxide nanoparticles for magnetic resonance imaging and photothermal therapy of colon cancer. *Colloids and Surfaces B: Biointerfaces*. **143**, pp.224–232.

Baglo, Y., Liang, B.J., Robey, R.W., Ambudkar, S. V., Gottesman, M.M. and Huang, H.-C. 2019. Porphyrin-lipid assemblies and nanovesicles overcome ABC transporter-mediated photodynamic therapy resistance in cancer cells. *Cancer Letters*. **457**, pp.110–118.

Balls, M. 2002. Future Improvements: Replacement In Vitro Methods. *ILAR Journal*. **43**(Suppl_1), pp.S69–S73.

Banfi, S., Caruso, E., Caprioli, S., Mazzagatti, L., Canti, G., Ravizza, R., Gariboldi, M. and Monti, E. 2004. Photodynamic effects of porphyrin and chlorin photosensitizers in human colon adenocarcinoma cells. *Bioorganic and Medicinal Chemistry*. **12**(18), pp.4853–4860.

Barkett, M. and Gilmore, T.D. 1999. Control of apoptosis by Rel/NF-kappaB transcription factors. *Oncogene*. **18**(49), pp.6910–24.

Barnes, J., Anderson, L.A. and Phillipson, J.D. 2001. St John's wort (Hypericum perforatum L.): a review of its chemistry, pharmacology and clinical properties. *Journal of Pharmacy and Pharmacology*. **53**(5), pp.583–600.

Barr, H., Krasner, N., Boulos, P.B., Chatlani, P. and Bown, S.G. 1990. Photodynamic therapy for colorectal cancer: a quantitative pilot study. *British Journal of Surgery*. **77**(1), pp.93–6.

Barr, H., Tralau, C.J., MacRobert, A.J., Krasner, N., Boulos, P.B., Clark, C.G. and Bown, S.G. 1987. Photodynamic therapy in the normal rat colon with phthalocyanine sensitisation. *British Journal of Cancer*. **56**(2), pp.111–118.

Bäumler, W., Abels, C., Karrer, S., Weiss, T., Messmann, H., Landthaler, M. and Szeimies, R.M. 1999. Photo-oxidative killing of human colonic cancer cells using indocyanine green and infrared light. *British Journal of Cancer*. **80**(3–4), pp.360–363.

Bender, B.F., Aijian, A.P. and Garrell, R.L. 2016. Digital microfluidics for spheroid-based invasion assays. *Lab on a chip*. **16**(8), pp.1505–13.

Benderra, Z., Faussat, A.M., Sayada, L., Perrot, J.-Y., Tang, R., Chaoui, D., Morjani, H., Marzac, C., Marie, J.-P. and Legrand, O. 2005. MRP3, BCRP, and P-glycoprotein activities are prognostic factors in adult acute myeloid leukemia. *Clinical cancer research : an official journal of the American Association for Cancer Research*. **11**(21), pp.7764–72.

Berg, K.C.G., Eide, P.W., Eilertsen, I.A., Johannessen, B., Bruun, J., Danielsen, S.A., Bjørnslett, M., Meza-Zepeda, L.A., Eknæs, M., Lind, G.E., Myklebost, O., Skotheim, R.I., Sveen, A. and Lothe, R.A. 2017. Multi-omics of 34 colorectal cancer cell lines - a resource for biomedical studies. *Molecular Cancer*. **16**(1), p.116.

Bhatti, M., Yahioglu, G., Milgrom, L.R., Garcia-Maya, M., Chester, K.A. and Deonarain, M.P. 2008. Targeted photodynamic therapy with multiply-loaded recombinant antibody fragments. *International Journal of Cancer*. **122**(5), pp.1155–1163.

Bieging, K.T., Mello, S.S. and Attardi, L.D. 2014. Unravelling mechanisms of p53-mediated tumour suppression. *Nature Reviews Cancer*. **14**(5), pp.359–370.

Bielenberg, D.R. and Zetter, B.R. 2015. The Contribution of Angiogenesis to the Process of Metastasis. *Cancer Journal*. **21**(4), pp.267–273.

Blank, M., Kostenich, G., Lavie, G., Kimel, S., Keisari, Y. and Orenstein, A. 2002. Wavelength-dependent properties of photodynamic therapy using hypericin in vitro and in an animal model. *Photochemistry and Photobiology*. **76**(3), pp.335–340.

Bown, S.G. 2012. How mainstream medicine sees photodynamic therapy in the United Kingdom. *Journal of the National Comprehensive Cancer Network : JNCCN*. **10 Suppl 2**(SUPP.2), pp.S69-74.

Braga, M., Vignali, a, Gianotti, L., Zuliani, W., Radaelli, G., Gruarin, P., Dellabona, P. and Di Carlo, V. 2002. Laparoscopic versus open colorectal surgery: a randomized trial on short-term outcome. *Annals of Surgery*. **236**(6), p.759–66; disscussion 767.

Breslin, S. and O'Driscoll, L. 2013. Three-dimensional cell culture: The missing link in drug discovery. *Drug Discovery Today*. **18**(5–6), pp.240–249.

De Bruijn, H.S., Brooks, S., Van Der Ploeg-Van Den Heuvel, A., Ten Hagen, T.L.M., De Haas, E.R.M. and Robinson, D.J. 2016. Light fractionation significantly increases the efficacy of photodynamic therapy using BF-200 ALA in normal mouse skin. *PLoS ONE*. **11**(2), pp.1–20.

Brunner, H., Hausmann, F., Krieg, R.C., Endlicher, E., Scholmerich, J., Knuechel, R. and Messmann, H. 2001. The effects of 5-aminolevulinic acid esters on protoporphyrin IX production in human adenocarcinoma cell lines Brunner H. *Photochemistry and Photobiology*. **74**(5), pp.721–725.

Bugaj, A., Kwitniewski, M., Iani, V., Juzeniene, A., Juzenas, P., Ma, L.W. and Moan, J. 2007. Photodynamic therapy with di-l-arginine protoporphyrinate on WiDr human colon adenocarcinoma xenografts in athymic nude mice. *Photodiagnosis and Photodynamic Therapy*. **4**(4), pp.237–241.

Cai, J., Yang, J. and Jones, D. 1998. Mitochondrial control of apoptosis: the role of cytochrome c. *Biochimica et Biophysica Acta (BBA) - Bioenergetics*. **1366**(1), pp.139–149.

Cancer Research UK 2016. Bowel cancer mortality statistics. [Accessed 25 January 2018]. Available from: https://www.cancerresearchuk.org/health-professional/cancer-statistics/statistics-by-cancer-type/bowel-cancer/mortality.

Cancer Research UK 2015. Bowel cancer statistics. [Accessed 25 January 2018]. Available from: https://www.cancerresearchuk.org/health-professional/cancer-statistics/statistics-by-cancer-type/bowel-cancer.

Carcenac, M., Larroque, C., Langlois, R., Van Lier, J.E., Artus, J.C. and Pèlegrin, A. 1999. Preparation, phototoxicity and biodistribution studies of anti-carcinoembryonic antigen monoclonal antibody-phthalocyanine conjugates. *Photochemistry and Photobiology*. **70**(6), pp.930–936.

Carrera, E.T., Dias, H.B., Corbi, S.C.T., Marcantonio, R.A.C., Bernardi, A.C.A., Bagnato, V.S., Hamblin, M.R. and Rastelli, A.N.S. 2016. The application of antimicrobial photodynamic therapy (aPDT) in dentistry: A critical review. *Laser Physics*. **26**(12).

Castano, A.P., Demidova, T.N. and Hamblin, M.R. 2005. Mechanisms in photodynamic therapy: part two—cellular signaling, cell metabolism and modes of cell death. *Photodiagnosis and Photodynamic Therapy*. **2**(1), pp.1–23.

Castano, A.P., Mroz, P. and Hamblin, M.R. 2006. Photodynamic therapy and anti-tumour immunity. *Nature reviews. Cancer*. **6**(7), pp.535–45.

Cekanova, M. and Rathore, K. 2014. Animal models and therapeutic molecular targets of cancer: Utility and limitations. *Drug Design, Development and Therapy*. **8**, pp.1911–1922.

Cengel, K.A., Simone, C.B. and Glatstein, E. 2016. PDT: What's past is prologue. *Cancer Research*. **76**(9), pp.2497–2499.

Chan, H.F., Zhang, Y., Ho, Y.-P., Chiu, Y.-L., Jung, Y. and Leong, K.W. 2013. Rapid formation of multicellular spheroids in double-emulsion droplets with controllable microenvironment. *Scientific Reports*. **3**(1), p.3462.

Chen, Y.-C., Lou, X., Zhang, Z., Ingram, P. and Yoon, E. 2015. High-Throughput Cancer Cell Sphere Formation for Characterizing the Efficacy of Photo Dynamic Therapy in 3D Cell Cultures. *Scientific Reports*. **5**(1), p.12175.

Chen, Y., Li, H., Deng, Y., Sun, H., Ke, X. and Ci, T. 2017. Near-infrared light triggered drug delivery system for higher efficacy of combined chemo-photothermal treatment. *Acta Biomaterialia*. **51**, pp.374–392.

Cherukuri, P., Glazer, E.S. and Curley, S.A. 2010. Targeted hyperthermia using metal nanoparticles. *Advanced Drug Delivery Reviews*. **62**(3), pp.339–345.

Chitgupi, U., Qin, Y. and Lovell, J.F. 2017. Targeted Nanomaterials for Phototherapy. *Nanotheranostics*. **1**(1), pp.38–58.

Chiu, S.M., Xue, L.Y., Azizuddin, K. and Oleinick, N.L. 2005. Photodynamic therapy-induced death of HCT 116 cells: Apoptosis with or without Bax expression. *Apoptosis*. **10**(6), pp.1357–1368.

Clark, R., Kerr, I.D. and Callaghan, R. 2006. Multiple drugbinding sites on the R482G isoform of the ABCG2 transporter. *British Journal of Pharmacology*. **149**(5), pp.506–515.

Clayton, N.P., Burwell, A., Jensen, H., Williams, B.F., Brown, Q.D., Ovwigho, P., Ramaiahgari, S., Hermon, T. and Dixon, D. 2018. Preparation of Three-dimensional (3-D) Human Liver (HepaRG) Cultures for Histochemical and Immunohistochemical Staining and Light Microscopic Evaluation. *Toxicologic Pathology*. **46**(6), pp.653–659.

Colucci, G., Gebbia, V., Paoletti, G., Giuliani, F., Caruso, M., Gebbia, N., Cartenì, G., Agostara, B., Pezzella, G., Manzione, L., Borsellino, N., Misino, A., Romito, S., Durini, E., Cordio, S., Di Seri, M., Lopez, M. and Maiello, E. 2005. Phase III randomized trial of FOLFIRI versus FOLFOX4 in the treatment of advanced colorectal cancer: A Multicenter Study of the Gruppo Oncologico Dell'Italia Meridionale. *Journal of Clinical Oncology*. **23**(22), pp.4866–4875.

Costa, E.C., Gaspar, V.M., Coutinho, P. and Correia, I.J. 2014. Optimization of liquid overlay technique to formulate heterogenic 3D co-cultures models. *Biotechnology and Bioengineering*. **111**(8), pp.1672–1685.

Costa, E.C., de Melo-Diogo, D., Moreira, A.F., Carvalho, M.P. and Correia, I.J. 2018. Spheroids Formation on Non-Adhesive Surfaces by Liquid Overlay Technique: Considerations and Practical Approaches. *Biotechnology Journal*. **13**(1), pp.1–12.

Crockett, S.L. and Robson, N.K.B. 2011. Taxonomy and Chemotaxonomy of the Genus Hypericum. *Medicinal and aromatic plant science and biotechnology*. **5**(Special Issue 1), pp.1–13.

Cui, Y. and Guo, G. 2016. Immunomodulatory function of the tumor suppressor p53 in host immune response and the tumor microenvironment. *International Journal of Molecular Sciences*. **17**(11).

van Cutsem, E., Köhne, C.-H., Hitre, E., Zaluski, J., Chang Chien, C.-R., Makhson, A., D'Haens, G., Pintér, T., Lim, R., Bodoky, G., Roh, J.K., Folprecht, G., Ruff, P., Stroh, C., Tejpar, S., Schlichting, M., Nippgen, J. and Rougier, P. 2009. Cetuximab and Chemotherapy as Initial Treatment for Metastatic Colorectal Cancer. *New England Journal of Medicine*. **360**(14), pp.1408–1417.

van Cutsem, E., Köhne, C.H., Láng, I., Folprecht, G., Nowacki, M.P., Cascinu, S., Shchepotin, I., Maurel, J., Cunningham, D., Tejpar, S., Schlichting, M., Zubel, A., Celik, I., Rougier, P. and Ciardiello, F. 2011. Cetuximab plus irinotecan, fluorouracil, and leucovorin as first-line treatment for metastatic colorectal cancer: Updated analysis of overall survival according to tumor KRAS and BRAF mutation status. *Journal of Clinical Oncology*. **29**(15), pp.2011–2019.

Damiano, M.G., Mutharasan, R.K., Tripathy, S., McMahon, K.M. and Thaxton, C.S. 2013. Templated high density lipoprotein nanoparticles as potential therapies and for molecular delivery. *Advanced Drug Delivery Reviews*. **65**(5), pp.649–662.

Denayer, T., Stöhrn, T. and Van Roy, M. 2014. Animal models in translational medicine: Validation and prediction. *New Horizons in Translational Medicine*. **2**(1), pp.5–11.

Dewaele, M., Martinet, W., Rubio, N., Verfaillie, T., de Witte, P.A., Piette, J. and Agostinis, P. 2011. Autophagy pathways activated in response to PDT contribute to cell resistance against ROS damage. *Journal of Cellular and Molecular Medicine*. **15**(6), pp.1402–1414.

Doke, S.K. and Dhawale, S.C. 2015. Alternatives to animal testing: A review. *Saudi Pharmaceutical Journal*. **23**(3), pp.223–229.

Dolmans, D.E.J.G.J., Fukumura, D. and Jain, R.K. 2003. Photodynamic therapy for cancer. *Nature reviews. Cancer*. **3**(5), pp.380–7.

Dougherty, T.J., Gomer, C.J., Henderson, B.W., Jori, G., Kessel, D., Korbelik, M., Moan, J. and Peng, Q. 1998. Photodynamic therapy. *Journal of the National Cancer Institute*. **90**(12), pp.889–905.

Dougherty, T.J., Kaufman, J.E., Goldfarb, A., Weishaupt, K.R., Boyle, D. and Mittleman, A. 1978. Photoradiation Therapy for the Treatment of Malignant Tumors Photoradiation Therapy for the Treatment of Malignant Tumors1. . **38**(August), pp.2628–2635.

Douillard, J.Y., Siena, S., Cassidy, J., Tabernero, J., Burkes, R., Barugel, M., Humblet, Y., Bodoky, G., Cunningham, D., Jassem, J., Rivera, F., Kocákova, I., Ruff, P., Błasińska-Morawiec, M., Šmakal, M., Canon, J.L., Rother, M., Oliner, K.S., Wolf, M. and Gansert, J. 2010. Randomized, Phase III trial of panitumumab with infusional fluorouracil, leucovorin, and oxaliplatin (FOLFOX4) Versus FOLFOX4 alone as first-line treatment in patients with previously untreated metastatic colorectal cancer: The PRIME study. *Journal of Clinical Oncology*. **28**(31), pp.4697–4705.

Du, D., Su, Z., Wang, D., Liu, W. and Wei, Z. 2018. Optimal Interval to Surgery After Neoadjuvant Chemoradiotherapy in Rectal Cancer: A Systematic Review and Meta-analysis. *Clinical Colorectal Cancer*. **17**(1), pp.13–24.

van Duijnhoven, F.H., Rovers, J.P., Engelmann, K., Krajina, Z., Purkiss, S.F., Zoetmulder, F.A.N., Vogl, T.J. and Terpstra, O.T. 2005. Photodynamic therapy with 5,10,15,20-tetrakis(m-hydroxyphenyl) bacteriochlorin for colorectal liver metastases is safe and feasible: Results from a phase I study. *Annals of Surgical Oncology*. **12**(10), pp.808–816.

van Duinen, V., Trietsch, S.J., Joore, J., Vulto, P. and Hankemeier, T. 2015. Microfluidic 3D cell culture: from tools to tissue models. *Current Opinion in Biotechnology*. **35**, pp.118–126.

Duncombe, T.A., Tentori, A.M. and Herr, A.E. 2015. Microfluidics: Reframing biological enquiry. *Nature Reviews Molecular Cell Biology*. **16**(9), pp.554–567.

Eder, T., Weber, A., Neuwirt, H., Grünbacher, G., Ploner, C., Klocker, H., Sampson, N. and Eder, I.E. 2016. Cancer-associated fibroblastsmodify the response of prostate cancer cells to androgen and anti-androgens in three-dimensional spheroid culture. *International Journal of Molecular Sciences*. **17**(9), pp.1–15.

Edmondson, R., Broglie, J.J., Adcock, A.F. and Yang, L. 2014. Three-Dimensional Cell Culture Systems and Their Applications in Drug Discovery and Cell-Based Biosensors. *ASSAY and Drug Development Technologies*. **12**(4), pp.207–218.

Edwards, M.S., Chadda, S.D., Zhao, Z., Barber, B.L. and Sykes, D.P. 2012. A systematic review of treatment guidelines for metastatic colorectal cancer. *Colorectal Disease*. **14**(2), pp.e31–e47.

Eichhorn, M.E., Strieth, S. and Dellian, M. 2004. Anti-vascular tumor therapy: Recent advances, pitfalls and clinical perspectives. *Drug Resistance Updates*. **7**(2), pp.125–138.

Einafshar, E., Asl, A.H., Nia, A.H., Mohammadi, M., Malekzadeh, A. and Ramezani, M. 2018. New cyclodextrin-based nanocarriers for drug delivery and phototherapy using an irinotecan metabolite. *Carbohydrate Polymers*. **194**(March), pp.103–110.

Eljamel, S. 2010. Photodynamic applications in brain tumors: A comprehensive review of the literature. *Photodiagnosis and Photodynamic Therapy*. **7**(2), pp.76–85.

Fadok, V.A., Bratton, D.L., Frasch, S.C., Warner, M.L. and Henson, P.M. 1998. The role of phosphatidylserine in recognition of apoptotic cells by phagocytes. *Cell Death and Differentiation*. **5**(7), pp.551–562.

Fang, X., Sittadjody, S., Gyabaah, K., Opara, E.C. and Balaji, K.C. 2013. Novel 3D Co-Culture Model for Epithelial-Stromal Cells Interaction in Prostate Cancer. *PLoS ONE*. **8**(9), pp.1–10.

Fang, Y. and Eglen, R.M. 2017. Three-Dimensional Cell Cultures in Drug Discovery and Development. *SLAS Discovery*. **22**(5), pp.456–472.

Ferreira, C.S.M., Cheung, M.C., Missailidis, S., Bisland, S. and Gariépy, J. 2009. Phototoxic aptamers selectively enter and kill epithelial cancer cells. *Nucleic Acids Research*. **37**(3), pp.866–876.

Fisher, A., Rucker, N., Wong, S. and Gomer, C. 1998. Differential photosensitivity in wild-type and mutant p53 human colon carcinoma cell lines. *Journal of Photochemistry and …*. **42**, pp.104–7.

Forster, J., Harriss-Phillips, W., Douglass, M. and Bezak, E. 2017. A review of the development of tumor vasculature and its effects on the tumor microenvironment. *Hypoxia*. **Volume 5**, pp.21–32.

Foty, R. 2011. A Simple Hanging Drop Cell Culture Protocol for Generation of 3D Spheroids. *Journal of Visualized Experiments*. **20**(51), pp.4–7.

Franken, A.C.W., Lokman, B.C., Ram, A.F.J., Punt, P.J., Van Den Hondel, C.A.M.J.J. and De Weert, S. 2011. Heme biosynthesis and its regulation: Towards understanding and improvement of heme biosynthesis in filamentous fungi. *Applied Microbiology and Biotechnology*. **91**(3), pp.447–460.

Frey, O., Misun, P.M., Fluri, D.A., Hengstler, J.G. and Hierlemann, A. 2014. Reconfigurable microfluidic hanging drop network for multi-tissue interaction and analysis. *Nature communications*. **5**(May), pp.1–11.

Friedrich, J., Seidel, C., Ebner, R. and Kunz-Schughart, L.A. 2009. Spheroid-based drug screen: considerations and practical approach. *Nature Protocols*. **4**(3), pp.309–324.

Fromm, D., Kessel, D. and Webber, J. 1996. Feasibility of photodynamic therapy using endogenous photosensitization for colon cancer. *Archives of surgery (Chicago, Ill. : 1960)*. **131**(6), pp.667–9.

Furukawa, K., Okunaka, T., Yamamoto, H., Tsuchida, T., Usuda, J., Kumasaka, H., Ishida, J., Konaka, C. and Kato, H. 1999. Effectiveness of Photodynamic Therapy and Nd-YAG Laser Treatment for Obstructed Tracheobronchial Malignancies. *Diagnostic and therapeutic endoscopy*. **5**(3), pp.161–6.

Gale, B., Jafek, A., Lambert, C., Goenner, B., Moghimifam, H., Nze, U. and Kamarapu, S. 2018. A Review of Current Methods in Microfluidic Device Fabrication and Future Commercialization Prospects. *Inventions*. **3**(3), p.60.

Ganin, D. V, Lapshin, K.E., Obidin, A.Z. and Vartapetov, S.K. 2018. High-precision cutting of polyimide film using femtosecond laser for the application in flexible electronics. *Journal of Physics: Conference Series*. **945**, p.012019.

Gariboldi, M.B., Ravizza, R., Baranyai, P., Caruso, E., Banfi, S., Meschini, S. and Monti, E. 2009. Photodynamic effects of novel 5,15-diaryl-tetrapyrrole derivatives on human colon carcinoma cells. *Bioorganic & Medicinal Chemistry*. **17**(5), pp.2009–2016.

Gaskell, H., Sharma, P., Colley, H.E., Murdoch, C., Williams, D.P. and Webb, S.D. 2016. Characterization of a functional C3A liver spheroid model. *Toxicology Research*. **5**(4), pp.1053–1065.

Gederaas, O.A., Rasch, M.H., Berg, K., Lagerberg, J.W.M. and Dubbelman, T.M.A.R. 1999. Photodynamically induced effects in colon carcinoma cells (WiDr) by endogenous photosensitizers generated by incubation with 5-aminolaevulinic acid. *Journal of Photochemistry and Photobiology B: Biology*. **49**(2–3), pp.162–170.

Ghosh, J.C., Dohi, T., Kang, B.H. and Altieri, D.C. 2008. Hsp60 Regulation of Tumor Cell Apoptosis. *Journal of Biological Chemistry*. **283**(8), pp.5188–5194.

Giantonio, B.J., Catalano, P.J., Meropol, N.J., O'Dwyer, P.J., Mitchell, E.P., Alberts, S.R., Schwartz, M.A. and Benson, A.B. 2007. Bevacizumab in combination with oxaliplatin, fluorouracil, and leucovorin (FOLFOX4) for previously treated metastatic colorectal cancer: Results from the Eastern Cooperative Oncology Group Study E3200. *Journal of Clinical Oncology*. **25**(12), pp.1539–1544.

Goldberg, R.M., Sargent, D.J., Morton, R.F., Fuchs, C.S., Ramanathan, R.K., Williamson, S.K., Findlay, B.P., Pitot, H.C. and Alberts, S.R. 2004. A randomized controlled trial of fluorouracil plus leucovorin, irinotecan, and oxaliplatin combinations in patients with previously untreated metastatic colorectal cancer. *Journal of Clinical Oncology*. **22**(1), pp.23–30.

Gomer, C.J. 1991. PRECLINICAL EXAMINATION OF FIRST and SECOND GENERATION PHOTOSENSITIZERS USED IN PHOTODYNAMIC THERAPY. *Photochemistry and Photobiology*. **54**(6), pp.1093–1107.

Goodrich, G.P., Bao, L., Gill-Sharp, K., Sang, K.L., Wang, J. and Payne, J.D. 2010. Photothermal therapy in a murine colon cancer model using near-infrared absorbing gold nanorods. *Journal of biomedical optics*. **15**(1), p.018001.

Goodwin, T.J., Prewett, T.L., Wolf, D.A. and Spaulding, G.F. 1993. Reduced shear stress: A major component in the ability of mammalian tissues to form three-dimensional assemblies in simulated microgravity. *Journal of Cellular Biochemistry*. **51**(3), pp.301–311.

Green, B.L., Marshall, H.C., Collinson, F., Quirke, P., Guillou, P., Jayne, D.G. and Brown, J.M. 2013. Long-term follow-up of the Medical Research Council CLASICC trial of conventional versus laparoscopically assisted resection in colorectal cancer. *British Journal of Surgery*. **100**(1), pp.75–82.

Gustavsson, B., Carlsson, G., MacHover, D., Petrelli, N., Roth, A., Schmoll, H.J., Tveit, K.M. and Gibson, F. 2015. A review of the evolution of systemic chemotherapy in the management of colorectal cancer. *Clinical Colorectal Cancer*. **14**(1), pp.1–10.

Hadler, C., Wissel, K., Brandes, G., Dempwolf, W., Reuter, G., Lenarz, T. and Menzel, H. 2017. Photochemical coating of Kapton® with hydrophilic polymers for the improvement of neural implants. *Materials Science and Engineering: C*. **75**, pp.286–296.

Hahn, S.M., Putt, M.E., Metz, J., Shin, D.B., Rickter, E., Menon, C., Smith, D., Glatstein, E., Fraker, D.L. and Busch, T.M. 2006. Photofrin uptake in the tumor and normal tissues of patients receiving intraperitoneal photodynamic therapy. *Clinical Cancer Research*. **12**(18), pp.5464–5470.

Hajri, A., Wack, S., Meyer, C., Smith, M.K., Leberquier, C., Kedinger, M. and Aprahamian, M. 2002. In vitro and in vivo efficacy of photofrin and pheophorbide a, a bacteriochlorin, in photodynamic therapy of colonic cancer cells. *Photochemistry and photobiology*. **75**(2), pp.140–8.

Halkia, E., Kopanakis, N., Nikolaou, G. and Spiliotis, J. 2015. Cytoreductive surgery and HIPEC for peritoneal carcinomatosis. A review on morbidity and mortality. *Journal of B.U.ON. : official journal of the Balkan Union of Oncology*. **20**, pp.S80–S87.

Hamdan, K.A., Tait, I.S., Nadeau, V., Padgett, M., Carey, F. and Steele, R.J. 2003. Treatment of grade III anal intraepithelial neoplasia with photodynamic therapy: report of a case. *Dis.Colon Rectum*. **46**(0012–3706 (Print)), pp.1555–1559.

Hanahan, D. and Weinberg, R.A. 2000. The Hallmarks of Cancer. *Cell*. **100**(1), pp.57–70.

Hanlon, J.G., Adams, K., Rainbow, A.J., Gupta, R.S. and Singh, G. 2001. Induction of Hsp60 by Photofrin-mediated photodynamic therapy. *Journal of Photochemistry and Photobiology B: Biology*. **64**(1), pp.55–61.

Harlow, S.P., Rodriguez-Bigas, M., Mang, T. and Petrelli, N.J. 1995. Intraoperative photodynamic therapy as an adjunct to surgery for recurrent rectal cancer. *Annals of surgical oncology*. **2**(3), pp.228–232.

Härmä, V., Virtanen, J., Mäkelä, R., Happonen, A., Mpindi, J.P., Knuuttila, M., Kohonen, P., Lötjönen, J., Kallioniemi, O. and Nees, M. 2010. A comprehensive panel of three-dimensional models for studies of prostate cancer growth, invasion and drug responses. *PLoS ONE*. **5**(5).

Hatakeyama, T., Murayama, Y., Komatsu, S., Shiozaki, A., Kuriu, Y., Ikoma, H., Nakanishi, M., Ichikawa, D., Fujiwara, H., Okamoto, K., Ochiai, T., Kokuba, Y., Inoue, K., Nakajima, M. and Otsuji, E. 2013. Efficacy of 5-aminolevulinic acid-mediated photodynamic therapy using light-emitting diodes in human colon cancer cells. *Oncology Reports*. **29**(3), pp.911–916.

Hauser, J., Zietlow, J., Köller, M., Esenwein, S.A., Halfmann, H., Awakowicz, P. and Steinau, H.U. 2009. Enhanced cell adhesion to silicone implant material through plasma surface modification. *Journal of materials science. Materials in medicine*. **20**(12), pp.2541–8.

Haylett, A.K. and Moore, J. V. 2002. Comparative analysis of foetal calf and human low density lipoprotein: Relevance for pharmacodynamics of photosensitizers. *Journal of Photochemistry and Photobiology B: Biology*. **66**(3), pp.171–178.

Herrera-Ornelas, L., Petrelli, N.J., Mittelman, A., Dougherty, T.J. and Boyle, D.G. 1986. Photodynamic therapy in patients with colorectal cancer. *Cancer*. **57**(3), pp.677–684.

Hirschhaeuser, F., Menne, H., Dittfeld, C., West, J., Mueller-Klieser, W. and Kunz-Schughart, L.A. 2010. Multicellular tumor spheroids: An underestimated tool is catching up again. *Journal of Biotechnology*. **148**(1), pp.3–15.

Ho, W.Y., Yeap, S.K., Ho, C.L., Rahim, R.A. and Alitheen, N.B. 2012. Development of Multicellular Tumor Spheroid (MCTS) Culture from Breast Cancer Cell and a High Throughput Screening Method Using the MTT Assay. *PLoS ONE*. **7**(9).

Hoffmann, O.I., Ilmberger, C., Magosch, S., Joka, M., Jauch, K.-W. and Mayer, B. 2015. Impact of the spheroid model complexity on drug response. *Journal of Biotechnology*. **205**, pp.14–23.

Home Office 2018. *Annual Statistics of Scientific Procedures on Living Animals Great Britain 2017* [Online]. Available from: https://assets.publishing.service.gov.uk/government/uploads/system/uploads/attachment_data/file/724611/annual-statistics-scientific-procedures-living-animals-2017.pdf.

Honjo, Y., Hrycyna, C.A., Yan, Q.W., Medina-Pérez, W.Y., Robey, R.W., van de Laar, A., Litman, T., Dean, M. and Bates, S.E. 2001. Acquired mutations in the MXR/BCRP/ABCP gene alter substrate specificity in MXR/BCRP/ABCP-overexpressing cells. *Cancer Research*. **61**(18), pp.6635–9.

Hosseinzadeh, H., Atyabi, F., Varnamkhasti, B.S., Hosseinzadeh, R., Ostad, S.N., Ghahremani, M.H. and Dinarvand, R. 2017. SN38 conjugated hyaluronic acid gold nanoparticles as a novel system against metastatic colon cancer cells. *International Journal of Pharmaceutics*. **526**(1–2), pp.339–352.

van Houdt, W.J., Hoogwater, F.J.H., de Bruijn, M.T., Emmink, B.L., Nijkamp, M.W., Raats, D.A.E., van der Groep, P., van Diest, P., Borel Rinkes, I.H.M. and Kranenburg, O. 2010. Oncogenic KRAS Desensitizes Colorectal Tumor Cells to Epidermal Growth Factor Receptor Inhibition and Activation. *Neoplasia*. **12**(6), pp.443-IN2.

Hu, Z., Pan, Y., Wang, J., Chen, J., Li, J. and Ren, L. 2009. Meso-tetra (carboxyphenyl) porphyrin (TCPP) nanoparticles were internalized by SW480 cells by a clathrin-mediated endocytosis pathway to induce high photocytotoxicity. *Biomedicine and Pharmacotherapy*. **63**(2), pp.155–164.

Huang, X. and El-Sayed, M.A. 2010. Gold nanoparticles: Optical properties and implementations in cancer diagnosis and photothermal therapy. *Journal of Advanced Research*. **1**(1), pp.13–28.

Huang, X. and El-Sayed, M.A. 2011. Plasmonic photo-thermal therapy (PPTT). *Alexandria Journal of Medicine*. **47**(1), pp.1–9.

Huang, X., Jain, P.K., El-Sayed, I.H. and El-Sayed, M.A. 2008. Plasmonic photothermal therapy (PPTT) using gold nanoparticles. *Lasers in medical science*. **23**(3), pp.217–28.

Huang, Z., Xu, H., Meyers, A.D., Musani, A.I., Wang, L., Tagg, R., Barqawi, A.B. and Chen, Y.K. 2008. Photodynamic therapy for treatment of solid tumors - potential and technical challenges. *Technology in cancer research & treatment*. **7**(4), pp.309–20.

Hughes, C.S., Postovit, L.M. and Lajoie, G.A. 2010. Matrigel: A complex protein mixture required for optimal growth of cell culture. *PROTEOMICS*. **10**(9), pp.1886–1890.

Ibbotson, S.H. 2011. Adverse effects of topical photodynamic therapy. *Photodermatology Photoimmunology and Photomedicine*. **27**(3), pp.116–130.

Inoue, K., Anai, S., Fujimoto, K., Hirao, Y., Furuse, H., Kai, F., Ozono, S., Hara, T., Matsuyama, H., Oyama, M., Ueno, M., Fukuhara, H., Narukawa, M. and Shuin, T. 2015. Oral 5-aminolevulinic acid mediated photodynamic diagnosis using fluorescence cystoscopy for non-muscle-invasive bladder cancer: A randomized, double-blind, multicentre phase II/III study. *Photodiagnosis and Photodynamic Therapy*. **12**(2), pp.193–200.

Ishiguro, T., Ohata, H., Sato, A., Yamawaki, K., Enomoto, T. and Okamoto, K. 2017. Tumor-derived spheroids: Relevance to cancer stem cells and clinical applications. *Cancer science*. **108**(3), pp.283–289.

Ivascu, A. and Kubbies, M. 2006. Rapid Generation of Single-Tumor Spheroids for High-Throughput Cell Function and Toxicity Analysis. *Journal of Biomolecular Screening*. **11**(8), pp.922–932.

Jaque, D., Martínez Maestro, L., Del Rosal, B., Haro-Gonzalez, P., Benayas, A., Plaza, J.L., Martín Rodríguez, E. and García Solé, J. 2014. Nanoparticles for photothermal therapies. *Nanoscale*. **6**(16), pp.9494–9530.

Jendželovská, Z., Jendželovský, R., Hiľovská, L., Kovaľ, J., Mikeš, J. and Fedoročko, P. 2014. Single pre-treatment with hypericin, a St. John's wort secondary metabolite, attenuates cisplatin- and mitoxantrone-induced cell death in A2780, A2780cis and HL-60 cells. *Toxicology in Vitro*. **28**(7), pp.1259–1273.

Jendželovská, Z., Jendželovský, R., Kuchárová, B. and Fedoročko, P. 2016. Hypericin in the Light and in the Dark: Two Sides of the Same Coin. *Frontiers in Plant Science*. **7**(May), p.560.

Jendželovský, R., Jendželovská, Z., Kuchárová, B. and Fedoročko, P. 2019. Breast cancer resistance protein is the enemy of hypericin accumulation and toxicity of hypericin-mediated photodynamic therapy. *Biomedicine & Pharmacotherapy*. **109**, pp.2173–2181.

Jendzelovsky, R., Mikes, J., Koval, J., Soucek, K., Prochazkova, J., Kello, M., Sackova, V., Hofmanova, J., Kozubik, A., Fedorocko, P., Jendzelovský, R., Mikes, J., Kovaľ, J., Soucek, K., Procházková, J., Kello, M., Sacková, V., Hofmanová, J., Kozubík, A. and Fedorocko, P. 2009. Drug efflux transporters, MRP1 and BCRP, affect the outcome of hypericin-mediated photodynamic therapy in HT-29 adenocarcinoma cells. *Photochemical & Photobiological Sciences*. **8**(12), pp.1716–1723.

Jeong, S.Y., Lee, J.H., Shin, Y., Chung, S. and Kuh, H.J. 2016. Co-culture of tumor spheroids and fibroblasts in a collagen matrix-incorporated microfluidic chip mimics reciprocal activation in solid tumor microenvironment. *PLoS ONE*. **11**(7), pp.1–17.

Jheon, S., Kim, T. and Kim, J.-K. 2011. Photodynamic therapy as an adjunct to surgery or other treatments for squamous cell lung cancers. *Laser therapy*. **20**(2), pp.107–116.

Jin, H.J., Kim, T., Cho, Y.H., Gu, J.M., Kim, J. and Oh, Y.S. 2011. A multicellular spheroid formation and extraction chip using removable cell trapping barriers. *Transactions of the Korean Society of Mechanical Engineers, A*. **35**(2), pp.131–134.

Jonker, J.W., Buitelaar, M., Wagenaar, E., Van Der Valk, M.A., Scheffer, G.L., Scheper, R.J., Plosch, T., Kuipers, F., Elferink, R.P.J.O., Rosing, H., Beijnen, J.H. and Schinkel, A.H. 2002. The breast cancer resistance protein protects against a major chlorophyll-derived dietary phototoxin and protoporphyria. *Proceedings of the National Academy of Sciences of the United States of America*. **99**(24), pp.15649–54.

Justice, B.A., Badr, N.A. and Felder, R.A. 2009. 3D cell culture opens new dimensions in cell-based assays. *Drug Discovery Today*. **14**(1–2), pp.102–107.

Juzeniene, A., Kaliszewski, M., Bugaj, A. and Moan, J. 2009. Clearance of protoporphyrin IX induced by 5-aminolevulinic acid from WiDr human colon carcinoma cells *In*: D. H. Kessel, ed., p.73802Q. Available from: http://proceedings.spiedigitallibrary.org/proceeding.aspx?articleid=782443.

Kamelian, F.S., Saljoughi, E., Shojaee Nasirabadi, P. and Mousavi, S.M. 2018. Modifications and research potentials of acrylonitrile/butadiene/styrene (ABS) membranes: A review. *Polymer Composites*. **39**(8), pp.2835–2846.

Kareliotis, G., Liossi, S. and Makropoulou, M. 2018. Assessment of singlet oxygen dosimetry concepts in photodynamic therapy through computational modeling. *Photodiagnosis and Photodynamic Therapy*. **21**, pp.224–233.

Karioti, A. and Bilia, A.R. 2010. Hypericins as potential leads for new therapeutics. *International Journal of Molecular Sciences*. **11**(2), pp.562–594.

Karnoub, A.E., Dash, A.B., Vo, A.P., Sullivan, A., Brooks, M.W., Bell, G.W., Richardson, A.L., Polyak, K., Tubo, R. and Weinberg, R.A. 2007. Mesenchymal stem cells within tumour stroma promote breast cancer metastasis. *Nature*. **449**(7162), pp.557–563.

Kashtan, H., Papa, M.Z., Wilson, B.C., Deutch, A.A. and Stern, H.S. 1991. Use of photodynamic therapy in the palliation of massive advanced rectal cancer. Phase I/II study. *Diseases of the colon and rectum*. **34**(7), pp.600–605.

Kato, H., Furukawa, K., Sato, M., Okunaka, T., Kusunoki, Y., Kawahara, M., Fukuoka, M., Miyazawa, T., Yana, T., Matsui, K., Shiraishi, T. and Horinouchi, H. 2003. Phase II clinical study of photodynamic therapy using mono-L-aspartyl chlorin e6 and diode laser for early superficial squamous cell carcinoma of the lung. *Lung Cancer*. **42**(1), pp.103–111.

Katt, M.E., Placone, A.L., Wong, A.D., Xu, Z.S. and Searson, P.C. 2016. In Vitro Tumor Models: Advantages, Disadvantages, Variables, and Selecting the Right Platform. *Frontiers in Bioengineering and Biotechnology*. **4**(February).

Kawczyk-Krupka, A., Bugaj, A.M., Latos, W., Wawrzyniec, K., Oleś, P., Mertas, A., Czuba, Z., Król, W., Sieroń-Stołtny, K. and Sieroń, A. 2015. ALA-mediated photodynamic effect on apoptosis induction and secretion of macrophage migration inhibitory factor (MIF) and of monocyte chemotactic protein (MCP-1) by colon cancer cells in normoxia and in hypoxia-like conditions in vitro. *Photodiagnosis and Photodynamic Therapy*. **12**(1), pp.27–35.

Kawczyk-Krupka, A., Bugaj, A.M., Latos, W., Zaremba, K., Wawrzyniec, K., Kucharzewski, M. and Sieroń, A. 2016. Photodynamic therapy in colorectal cancer treatment-The state of the art in preclinical research. *Photodiagnosis and Photodynamic Therapy*. **13**, pp.158–174.

Kawczyk-Krupka, A., Bugaj, A.M., Latos, W., Zaremba, K., Wawrzyniec, K. and Siero, A. 2015. Photodynamic therapy in colorectal cancer treatment: The state of the art in clinical trials. *Photodiagnosis and Photodynamic Therapy*. **12**(3), pp.545–553.

Kelm, J.M., Timmins, N.E., Brown, C.J., Fussenegger, M. and Nielsen, L.K. 2003. Method for generation of homogeneous multicellular tumor spheroids applicable to a wide variety of cell types. *Biotechnology and Bioengineering*. **83**(2), pp.173–180.

Khan, I., Smith, N., Jones, E., Finch, D.S. and Cameron, R.E. 2005. Analysis and evaluation of a biomedical polycarbonate urethane tested in an in vitro study and an ovine arthroplasty model. Part I: materials selection and evaluation. *Biomaterials*. **26**(6), pp.621–631.

Khunweeraphong, N., Stockner, T. and Kuchler, K. 2017. The structure of the human ABC transporter ABCG2 reveals a novel mechanism for drug extrusion. *Scientific Reports*. **7**(1), p.13767.

Kim, J.-Y.J.-Y., Fluri, D.A., Kelm, J.M., Hierlemann, A. and Frey, O. 2015. 96-Well Format-Based Microfluidic Platform for Parallel Interconnection of Multiple Multicellular Spheroids. *Journal of Laboratory Automation*. **20**(3), pp.274–282.

Kim, J. Bin 2005. Three-dimensional tissue culture models in cancer biology. *Seminars in Cancer Biology*. **15**(5), pp.365–77.

Kim, J.H., Park, J.M., Roh, Y.J., Kim, I.-W., Hasan, T. and Choi, M.-G. 2015. Enhanced efficacy of photodynamic therapy by inhibiting ABCG2 in colon cancers. *BMC Cancer*. **15**(1), p.504.

Kim, M., Jung, H.Y. and Park, H.J. 2015. Topical PDT in the treatment of benign skin diseases: Principles and new applications. *International Journal of Molecular Sciences*. **16**(10), pp.23259–23278.

Kim, S.A., Lee, E.K. and Kuh, H.J. 2015. Co-culture of 3D tumor spheroids with fibroblasts as a model for epithelial-mesenchymal transition in vitro. *Experimental Cell Research*. **335**(2), pp.187–196.

Kirui, D.K., Khalidov, I., Wang, Y. and Batt, C.A. 2013. Targeted near-IR hybrid magnetic nanoparticles for in vivo cancer therapy and imaging. *Nanomedicine: Nanotechnology, Biology, and Medicine*. **9**(5), pp.702–711.

Kleinman, H.K. and Martin, G.R. 2005. Matrigel: Basement membrane matrix with biological activity. *Seminars in Cancer Biology*. **15**(5 SPEC. ISS.), pp.378–386.

Koonce, S.L. and Newman, M.I. 2017. Clinics in Oncology A Systematic Review of Concordance between Indocyanine Green and 99m Technetium Sentinel Lymph Node Identification in Melanoma. . **2**, pp.1–5.

Koren, G. 1984. CO2 laser assisted UV ablative photoetching of Kapton films. *Applied Physics Letters*. **45**(1), pp.10–12.

Korir, G. and Prakash, M. 2015. Punch card programmable microfluidics. *PLoS ONE*. **10**(3), pp.1–17.

Krasner, N. 1989. Laser therapy in the management of benign and malignant tumours in the colon and rectum. *International Journal of Colorectal Disease*. **4**(1), pp.2–5.

Krieg, R.C., Messmann, H., Rauch, J., Seeger, S. and Knuechel, R. 2002. Metabolic characterization of tumor cell-specific protoporphyrin IX accumulation after exposure to 5-aminolevulinic acid in human colonic cells. *Photochemistry and photobiology*. **76**(5), pp.518–25.

Kubin, A., Wierrani, F., Burner, U., Alth, G. and Grunberger, W. 2005. Hypericin - The Facts About a Controversial Agent. *Current Pharmaceutical Design*. **11**(2), pp.233–253.

Kuchárová, B., Mikeš, J., Jendželovský, R., Vargová, J., Mikešová, L., Jendželovská, Z., Kovaľ, J. and Fedoročko, P. 2015. Potentiation of hypericin-mediated photodynamic therapy cytotoxicity by MK-886: Focus on ABC transporters, GDF-15 and redox status. *Photodiagnosis and Photodynamic Therapy*. **12**(3), pp.490–503.

Kuliková, L., Mikeš, J., Hýžďalová, M., Palumbo, G. and Fedoročko, P. 2010. NF-κB is not directly responsible for photoresistance induced by fractionated light delivery in HT-29 colon adenocarcinoma cells. *Photochemistry and Photobiology*. **86**(6), pp.1285–1293.

Kuo, C. Te, Wang, J.Y., Lin, Y.F., Wo, A.M., Chen, B.P.C. and Lee, H. 2017. Three-dimensional spheroid culture targeting versatile tissue bioassays using a PDMS-based hanging drop array. *Scientific Reports*. **7**(1), pp.1–10.

Kurokawa, H., Ito, H., Terasaki, M. and Matsui, H. 2019. Hyperthermia enhances photodynamic therapy by regulation of HCP1 and ABCG2 expressions via high level ROS generation. *Scientific Reports*. **9**(1), p.1638.

Kurosawa, H. 2007. Methods for inducing embryoid body formation: in vitro differentiation system of embryonic stem cells. *Journal of Bioscience and Bioengineering*. **103**(5), pp.389–398.

Kwapiszewska, K., Michalczuk, A., Rybka, M., Kwapiszewski, R. and Brzózka, Z. 2014. A microfluidic-based platform for tumour spheroid culture, monitoring and drug screening. *Lab on a chip*. **14**(12), pp.2096–104.

Kye, B. and Cho, H. 2014. Overview of radiation therapy for treating rectal cancer. *Annals of coloproctology*. **30**(4), pp.165–166.

Landau, M.J., Gould, D.J. and Patel, K.M. 2016. Advances in fluorescent-image guided surgery. *Annals of Translational Medicine*. **4**(20), pp.392–392.

Langan, L.M., Dodd, N.J.F., Owen, S.F., Purcell, W.M., Jackson, S.K. and Jha, A.N. 2016. Correction: Direct measurements of oxygen gradients in spheroid culture system using electron paramagnetic resonance oximetry. *PLoS ONE*. **11**(8), pp.1–13.

Langhans, S.A. 2018. Three-Dimensional in Vitro Cell Culture Models in Drug Discovery and Drug Repositioning. *Frontiers in Pharmacology*. **9**.

Lantz, J.M., Meyer, C., Saussine, C., Leberquier, C., Heysel, F., Miehe, J., Marescaux, J., Sultan, R. and Kedinger, M. 1992. Experimental photodynamic therapy with a copper metal vapor laser in colorectal cancer. *International Journal of Cancer*. **52**(3), pp.491–8.

Leal, F., Ferreira, F.P. and Sasse, A.D. 2017. FOLFOXIRI Regimen for Metastatic Colorectal Cancer: A Systematic Review and Meta-Analysis. *Clinical Colorectal Cancer*. **16**(4), p.405–409.e2.

Lee, S.-A., No, D.Y., Kang, E., Ju, J., Kim, D.-S. and Lee, S.-H. 2013. Spheroid-based three-dimensional liver-on-a-chip to investigate hepatocyte–hepatic stellate cell interactions and flow effects. *Lab on a Chip*. **13**(18), p.3529.

Leung, W.N., Sun, X., Mak, N.K. and Yow, C.M. 2002. Photodynamic effects of mTHPC on human colon adenocarcinoma cells: photocytotoxicity, subcellular localization and apoptosis. *Photochemistry and photobiology*. **75**(4), pp.406–411.

Levenstein, M.A., Bawazer, L.A., Mc Nally, C.S., Marchant, W.J., Gong, X., Meldrum, F.C. and Kapur, N. 2016. A reproducible approach to the assembly of microcapillaries for double emulsion production. *Microfluidics and Nanofluidics*. **20**(10), pp.1–11.

Li, J., Chen, F., Cona, M.M., Feng, Y., Himmelreich, U., Oyen, R., Verbruggen, A. and Ni, Y. 2012. A review on various targeted anticancer therapies. *Targeted Oncology*. **7**(1), pp.69–85.

Li, X., Wu, N., Rojanasakul, Y. and Liu, Y. 2013. Selective stamp bonding of PDMS microfluidic devices to polymer substrates for biological applications. *Sensors and Actuators, A: Physical*. **193**, pp.186–192.

Li, X.J., Valadez, A. V, Zuo, P. and Nie, Z. 2012. Microfluidic 3D cell culture: potential application for tissue-based bioassays. *Bioanalysis*. **4**(12), pp.1509–25.

Lim, Y.C., Yoo, J.O., Park, D., Kang, G., Hwang, B.M., Kim, Y.M. and Ha, K.S. 2009. Antitumor effect of photodynamic therapy with chlorin-based photosensitizer DH-II-24 in colorectal carcinoma. *Cancer Science*. **100**(12), pp.2431–2436.

Lin, C.-Y. and Shieh, M.-J. 2018. Near-Infrared Fluorescent Dye-Decorated Nanocages to Form Grenade-like Nanoparticles with Dual Control Release for Photothermal Theranostics and Chemotherapy. *Bioconjugate chemistry*. **29**(4), pp.1384–1398.

Lin, R.Z. and Chang, H.Y. 2008. Recent advances in three-dimensional multicellular spheroid culture for biomedical research. *Biotechnology Journal*. **3**(9–10), pp.1172–1184.

Liska, D., Stocchi, L., Karagkounis, G., Elagili, F., Dietz, D.W., Kalady, M.F., Kessler, H., Remzi, F.H. and Church, J. 2017. Incidence, Patterns, and Predictors of Locoregional Recurrence in Colon Cancer. *Annals of surgical oncology*. **24**(4), pp.1093–1099.

Liu, H.G., Pan, Y.F., You, J., Wang, O.C., Huang, K. Te and Zhang, X.H. 2010. Expression of ABCG2 and its significance in colorectal cancer. *Asian Pacific Journal of Cancer Prevention*. **11**(4), pp.845–8.

Liu, L.J., Brown, S.L., Ewing, J.R., Ala, B.D., Schneider, K.M. and Schlesinger, M. 2016. Estimation of Tumor Interstitial Fluid Pressure (TIFP) Noninvasively T. W. Secomb, ed. *PLOS ONE*. **11**(7), p.e0140892.

Liu, T., Lin, B. and Qin, J. 2010. Carcinoma-associated fibroblasts promoted tumor spheroid invasion on a microfluidic 3D co-culture device. *Lab on a Chip*. **10**(13), p.1671.

Lo, P.-C., Leung, S.C.H., Chan, E.Y.M., Fong, W.-P., Ko, W.-H. and Ng, D.K.P. 2007. Photodynamic effects of a novel series of silicon(IV) phthalocyanines against human colon adenocarcinoma cells. *Photodiagnosis and Photodynamic Therapy*. **4**(2), pp.117–123.

Loschenov, V., Konov, V. and Prokhorov, A. 2000. Photodynamic therapy and fluorescence diagnostics. *Laser Physics*. **10**(6), pp.1188–1207.

Lu, Y.-J., Lin, P.-Y., Huang, P.-H., Kuo, C.-Y., Shalumon, K.T., Chen, M.-Y. and Chen, J.-P. 2018. Magnetic Graphene Oxide for Dual Targeted Delivery of Doxorubicin and Photothermal Therapy. *Nanomaterials*. **8**(4), p.193.

Ludwig, K., Tse, E.S. and Wang, J.Y. 2013. Colon cancer cells adopt an invasive phenotype without mesenchymal transition in 3-D but not 2-D culture upon combined stimulation with EGF and crypt growth factors. *BMC Cancer*. **13**(1), p.221.

Lustig, R.A., Vogl, T.J., Fromm, D., Cuenca, R., Hsi, R.A., D'Cruz, A.K., Krajina, Z., Turić, M., Singhal, A. and Chen, J.C. 2003. A multicenter phase I safety study of intratumoral photoactivation of talaporfin sodium in patients with refractory solid tumors. *Cancer*. **98**(8), pp.1767–1771.

Lyssiotis, C.A. and Kimmelman, A.C. 2017. Metabolic Interactions in the Tumor Microenvironment. *Trends in Cell Biology*. **27**(11), pp.863–875.

Maduray, K. and Davids, L. 2011. The Anticancer Activity of Hypericin in Photodynamic Therapy. *Journal of Bioanalysis & Biomedicine*. **s6**(01), pp.4–6.

Mak, I.W., Evaniew, N. and Ghert, M. 2014. Lost in translation: animal models and clinical trials in cancer treatment. *Am J Transl Res*. **6**(2), pp.114–118.

Manoto, S.L., Houreld, N., Hodgkinson, N. and Abrahamse, H. 2017. Modes of Cell Death Induced by Photodynamic Therapy Using Zinc Phthalocyanine in Lung Cancer Cells Grown as a Monolayer and Three-Dimensional Multicellular Spheroids. *Molecules*. **22**(5).

Manoto, S.L., Sekhejane, P.R., Houreld, N.N. and Abrahamse, H. 2012. Localization and phototoxic effect of zinc sulfophthalocyanine photosensitizer in human colon (DLD-1) and lung (A549) carcinoma cells (in vitro). *Photodiagnosis and Photodynamic Therapy*. **9**(1), pp.52–59.

Martinez, M.A., Abenojar, J. and Lopez de Armentia, S. 2018. Environmentally Friendly Plasma Activation of Acrylonitrile–Butadiene–Styrene and Polydimethylsiloxane Surfaces to Improve Paint Adhesion. *Coatings*. **8**(12), p.428.

Mathews, M.S., Angell-Petersen, E., Sanchez, R., Sun, C.H., Vo, V., Hirschberg, H. and Madsen, S.J. 2009. The effects of ultra low fluence rate single and repetitive photodynamic therapy on glioma spheroids. *Lasers in Surgery and Medicine*. **41**(8), pp.578–584.

Matroule, J.Y., Bonizzi, G., Morlière, P., Paillous, N., Santus, R., Bours, V. and Piette, J. 1999. Pyropheophorbide-a methyl ester-mediated photosensitization activates transcription factor NF-kappaB through the interleukin-1 receptor-dependent signaling pathway. *The Journal of biological chemistry*. **274**(5), pp.2988–3000.

Matroule, J.Y., Hellin, A.C., Morlière, P., Fabiano, A.S., Santus, R., Merville, M.P. and Piette, J. 1999. Role of nuclear factor-kappa B in colon cancer cell apoptosis mediated by aminopyropheophorbide photosensitization. *Photochemistry and photobiology*. **70**(4), pp.540–8.

McDonald, J.R., Renehan, A.G., O'Dwyer, S.T. and Haboubi, N.Y. 2012. Lymph node harvest in colon and rectal cancer: Current considerations. *World journal of gastrointestinal surgery*. **4**(1), pp.9–19.

McMillan, K.S., Boyd, M. and Zagnoni, M. 2016. Transitioning from multi-phase to single-phase microfluidics for long-term culture and treatment of multicellular spheroids. *Lab on a chip*. **16**(18), pp.3548–57.

Mehta, G., Hsiao, A.Y., Ingram, M., Luker, G.D. and Takayama, S. 2012. Opportunities and challenges for use of tumor spheroids as models to test drug delivery and efficacy. *Journal of Controlled Release*. **164**(2), pp.192–204.

Messmann, H., Mlkvy, P., Buonaccorsi, G., Davies, C.L., MacRobert, A.J. and Bown, S.G. 1995. Enhancement of photodynamic therapy with 5-aminolaevulinic acid-induced porphyrin photosensitisation in normal rat colon by threshold and light fractionation studies. *British Journal of Cancer*. **72**(3), pp.589–594.

Mikeš, J., Hýžďalová, M., Kočí, L., Jendželovský, R., Kovaľ, J., Vaculová, A., Hofmanová, J., Kozubík, A. and Fedoročko, P. 2011. Lower sensitivity of FHC fetal colon epithelial cells to photodynamic therapy compared to HT-29 colon adenocarcinoma cells despite higher intracellular accumulation of hypericin. *Photochemical & Photobiological Sciences*. **10**(4), pp.626–32.

Mikes, J., Kleban, J., Sacková, V., Horváth, V., Jamborová, E., Vaculová, A., Kozubík, A., Hofmanová, J. and Fedorocko, P. 2007. Necrosis predominates in the cell death of human colon adenocarcinoma HT-29 cells treated under variable conditions of photodynamic therapy with hypericin. *Photochemical & Photobiological Sciences*. **6**(7), pp.758–66.

Mikes, J., Kovaľ, J., Jendzelovský, R., Sacková, V., Uhrinová, I., Kello, M., Kuliková, L. and Fedorocko, P. 2009. The role of p53 in the efficiency of photodynamic therapy with hypericin and subsequent long-term survival of colon cancer cells. *Photochemical & Photobiological Sciences*. **8**(11), pp.1558–67.

Miller, J.D., Baron, E.D., Scull, H., Hsia, A., Berlin, J.C., McCormick, T., Colussi, V., Kenney, M.E., Cooper, K.D. and Oleinick, N.L. 2007. Photodynamic therapy with the phthalocyanine photosensitizer Pc 4: the case experience with preclinical mechanistic and early clinical-translational studies. *Toxicology and Applied Pharmacology*. **224**(3), pp.290–9.

Milsom, J.W., Bohm, B., Hammerhofer, K.A., Fazio, V., Steiger, E. and Elson, P. 1998. A prospective, randomized trial comparing laparoscopic versus conventional techniques in colorectal cancer surgery: a preliminary report. *Journal of the American College of Surgeons*. **187**(1), pp.46–54.

Mimikos, C., Shafirstein, G. and Arshad, H. 2016. Current state and future of photodynamic therapy for the treatment of head and neck squamous cell carcinoma. *World Journal of Otorhinolaryngology-Head and Neck Surgery*. **2**(2), pp.126–129.

Minnich, D.J., Bryant, A.S., Dooley, A. and Cerfolio, R.J. 2010. Photodynamic Laser Therapy for Lesions in the Airway. *Annals of Thoracic Surgery*. **89**(6), pp.1744–1749.

Misiakos, E.P., Karidis, N.P. and Kouraklis, G. 2011. Current treatment for colorectal liver metastases. *World Journal of Gastroenterology*. **17**(36), pp.4067–4075.

Mitsunaga, M., Tsubota, A., Nariai, K., Namiki, Y., Sumi, M. and Yoshikawa, T. 2007. Early apoptosis and cell death induced by ATX-S10Na ( ) -mediated photodynamic therapy are Bax- and p53-dependent in human colon cancer cells. . **13**(5), pp.692–698.

Mlkvy, P., Messmann, H., Debinski, H., Regula, J., Conio, M., MacRobert, A., Spigelman, A., Phillips, R. and Bown, S.G. 1995. Photodynamic therapy for polyps in familial adenomatous polyposis-a pilot study. *European Journal of Cancer*. **31**(7–8), pp.1160–1165.

Mĺkvy, P., Messmann, H., Regula, J., Conio, M., Pauer, M., Millson, C.E., MacRobert, A.J. and Bown, S.G. 1998. Photodynamic therapy for gastrointestinal tumors using three photosensitizers--ALA induced PPIX, Photofrin and MTHPC. A pilot study. *Neoplasma*. **45**(3), pp.157–61.

Mo, W. and Zhang, J. 2012. Review Article Human ABCG2 : structure , function , and its role in multidrug resistance. *International Journal of Biochemistry and Molecular Biology*. **3**(1), pp.1–27.

Mochida, A., Ogata, F., Nagaya, T., Choyke, P.L. and Kobayashi, H. 2017. Activatable fluorescent probes in fluorescence-guided surgery: Practical considerations. *Bioorganic & Medicinal Chemistry*.

Moghissi, K., Dixon, K. and Gibbins, S. 2015. A Surgical View of Photodynamic Therapy in Oncology: A Review. *Surgery journal (New York, N.Y.)*. **1**(1), pp.e1–e15.

Moghissi, K., Dixon, K., Stringer, M., Freeman, T., Thorpe, A. and Brown, S. 1999. The place of bronchoscopic photodynamic therapy in advanced unresectable lung cancer: experience of 100 cases. *European journal of cardio-thoracic surgery : official journal of the European Association for Cardio-thoracic Surgery*. **15**(1), pp.1–6.

Mohanty, N., Jalaluddin, M., Kotina, S., Routray, S. and Ingale, Y. 2013. Photodynamic therapy: The imminent milieu for treating oral lesions. *Journal of Clinical and Diagnostic Research*. **7**(6), pp.1254–1257.

Mondal, S.B., Gao, S., Zhu, N., Liang, R., Gruev, V. and Achilefu, S. 2014. Real-time fluorescence image-guided oncologic surgery. *Advances in cancer research*. **124**, pp.171–211.

Morisaki, K., Robey, R.W., Özvegy-Laczka, C., Honjo, Y., Polgar, O., Steadman, K., Sarkadi, B. and Bates, S.E. 2005. Single nucleotide polymorphisms modify the transporter activity of ABCG2. *Cancer Chemotherapy and Pharmacology*. **56**(2), pp.161–172.

Moriyama, T., Ohuchida, K., Mizumoto, K., Cui, L., Ikenaga, N., Sato, N. and Tanaka, M. 2010. Enhanced cell migration and invasion of CD133+ pancreatic cancer cells cocultured with pancreatic stromal cells. *Cancer*. **116**(14), pp.3357–3368.

Motoori, M., Yano, M., Tanaka, K., Kishi, K., Takahashi, H., Inoue, M., Saito, T., Sugimura, K., Fujiwara, Y., Ishikawa, O. and Sakon, M. 2015. Intraoperative photodynamic diagnosis of lymph node metastasis in esophageal cancer patients using 5-aminolevulinic acid. *Oncology Letters*. **10**(5), pp.3035–3039.

Mouratidis, P.X.E., Rivens, I. and Ter Haar, G. 2015. A study of thermal dose-induced autophagy, apoptosis and necroptosis in colon cancer cells. *International Journal of Hyperthermia*. **31**(5), pp.476–488.

Mukhopadhyay, R. 2007. When PDMS isn't the best. What are its weaknesses, and which other polymers can researchers add to their toolboxes? *Analytical chemistry*. **79**(9), pp.3248–53.

Muz, B., de la Puente, P., Azab, F. and Azab, A.K. 2015. The role of hypoxia in cancer progression, angiogenesis, metastasis, and resistance to therapy. *Hypoxia*., p.83.

Nakajima, N. and Kawashima, N. 2012. A basic study on hypericin-PDT in vitro. *Photodiagnosis and Photodynamic Therapy*. **9**(3), pp.196–203.

Nakamura, Y., Mochida, A., Choyke, P.L. and Kobayashi, H. 2016. Nanodrug Delivery: Is the Enhanced Permeability and Retention Effect Sufficient for Curing Cancer? *Bioconjugate Chemistry*. **27**(10), pp.2225–2238.

Namikawa, T., Yatabe, T., Inoue, K., Shuin, T. and Hanazaki, K. 2015. Clinical applications of 5-aminolevulinic acid-mediated fluorescence for gastric cancer. *World Journal of Gastroenterology*. **21**(29), pp.8817–8825.

Narang, A.S. and Varia, S. 2011. Role of tumor vascular architecture in drug delivery. *Advanced Drug Delivery Reviews*. **63**(8), pp.640–658.

National Institute for Health and Care Excellence 2011. *Colorectal cancer: diagnosis and management* [Online]. Available from: https://www.nice.org.uk/guidance/cg131.

Newton, A.D., Bartlett, E.K. and Karakousis, G.C. 2016. Cytoreductive surgery and hyperthermic intraperitoneal chemotherapy: A review of factors contributing to morbidity and mortality. *Journal of Gastrointestinal Oncology*. **7**(1), pp.99–111.

Niu, G. and Chen, X. 2010. Vascular endothelial growth factor as an anti-angiogenic target for cancer therapy. *Current drug targets*. **11**(8), pp.1000–17.

Norouzi, H., Khoshgard, K. and Akbarzadeh, F. 2018. In vitro outlook of gold nanoparticles in photo-thermal therapy: a literature review. *Lasers in Medical Science*. **33**(4), pp.917–926.

Norum, O.J., Fremstedal, A.S.V., Weyergang, A., Golab, J. and Berg, K. 2017. Photochemical delivery of bleomycin induces T-cell activation of importance for curative effect and systemic anti-tumor immunity. *Journal of Controlled Release*. **268**(July), pp.120–127.

Nyga, A., Cheema, U. and Loizidou, M. 2011. 3D tumour models: Novel in vitro approaches to cancer studies. *Journal of Cell Communication and Signaling*. **5**(3), pp.239–248.

O'Neal, D.P., Hirsch, L.R., Halas, N.J., Payne, J.D. and West, J.L. 2004. Photo-thermal tumor ablation in mice using near infrared-absorbing nanoparticles. *Cancer Letters*. **209**(2), pp.171–176.

Ogawa, M., Kosaka, N., Choyke, P.L. and Kobayashi, H. 2009. In vivo molecular imaging of cancer with a quenching near-infrared fluorescent probe using conjugates of monoclonal antibodies and indocyanine green. *Cancer Research*. **69**(4), pp.1268–1272.

Okuyama, T., Yamazoe, H., Mochizuki, N., Khademhosseini, A., Suzuki, H. and Fukuda, J. 2010. Preparation of arrays of cell spheroids and spheroid-monolayer cocultures within a microfluidic device. *Journal of Bioscience and Bioengineering*. **110**(5), pp.572–576.

Olsen, C.E., Weyergang, A., Edwards, V.T., Berg, K., Brech, A., Weisheit, S., Høgset, A. and Selbo, P.K. 2017. Development of resistance to photodynamic therapy (PDT) in human breast cancer cells is photosensitizer-dependent: Possible mechanisms and approaches for overcoming PDT-resistance. *Biochemical Pharmacology*. **144**, pp.63–77.

Orenstein, A., Kostenich, G., Roitman, L., Shechtman, Y., Kopolovic, Y., Ehrenberg, B. and Malik, Z. 1996. A comparative study of tissue distribution and photodynamic therapy selectivity of chlorin e6, Photofrin II and ALA-induced protoporphyrin IX in a colon carcinoma model. *British Journal of Cancer*. **73**(8), pp.937–944.

Ormond, A.B. and Freeman, H.S. 2013. Dye Sensitizers for Photodynamic Therapy. *Materials*. **6**(3), pp.817–840.

Palasuberniam, P., Yang, X., Kraus, D., Jones, P., Myers, K.A. and Chen, B. 2015. ABCG2 transporter inhibitor restores the sensitivity of triple negative breast cancer cells to aminolevulinic acid-mediated photodynamic therapy. *Scientific reports*. **5**(July), p.13298.

Panzarini, E., Inguscio, V. and Dini, L. 2011. Overview of Cell Death Mechanisms Induced by Rose Bengal Acetate-Photodynamic Therapy. *International Journal of Photoenergy*. **2011**, pp.1–11.

Panzarini, E., Tenuzzo, B. and Dini, L. 2009. Photodynamic therapy-induced apoptosis of HeLa cells. *Annals of the New York Academy of Sciences*. **1171**, pp.617–626.

Patel, N., Pera, P., Joshi, P., Dukh, M., Tabaczynski, W.A., Siters, K.E., Kryman, M., Cheruku, R.R., Durrani, F., Missert, J.R., Watson, R., Ohulchanskyy, T.Y., Tracy, E.C., Baumann, H. and Pandey, R.K. 2016. Highly Effective Dual-Function Near-Infrared (NIR) Photosensitizer for Fluorescence Imaging and Photodynamic Therapy (PDT) of Cancer. *Journal of Medicinal Chemistry*. **59**(21), pp.9774–9787.

Patra, B., Chen, Y.H., Peng, C.C., Lin, S.C., Lee, C.H. and Tung, Y.C. 2013. A microfluidic device for uniform-sized cell spheroids formation, culture, harvesting and flow cytometry analysis. *Biomicrofluidics*. **7**(5), pp.1–11.

Patra, B., Peng, C.-C., Liao, W.-H., Lee, C.-H. and Tung, Y.-C. 2016. Drug
testing and flow cytometry analysis on a large number of uniform sized
tumor spheroids using a microfluidic device. *Scientific Reports*. **6**(1),
p.21061.

Patrice, T., Foultier, M.T., Yactayo, S., Douet, M.C., Maloisel, F. and Le Bodic,
L. 1990. Endoscopic photodynamic therapy with haematoporphyrin
derivative in gastroenterology. *Journal of Photochemistry and
Photobiology, B: Biology*. **6**(1–2), pp.157–165.

Peltomäki, P. 2001. DNA mismatch repair and cancer. *Mutation research*.
488(1), pp.77–85.

Pereira, P.M.R., Berisha, N., Bhupathiraju, N.V.S.D.K., Fernandes, R., Tomé,
J.P.C. and Drain, C.M. 2017. Cancer cell spheroids are a better screen for
the photodynamic efficiency of glycosylated photosensitizers. *PloS one*.
12(5), p.e0177737.

Petrelli, F., Sgroi, G., Sarti, E. and Barni, S. 2016. Increasing the interval
between neoadjuvant chemoradiotherapy and surgery in rectal cancer : A
meta-analysis of published studies. *Annals of Surgery*. **263**(3), pp.458–
464.

Petrova, V., Annicchiarico-Petruzzelli, M., Melino, G. and Amelio, I. 2018. The
hypoxic tumour microenvironment. *Oncogenesis*. **7**(1).

Phung, Y.T., Barbone, D., Broaddus, V.C. and Ho, M. 2011. Rapid generation
of in vitro multicellular spheroids for the study of monoclonal antibody
therapy. *Journal of Cancer*. **2**(1), pp.507–514.

Piccinini, F., Tesei, A., Arienti, C. and Bevilacqua, A. 2017. Cell Counting and
Viability Assessment of 2D and 3D Cell Cultures: Expected Reliability of
the Trypan Blue Assay. *Biological Procedures Online*. **19**(1), p.8.

Pickl, M. and Ries, C.H. 2009. Comparison of 3D and 2D tumor models reveals enhanced HER2 activation in 3D associated with an increased response to trastuzumab. *Oncogene*. **28**(3), pp.461–468.

Poleshko, A.G. and Volotovski, I.D. 2016. The role of ABCG2 in maintaining the viability and proliferative activity of bone marrow mesenchymal stem cells in hypoxia. *Biophysics*. **61**(2), pp.271–276.

Polo, L., Valduga, G., Jori, G. and Reddi, E. 2002. Low-density lipoprotein receptors in the uptake of tumour photosensitizers by human and rat transformed fibroblasts. *International Journal of Biochemistry and Cell Biology*. **34**(1), pp.10–23.

Poon, M.A., O'Connell, M.J., Moertel, C.G., Wieand, H.S., Cullinan, S.A., Everson, L.K., Krook, J.E., Mailliard, J.A., Laurie, J.A. and Tschetter, L.K. 1989. Biochemical modulation of fluorouracil: evidence of significant improvement of survival and quality of life in patients with advanced colorectal carcinoma. *Journal of Clinical Oncology*. **7**(10), pp.1407–1418.

Prabhakarpandian, B., Shen, M.C., Nichols, J.B., Garson, C.J., Mills, I.R., Matar, M.M., Fewell, J.G. and Pant, K. 2015. Synthetic tumor networks for screening drug delivery systems. *Journal of Controlled Release*. **201**, pp.49–55.

Pugh, S.A., Shinkins, B., Fuller, A., Mellor, J., Mant, D. and Primrose, J.N. 2016. Site and Stage of Colorectal Cancer Influence the Likelihood and Distribution of Disease Recurrence and Postrecurrence Survival: Data From the FACS Randomized Controlled Trial. *Annals of surgery*. **263**(6), pp.1143–7.

Quirk, B.J., Brandal, G., Donlon, S., Vera, J.C., Mang, T.S., Foy, A.B., Lew, S.M., Girotti, A.W., Jogal, S., LaViolette, P.S., Connelly, J.M. and Whelan, H.T. 2015. Photodynamic therapy (PDT) for malignant brain tumors - Where do we stand? *Photodiagnosis and Photodynamic Therapy*. **12**(3), pp.530–544.

Ratnayaka, S.H., Hillburn, T.E., Forouzan, O., Shevkoplyas, S.S. and Khismatullin, D.B. 2013. PDMS well platform for culturing millimeter-size tumor spheroids. *Biotechnology Progress*. **29**(5), pp.1265–1269.

Ravi, M., Paramesh, V., Kaviya, S.R., Anuradha, E. and Paul Solomon, F.D. 2015. 3D cell culture systems: Advantages and applications. *Journal of Cellular Physiology*. **230**(1), pp.16–26.

Rick, K., Sroka, R., Stepp, H., Kriegmair, M., Huber, M., Jacob, K. and Baumgartner, R. 1997. Pharmacokinetics of 5aminolevulinic acid-induced protoporphyrin IX in skin and blood. *Journal of Photochemistry and Photobiology B: Biology*. **40**, pp.313–319.

Riihimäki, M., Hemminki, A., Sundquist, J. and Hemminki, K. 2016. Patterns of metastasis in colon and rectal cancer. *Scientific reports*. **6**, p.29765.

Riley, R.S. and Day, E.S. 2017. Gold nanoparticle-mediated photothermal therapy: applications and opportunities for multimodal cancer treatment. *Wiley Interdisciplinary Reviews: Nanomedicine and Nanobiotechnology*. **9**(4).

Ritz, R., Scheidle, C., Noell, S., Roser, F., Schenk, M., Dietz, K. and Strauss, W.S.L. 2012. In Vitro Comparison of Hypericin and 5-Aminolevulinic Acid-Derived Protoporphyrin IX for Photodynamic Inactivation of Medulloblastoma Cells. *PLoS ONE*. **7**(12), pp.1–11.

Robertson, C.A., Evans, D.H. and Abrahamse, H. 2009. Photodynamic therapy (PDT): a short review on cellular mechanisms and cancer research applications for PDT. *Journal of photochemistry and photobiology. B, Biology*. **96**(1), pp.1–8.

Robey, R.W., Steadman, K., Polgar, O. and Bates, S.E. 2005. ABCG2-mediated transport of photosensitizers: potential impact on photodynamic therapy. *Cancer Biology & Therapy*. **4**(2), pp.187–194.

Rodday, B., Hirschhaeuser, F., Walenta, S. and Mueller-Klieser, W. 2011. Semiautomatic growth analysis of multicellular tumor spheroids. *Journal of Biomolecular Screening*. **16**(9), pp.1119–1124.

Rovers, J.P., Saarnak, A.E., Molina, A., Schuitmaker, J.J., Sterenborg, H.J.C.M. and Terpstra, O.T. 1999. Effective treatment of liver metastases with photodynamic therapy, using the second-generation photosensitizer meta-tetra(hydroxyphenyl)chlorin (mTHPC), in a rat model. *British Journal of Cancer*. **81**(4), pp.600–608.

Ruppen, J., Cortes-Dericks, L., Marconi, E., Karoubi, G., Schmid, R.A., Peng, R., Marti, T.M. and Guenat, O.T. 2014. A microfluidic platform for chemoresistive testing of multicellular pleural cancer spheroids. *Lab Chip*. **14**(6), pp.1198–1205.

Sabhachandani, P., Motwani, V., Cohen, N., Sarkar, S., Torchilin, V. and Konry, T. 2016. Generation and functional assessment of 3D multicellular spheroids in droplet based microfluidics platform. *Lab on a Chip*. **16**(3), pp.497–505.

Sackmann, E.K., Fulton, A.L. and Beebe, D.J. 2014. The present and future role of microfluidics in biomedical research. *Nature*. **507**(7491), pp.181–189.

Sacková, V., Kuliková, L., Mikes, J., Kleban, J. and Fedorocko, P. 2005. Hypericin-mediated photocytotoxic effect on HT-29 adenocarcinoma cells is reduced by light fractionation with longer dark pause between two unequal light doses. *Photochemistry and Photobiology*. **81**(6), pp.1411–6.

Safavieh, R. and Juncker, D. 2013. Capillarics: pre-programmed, self-powered microfluidic circuits built from capillary elements. *Lab on a Chip*. **13**(21), p.4180.

Salahudeen, A.A. and Kuo, C.J. 2015. Toward recreating colon cancer in human organoids. *Nature Medicine*. **21**(3), pp.215–216.

Sant, S. and Johnston, P.A. 2017. The production of 3D tumor spheroids for cancer drug discovery. *Drug Discovery Today: Technologies*. **23**, pp.27–36.

Dos Santos, A.F., De Almeida, D.R.Q., Terra, L.F., Baptista, M.S. and Labriola, L. 2019. Photodynamic therapy in cancer treatment - an update review. *Journal of Cancer Metastasis and Treatment*. **5**(25).

Sato, T., Stange, D.E., Ferrante, M., Vries, R.G.J., Van Es, J.H., Van Den Brink, S., Van Houdt, W.J., Pronk, A., Van Gorp, J., Siersema, P.D. and Clevers, H. 2011. Long-term expansion of epithelial organoids from human colon, adenoma, adenocarcinoma, and Barrett's epithelium. *Gastroenterology*. **141**(5), pp.1762–1772.

Schmidt, J.J., Rowley, J. and Hyun, J.K. 2008. Hydrogels used for cell-based drug delivery. *Journal of Biomedical Materials Research - Part A*. **87**(4), pp.1113–1122.

Schwarz, V.A., Hornung, R., Fedier, A., Fehr, M.K., Walt, H., Haller, U. and Fink, D. 2002. Photodynamic therapy of DNA mismatch repair-deficient and -proficient tumour cells. *British Journal of Cancer*. **86**(7), pp.1130–5.

Sekhejane, P.R., Houreld, N.N. and Abrahamse, H. 2014. Multiorganelle localization of metallated phthalocyanine photosensitizer in colorectal cancer cells (DLD-1 and CaCo-2) enhances efficacy of photodynamic therapy. *International Journal of Photoenergy*. **2014**(Ldl).

Selbo, P.K., Weyergang, A., Høgset, A., Norum, O.J., Berstad, M.B., Vikdal, M. and Berg, K. 2010. Photochemical internalization provides time- and space-controlled endolysosomal escape of therapeutic molecules. *Journal of Controlled Release*. **148**(1), pp.2–12.

Šemeláková, M., Jendželovský, R. and Fedoročko, P. 2016. Drug membrane transporters and CYP3A4 are affected by hypericin, hyperforin or aristoforin in colon adenocarcinoma cells. *Biomedicine & pharmacotherapy = Biomedecine & pharmacotherapie*. **81**, pp.38–47.

Šemeláková, M., Mikeš, J., Jendželovský, R. and Fedoročko, P. 2012. The pro-apoptotic and anti-invasive effects of hypericin-mediated photodynamic therapy are enhanced by hyperforin or aristoforin in HT-29 colon adenocarcinoma cells. *Journal of Photochemistry and Photobiology B: Biology*. **117**, pp.115–125.

Sharma, M., Sahu, K., Dube, A. and Gupta, P.K. 2005. Extracellular pH influences the mode of cell death in human colon adenocarcinoma cells subjected to photodynamic treatment with chlorin p6. *Journal of Photochemistry and Photobiology B: Biology*. **81**(2), pp.107–113.

Shen, S., Callaghan, D., Juzwik, C., Xiong, H., Huang, P. and Zhang, W. 2010. ABCG2 reduces ROS-mediated toxicity and inflammation: A potential role in Alzheimer's disease. *Journal of Neurochemistry*. **114**(6), pp.1590–1604.

Shiga, K., Hara, M., Nagasaki, T., Sato, T., Takahashi, H. and Takeyama, H. 2015. Cancer-associated fibroblasts: Their characteristics and their roles in tumor growth. *Cancers*. **7**(4), pp.2443–2458.

Shin, B.H., Kim, B.H., Kim, S., Lee, K., Choy, Y. Bin and Heo, C.Y. 2018. Silicone breast implant modification review: overcoming capsular contracture. *Biomaterials Research*. **22**(1), p.37.

Shin, C.S., Kwak, B., Han, B. and Park, K. 2013. Development of an *in Vitro* 3D Tumor Model to Study Therapeutic Efficiency of an Anticancer Drug. *Molecular Pharmaceutics*. **10**(6), pp.2167–2175.

Shri, M., Agrawal, H., Rani, P., Singh, D. and Onteru, S.K. 2017. Hanging drop, a best three-dimensional (3D) culture method for primary buffalo and sheep hepatocytes. *Scientific Reports*. **7**(1), pp.1–13.

Shu, Z. and Wang, X. 2012. Environment-friendly Pd free surface activation technics for ABS surface. *Applied Surface Science*. **258**(14), pp.5328–5331.

Sibata, C.H., Colussi, V.C., Oleinick, N.L. and Kinsella, T.J. 2000. Photodynamic therapy: a new concept in medical treatment. *Brazilian journal of medical and biological research = Revista brasileira de pesquisas médicas e biológicas / Sociedade Brasileira de Biofísica ... [et al.]*. **33**(8), pp.869–80.

Siboni, G., Weitman, H., Freeman, D., Mazur, Y., Ehrenberg, B. and Malik, Z. 2002. The correlation between hydrophilicity of hypericins and helianthrone: internalization mechanisms, subcellular distribution and photodynamic action in colon carcinoma cells. *Photochemical & Photobiological Sciences*. **1**(7), pp.483–491.

Simkens, G.A., Rovers, K.P., Nienhuijs, S.W. and de Hingh, I.H. 2017. Patient selection for cytoreductive surgery and HIPEC for the treatment of peritoneal metastases from colorectal cancer. *Cancer management and research*. **9**, pp.259–266.

Simon, V., Devaux, C., Darmon, A., Donnet, T., Thiénot, E., Germain, M., Honnorat, J., Duval, A., Pottier, A., Borghi, E., Levy, L. and Marill, J. 2010. Pp IX silica nanoparticles demonstrate differential interactions with in vitro tumor cell lines and in vivo mouse models of human cancers. *Photochemistry and Photobiology*. **86**(1), pp.213–222.

Simone, C.B. and Cengel, K.A. 2014. Photodynamic therapy for lung cancer and malignant pleural mesothelioma. *Seminars in oncology*. **41**(6), pp.820–30.

Sirenko, O., Mitlo, T., Hesley, J., Luke, S., Owens, W. and Cromwell, E.F. 2015. High-Content Assays for Characterizing the Viability and Morphology of 3D Cancer Spheroid Cultures. *ASSAY and Drug Development Technologies*. **13**(7), pp.402–414.

Slingerland, M., Guchelaar, H.J. and Gelderblom, H. 2012. Liposomal drug formulations in cancer therapy: 15 years along the road. *Drug Discovery Today*. **17**(3–4), pp.160–166.

Smith, P.G., Burchill, S.A., Brooke, D., Coletta, P.L. and Whitehouse, A. 2005. Efficient infection and persistence of a herpesvirus saimiri-based gene delivery vector into human tumor xenografts and multicellular spheroid cultures. *Cancer Gene Therapy*. **12**(3), pp.248–256.

Sodunke, T.R., Turner, K.K., Caldwell, S.A., McBride, K.W., Reginato, M.J. and Noh, H.M. 2007. Micropatterns of Matrigel for three-dimensional epithelial cultures. *Biomaterials*. **28**(27), pp.4006–4016.

Spyratou, E., Makropoulou, M., Efstathopoulos, E.P., Georgakilas, A.G. and Sihver, L. 2017. Recent Advances in Cancer Therapy Based on Dual Mode Gold Nanoparticles. *Cancers*. **9**(12).

Stacy, A.E., Jansson, P.J. and Richardson, D.R. 2013. Molecular Pharmacology of ABCG2 and Its Role in Chemoresistance. *Molecular Pharmacology*. **84**(5), pp.655–669.

Star, W.M., van't Veen, A.J., Robinson, D.J., Munte, K., de Haas, E.R.M. and Sterenborg, H.J.C.M. 2006. Topical 5-aminolevulinic acid mediated photodynamic therapy of superficial basal cell carcinoma using two light fractions with a two-hour interval: long-term follow-up. *Acta dermato-Venereologica*. **86**(5), pp.412–417.

Stock, K., Estrada, M.F., Vidic, S., Gjerde, K., Rudisch, A., Santo, V.E., Barbier, M., Blom, S., Arundkar, S.C., Selvam, I., Osswald, A., Stein, Y., Gruenewald, S., Brito, C., Van Weerden, W., Rotter, V., Boghaert, E., Oren, M., Sommergruber, W., Chong, Y., De Hoogt, R. and Graeser, R. 2016. Capturing tumor complexity in vitro: Comparative analysis of 2D and 3D tumor models for drug discovery. *Scientific Reports*. **6**, pp.1–15.

Stoka, V., Turk, V. and Turk, B. 2006. Do lysosomes induce cell death? *IUBMB Life*. **58**(8), pp.493–494.

Stummer, W., Novotny, A., Stepp, H., Goetz, C., Bise, K. and Reulen, H.J. 2000. Fluorescence-guided resection of glioblastoma multiforme utilizing 5-ALA-induced porphyrins: a prospective study in 52 consecutive patients. *Journal of Neurosurgery*. **93**(6), pp.1003–1013.

Stummer, W., Pichlmeier, U., Meinel, T., Wiestler, O.D., Zanella, F. and Reulen, H.J. 2006. Fluorescence-guided surgery with 5-aminolevulinic acid for resection of malignant glioma: a randomised controlled multicentre phase III trial. *Lancet Oncology*. **7**(5), pp.392–401.

Sultan, A.A., Jerjes, W., Berg, K., Høgset, A., Mosse, C.A., Hamoudi, R., Hamdoon, Z., Simeon, C., Carnell, D., Forster, M. and Hopper, C. 2016. Disulfonated tetraphenyl chlorin (TPCS2a)-induced photochemical internalisation of bleomycin in patients with solid malignancies: a phase 1, dose-escalation, first-in-man trial. *The Lancet Oncology*. **17**(9), pp.1217–1229.

Sun, D., Lu, J., Chen, Z., Yu, Y. and Li, Y. 2014. A novel three-dimensional microfluidic platform for on chip multicellular tumor spheroid formation and culture. *Microfluidics and Nanofluidics*. **17**(5), pp.831–842.

Sun, Y., Lacour, S.P., Brooks, R.A., Rushton, N., Fawcett, J. and Cameron, R.E. 2009. Assessment of the biocompatibility of photosensitive polyimide for implantable medical device use. *Journal of Biomedical Materials Research Part A*. **90A**(3), pp.648–655.

Swietach, P., Vaughan-Jones, R.D., Harris, A.L. and Hulikova, A. 2014. The chemistry, physiology and pathology of pH in cancer. *Philosophical Transactions of the Royal Society B: Biological Sciences*. **369**(1638), pp.20130099–20130099.

Sznarkowska, A., Maleńczyk, K., Kadziński, L., Bielawski, K.P., Banecki, B. and Zawacka-Pankau, J. 2011. Targeting of p53 and its homolog p73 by protoporphyrin IX. *FEBS Letters*. **585**(1), pp.255–260.

Tanaka, M., Kataoka, H., Mabuchi, M., Sakuma, S., Takahashi, S., Tujii, R., Akashi, H., Ohi, H., Yano, S., Morita, A. and Joh, T. 2011. Anticancer effects of novel photodynamic therapy with glycoconjugated chlorin for gastric and colon cancer. *Anticancer Research*. **31**(3), pp.763–769.

Thirion, P., Michiels, S., Pignon, J.P., Buyse, M., Braud, A.C., Carlson, R.W., O'Connell, M., Sargent, P., Piedbois, P. and Meta-Analysis Group in Cancer 2004. Modulation of fluorouracil by leucovorin in patients with advanced colorectal cancer: an updated meta-analysis. *Journal of Clinical Oncology*. **22**(18), pp.3766–75.

Toley, B.J., Tropeano Lovatt, Z.G., Harrington, J.L. and Forbes, N.S. 2013. Microfluidic technique to measure intratumoral transport and calculate drug efficacy shows that binding is essential for doxorubicin and release hampers Doxil. *Integrative Biology*. **5**(9), p.1184.

Tong, L., Wei, Q., Wei, a and Cheng, J. 2009. Gold nanorods as contrast agents for biological imaging: optical properties, surface conjugation and photothermal effects. *Photochemistry and photobiology*. **85**(1), pp.21–32.

Tournigand, C., André, T., Achille, E., Lledo, G., Flesh, M., Mery-Mignard, D., Quinaux, E., Couteau, C., Buyse, M., Ganem, G., Landi, B., Colin, P., Louvet, C. and De Gramont, A. 2004. FOLFIRI followed by FOLFOX6 or the reverse sequence in advanced colorectal cancer: A randomized GERCOR study. *Journal of Clinical Oncology*. **22**(2), pp.229–237.

Tralau, C.J., Barr, H., Sandeman, D.R., Barton, T., Lewin, M.R. and Bown, S.G. 1987. ALUMINUM SULFONATED PHTHALOCYANINE DISTRIBUTION IN RODENT TUMORS OF THE COLON, BRAIN and PANCREAS. *Photochemistry and Photobiology*. **46**(5), pp.777–781.

Tsai, M.-H., Peng, C.-L., Yang, S.-J. and Shieh, M.-J. 2017. Photothermal, Targeting, Theranostic Near-Infrared Nanoagent with SN38 against Colorectal Cancer for Chemothermal Therapy. *Molecular pharmaceutics*. **14**(8), pp.2766–2780.

Tuy, H.D., Shiomi, H., Mukaisho, K.I., Naka, S., Shimizu, T., Sonoda, H., Mekata, E., Endo, Y., Kurumi, Y., Sugihara, H., Tani, M. and Tani, T. 2016. ABCG2 expression in colorectal adenocarcinomas may predict resistance to irinotecan. *Oncology Letters*. **12**(4), pp.2752–2760.

Upreti, M., Jamshidi-Parsian, A., Koonce, N.A., Webber, J.S., Sharma, S.K., Asea, A.A.A., Mader, M.J. and Griffin, R.J. 2011. Tumor-Endothelial Cell Three-dimensional Spheroids: New Aspects to Enhance Radiation and Drug Therapeutics. *Translational Oncology*. **4**(6), pp.365-IN3.

Uzdensky, A.B., Ma, L.-W., Iani, V., Hjortland, G.O., Steen, H.B. and Moan, J. 2001. Intracellular Localisation of Hypericin in Human Glioblastoma and Carcinoma Cell Lines. *Lasers in Medical Science*. **16**(4), pp.276–283.

Vansevičiūtė, R., Venius, J. and Letautienė, S. 2014. 5-Aminolevulinic acid-based fluorescence diagnostics of cervical preinvasive changes. *Medicina (Kaunas, Lithuania)*. **50**(3), pp.137–143.

Verteporfin In Photodynamic Therapy Study Group 2001. Verteporfin therapy of subfoveal choroidal neovascularization in age-related macular degeneration: two-year results of a randomized clinical trial including lesions with occult with no classic choroidal neovascularization - Verteporfin In Photodynamic The. *American Journal of Ophthalmology*. **131**(5), pp.541–60.

de Vijlder, H.C., Sterenborg, H.J.C.M., Neumann, H.A.M., Robinson, D.J. and de Haas, E.R.M. 2012. Light fractionation significantly improves the response of superficial basal cell carcinoma to aminolaevulinic acid photodynamic therapy: five-year follow-up of a randomized, prospective trial. *Acta dermato-Venereologica*. **92**(6), pp.641–7.

Vinci, M., Gowan, S., Boxall, F., Patterson, L., Zimmermann, M., Court, W., Lomas, C., Mendiola, M., Hardisson, D. and Eccles, S.A. 2012. Advances in establishment and analysis of three-dimensional tumor spheroid-based functional assays for target validation and drug evaluation. *BMC Biology*. **10**(1), p.29.

Vonarx-Coinsmann, V., Foultier, M.T., Cempel, N., Morlet, L., Combre, A. and Patrice, T. 1994. In vitro and in vivo photodynamic effects of a new photosensitizer: Tetra(m-hydroxyphenyl)chlorin. *Lasers in Medical Science*. **9**(3), pp.173–181.

Wallace, D.I. and Guo, X. 2013. Properties of tumor spheroid growth exhibited by simple mathematical models. *Frontiers in Oncology*. **3**, p.51.

Wan, M.T. and Lin, J.Y. 2014. Current evidence and applications of photodynamic therapy in dermatology. *Clinical, Cosmetic and Investigational Dermatology*. **7**, pp.145–63.

Wang, M., Zhao, J., Zhang, L., Wei, F., Lian, Y., Wu, Y., Gong, Z., Zhang, S., Zhou, J., Cao, K., Li, X., Xiong, W., Li, G., Zeng, Z. and Guo, C. 2017. Role of tumor microenvironment in tumorigenesis. *Journal of Cancer*. **8**(5), pp.761–773.

Wang, Y. and Wang, J. 2014. Mixed hydrogel bead-based tumor spheroid formation and anticancer drug testing. *The Analyst*. **139**(10), pp.2449–2458.

Wang, Z., Wang, J., Li, M., Sun, K. and Liu, C. 2014. Three-dimensional printed acrylonitrile butadiene styrene framework coated with Cu-BTC metal-organic frameworks for the removal of methylene blue. *Scientific reports*. **4**(1), p.5939.

Webber, J., Leeson, B., Fromm, D. and Kessel, D. 2005. Effects of photodynamic therapy using a fractionated dosing of mono-L-aspartyl chlorin e6 in a murine tumor. *Journal of Photochemistry and Photobiology B: Biology*. **78**(2), pp.135–140.

Weijer, R., Broekgaarden, M., van Golen, R.F., Bulle, E., Nieuwenhuis, E., Jongejan, A., Moerland, P.D., van Kampen, A.H.C., van Gulik, T.M. and Heger, M. 2015. Low-power photodynamic therapy induces survival signaling in perihilar cholangiocarcinoma cells. *BMC Cancer*. **15**(1), p.1014.

Westover, D. and Li, F. 2015. New trends for overcoming ABCG2/BCRP-mediated resistance to cancer therapies. *Journal of Experimental & Clinical Cancer Research*. **34**(1), p.159.

van De Wetering, M., Francies, H.E., Francis, J.M., Bounova, G., Iorio, F., Pronk, A., Van Houdt, W., Van Gorp, J., Taylor-Weiner, A., Kester, L., McLaren-Douglas, A., Blokker, J., Jaksani, S., Bartfeld, S., Volckman, R., Van Sluis, P., Li, V.S.W., Seepo, S., Sekhar Pedamallu, C., Cibulskis, K., Carter, S.L., McKenna, A., Lawrence, M.S., Lichtenstein, L., Stewart, C., Koster, J., Versteeg, R., Van Oudenaarden, A., Saez-Rodriguez, J., Vries, R.G.J., Getz, G., Wessels, L., Stratton, M.R., McDermott, U., Meyerson, M., Garnett, M.J. and Clevers, H. 2015. Prospective derivation of a living organoid biobank of colorectal cancer patients. *Cell*. **161**(4), pp.933–945.

Weyergang, A., Selbo, P.K. and Berg, K. 2006. Photochemically stimulated drug delivery increases the cytotoxicity and specificity of EGF-saporin. *Journal of Controlled Release*. **111**(1–2), pp.165–173.

Wheatley, D. 1999. Hypericum *in Seasonal Affective Disorder (SAD)*. *Current Medical Research and Opinion*. **15**(1), pp.33–37.

Whitacre, C.M., Feyes, D.K., Satoh, T., Grossmann, J., Mulvihill, J.W. and Mukhtar, H. 2000. Photodynamic Therapy with the Phthalocyanine Photosensitizer Pc 4 of SW480 Human Colon Cancer Xenografts in Athymic Mice Photodynamic Therapy with the Phthalocyanine Photosensitizer Pc 4 of SW480 Human Colon Cancer Xenografts in Athymic Mice 1. . **6**(May), pp.2021–2027.

Wilkinson, N.W., Yothers, G., Lopa, S., Costantino, J.P., Petrelli, N.J. and Wolmark, N. 2010. Long-term survival results of surgery alone versus surgery plus 5-fluorouracil and leucovorin for stage ii and stage iii colon cancer: Pooled analysis of NSABP C-01 through C-05. A baseline from which to compare modern adjuvant trials. *Annals of Surgical Oncology*. **17**(4), pp.959–966.

Wilson, B.C., Olivo, M. and Singh, G. 1997. Subcellular localization of Photofrin and aminolevulinic acid and photodynamic cross-resistance in vitro in radiation-induced fibrosarcoma cells sensitive or resistant to photofrin-mediated photodynamic therapy. *Photochemistry and photobiology*. **65**(1), pp.166–76.

Winner, M., Koong, A.C., Rendon, B.E., Zundel, W. and Mitchell, R.A. 2007. Amplification of tumor hypoxic responses by macrophage migration inhibitory factor-dependent hypoxia-inducible factor stabilization. *Cancer Research*. **67**(1), pp.186–193.

Wu, R.W.K., Chu, E.S.M., Huang, Z., Olivo, M.C., Ip, D.C.W. and Yow, C.M.N. 2015. An in vitro investigation of photodynamic efficacy of FosPeg ® on human colon cancer cells. *Journal of Innovative Optical Health Sciences*. **08**(05), p.1550027.

Xiao, Z., Halls, S., Dickey, D., Tulip, J. and Moore, R.B. 2007. Fractionated versus standard continuous light delivery in interstitial photodynamic therapy of dunning prostate carcinomas. *Clinical Cancer Research*. **13**(24), pp.7496–7505.

Xie, S.-M., Xiong, J.-J., Liu, X.-T., Chen, H.-Y., Iglesia-García, D., Altaf, K., Bharucha, S., Huang, W., Nunes, Q.M., Szatmary, P. and Liu, X.-B. 2017. Laparoscopic Versus Open Liver Resection for Colorectal Liver Metastases: A Comprehensive Systematic Review and Meta-analysis. *Scientific Reports*. **7**(1), p.1012.

Xu, C.S., Leung, A.W.N., Liu, L. and Xia, X.S. 2010. LED-activated pheophorbide a induces cellular destruction of colon cancer cells. *Laser Physics Letters*. **7**(7), pp.544–548.

Xu, Y., Wang, D., Zhuang, Z., Jin, K., Zheng, L., Yang, Q. and Guo, K. 2015. Hypericin-mediated photodynamic therapy induces apoptosis in K562 human leukemia cells through JNK pathway modulation. *Molecular Medicine Reports*. **12**(5), pp.6475–6482.

Yamazoe, H., Hagihara, Y. and Kobayashi, H. 2016. Multicomponent Coculture System of Cancer Cells and Two Types of Stromal Cells for *In Vitro* Evaluation of Anticancer Drugs. *Tissue Engineering Part C: Methods*. **22**(1), pp.20–29.

Yang, X., Xue, X., Luo, Y., Lin, T. yin, Zhang, H., Lac, D., Xiao, K., He, Y., Jia, B., Lam, K.S. and Li, Y. 2017. Sub-100 nm, long tumor retention SN-38-loaded photonic micelles for tri-modal cancer therapy. *Journal of Controlled Release*. **261**(June), pp.297–306.

Yang, Y., Yang, X., Zou, J., Jia, C., Hu, Y., Du, H. and Wang, H. 2015. Evaluation of photodynamic therapy efficiency using an in vitro three-dimensional microfluidic breast cancer tissue model. *Lab on a Chip - Miniaturisation for Chemistry and Biology*. **15**(3), pp.735–744.

Yoon, I., Li, J.Z. and Shim, Y.K. 2013. Advance in photosensitizers and light delivery for photodynamic therapy. *Clinical Endoscopy*. **46**(1), pp.7–23.

Yoon, S., Kim, J.A., Lee, S.H., Kim, M. and Park, T.H. 2013. Droplet-based microfluidic system to form and separate multicellular spheroids using magnetic nanoparticles. *Lab on a Chip*. **13**(8), p.1522.

Young, E.W.K. and Beebe, D.J. 2010. Fundamentals of microfluidic cell culture in controlled microenvironments. *Chemical Society reviews*. **39**(3), pp.1036–48.

Yu, L., Chen, M.C.W. and Cheung, K.C. 2010. Droplet-based microfluidic system for multicellular tumor spheroid formation and anticancer drug testing. *Lab on a Chip*. **10**(18), p.2424.

Yu, L., Ni, C., Grist, S.M., Bayly, C. and Cheung, K.C. 2015. Alginate core-shell beads for simplified three-dimensional tumor spheroid culture and drug screening. *Biomedical Microdevices*. **17**(2).

Yu, X., Trase, I., Ren, M., Duval, K., Guo, X. and Chen, Z. 2016. Design of Nanoparticle-Based Carriers for Targeted Drug Delivery. *Journal of Nanomaterials*. **2016**.

Yuan, Y., Jiang, Y.-C., Sun, C.-K. and Chen, Q.-M. 2016. Role of the tumor microenvironment in tumor progression and the clinical applications (Review). *Oncology reports*. **35**(5), pp.2499–515.

Zawacka-Pankau, J., Issaeva, N., Hossain, S., Pramanik, A., Selivanova, G. and Podhajska, A.J. 2007. Protoporphyrin IX interacts with wild-type p53 protein in vitro and induces cell death of human colon cancer cells in a p53-dependent and -independent manner. *Journal of Biological Chemistry*. **282**(4), pp.2466–2472.

Zhang, J., Jiang, C., Figueiró Longo, J.P., Azevedo, R.B., Zhang, H. and Muehlmann, L.A. 2017. An updated overview on the development of new photosensitizers for anticancer photodynamic therapy. *Acta Pharmaceutica Sinica B.*, pp.0–9.

Zhang, Q., Li, Z., Li, Y., Shi, S., Zhou, S., Fu, Y., Zhang, Q., Yang, X., Fu, R. and Lu, L. 2015. Hypericin-photodynamic therapy induces human umbilical vein endothelial cell apoptosis. *Scientific Reports*. **5**, p.18398.

Zheng, Y., Yin, G., Le, V., Zhang, A., Chen, S.Y., Liang, X. and Liu, J.W. 2016. Photodynamic-therapy activates immune response by disrupting immunity homeostasis of tumor cells, which generates vaccine for cancer therapy. *International Journal of Biological Sciences*. **12**(1), pp.120–132.

Ziółkowska, K., Stelmachowska, A., Kwapiszewski, R., Chudy, M., Dybko, A. and Brzózka, Z. 2013. Long-term three-dimensional cell culture and anticancer drug activity evaluation in a microfluidic chip. *Biosensors and Bioelectronics*. **40**(1), pp.68–74.

Zuchowska, A., Jastrzebska, E., Chudy, M., Dybko, A. and Brzozka, Z. 2016. Advanced 3D Spheroid Culture for Evaluation of Photodynamic Therapy in Microfluidic System. *Procedia Engineering*. **168**, pp.403–406.

APPENDIX

9 APPENDIX

9.1 Calculation of light dose for PDT experiments

1. Equation to convert power: $Watt(W) = \dfrac{Joule(J)}{Second(s)}$

2. Rearrange equation: $J = W * s$

3. Divide both sides of equation by unit of surface area: $\dfrac{J}{cm^2} = \dfrac{W}{cm^2} * s$

4. Light fluency rate of light box: $\dfrac{0.00023W}{cm^2}$

5. Amount of light dose required for PDT experiment: $\dfrac{1J}{cm^2}$

<u>Calculating the time for PDT experiments</u>

1. $\dfrac{1J}{cm^2} = \dfrac{0.00023W}{cm^2} * s \rightarrow 1J = 0.00023W * s$

2. $\dfrac{1J}{0.00023W} = s$

3. $s = 4348$

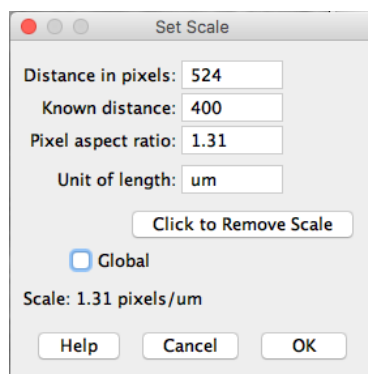4. $4348\ seconds =$ ==*72 minutes and 28 seconds*==

To administer 1J/cm^2 of light, it would take 72mins and 28secs using the lightbox.

## 9.2 Example step-by-Step calculation of spheroid volume

1. Transillumination Images of spheroids were taken and analysed using

    ImageJ
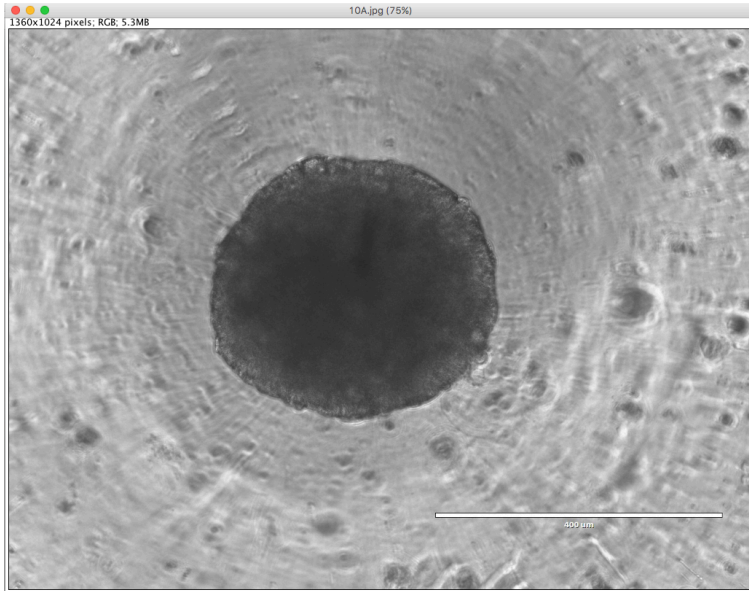
2. Using the scalebar (bottom right corner), a scale ratio was measured and

    applied

3. Once the scale ratio is determined, a horizontal line was drawn from the

    centre of the spheroid to the edge to determine the radius (193.384µm in

    this example)
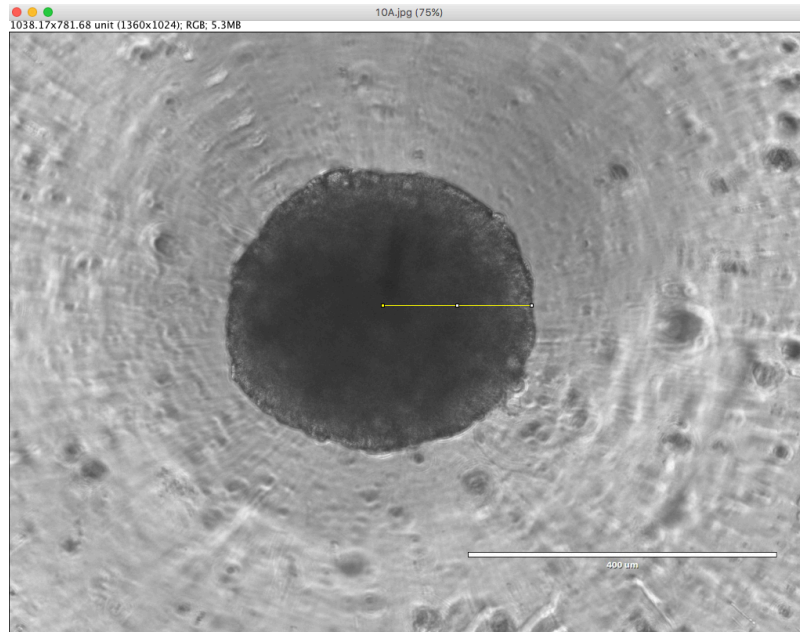
4. The equation to determine the volume of a spheroid was then used

    i.   Equation to calculate the volume (V) of spheroid: $V = \frac{4}{3}\pi r^3$

    ii. $193.384\mu m = 0.193384 mm$

    iii. $V = \frac{4}{3} * \pi * 0.193384^3$

    iv. $V = 0.03 mm^3$

9.3 Cost Analysis of using commercially available ULA 96-well plates and 'in-house' prepared 1% (w/v) agarose-coated.

Commercially available ULA plate

1. One box of plates costs €150.15 (**£133.50**) and contains five plates. *(https://ecatalog.corning.com/life-sciences/b2c/EUOther/en/Microplates/Assay-Microplates/96-Well-Microplates/Corning-96-well-Spheroid-Microplates/p/4515)* Price and exchange rate is correct as of 25/07/18.

2. £133.50/box ➕ 5 plates/box ➔ <mark>**£26.70/plate**</mark>

'In-house' prepared 1% (w/v) agarose-coated plate

1. One box of plates costs €142.30 (**£126.52**) and contains fifty plates. *(https://ecatalog.corning.com/life-sciences/b2c/EUOther/en/Permeable-Supports/Inserts/Corning®-96-well-Clear-Polystyrene-Microplates/p/3799)* Price and exchange rate is correct as of 25/07/18.

2. £126.52/box ➕ 50 plates/box ➔ **£2.53/plate**

3. 500g of Agarose powder (Sigma Aldrich) costs **£692.00**. *(https://www.sigmaaldrich.com/catalog/product/sigma/a9539?lang=en&region=GB)* Price and exchange rate is correct as of 25/07/18.

4. £692.00/500g of Agarose ➔ **£1.38/g of Agarose**

5. 50µL of 1% (w/v) agarose is added per well ➔ 96-wells/plate x 50µL/well = 4800µL (4.8mL) per plate

6. 1% (w/v) = 1g in 100mL ➔ 0.01g in 1mL ➔ 0.048g in 4.8mL

7. 0.048g of agarose at £1.38/g of agarose = **£0.07 of agarose per plate**

8. £2.53 (cost of one plate) **+** £0.07 (cost of agarose per plate) = <mark>**£2.60/plate**</mark>

It costs **£26.70** and **£2.60** to use one commercial ULA plate and one 'in-house' prepared 1% (w/v) agarose-coated plate respectively. Therefore, it costs 10x more to purchase and use commercial ULA plates to culture spheroids as compared to preparing plates 'in-house'.